cidepint

ISSN - 0325 - 4186

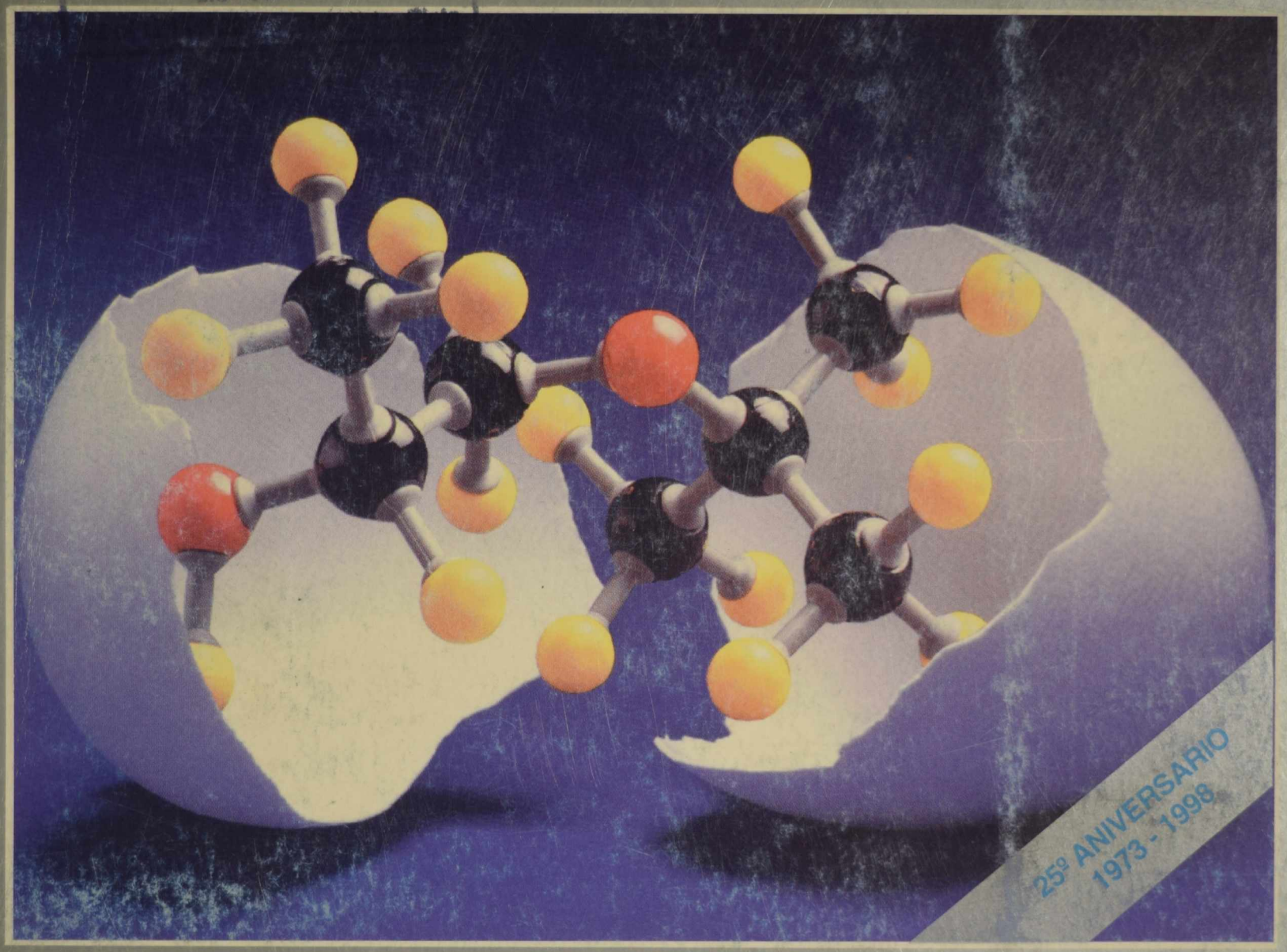

CENTRO DE INVESTIGACION Y DESARROLLO
EN TECNOLOGIA DE PINTURAS
CIC - CONICET

ANALES 1997-98

El Centro de Investigación y Desarrollo en Tecnología de Pinturas es patrocinado actualmente por la Comisión de Investigaciones Científicas de la Provincia de Buenos Aires (CIC) y por el Consejo Nacional de Investigaciones Científicas y Técnicas (CONICET).

Los objetivos fundamentales de su creación fueron los siguientes: obtener nuevos desarrollos tecnológicos relativos a pinturas y revestimientos protectores, particularmente en aquellos aspectos que puedan resultar de mayor interés desde el punto de vista nacional; formar y perfeccionar investigadores y técnicos; y, finalmente, asesorar y prestar asistencia técnica a entidades estatales y privadas, realizar peritajes y efectuar estudios especiales y tareas de control de calidad en los temas de su especialidad.

Desarrolla sus actividades en las siguientes áreas de investigación: estudios electroquímicos aplicados a problemas de corrosión y anticorrosión; análisis electroquímico; propiedades fisicoquímicas de películas de pintura; propiedades protectora de películas de pintura; planta piloto; análisis orgánico; química analítica general, cromatografía e inscrustaciones biológicas.

Durante los últimos treinta años los trabajos realizados se han publicado en diferentes revistas nacionales e internacionales: Anales de la Asociación Química Argentina, Revista de Ingeniería, Revista Latinoamericana de Ingeniería Química y Química Aplicada y Revista del Museo de Ciencias Naturales Bernardino Rivadavia (Argentina); Revista Iberoamericana de Corrosión y Protección (España); Journal of Coatings Technology, Industrial Engineering Chemistry Research, Journal of Solution Chemistry, Journal of Chromatography, Journal of Chromatographic Science, Journal of Colloid and Interface Science y Journal of Physical Chemistry (EE.UU.); Marine Biology, European Coatings Journal (Alemania Occidental); Journal of the Oil and Colour Chemists' Association y Journal of Chemical Technology and Biotechnology (Gran Bretaña); Progress in Organic Coatings (Suiza); Pitture e Vernice (Italia); Revista de la Sociedad Química de México (México); Peintures, Pigments, Vernis y Corrosion-Marine Fouling (Francia).

Otros trabajos han aparecido en Anales y Proccedings de diferentes Congresos Internacionales: Seminario Nacional de Corrosão (Brasil); Protection of Materials in the Sea (India); ACS Organic Coatings and Applied Polymer Science (EE.UU.); Congress on Metallic Corrosion (Brasil, Alemania Occidental, Canadá, India, Italia); Congress on Marine Corrosion and Fouling (Francia, EE.UU., Grecia, España); Congreso Nacional de Corrosión y Protección (España); etc.

CIDEPINT agradece expresamente el apoyo económico que los organismos promotores (Comisión de Investigaciones Científicas de la Provincia de Buenos Aires y Consejo Nacional de Investigaciones Científicas y Técnicas) prestaron para la realización de los trabajos que constituyen el presente volumen.

Editor: CENTRO DE INVESTIGACION Y DESARROLLO EN TECNOLOGIA DE PINTURAS

Dirección: 52 entre 121 y 122
1900 La Plata - Argentina
Teléfonos: (021) 831141/44 y (021) 216214
Fax: 54-21-271537

CIDEPINT-Anales es indizado periódicamente en:

Aquatic Sciences and Fisheries Abstracts (México)
Chemical Abstracts (EE.UU.)
Referativnyi Zhurnal (Rusia)
World Surface Coatings Abstracts (Gran Bretaña)

Diagramación: Prof. Viviana M. Segura

COMITE DE REPRESENTANTES

Comisión de Investigaciones Científicas
de la Provincia de Buenos Aires
(CIC)

Ing. Carlos Mayer (Titular)
Ing. Carlos Gigola (Alterno)

Consejo Nacional de Investigaciones
Científicas y Técnicas
(CONICET)

Dra. Noemí Walsöe de Reca (Titular)
Dr. José María Carella (Alterno)

DIRECTOR

Dr. Vicente J. D. Rascio

SUBDIRECTOR

Dr. en Ing. Alejandro R. Di Sarli

JEFES DE AREA

Dr. Javier I. Amalvy
Materiales Poliméricos

Dr. en Ing. Carlos A. Giúdice
Estudios en Planta Piloto

Dr. Vicente F. Vetere
Estudios Electroquímicos Aplicados a Problemas
de Corrosión y Anticorrosión

Dr. en Ing. Alejandro R. Di Sarli
Análisis Electroquímico de Pinturas y Revestimientos

Dr. Reynaldo C. Castells
Cromatografía

Tco. Quím. Rodolfo R. Iasi
Absorción Atómica

Ing. Quím. Silvia Zicarelli
Espectrofotometría

Lic. Mirta E. Stupak
Incrustaciones Biológicas

Ing. Ricardo A. Armas
Asistencia Técnica al Sector Productivo

COMENTARIOS DE LA DIRECCION DEL CIDEPINT

El presente volumen, como se indica en la tapa, se corresponde con el 25° Aniversario de la creación del Centro. A este lapso debe sumarse el transcurrido entre 1949 y 1972. Es precisamente en 1949 que, durante la gestión directiva de los Dres. Pedro J. Carriquiriborde y Humberto Giovambattista, el que suscribe se hizo cargo de la Sección Pinturas, Barnices y Plásticos del entonces Laboratorio de Ensayo de Materiales e Investigaciones Tecnológicas de la Provincia de Buenos Aires. Dicha Sección se transformó luego en División Pinturas y posteriormente en el Departamento de Análisis en Ensayo de Materiales.

A partir de la actividad inicial de control de calidad de los productos de la industria nacional y de servicios para entes privados y oficiales (nacionales y provinciales) se comenzó a incursionar en el campo de la investigación tecnológica. Este último aspecto fue encarado privilegiando proyectos relacionados con la capacidad protectora de las pinturas sobre el aspecto decorativo, pero sin separar taxativamente ambos campos, ya que una cubierta orgánica es un sistema integrado por capas de productos con diferentes características (imprimaciones, reactivas o no; pinturas de fondo, anticorrosivas o no, de acuerdo con el sustrato que se utilice; pinturas intermedias o "sealers"; y, finalmente, pinturas de terminación). Todas ellas deben complementarse para lograr una mayor vida útil, manteniendo su cohesión y la adhesión al sustrato durante lapsos prolongados.

Por ese camino se detectaron fallas en algunos de los productos existentes en el mercado, lo que indujo a profundizar en el por qué del problema. Simultáneamente se colaboró con el IRAM en el estudio de las Normas de la especialidad, revisándose las existentes o implementando otras nuevas, siempre en base a los valores que surgían de datos experimentales.

De la asociación de esfuerzos entre aquel LEMIT, la Comisión de Investigaciones Científicas de la Provincia de Buenos Aires (CIC) y el Consejo Nacional de Investigaciones Científicas y Técnicas (CONICET) surgió el CIDEPINT. El objetivo fundamental del Centro, establecido en el Convenio de formación, apuntó a la realización de investigaciones científicas y desarrollo de tareas técnicas en el campo de la tecnología de pinturas y/o

recubrimientos protectores. La financiación e infraestructura básica, proporcionada en su primera etapa por el LEMIT, se complementó con subsidios y aportes presupuestarios por parte de la CIC y del CONICET. Actualmente el CIDEPINT es un Centro del sistema CIC y continúa vigente el acuerdo con el CONICET.

Dentro del marco citado se han ejecutado numerosos proyectos de investigación, con objetivos concretos y con una planificación y cronogramas preestablecidos. Se ha logrado la formación de recursos humanos (investigadores, profesionales, becarios, técnicos, etc.) en las diferentes especialidades del Centro (materiales poliméricos; planta piloto; estudios electroquímicos aplicados a problemas de corrosión y protección; análisis electroquímico de pinturas y recubrimientos; cromatografía; absorción atómica; espectrofotometría de infrarrojo, ultravioleta y visible; e incrustaciones biológicas). El último de los temas citados, de carácter esencialmente biológico, está íntimamente asociado con la protección de estructuras tanto móviles como fijas, sumergidas en medio marino. Las líneas de investigación citadas se complementan con el apoyo de una secretaría ejecutiva que coordina las actividades administrativas, documentación científica e informática.

Durante el año en curso finaliza el proyecto trienal 1996-98, y se ha elaborado uno nuevo para el período 1999-2001. Por diferentes caminos, todas las acciones propuestas apuntan a un mismo objetivo: lograr productos ajustados a las normas ecológicas actualmente vigentes en los países desarrollados (bajo nivel de compuestos orgánicos volátiles o eliminación total de disolventes, empleo de pigmentos no tóxicos, métodos de elaboración o de aplicación no contaminantes, etc.).

En este proyecto se indica explícitamente que la implementación de las Normas ISO 25, destinadas a la acreditación de ensayos y laboratorios, constituye una preocupación constante del nivel directivo del Centro, habiendo profesionales y técnicos asistido a conferencias y cursos sobre dicha temática. Las etapas previstas, de ejecución sucesiva, permitirán establecer un sistema de calidad (precisión de tareas), control de calidad (diseño de actividades), garantía de calidad y manuales de procedimientos, conducentes a lograr el reconocimiento final de un organismo externo en el sentido que el sector involucrado es competente para las tareas que se realizan en el mismo.

Lo expuesto precedentemente será de utilidad no sólo para mejorar la asistencia técnica al sector productivo sino también para las tareas de investigación que se realizan.

Como ha ocurrido permanentemente, la casi totalidad de los trabajos incluidos en este volumen han sido publicados en las revistas más importantes de la especialidad. Otros han sido aceptados para su publicación o están siendo evaluados con el mismo fin. En un Anexo se incluye un listado completo de los trabajos de investigación publicados en los últimos seis años, complementado por las presentaciones a congresos científicos o por artículos técnicos.

Dr. Vicente J. D. Rascio
Director del CIDEPINT

INDICE CONTENTS

Algunos de los trabajos de investigación incluídos en este volumen han sido publicados, aceptados o remitidos para su publicación en revistas científicas de difusión internacional o presentados en Congresos y Reuniones Científicas de la especialidad *(Some of the research papers issued in this volume have been published, accepted or submitted for publication to international journals or submitted to Congress and Scientific Meetings on the speciality).*

[1] Proceedings 16th Conference on Waterborne, High Solids and Radcure Technologies, Frankfurt, Alemania, 11-13 de noviembre 1996.
[2] Proceedings 1997 Joint International Meeting de ISE y The Electrochemistry Society, Paris, Francia, 31 de agosto al 5 de setiembre de 1997.
[3] Anales VII Jornadas Argentinas de Corrosión y Protección, Mendoza, Argentina, 17-19 de setiembre de 1996.
[4] European Coatings Journal, 1-2, 52-59 (1998).
[5] Pitture e Vernici, 73 (14), 9-16 (1997).
[6] Pitture e Vernici, 73 (11), 10-16 (1997).
[7] Pitture e Vernici. Aceptado para su publicación, octubre 1997.
[8] The Journal of Scanning Microscopies, 19 (3), 244-45 (1997).
[9] Journal of Chromatography A, 775, 73 (1997).
[10] Journal of Colloid Interface Science, 192, 142 (1997).
[11] Journal of Chromatography A, 757, 97 (1997).
[12] Journal of Chromatography A, 757, 109 (1997).
[13] Journal of Chromatography A, 766, 147 (1997).
[14] Oceanologica Acta. Remitido para su publicación, mayo 1998.
[15] 3rd NACE Latin American Region Corrosion Congress, Cancún, del 30 de agosto al 4 de setiembre de 1998. Aceptado.
[16] 3rd NACE Latin American Region Corrosion Congress, Cancún, del 30 de agosto al 4 de setiembre de 1998. Aceptado.

THE USE OF POLYMERIZABLE SURFACTANTS IN EMULSION COPOLYMERIZATIONS FOR COATINGS APPLICATIONS

EL USO DE SURFACTANTES POLIMERIZABLES EN COPOLIMERIZACION EN EMULSION PARA APLICACIONES EN PINTURAS

J.I. Amalvy[1], M.J. Unzué[2], H.A.S. Schoonbrood[3], J.M. Asua[2]

SUMMARY

In this paper results obtained in high solids content emulsion copolymerizations using polymerizable surfactants (surfmers) have been reviewed.

On the basis of the interpretation of the behavior of the surfmers (the conversion vs. time and their performance in stability tests and film properties), an optimal surfmer behavior has been defined, which means that all the added surfmer groups end up on the particle surface rather than being buried, which leads to inferior latex stability. One of the strategies that have been proposed to achieve this has been applied to prepare a well-defined styrene-butyl acrylate latex of which film can be easily be cast. Its properties in terms of mechanical stability, film water absorption, and film surfactant exhudation have been assessed and compared with these of a similar latex with sodium dodecyl sulfate. Other comonomer systems have been studied as well with the maleic surfmer. In these systems the surfmer behavior was less "optimum". For these latices both mechanical stability and water absorption was assessed.

Keywords: *polymerizable surfactants, surfmers, reactive surfactants, emulsion polymerization, latex, kinetics, film properties.*

INTRODUCTION

In the process of emulsion polymerization surfactants play a very significant role. They are very important for fast nucleation of latex particles, emulsification of monomer droplets and stabilization of the latex particles during the polymerization, and during the shelf life of the latex. When the latex is used in films and coatings however, the presence of surfactant can have negative effects. These effects are caused by the fact that the surfactant can desorb from the latex particle surface and can migrate through the product. For example they can desorb from the particle surface under high shear and cause mechanical instability or concentrate in aggregates **[1]**, increasing the water-sensitivity of the product Additionally in films exhudation of the surfactant **[2-4]** can take place towards the film-air (F-A) interface, or even towards the film-substrate (F-S) interface. This fact increases the water sensitivity of the film-air surface, and can have a negative effect on the adhesion properties of the film at the substrate interface.

---

[1] Miembro de la Carrera del Investigador de la CIC
[2] Grupo de Ingeniería Química, Departamento de Química Aplicada, Facultad de Química, Universidad del País Vasco, España
[3] Dirección actual: Rhône-Poulenc, Centre de Recherches d'Aubervilliers, Francia

The use of reactive surfactants could be a solution to some of these problems, due to the fact that the surfactant moiety is bound covalently to the polymer material and the deabsorption from the latex particle surface is impeded. The migration in the polymer film is also impeded. These reactive surfactants can be the combination of a part with surfactant activity and a part with an initiating capacity called inisurf **[5-7]**. If the reactive group is a transfer agent it is called a transurf **[8]** and if the reactive group is polymerizable, it is a surfmer **[9,10]**. These have been described before as polymerizable surfactants and are the most promising possibility in emulsion polymerization. There are several examples which include anionic surfmers with sulfate or sulfonate head groups, **[11-17]** cationic surfmers **[18,19]** and non-ionic surfmers **[20,21]**. The reactive groups can be of different types, for example: allylics **[22,23]**, acrylamides **[16]**, (meth)acrylates **[21,24]**, styrenics **[14,25]**, or maleates.

Examples of emulsion polymerizations with surfmers can be found in refs. 13, 24-30 improvements in properties caused by the use of surfmers have been reported in several cases. For example in mechanical stability **[26]** and electrolyte stability of the latex **[24]**. Has been reported **[13]** that when a surfmer is used the surfactant migration is reduced and the water resistance **[12,14,20,31,32]** and adhesivity **[14,20,32]** are improved.

SCOPE OF THE PRESENT PAPER

This paper is part of a series **[10,33-35]** where several surfmers with very different reactivities in copolymerization have been investigated. We will firstly review results obtained in a styrene-acrylic monomer system with several surfmers with varying reactive groups: two maleic acid diesters, a methacrylic acid ester and a crotonic acid ester. The results include the analyses of conversion versus time of both surfmers and main monomers in high solids semicontinuous reactions, and the amount of coagulum formed and particle size.

This is followed by a review of results obtained **[35]** when using the maleic acid diesthers in other comonomer systems, to illustrate the fact of changing the reactivity of the main monomers. In the last part we will give the results of some tests that determine the performance of a few of these latices with respect to mechanical stability as well as the performance when applied as films (water sensitivity and surfactant exhudation). For this purpose two new styrene acrylic latices were prepared following a strategy as proposed in ref. 35 to obtain an ideal surfmer behavior, which means that all the surfmer is bound to the surface of the particles and that none is buried in the particles interior, where they can not contribute to the latex stability. These latices only differ in the nature of the surfactant: a bound maleic acid diester and the unbound sodium dodecyl sulfate.

EXPERIMENTAL

The experimental details of preparation of latices, surfactant and main monomer conversion, cleaning of latices and water ababsorption are given in ref. 10, 33 and 35.

For the mechanical stability test 25 g of latex was stirred at 12.000 rpm for 5 minutes and the coagulum formed was filtered through a # 63 mesh sieve. The residue was rinsed with

water and dried. The weight of the residue was expressed in percentage based on the solid content of the emulsion.

Films from latices, for water ababsorption and spectral measurements, were cast on glass substrate and peeled off.

Transmission spectra of films and surfactants were performed in the common way. The attenuated total reflectance (ATR) spectra of film-air and film-substrate interfaces were performed using a KRS-5 crystal. The spectrum were normalized with respect to the 852 cm^{-1} band due to the C-C skeletal mode of the C-C main chain.

RESULTS AND DISCUSSIONS

The surfmers used in the work are summarized in Table 1. Sodium dodecyl sulfate (SDS) was used as a non-polymerizable reference surfactant.

The systems investigated include the following:

I) Styrene (S)/butyl acrylate (BA)/acrylic acid(AA) (49.5/49.5/1 (w%)).
II) Vinyl acetate (VAc)/VEOVA10/AA (69/30/1 (w%))
III) VAc/BA/AA (79/20/1 (w%))
IV) Methyl methacrylate (MMA)/BA/VAc (50/35/15 (w%))

Table 1

Name, code, chemical structure and cmc value of surfactants used

surfactant	code	chemical structure	cmc (g/L)
Sodium 3-sulfopropyl dodecyl maleate	M12	$C_{12}H_{25}OOC\text{-}CH{=}CH\text{-}COOC_3H_6SO_3Na$	0.693
Sodium 3-sulfopropyl tetradecyl maleate	M14	$C_{14}H_{29}OOC\text{-}CH{=}CH\text{-}COOC_3H_6SO_3Na$	0.12/0.085
Sodium 11-crotonoyl undecan-1-yl sulfate	CRO	$NaSO_4C_{11}H_{22}OOC\text{-}CH{=}CH(CH_3)$	4.9
sodium 11-methacryloyl undecan-1-sulfate	MET	$NaSO_4C_{11}H_{22}OOC\text{-}C(CH_3){=}CH_2$	2.5
sodium dodecyl sulfate	SDS	$C_{12}H_{25}\ SO_4Na$	1.15

These systems are of practical interest and at the same time the monomers present widely different reactivities in copolymerization (Table 2).

Table 2

Reactivity ratios of surfmers (or corresponding monomers) with main monomers

Surfmer or equivalent monomer	styrene	butyl acrylate	vinyl acetate	methyl methacrylate
	r_S , $r_{surfmer}$	r_{BA} , $r_{surfmer}$	r_{VAc} , $r_{surfmer}$	r_{MMA} , $r_{surfmer}$
Diethyl maleate (M14 or M12)	8-10 , 0[36]	>>10 , 0*	0.04 , 0.17[36]	354 , 0[37]
Methyl crotonate (CRO)	26 , 0.01[38]	-	-	-
Dodecyl/methyl methacrylate (MET)	0.53 , 0.30[36]	0.32 , 2.6[39]	-	-

* estimated on the basis of results of a reaction between BA and M14 (33), where M14 did not polymerize at all in the presence of BA.

I) The styrene/butyl acrylate/acrylic acid system.

Three surfmers differing in the nature of the polymerizable group were used. One of the surfmers is an ester of methacrylic acid (MET), one is an ester of crotonic acid (CRO), and the third is a diester of maleic acid (M14). The methacrylic derivative is an example of a very reactive surfmer, the crotonic derivative an example of a generally non-reactive surfmer. The maleic derivative was chosen for its intermediate reactivity and for the fact that it cannot homopolymerize (in the aqueous phase). This feature is common to all maleic diesters **[40,41]**. The intrinsic reactivity of the polymerizable groups in the surfmers can provide a basic idea about the suitability of the surfmer. One can see in Table 2, that on the basis of the reactivity with S, the MET surfmer can be expected to be the most reactive, and the CRO surfmer the least reactive. In order to maximize the differences between the performance in the emulsion polymerizations, the concentrations of the surfmers were chosen in such way that the system were close to the stability limit.

In Table 3 the amount of coagulum obtained in some reactions are given together with the particle diameter.

When MET is used as the surfmer, the amount of coagulum increases and reaches 24 %, an unacceptable level. This could be due to the fact that the MET can homopolymerize and is quite reactive with the main monomers (see Table 2) in contrast to M14. This fact could lead to polyelectrolyte formation in the aqueous phase, which in turn could destabilize existing particles by bridging flocculation or, if the amount of polyelectrolyte is significant with respect to the amount available for adabsorption on the latex particle surface, the minimum coverage for stabilization is not attained.

If we compare the reactions M14B1 and CRO, in which the initiator was charged completely at the beginning, it can be seen that the surface tension is lower in the case of CRO, which also has less coagulum. This may be caused by the fact that CRO is less reactive than M14, so that when all M14 is charged in the beginning, more of this surfmer may become buried in the particle, whereas the less reactive CRO remains at the particle surface.

Table 3

Amount of coagulum[a] and diameter[b,c] of latex in non-seeded reactions in the S/BA/AA system (50% solid content), with SDS and various anionic surfmers, using KPS as initiator and at 80 °C.

reaction code	initiator charge/feed	surfactant	coagulum (%)	diameter (nm)
SDS	50/50	SDS (1 w%)[d]	1.1	99
M141	50/50	M14 (1 w%)	2.5	152[c]
M142	50/50	M14 (2 w%)	0.5	130[c]
M145	50/50	M14 (5 w%)	0.6	102[c]
MET	50/50	MET (1 w%)	24	-
M14B1	100/0	M14 (1 w%)	5.6	129
CRO	100/0	CRO(1 w%)	1.5	186

[a] % on total monomer; [b] from light scattering; [c] from transmission electron microscopy
[d] based on monomers.

In case of the maleates (M14 and M12) the results indicate that the level of conversion is between that of the crotonate and methacrylate surfmers. This is in line with its general copolymerization reactivity. In Table 4 the properties of some latices of system I with maleate surfmers are presented.

Table 4

Properties of latices of system I

Code	Monomers (w%)	solids content (%)	surfmer, w%	final particle size (nm)	coagulum (w%)*
30IM141	S/BA/AA (49.5/49.5/1)	30	M14, 1	98	1.3
50M142	S/BA/AA (49.5/49.5/1) seed S/BA (50/50)	50	M14, 2	114	1.4
50M122	S/BA/AA (49.5/49.5/1) seed S/BA (50/50)	50	M12, 2	109	1.2

* w% based on monomers.

Figure 1 shows an example of a seeded semi-continuous reaction with M14 (50M142S) and the equivalent reaction with M12 (50M122S).

The evolution of the total conversion of the main monomers with time is virtually the same for both reactions, due to the fact that these are seeded reactions. An equivalent reaction with SDS gave conversion results identical to 50M142. The use of the maleate surfmers in these reactions does not seem to affect the kinetics.

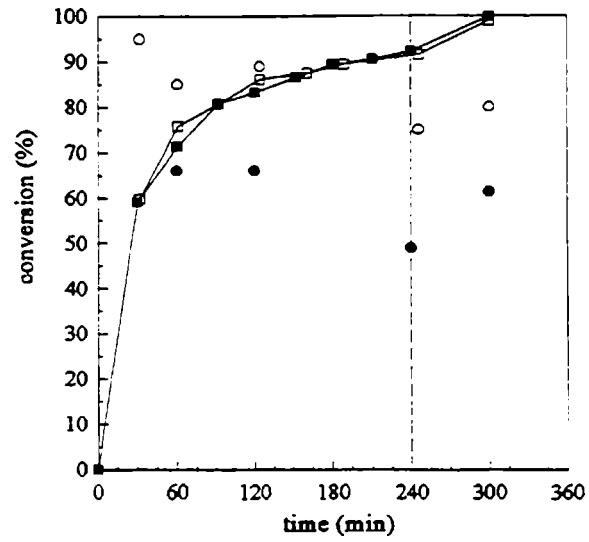

Fig.1. System I. Main monomer conversion (squares) and surfmer conversion (circles) versus time in reactions 50M142 (with M14 as surfmer, open symbols) and 50M122 (with M12 as surfmer, closed symbols).

It can be seen that M14 had a relatively high conversion throughout the reaction and a final conversion of 80 %. The conversion of M12 is somewhat lower and its final conversion is 62 %, which is perhaps due to the higher water solubility of M12. Anyway, the pattern of the conversion versus time shows the same characteristics for both maleates.

It was observed in a non-seeded reaction with a final particle size of 98 nm (30IM141 in Table 5), that the conversion of M14 during the reaction reached levels higher than 95 %. The surface-charge density analysis showed that only 40 % of the original M14 surfactant groups were present at the particle surface, indicating that a large proportion remains buried in the particle interior due to the high conversion of M14 from the beginning of the reaction. This is corroborated by the results of other reactions with styrene and M12 or M4 **[34]**, where the surfmers reached very high levels of conversion at low overall conversion.

II) The VAc/VEOVA10/AA system

We applied M12 as a surfmer in the monomer system VAc/VEOVA10/AA (Table 5).

In Figure 2 are shown the conversion results of the reaction 30IIM12. It can be seen that in reaction 30IIM12 the conversion of M12 is very high from the beginning.

The amount of coagulum is not very high, however, and no signs of instability were observed. This can be a result of the fact that the solids content was low. A reaction at 50 % of solids (50IIM12 in Table 5) was carried out, using a seed of latex to ensure a similar particle size to that of 30IIM12. The conversion of the main monomers (not shown here) follows the same pattern as in 30IIM12, but as indicated in Table 5, the amount of coagulum is quite high

and at the same time, the particle size is much higher than expected on the basis of the number of seed particles.

Table 5

Properties of latices of system II

Code	monomers (w%)	Solids content (%)	surfmer, w%	final particle size (nm)	coagulum (w%)*
30IIM12	VAc/VEOVA10/AA (69/30/1)	30	M12, 1	128	0.6
50IIM12	VAc/VEOVA10/AA (69/30/1) seed VAc/VEOVA10 (75/25)	50	M12,2	>170	15

*w% based on monomers.

This indicates that the reaction 50IIM12 is unstable, probably because of the high conversion of the surfmer. This high conversion is somehow expected if we look the reactivity ratios (see Table 2) between diethyl maleate and VAc: $r_{\text{diethyl maleate}} = 0.04$, $r_{VAc} = 0.17$ (ref. 36).

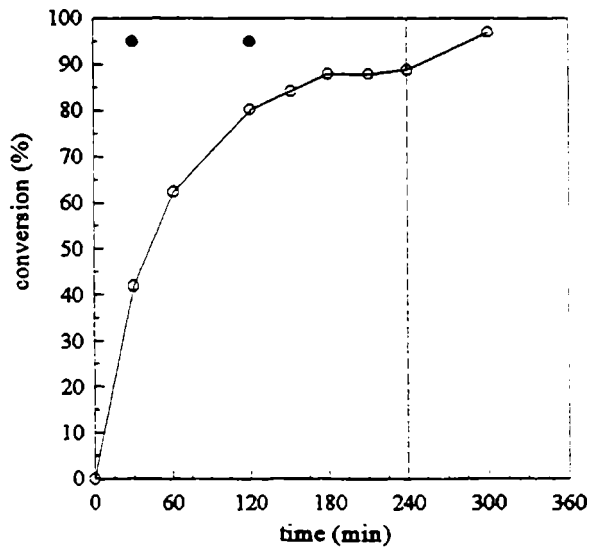

Fig. 2. Main monomer conversion (o) and M12 conversion (●) versus time in reaction 30IIM12.

III) The VAc/BA/AA system.

In this monomer system (ref. 35) BA is far more reactive than VAc, and at the end of the feeding period there will be a certain amount of VAc left even under starved conditions. In ref. 33 it was shown that M14 does not react with BA. Therefore it was expected that during the feeding time of a semi-continuos reaction with this monomer system, when there is some BA present, the maleate surfmer would not react to high conversion as it does in a system with only vinyl esters (II), and that the maleate would react with the remaining part of the VAc after stopping the feed.

Three reactions were carried out with this monomer system, two at 54 % solids with SDS and M12 and one at 30 % solids with M12 (see Figure 3).

The reaction with SDS (54IIISDS) gave a stable latex with very little macroscopic coagulum. However, the latex completely coagulated on the shelf after a few weeks. The reaction 54IIIM12 with M12, ended in total coagulation after 90 minutes of reaction. The reaction 30IIIM12 was carried out at 30% solids content and the conversion of M12 was very high from the beginning.

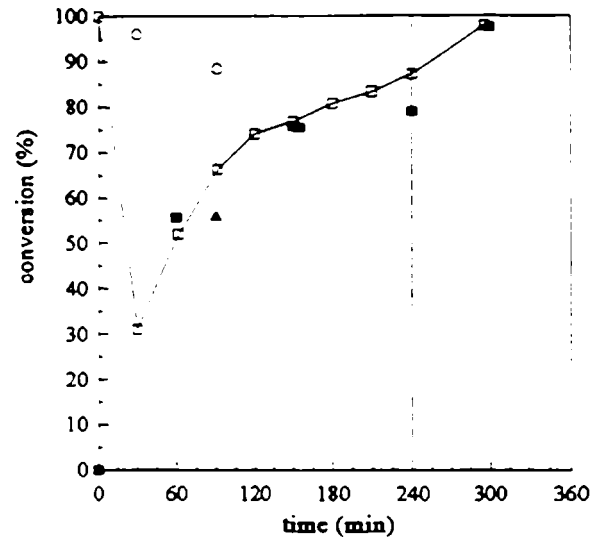

Fig. 3. Main monomer conversion and surfmer conversion versus time in reactions 54IIISDS (main monomer: ■), 54IIIM12 (main monomer ▲) and 30IIIM12 (main monomer ❑, M12: o).

This high conversion probably led to the observed instability. The conclusion therefore is that the maleate surfmers are too reactive, just as in the previous system, due to the presence of the vinyl esters.

IV) The MMA/BA/VAc system

In this system (ref. 35) due to the fact that VAc is by far the least reactive monomer, in semi-continuous reactions, during the period of feeding, the instantaneous conversions of both BA and MMA are quite high and that of VAc relatively low **[39]**, which means that at the end of the feeding period the unreacted monomer will be mainly VAc. This unreacted VAc is expected to copolymerize with M12 after feeding has stopped and a high conversion of the surfmer at the end of the reaction should be found. Using a variable feed flow rate so that the instantaneous conversion of the monomers (mainly VAc) was not high at the end the conversion-time behavior found was as shown in figure 4 (see ref. 35).

The instantaneous conversion of the monomers was approximately 90 % at the end of the feed period. The M12 conversion after the nucleation period is relatively high, due to the fact that the charge is allowed to react in batch mode. At the end of that batch period the mixture is enriched in VAc. However, after this initial period the instantaneous conversion drops to a lower level, and at the end of the feeding period it is about 60 %. The amount of VAc (15 %) seems to high enough to allow some reaction of M12. When the feeding has been stopped, and the reaction is in batch mode with a large amount of unreacted VAc, it can be seen that the conversion of M12 starts to increase rapidly, having reached complete conversion when all main monomers have reacted.

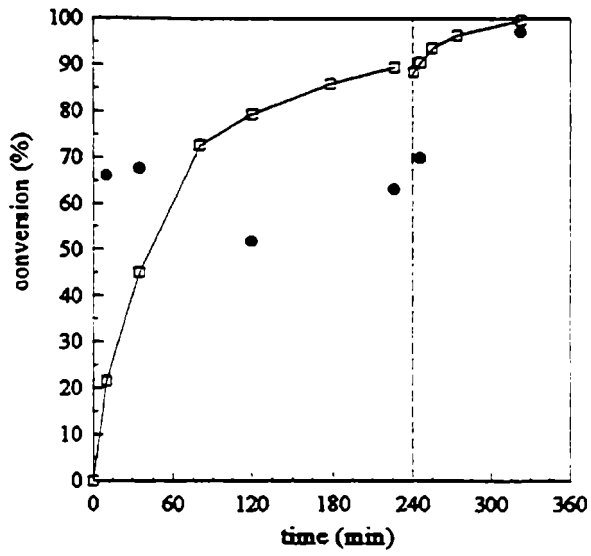

Fig. 4. Main monomer conversion and surfmer conversion versus time in reaction 30IVM12 (main monomer: □, surfmer ●).

Based on the above mentioned results it can be concluded that the reactivity of the surfmer relative to the main monomers plays an important role [35]. However, the results of various reactions with M14 in system I suggest that the level of conversion can vary significantly within the same monomer/surfmer system. Combining M14 conversion data in several reactions with monomer system I shows the interesting result [35] that the conversion of M14 is strongly dependent upon the particle diameter and reaches high levels for small particles up to 100 nm, and decreases steadily at higher particle diameters. The different M14 conversions found in various reactions could be explained by the difference in particle size. The rate of polymerization of M14 relative to the monomers decreases as a function of particle size. This result points strongly in the direction of M14 reacting at the surface, where the free, unreacted M14 will mainly be present. The locus of polymerization for the main monomers is the whole polymer particle. If the M14 only reacts in an outer shell of the particle with a set thickness, an increase in particle diameter should cause a decrease in the extent of reaction of M14, if we discard any radial radical concentration profile.

LATEX AND FILM PROPERTIES

The use of polymerizable surfactants instead of classic surfactants is only valid if there is an improvement in latex or film properties that warrants their use. Obviously the polymerizable surfactant serves best if at the end of the polymerization it resides at the particle surface, rather than being partly buried. To achieve this, in most cases both a well chosen type of polymerizable surfactant has to be used as well as a special polymerization strategy (see ref. 35). As we have seen in the above, this has probably not been achieved in any of the latices, except perhaps in latex 30IVM12. Some of the latices described above, including 30IVM12 have been analyzed with respect to mechanical stability and the corresponding films with respect to water ababsorption. To offset the results, we have not used the latices of monomer system I as mentioned above, but rather we have synthetized two new latices with the objective to have two very similar latices, only differing in the nature of the surfactant groups at the surface: one latex with the unbound SDS (35ISDS), and the second latex with the SDS

replaced by M14, all bound to the particle surface. The latter latex was prepared by replacing the initially used SDS with M14 using dialysis, followed by addition of KPS and a 70:30 mixture of VAc and VEOVA10 which react very well with M14. This procedure ensures the inmobilization of the M14 groups at the particle surface (35IM14).

In addition to the latex mechanical stability and water ababsorption of the film, in this case also the exhudation of the surfactant to the film surface was investigated with attenuated total reflectance (ATR) -FTIR spectroscopy.

MECHANICAL STABILITY

Table 6 shows the amount of coagulum after the mechanical stability test of some latices.

The results were interpreted taking into account the surfactant distributions.

System I, 35ISDS and 35IM14

In this case the small amount of coagulum indicates a good stability of both latices, but the one prepared with the surfmer is better. This is in accordance that the observations of Greene and Sheetz **[26]** that when the charges are immobilized on the latex surface, deabsorption is highly improbable and the latices are more stable.

Table 6

Properties and mechanical stability[a] of the latices tested

System	reaction code	Surfactant (1% w)	solids content(%)	particle size (nm)	coagulum (w%)[b]
I	35IM14	M14	35	164	1.5
	35ISDS	SDS	35	153	3.3
II	30IIM12	M12	30	128	10.4
	B5	DDBS[c]	30	127	25.4
III	30IIIM12	M12	30	109	28.3
	30IIISDS	SDS	30	76.2	8.9
IV	30IVM12	M12	30	114	30.7
	30IVSDS	SDS	30	236	11.2

[a] 12,000 rpm, 5 minutes. [b] w% based on solid content.
[c] In this case a non-ionic surfactant was used in conjunction with dodecyl benzene sulfonate (DDBS).

System II (VAc/VEOVA10/AA - 69/30/1)

The high amount of coagulum could be due to the fact that the surfmer has an elevated conversion from the beginning of reaction (Fig. 2), i.e., it is likely that a high proportion is buried inside the particle. Greene *et al* **[26]**, found that the amount of coagulum formed after a

mechanical test decreased with increasing surface coverage and due to the fact that when the surfmers are bound in parts of the particle other than the surface, the stabilization is not achieved until an optimum coverage is reached.

System III (BA/VAc/AA - 20/79/1) and system IV (MMA/BA/VAc - 50/35/15)

In systems III and IV the situation is more complex. The latices with SDS obviously have all the surfactant on the particle surface. On the other hand the latex with M12 in system III probably has few surfactant groups on the surface due to burying. Reaction 30IVM12 was carried out so as to obtain a latex with most M12 bound to the surface, by maintaining a low surfmer conversion during the feeding period (ref. 35) However, the remaining amount of M12 at the end of the feeding period reacts very rapidly with VAc, possibly leading to copolymer chain which are very rich in M12 (1:1). This means that although the problem of burying surfactant groups is (partly) circumvented, it is possible that the 1:1 polymer formed at the end does not stabilize the particles as effectively as free M12 or M12 bound more homogeneously to the particle surface. This a matter for further investigations. The stability results suggest the present situation (1:1 polymer) is not good. Perhaps the reactivity of the remaining main monomer needs to be higher than 0 (as in this case).

WATER ABABSORPTION

Figure 5 shows the water ababsorption of films prepared from latices discussed here. It can be seen that in general films with surfmers have a lower final water absorption than films with SDS.

In system I, we had an example where there was not much difference in the initial stage, between M14 and SDS (although $X_{final, M14}$ was not very high (64%)), but the final water absorption is lower in the latex with M14. So it seems that there is a general improvement in water absorption. Comparing films cast from the different systems (prepared with surfmers), we observe that the final water uptake is similar for systems I, II and III (about 45 % after 30 days) and lower for system IV (33 % after 30 days). These differences are due to the presence of the more hydrophilic AA monomer in the first three systems.

SURFACTANT MIGRATION

The latex from reaction 35IM14 and its counterpart with SDS, were cast on glass and peeled off, to study surfactant migration to the interfaces, using FTIR-ATR spectroscopy.

Figure 6 shows the spectra in the low wavenumber region where the bending modes of the $-SO_3$ or the $-OSO_3$ groups appear.

It can be seen that in the SDS latex, the spectrum of film-air (F-A) interface shows a somewhat different pattern than the transmission spectrum (bulk), indicating that there is surfactant migration during coalescence. The relative intensities of band of 635 cm^{-1} due to SDS and that of ca. 620 cm^{-1},due to the polymer, indicates an exhudation of SDS to the film-air interface.

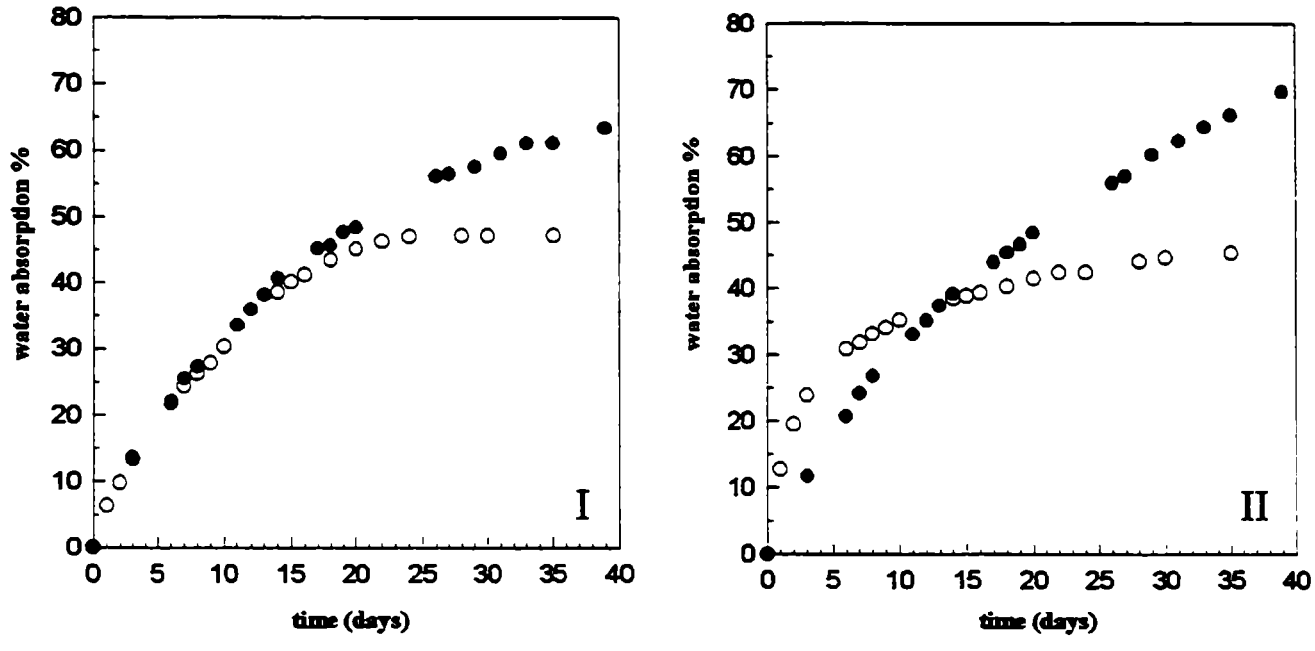

Fig. 5. Water absorption vs. time of latices from systems I to IV. Open circles with surfmer and closed circles with SDS.

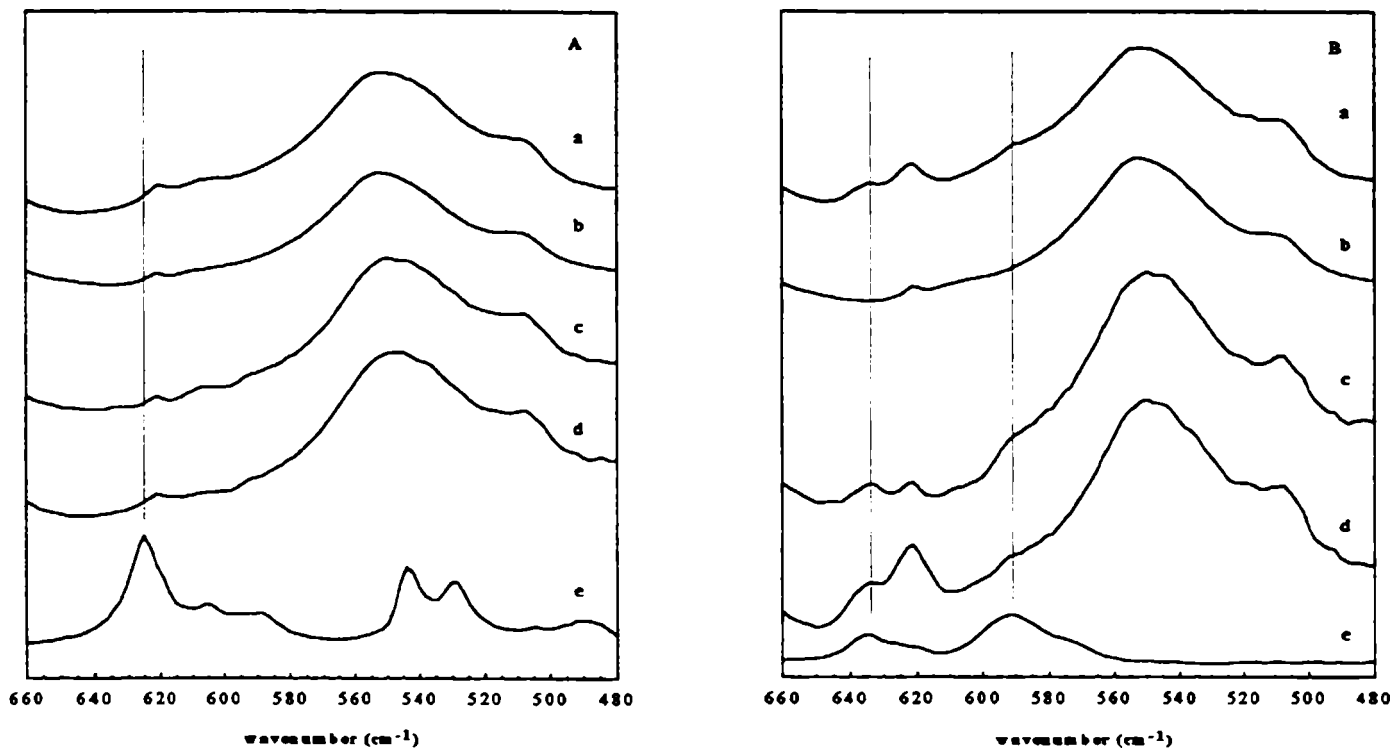

Fig. 6. FTIR spectra in the low wavenumber region of latices cast from 35IM14 (A), 35ISDS (B) and surfactants. Film transmission (a), film transmission of latex without surfactant (b), ATR of film-air interface (c), ATR of film-substrate interface (d) and pure surfactant (e).

In the case of films cast from 30IM14, no difference between transmission (bulk), F-A or F-S interfaces is observed, indicating that due to the surfmer is chemically bounded, the migration is prevented. However, it has to be pointed out that between both surfactants there are differences in molecular weight, in polarity and consequently in compatibility with the polymer. These should contribute to a lower migration of M14 in comparison with SDS. Anyway, it can conclude that the use of a surfmer hinder the surfactant migration.

CONCLUSIONS

It can concluded clearly that water ababsorption is improved by using reactive surfactants. At the same time it can be conclude that exhudation of surfactant to the film surface can be prevented. The mechanical stability of the latex can be improved as well, although this requires all of the surfactant to be bound to the latex particle surface, but possibly not in highly enriched polymer chains. This can only be achieved by using what was coined as "optimum surface behavior" in a previous publication **[35]**, where ways of avoiding burying of surfactant groups, but ensuring 100% incorporation, are suggested. This optimum behavior was "attained" in reaction 35IM14.

ACKNOWLEDGEMENTS

This work was carried out as part of a European Union sponsored network (CHRX CT 930159). MJU was financially supported by the Basque Government. HASS acknowledges a grant of the Training and Mobility of Researchers Program (ERB4001GT953910). J.I.A acknowledges the fellowship from AECI-UPV.

REFERENCES

[1] Roulstone, B.J.; Wilkinson, M.J.; Hearn J.- **Polym. Intern.**, **27**, 43 (1992).

[2] Zhao, C.I.; Holl, Y.; Pith, T.; Lambla, M.- **Colloid & Polym. Sci.** , **265**, 823 (1987).

[3] (a) Evanson, K.W.; Urban, M.W.- **J. Appl. Polym. Sci.** , **42**, 2287 (1991), (b) Evanson, K.W.; Thorstenson, T.A.; Urban, M.W.- **J. Appl. Polym. Sci.** , **42**, 2297 (1991).

[4] Juhuë, D.; Wang, Y.; Lang, J.; Leung, O.-M.; Goh, M.C.; Winnik, M.A.- **Polym. Mater. Sci.**, **73**, 86 (1995).

[5] Tauer K.; Goebel, K-H.; Kosmella, S.; Neelsen, J.; and Stähler, K.- **Plaste Kautsch.**, **35**, 373 (1988).

[6] Tauer, K. and Kosmella, S.- **Polym. Int.**, **30**, 253 (1993).

[7] Kusters, J.M.H.; Napper, D.H.; Gilbert, R.G. and German, A.L.- **Macromolecules**, **25**, 7043 (1992).

[8] Vidal, F.; Guillot, J. and Guyot, A.- **Polym. Adv. Technol., 6**, 473 (1994).

[9] Guyot, A.; Tauer,K.- **Adv. Polym. Sci., 43**, 111 (1994).

[10] Unzué, M.J.; Schoonbrood, H.A.S.; Asua, J.M.; Montoya Goñi, A.; Sherrington, D.C.; Stähler, K.; Goebel, K.H.; Tauer, K.; Sjöberg, M.; Holmberg, K.- **J. Appl. Polym. Sci., 66**, 1803 (1997).

[11] Parker, III, J.E.; Alford, J.A.- **US Patent** 5, 306, 793 (1994).

[12] Onodera, S; Yamamoto, S.; Tamai,T.; Takahashi, H.- **Jpn Pat.** 06, 239, 908 (1994).

[13] Chen, S.A.; Chang, H.S.- **J. Polym. Sci.:Part A: Polym. Chem. Ed., 23** , 2615, 1985.

[14] Yokota, K.; Ichihara, A.; Shinike,H.- **US Patent**, 5, 324, 862 (1994).

[15] Nagai, K.; Satoh, H.; Kuramoto, N.- **Polymer, 34**, 4969 (1993).

[16] Baumgartner, E; et al.- **Germ. Pat.,** DE 32 39 527 (1984).

[17] Kozuka, K.; Kobayashi, S.; Watanabe, A.; Yokoe, M.; Iki, Y.- **US Pat.,** US 3, 980, 622 (1976).

[18] Cochin, D.; Zana, R.; Candau, F.- **Macromolecules, 26**, 5765 (1993).

[19] Choubal, H.; Ford, W.T.- **J. Polym. Sci.: Part A: Polym. Chem. , 27**, 1873 (1989).

[20] Kinoshita, K.; et al.- **Jpn. Pat.** 94/49, 108 (1994).

[21] Ferguson, P.; Sherrington, D.C.; Gough, A.- **Polymer, 34**, 3281 (1993).

[22] Larrabee, Jr, C.E.; Sprague, E.D.- **J. Polym. Sci., Polym. Lett. , 17**, 749 (1979).

[23] Denton, J.M.; Duecker, D.C., Sprague, E.D.- **J. Phys. Chem., 97**, 756 (1993).

[24] Green, B.W.; Saunders, F.L.- **J. Colloid and Interf. Sci., 33**, 393 (1970).

[25] Tsaur, S.L.; Fitch, R.B.- **J. Colloid and Interf. Sci., 115**, 450 (1987).

[26] Green, B.W.; Sheetz, D.P.- **J. Colloid and Interf. Sci., 32**, 96 (1970).

[27] Guillaume, J.L.; Pichot, C.; Guillot, J.- **J. Polym. Sci.: Part A: Polym. Chem., 28**, 137 (1990).

[28] Urquiola, M.B.; Dimonie, V.L.; Sudol, E.D.; El-Aasser, M.S.- **J. Polym. Sci.: Part A: Polym. Chem.** , **30,** 2619 (1992).

[29] Urquiola, M.B.; Dimonie, V.L.; Sudol, E.D.; El-Aasser, M.S.- **J. Polym. Sci.: Part A: Polym. Chem.** , **30**, 2631 (1992).

[30] Urquiola, M.B.; Dimonie, V.L.; Sudol, E.D.; El-Aasser, M.S.- **J. Polym. Sci.: Part A: Polym. Chem.** , **31**, 1403 (1993).

[31] Tang, R.H.; Chakrabarti, P.M.- **US Pat.**, US 5, 296, 627 (1994).

[32] Usai, S.- **Jpn. Pat.,** 94/65, 551 (1994).

[33] Schoonbrood, H.A.S.; Unzué, M.J.; Beck, O-J.; Asua, J.M.; Montoya Goñi, A.; Sherrington, D.C.- **Macromolecules, 30**, 6024 (1997).

[34] Schoonbrood, H.A.S.; Unzué, M.J.; Amalvy, J.I.; Asua, J.M.- **J. Polym. Sci., 35**, 2561 (1997).

[35] Schoonbrood, H.A.S.; Asua, J.M.- **Macromolecules, 30**, 6034 (1997).

[36] Polymer Handbook, 3rd Ed., J. Brandrup and E.H. Immergut, editors, John Wiley & Sons, New York 1989.

[37] Bengough, W.I.; Goldrich, D.; Young, R.A.- **Eur. Polym. J.** , **3**, 117 (1967).

[38] Minoura,Y.; Tadokoro, T.; Suzuki, Y.- **J. Polym. Sci.: Part A1, 5**, 2641 (1967).

[39] Urretabizkaia, A.; Asua, J.M.- **J. Polym. Sci.: Part A: Polym. Chem.** , **32**, 1761 (1994).

[40] Urushido, K.; Matsumoto A.; Oiwa, M.- **J. Polym. Sci., Polym. Chem., 19**, 59 (1981).

[41] Otsu T.; Toyoda, N.- **Makromol. Chem., Rapid Commun.**, **2**, 79 (1981).

THE PERFORMANCE OF ZINC MOLYBDENUM PHOSPHATE IN ANTICORROSIVE PAINTS BY ACCELERATED AND ELECTROCHEMICAL TESTS

ESTUDIO DEL COMPORTAMIENTO DEL MOLIBDOFOSFATO DE CINC EN PINTURAS ANTICORROSIVAS POR MEDIO DE ENSAYOS ACELERADOS Y ELECTROQUIMICOS

B. del Amo[1], R. Romagnoli[2], V.F. Vetere[3]

SUMMARY

Red lead and zinc chromates are doubtless efficient pigments to protect metals against corrosion. Their use in paints formulation is being restricted due to their deleterious action. Zinc phosphate was firstly suggested to replace toxic chromates. However, data on their anticorrosive properties are not conclusive; so, a second generation of phosphate pigments, including zinc molybdenum phosphate, was developed.

In this paper, the anticorrosive behavior of micronized zinc molybdenum phosphate in paints with 30% of the pigment by volume and a PVC/CPVC ratio 0.8, formulated with different binders (alkyd, vinyl, chlorinated rubber and epoxy resins), was assessed by accelerated (salt spray cabinet and accelerated weathering) and electrochemical tests.

Epoxy and chlorinated rubber paints showed the best anticorrosive performance. The inhibitive action of zinc molybdenum phosphate was confirmed. Good correlation has been obtained between salt spray and electrochemical tests.

Keywords: *ecological pigments; zinc molybdenum phosphate; alkyd, vinyl, chlorinated rubber and epoxy resins; anticorrosive paints; salt spray test; electrochemical assays.*

INTRODUCTION

Organic coatings are an effective mean to protect steel against corrosive environments. Usually, anticorrosive paints contain lead or hexavalent chromium compounds; these pigments are particularly hazardous and contribute to contaminate the environment. Coatings today, and in the future, need to meet stringent environmental health and safety rules. Although heavy metal-containing primers have performed admirably in the past, today their use is not recommended. Zinc phosphate became one of the leading substitute for carcinogenic zinc chromate pigments **[1-3]**.

---

[1] Miembro de la Carrera del Investigador del CONICET
[2] Miembro de la Carrera del Investigador del CONICET; Profesor Adjunto, UNLP
[3] Profesor Titular, UNLP, Jefe Area Estudios Electroquimicos Aplicados a Problemas de Corrosión y Anticorrosión

The protective action of zinc phosphate results from phosphatization of the metal substrate and the formation of complex substances with binder components **[1,2]**. More recent studies confirmed the presence of an oxyhydroxide film on the steel surface **[4-6]**. The protection mechanism would also imply the polarization of cathodic areas by the precipitation of sparingly soluble salts on the metal substrate **[6-8]**. The low solubility of zinc phosphate and the fact that this pigment is a coarse crystalline precipitate do not assist the growth of an effective anticorrosive film **[3, 9-12]**.

Accelerated tests of zinc phosphate pigmented coatings led to disappointing results whereas outdoor long exposure tests showed the good performance of these paints **[10, 13-22]**. Present investigations point out that the protective properties of zinc chromate cannot be achieved by zinc phosphate **[10, 13, 15, 23]** except for alkyd paints **[24]**. As a consequence a second generation of modified zinc phosphate-based pigments was developed **[10, 13-17]**.

Efforts to produce improved phosphate pigments were concentrated on the modification of the particle size and the pigment chemical composition. Smaller particle size results in optimum pigment packing. The chemical composition of the pigments was modified by adding molybdates, aluminium or by the use of surface organic pre-treatments.

Zinc molybdenum phosphate belongs to the so called second generation phosphate pigments; it is composed by zinc phosphate with zinc molybdate up to 1% (expressed as MoO_3) and is claimed to have equal or higher anticorrosive behavior than chromates and undoubtedly better than zinc phosphate alone **[25]**. The pigment active inhibitive species is molybdate anion which repassivates corrosion pits in steel **[26]**. However, little information is available in the literature about its anticorrosive performance. Adrian and Bittner **[3, 10, 13]** reported the behavior of zinc molybdenum phosphate in alkyd paints in comparison with zinc phosphate and zinc chromate. The employment of zinc molybdenum phosphate and other pigments belonging to the second generation phosphate pigments series in compliant primers was also tested **[13, 27]**.

The purpose of the present research is to study the anticorrosive properties of zinc molybdenum phosphate in solvent borne paints. Four binders were selected: alkyd, vinyl, chlorinated rubber and epoxy resins. Paints were formulated with a 30% pigment content by volume and a PVC/CPVC ratio 0.8. Their anticorrosive behavior was evaluated by accelerated and electrochemical tests. This paper continues previous research about zinc phosphate in paints formulated with different binders **[24, 28]**.

EXPERIMENTAL

Paints composition and manufacture

Binder. The film forming materials were the followings: a medium oil alkyd (50 % linseed and tung oils, 30 % o-phtalic anhydride, 8 % pentaerythritol and glycerol and 12 % pentaerythritol resinate), vinyl resin (91 % vinyl chloride, 3 % vinyl acetate, 5.7 % alcohols)/tricresyl phosphate (4/1 ratio by volume) **[29]**; chlorinated rubber 10 cP/chlorinated paraffin 42 % (70/30 ratio by volume) and bisphenol A epoxy resin/polyamide (1/1 ratio by volume).

Solvents. The solvents employed were: white spirit for alkyd paints; cellosolve acetate/methyl isobutyl ketone/xylene (70/ 10/ 20, % by weight) for vinyl resin; xylene/Solvesso 100 (4/1 ratio by weight) for chlorinated rubber paints and toluene/methyl isobutyl ketone/butyl alcohol (36/52/12, % by weight) for epoxy paints.

Pigment. Micronized zinc molybdenum phosphate was employed as anticorrosive pigment, with two different contents, 15 and 30 % by volume with respect to the total pigment content. Titanium dioxide, talc and barium sulfate were also incorporated to the formulation to complete the pigment formula. The PVC/CPVC relationship was 0.8. The composition of the tested paints is shown in Table I.

Table I

Solids in paint composition (% by volume)

Paints	1	2	3	4	5	6	7	8
Zinc molybdenum phosphate	5.8	11.6	5.8	11.6	5.8	11.6	5.8	11.6
Titanium dioxide	5.6	4.8	5.6	4.8	5.6	4.8	5.6	4.8
Talc	13.8	11.3	13.8	11.3	13.8	11.3	13.8	11.3
Barium sulfate	13.8	11.3	13.8	11.3	13.8	11.3	13.8	11.3
Epoxy resin/polyamide resin (1/1 ratio)	61.0	61.0	--	--	--	--	--	--
Chlorinated rubber/ chlorinated paraffin (70/30 ratio)	--	--	61.0	61.0	--	--	--	--
Vinyl resin/tricresyl phosphate (4/1 ratio)	--	--	--	--	61.0	61.0	--	--
Medium oil alkyd	--	--	--	--	--	--	61.0	61.0

NOTE: The solvent mixture employed for epoxy paints was toluene/ methyl isobutyl ketone/ butyl alcohol (36/52/12, % by weight); for chlorinated rubber paints was xylene/Solvesso 100 (4/1 ratio by weight); for vinyl resin was cellosolve acetate/methyl isobutyl ketone/xylene (70/10/20, % by weight) while white spirit was used for alkyd paints.

Paints manufacture and application. Paint manufacture was carried out employing a ball mill with a 3.3 liters jar. The pigments were dispersed in the vehicle for 24 hours to achieve an acceptable dispersion degree **[30]**.

The paints were applied by means of a spray gun on SAE 1010 steel panels (15.0x7.5x0.2 cm) up to a thickness of 75 $\pm$ 5 µm. SAE 1010 steel composition is as follows: C: 0.12%, Si: 0.01%, Mn: 0.35%, S: 0.02%, P: 0.02%. Tested panels were previously sandblasted to Sa 2 1/2 (SIS 05 59 00) attaining 20 $\pm$ 4 µm maximum roughness and degreased with toluene. A second series of panels was prepared by topcoating primed specimens with a dry film thickness of 40 $\pm$ 5 µm. The painted panels were kept in the laboratory for 7 days before testing.

Laboratory tests

Salt spray test (ASTM B 117). A scratch line was made through the coating with a sharp instrument so as to expose the underlying metal to the aggressive environment. After 650 and 1300 hours exposure, the panels were evaluated to establish the rusting degree (ASTM D 610) and to assess failure at the scribe (ASTM D 1654). In all cases experiences were carried out in triplicate, determining the mean value of the results obtained.

Accelerated weathering (ASTM G 26). The accelerated degradation of painted samples was carried out in an Atlas Weather-Ometer (Xenon arc type). The test program consisted of a 102 minutes light cycle followed by a 18 minutes light and water spray cycle. The overall time of each cycle was 2 hours and that of the complete test 720 hours. Test specimens were observed and evaluated for blister formation, degree of rusting and failure at the scribe marks, according to the above mentioned standard specification.

Corrosion potential measurements. The electrochemical cells were constructed by delimiting 3 cm^2 circular zones on the painted surface. An acrylic tube, with one flat end and 7 cm high, was then placed on the specimen and filled with the electrolyte (0.5 M sodium perchlorate solution). The measurements of the corrosion potential of the coated steel were made using a calomel electrode as reference and a high impedance voltmeter.

Resistance measurements. The resistance between the steel substrate and a platinum electrode was also measured employing the cells described previously and an ATI Orion, model 170 conductivity meter which operates at a 1000 Hz frequency. Similar measurements were performed on uncoated steel.

Polarization resistance measurements. The polarization resistance of painted specimens was determined as a function of immersion time employing an electrochemical cell with three electrodes. The reference electrode was a calomel one and the counterelectrode a platinum grid. The voltage swept was $\pm$ 10 mV, starting from the corrosion potential. Measurements were done employing an EG&G PAR Potentiostat/Galvanostat, Model 273A and the software SOFTCORR 352. Polarization resistance of uncoated steel was also monitored as a function of the immersion time.

RESULTS AND DISCUSSION

Salt spray test (ASTM B 117). The results obtained in the salt spray cabinet after 650 and 1300 hours of testing are shown in Tables II and III. None of the paints showed blistering during this test. The anticorrosive protection achieved with the epoxy resin was the most efficient for both pigment contents (Fig. 1 and 2). A similar behavior was observed for paints formulated with chlorinated rubber.

Topcoating of panels improved notably the anticorrosive behavior in such a way that all paint systems showed a good performance in this test after 1300 hours exposure (Fig. 3) and no corrosion spots were observed in the intercoat zone. After removing the anticorrosive paint only a slight uniform non aggressive corrosion products film was detected in the case of panels coated with vinyl and alkyd paints pigmented with 15% of zinc molybdenum

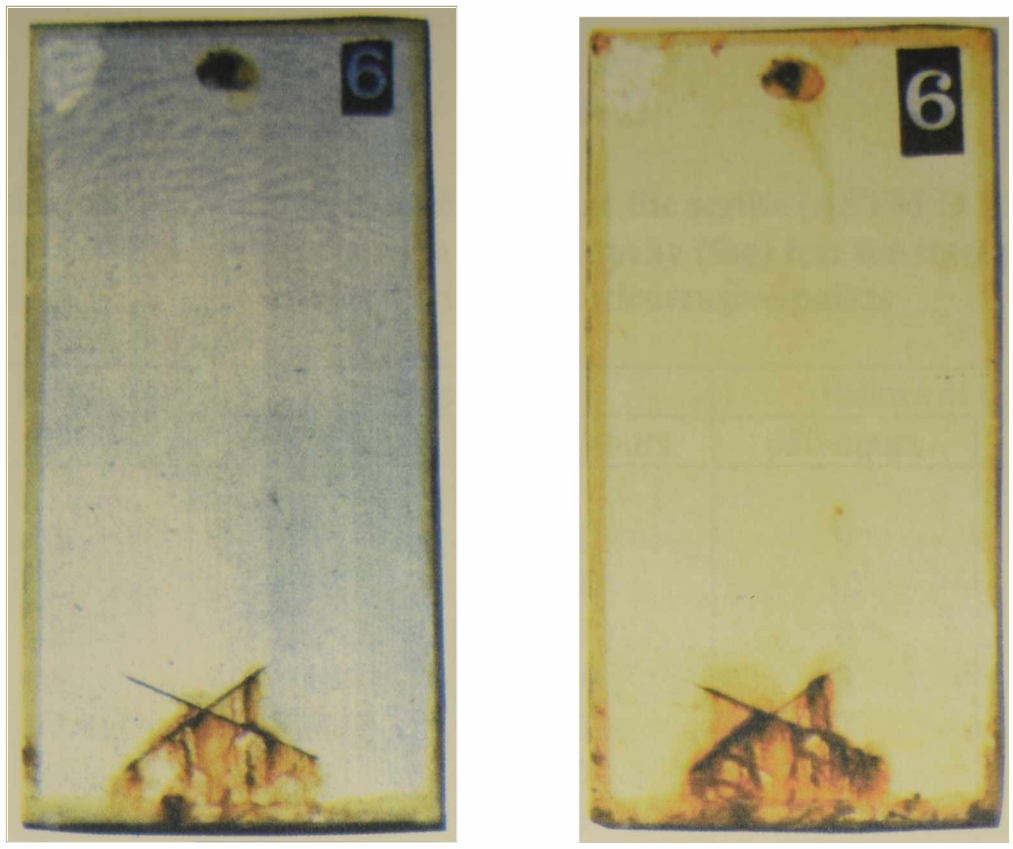

Fig.1.- Panels covered with the epoxy paint (30% zinc molybdenum phosphate) exposed for 650 (left) and 1300 (right) hours to the salt spray cabinet (ASTM B 117).

Fig.2.- Panel covered with the epoxy paint (15% zinc molybdenum phosphate) exposed for 1300 hours to the salt spray cabinet (ASTM B 117).

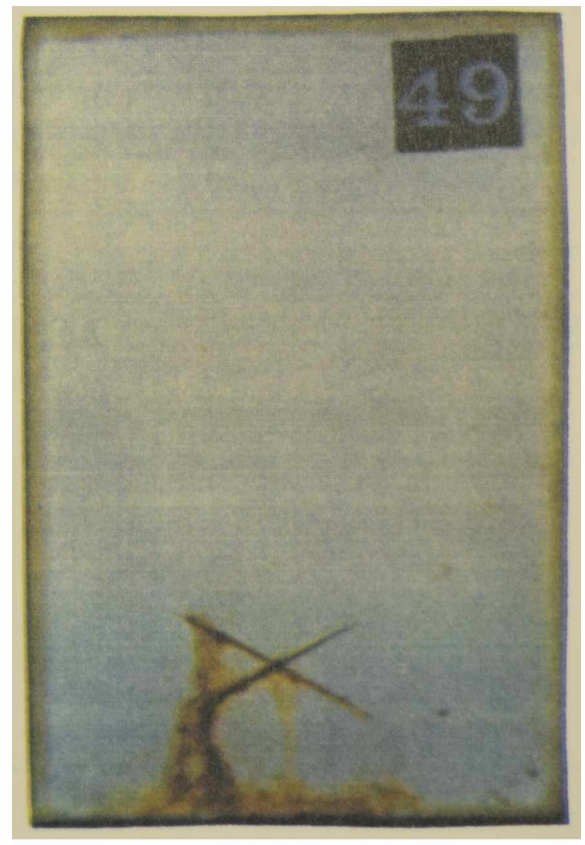

Fig. 3.- Panels covered with the vinyl paint (15% zinc molybdenum phosphate) and a topcoating, exposed during 1300 hours to the salt spray cabinet (ASTM B 117).

phosphate. Obviously, the improved behavior was due to the increased barrier effect obtained by topcoating the primed panels.

Table II

Rusting degree (ASTM D 610) and failure at the scribe (ASTM D 1654) after 650 and 1300 hours exposure in the salt spray (fog) test for steel panels covered with the anticorrosive paints

Paint	Rusting		Failure at the scribe	
	650 hours	1300 hours	650 hours	1300 hours
1	8	8	9	9
2	10	10	10	10
3	9	9	8	7
4	10	10	9	8
5	8	7	7	6
6	6	5	6	5
7	6	5	6	5
8	7	6	8	7

Table III

Rusting degree (ASTM D 610) and failure at the scribe (ASTM D 1654) after 650 and 1300 hours exposure in the salt spray (fog) test for steel panels covered with the anticorrosive paint plus a topcoat

Paint	Rusting		Failure at the scribe	
	650 hours	1300 hours	650 hours	1300 hours
1	10	10	10	10
2	10	10	10	10
3	9	9	9	9
4	10	10	10	10
5	9	8	9	7
6	10	10	8	8
7	8	6	7	6
8	9	7	6	5

In this test, the anticorrosive behavior of epoxy and chlorinated rubber paints pigmented with zinc molybdenum phosphate was notably improved with respect to similar paints formulated with zinc phosphate; to achieve a similar performance the latter paints needed a topcoat (40 μm thickness). In the case of chlorinated rubber, in spite of being topcoated, 0.03% of the metallic surface showed signs of corrosion **[31]**.

Vinyl paints containing zinc molybdenum phosphate showed an extended life with respect to those containing zinc phosphate. Both types of paints obtained the same qualification but the former after a 650 exposure period and the latter after 400 hours **[32]**. A similar feature was noticed with the alkyd binder **[31]**.

If comparison is made with respect to paints formulated with zinc chromate and the less resistant resins (vinyl and alkyd), it must be pointed out that paints with vinyl resin failed in this test after 96 hours exposure developing pits on the painted surface **[32]** and substitution by zinc molybdenum phosphate resulted clearly advantageous. Non significant differences in the anticorrosive performance were observed between alkyd paints pigmented either with zinc chromate or with zinc molybdenum phosphate **[24]**.

Undercutting rusting was similar for paints containing zinc phosphate and for paints pigmented with zinc molybdenum phosphate; however results obtained with phosphate pigments and alkyd binder are notably improved with respect to zinc chromate **[24, 32]**.

Accelerated Weathering (ASTM G 26). All paints exhibited a good behavior after 720 hours exposure. No blister or significant signs of corrosion were observed on the surface of the painted panel. Again, topcoating of panels covered with anticorrosive paints enhanced barrier properties of the system improving the behavior of vinyl and alkyd systems (Table IV). It may be expected that these paint systems would perform acceptably in outdoor exposures for at least two years without showing signs of corrosion because 700 hours of accelerated weathering are approximately equivalent to 2 years outdoor exposure **[33]**.

Table IV

Rusting degree (ASTM D 610) and failure at the scribe (ASTM D 1654) after 360 and 720 hours exposure in the Weather-Ometer for steel panels covered with the anticorrosive paints plus a topcoat

Paint	Rusting		Failure at the scribe	
	360 hours	720 hours	360 hours	720 hours
1	10	10	10	10
2	10	10	10	10
3	10	10	10	10
4	10	10	10	10
5	10	9	10	9
6	10	10	10	10
7	10	8	10	8
8	10	9	10	9

NOTE: None of the samples presented blistering.

Corrosion potential measurements (Fig. 4). The corrosion potential of panels coated with paints formulated with chlorinated rubber and epoxy resins shifted towards more positive values as time elapsed to finally decay slightly after 25 and 50 days of immersion, respectively.

For chlorinated rubber paints, the corrosion potential rised again after 40 days of immersion due to the sealing of the small pores of the paint film by corrosion products as it was observed by a visual inspection. Pigment-binder interaction could also be responsible for the shifting of the corrosion potential during the test period in epoxy paints; but this requires a deeper study. Accordingly, both paints showed the best anticorrosive performance in the salt spray test, so corrosion potential measurements support the results obtained in this test.

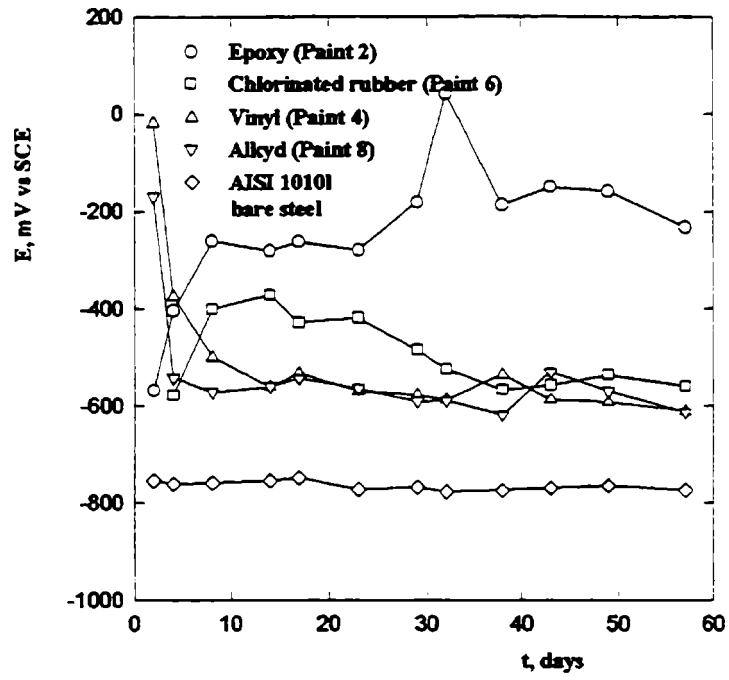

Fig. 4.- Corrosion potential of painted steel panels as a function of the exposure time in 0.5 M sodium perchlorate solution.

The corrosion potential of panels covered with paints formulated with alkyd and vinyl resins shifted towards more positive values with respect to the corrosion potential of bare steel in 0.5 M sodium perchlorate solution during the first 24 hours of immersion. After one day, the corrosion potential derived quickly towards more negative values because of the increasing number of conductive paths through the paint film and the concomitant incoming of the electrolyte solution (Fig.5); after a few days these paints attained the final value which was displaced, at least, +150 mV with respect to the corrosion potential of bare steel.

The corrosion potential of painted steel changed as the corroded area increased but it never matched the corrosion potential of bare steel because a fractional area of the test specimen remained undamaged, free from blisters and corrosion spots (99 % for chlorinated rubber paint, 100 % for epoxy, 94 % for vinyl and 40 % for alkyd paints) at the end of the test part of the attacked area is passivated as it would be seen later.

In every case, the shifting of the corrosion potential to more noble values is due to the low film permeability and to the presence of zinc molybdate in the paint film **[34, 35]**. Mo(VI) compounds constitute the passive layer together with phosphates **[36]**. Ambrose **[26]** found that molybdenum compounds are effective in increasing the repasivation rate in crevices and pits.

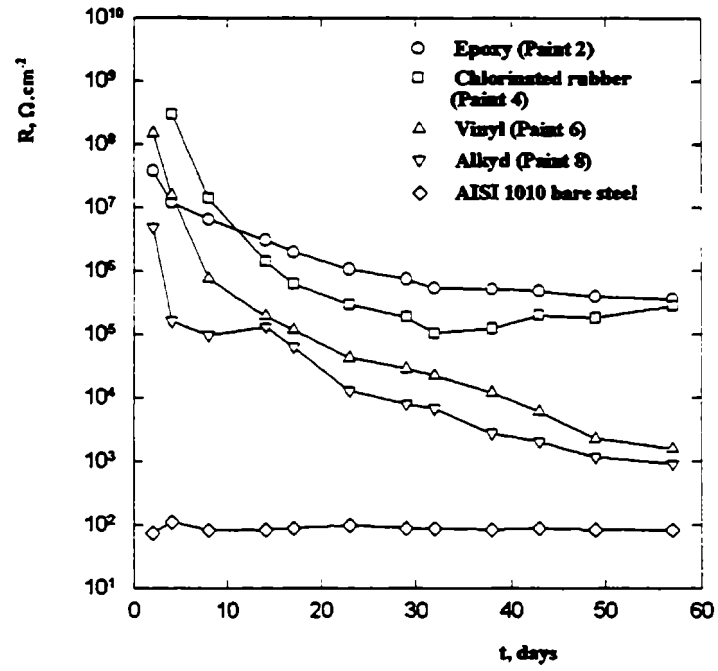

Fig. 5.- Resistance of painted steel as a function of the exposure time in 0.5 M sodium perchlorate solution.

A diminishing of the zinc molybdenum phosphate content to 15 % impaired the anticorrosive protection since the corrosion potential shifted towards more negative values with the immersion time; however, epoxy paints still showed good anticorrosive performance. No significant changes were detected among panels covered with paints formulated with alkyd and vinyl resins which, anyway, rapidly acquired the final corrosion potential. For the sake of simplicity, only paints formulated with a 30 % of the pigment were plotted.

Resistance measurements (Fig. 5). The measured resistance is composed of two contributions: the solution resistance and the paint film resistance. As the solution resistance is low (84 Ω) the paint film resistance is responsible of the measured values. Polarization effects may be neglected at the measuring frequency employed in this test. The initial values for the ionic resistance decreased as follows:

$$R_{\text{paint 3 and 4}} > R_{\text{paint 6}} > R_{\text{paint 5}} > R_{\text{paint 2}} > R_{\text{paint 7 and 8}} > R_{\text{paint 1}}$$

and the final values decreased according to:

$$R_{\text{paint 3 and 4}} = R_{\text{paint 2}} > R_{\text{paint 1}} > R_{\text{paint 6}} = R_{\text{paint 5}} > R_{\text{paint 7 and 8}}$$

The initial values of the ionic resistance are of crucial importance because they are employed to predict the useful life of the coating. All paints originated films with an initial ionic resistance high enough ($>10^6$ $\Omega.cm^{-2}$) to protect steel by a barrier effect, however, full protection is achieved when the ionic resistance exceeds 10^8 $\Omega.cm^{-2}$ **[37, 38]**. In this sense, vinyl and chlorinated rubber paints exhibited the highest initial barrier effect. However, as time went on, chlorinated rubber and epoxy coatings proved to be the most resistant ones to water

and ion penetration and this fact ensured and excellent performance of both paints during the immersion period.

Although chlorinated rubber paint showed the highest ionic resistance values at the beginning of the test, it also denoted a higher tendency to produce pinholes with respect to epoxy paints. Pore sealing by corrosion products in chlorinated rubber paints, after 32 days of immersion, is noticed by the slight increment of the ionic resistance at the end of the immersion period. Epoxy paints did not show spots of iron oxides neither on the paint film nor under it during the test period, the ionic resistance decreased slowly as time elapsed.

Vinyl and alkyd paints showed abrupt changes in the ionic resistance during the first days of immersion resulting in an increasing permeability to the electrolyte solution through macropores which reach the base metal. It was demonstrated that the electrolyte located inside the polymer net does not affect the conduction through coating **[39]**. When the ionic resistance fell in the 10^4-10^5 range, the corrosion potential reached its final average value and it coincided with total electrolyte penetration through the coating and, eventually, blister formation, as stated by Szauer **[38]**.

When the pigment content was lowered from 30 to 15% the initial ionic resistance decreased, as an average, by two orders of magnitude; this means that in the case of vinyl and alkyd paints the initial barrier effect is lost and in the other cases diminished.

Polarization resistance measurements (Fig. 6). Polarization resistance, as measured in this research, is not a true one because it includes the ionic resistance. However, in all cases it is higher than the ionic resistance, this fact reveals that the tested pigment has inhibitive properties **[38]** which is in agreement with previous results where zinc phosphate (the main component of the so called zinc molybdenum phosphate) reduced the corrosion rate of iron **[6]**. The inhibitive action of the pigment is due to the precipitation of a ferric phosphate layer on the metal surface. Phosphate adheres partially to the metal surface and loose ferric phosphate plugging paint film pores. Ferrous phosphate may be formed as a previous stage and iron oxides precipitated on the metal surface too **[40]**. Visual inspection of exposed panel showed that ferric oxide spots were partially converted in more stable ferric phosphate. It was demonstrated that molybdenum compounds increase the polarization resistance of steel and improved the corrosion resistant of the substrate still in the presence of chlorides **[34]**. The addition of molybdenum hexavalent anions decreases the critical current density for passivation and increases the stability of passive films. The presence of silicon in the steel employed in this research may contribute to enhance the effect of molybdenum **[41]**.

Panels painted with chlorinated rubber and epoxy paints showed the highest polarization resistance values and vinyl and alkyd paints showed an important decrease of this magnitude with the immersion time. As a general rule, changes in polarization resistance are correlated with changes in the ionic resistance.

Alkyd paints polarization resistance may be ten times higher than the electrolyte resistance (84 Ω) and this may be attributed not only to the inhibitive action of the pigment but also to the high reactivity of this pigment with the alkyd resin; the inhibition of corrosion of steel by soap formation was known from early times **[1, 2, 42, 43]**. As a consequence, it presented less ferric oxide spots than it could be expected from the low electrolyte resistance

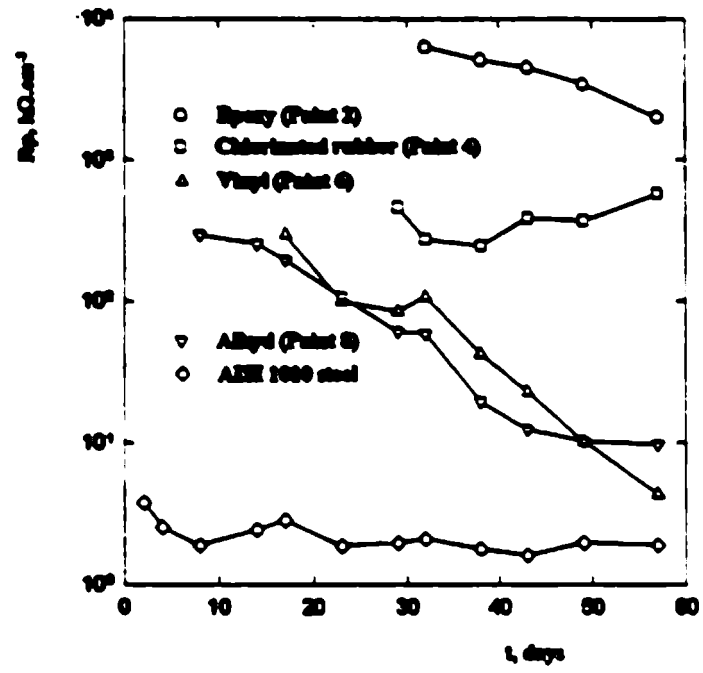

Fig. 6.- Polarization resistance of painted steel panels as a function of the exposure time in 0.5 M sodium perchlorate solution.

values registered during the test. However, it formed some blisters; under which the metal surface remained free from oxides.

Visual examination of painted panels revealed that ferric oxide spots were partially converted into non adherent non expansible ferric phosphate by the action of the pigment.

CONCLUSIONS

1. Paints formulated with epoxy and chlorinated rubber resins still showed a good anticorrosive performance with a zinc molybdenum phosphate content as low as 15% by volume with respect to the total amount of pigments. However, a 30% content is recommendable to obtain the best performance of each type of binder.

2. The higher values of the polarization resistance with respect to the ionic one show that zinc molybdenum phosphate has inhibitive properties against corrosion.

3. In general, due to the efficiency of the total scheme applied on steel, all samples showed a good behavior in the Weather-Ometer test after 720 hours of exposition.

4. Good correlation was found between salt spray test and electrochemical tests. A relationship was noticed among corrosion potential, ionic resistance and polarization resistance but this aspect deserves a further research.

AGKNOWLEDGEMENTS

The authors are grateful to CONICET (Consejo Nacional de Investigaciones Científicas y Técnicas) and CIC (Comisión de Investigaciones Científicas de la Provincia de Buenos Aires) for their sponsorship to do this research and to Colores Hispania for providing the anticorrosive pigment.

REFERENCES

[1] Meyer, G.- **Farbe+Lack, 69(7)**, 528 (1963).
[2] Meyer, G.- **Farbe+Lack, 71(2)**, 113 (1965).
[3] Adrian, G.; Gerhard, A.; Bittner, A.; Gawol, M.- **European Supplement to Polymer Paint Colour Journal**, 62 (1981).
[4] Leidheiser (Jr.), L.H.- **J. Coat. Tech., 53(678)**, 29 (1981).
[5] Kozlowski, W.; Flis, J.- Corr. Sci., **32(8)**, 861 (1991).
[6] Romagnoli, R.; Vetere, V.F.- **Corrosion** (NACE), **51(2)**, 16 (1995).
[7] Clay, M.F.; Cox, J.H.- **J. Oil Colour Chem. Assoc., 56**, 13 (1973).
[8] Szklarska-Smialowska, Z.; Mankowsky, J.- **Br. Corros. J., 4(9)**, 271 (1969).
[9] Burkill, J.A.; Mayne, J.E.O.- **J. Oil Colour Chem. Assoc., 71(9)**, 273 (1988).
[10] Gerhard, A.; Bittner, A.- **J. Coat. Tech., 58(740)**, 59 (1986).
[11] Kresse, P.- **Farbe+Lack, 80(2)**, 85 (1977).
[12] Pfizer Pigments, Inc., Zinc Phosphate. Technical Specification (1988).
[13] Bittner, A.- **J. Coat.Tech., 61(777)**, 111 (1989).
[14] Pietsch, S.- **Plaste Kautschuk, 36(7)**, 246 (1989).
[15] Kukla, J.; Tyrka, E.; Polen, S.- Hydrokorr-Organokorr'86 Seminar 42 (1986).
[16] Hare, C.H.- **J. Protect. Coat. & Linings, 7(10)**, 61 (1990).
[17] Chromy, L.; Kaminska, E.- **Prog. Org. Coat., 18(4)**, 319 (1990).
[18] Barraclough, J.; Harrison, J.B.- **J. Oil Col. Chem. Assoc., 48(4)**, 341 (1965).
[19] Fragata, F. de L.; Dopico, J.- **J. Oil Col. Chem. Assoc., 74**, 3 (1991).
[20] Rendu, M.- **Paint, Oil and Colour J., Set. 25**, 477 (1970).
[21] Goma, A. Z.; Gad, H. A.- **J. Oil Col. Chem. Assoc., 70(2)**, 50 (1988).
[22] Williams-Wynn, D. E. A.- **J. Oil Colour Chem. Assoc., 60**, 263 (1977).
[23] Depireux, J.; Piens, M.- 18th FATIPEC Congress, vol. **3,** 183 (1987).
[24] del Amo,B.; Romagnoli, R.; Vetere, V.F.- **Corrosion Reviews, 14(1-2)**, 121 (1996).
[25] H. Heubach GmbH. HEUCOPHOS. Three Generations nontoxic anticorrosive pigments.
[26] Ambrose, J.R.- **Corrosion** (NACE), **34(1)**, 27 (1978).
[27] Kopecny, F.; Sranck, Z.- FATIPEC Congress, pp **III**-61-66, Budapest, 15-19th May 1994.
[28] del Amo, B.; Romagnoli, R.; Vetere, V.F.- Libro de Resúmenes del XII Congreso Iberoamericano de Electroquímica (SIBAE), pp 408-409, Mérida, Venezuela, 24-29 de marzo de 1996.
[29] Caprari, J.J.; del Amo, B.; Giúdice, C.A.; Ingeniero, R.D.- **Corrosión y Protección, 9(9-10)**, 35 (1987).
[30] Giúdice, C.A.; Benítez, J.C.; Rascio, V.- **J.Oil Col. Chem Assoc., 62(3)**, 151 (1980).
[31] Koopmans, A.- XIV FATIPEC Congress, Congress Book, 321-328 (1978).
[32] del Amo, B.; Romagnoli, R.; Vetere, V.F.- Accepted for publication in Progress in Organic Coatings.

[33] Rascio, V.J.D.; Caprari, J.J.; del Amo, B.; Ingeniero, R.- **J.Oil Col. Chem Assoc., 62(12)**, 475 (1979).
[34] Roberge, P.R.; Sastri, V.S.- **Br. Corros.J., 29(1)**, 38 (1994).
[35] Garnaud, M.H.L.- **Polymer Paint Colour J., 18(4)**, 268 (1984).
[36] Guenbour, A.; Faunchen, J.; Ben Bachir, A.- **Corrosion** (NACE), **44(4)**, 214 (1988).
[37] Elsner, C.I.; Di Sarli, A.R.- **J. of the Brazilian Chemical Society, 5(1)**, 15 (1994).
[38] Szauer, T.- **Prog. Org. Coatings**, **10**, 157 (1982).
[39] Miskovic-Stankovic, V.B.; Drazic, D.M.; Teodorovic, M.J.- **Corrosion Science**, **37(2)**, 241 (1995).
[40] Lezna, R.O.; Borrás, C.; Romagnoli, R.- Research in progress.
[41] Lizlous, E.A.- **Corrosion** (NACE), **22(11)**, 297 (1966).
[42] Mayne, J.E.O.- **Br. Corros. J., 5(5)**, 106 (1970).
[43] Romagnoli, R.; Vetere, V.F.- **Corrosion Reviews, 13(1)** 45 (1995).

FORMULATION AND TESTING OF A WATER-BORNE PRIMER CONTAINING CHESTNUT TANNIN

FOMULACION Y EVALUACION DE UN PRETRATAMIENTO DE BASE ACUOSA CONTENIENDO TANINO DE CASTAÑO

O.R. Pardini, J.I. Amalvy[1], R. Romagnoli[2], V. F. Vetere[3]

SUMMARY

In this work an aqueous primer containing chestnut tannin and phosphoric acid was developed and its anticorrosive properties assessed by different conventional tests. Treated steel panels coated with an anticorrosive paint and a topcoat were subjected to the salt spray test, humidity chamber, mechanical tests (adhesion and flexibility) and electrochemical tests (corrosion potential, ionic resistance and polarization resistance). Electrochemical tests were done employing only panels primed with the primer. The binder employed in this research was prepared in the laboratory by emulsion polymerization of acrylic monomers.

It was found that the tested formulation protected steel against corrosion incorporating corrosion products to the film as ferric tannates and avoiding oxide formation. Undercutting rusting was not significant and the scratch line stood free from oxides. The good stability of the binder in low pH media and the interaction of the binder with the substrate are decisive factors in the performance of this aqueous pretreatment system.

Keywords: *corrosion protection, water-based pretreatment, acrylic emulsion, phosphoric acid, tannin.*

INTRODUCTION

Wash primers designed to protect steel structures against corrosion normally contain chromates, which, because of their toxicity, constitute a hazard that needs to be replaced by more environmentally acceptable corrosion inhibitors. In this sense tannins, a class of natural, non-toxic, biodegradable organic compound, is being proposed as an alternative in primer paint systems.

Tannins as corrosion inhibitors are applied both in solvent and in waterborne paints. Tannin based paints could be applied on partially rusted substrates, reducing in this way the effort needed for cleaning the surface by sandblasting or other methods. They have been

[1] Miembro de la Carrera del Investigador de la CIC
[2] Miembro de la Carrera del Investigador del CONICET; Profesor Adjunto, UNLP
[3] Profesor Titular, UNLP, Jefe Area Estudios Electroquímicos Aplicados a Problemas de Corrosión y Anticorrosión

referred, sometimes, as rust stabilizers modifying the active rust into an unreactive protective compound.

Solvent-based primer formulations were developed and tested employing electrochemical techniques. The total amount of iron dissolved in this case was compared with a blank consisting of steel covered either with a varnish film or with a paint system (anticorrosive paint plus a topcoat). Rusting, blistering and adhesion were also assessed over time. It was shown that paint adhesion and anticorrosive properties of the tested paints were improved when they were applied in combination with pretreatment formulations containing tannins. These pretreatments reduce steel corrosion rate by a factor of three with respect to conventional ones and may be used on clean or slightly rusted surfaces of variable roughness [1-3]. However, their behavior not only depends on their composition but also on the properties of the whole paint system. Results showed that tannins could not be employed alone when subjected to different tests **[1-5]**.

The reaction mechanism of tannins added to priming paints for steel protection is not well understood and their efficiency questioned by some authors **[4, 6-9]**. Tannins are polyphenols of vegetal origin and the vicinity of hydroxyl groups on the aromatic rings makes them able to form chelates with iron. Ferric tannates of dark blue color are highly insoluble and act as electric insulators between cathodic and anodic sites on the metal surface **[4, 5, 8-13].** The influence of phosphoric acid on the performance of these systems, has also been studied **[14, 15].**

Scarce information concerning the preparation and performance of aqueous pretreatment systems containing tannins was found in the literature **[3, 16, 17]** although formulations without incorporating a resin have been developed **[18].** It is the aim of this research to formulate a water based anticorrosive primer and to study its anticorrosive performance through mechanical, chemical and electrochemical assays. The synthesis of the binder was carried out in the laboratory in order to achieve a product with well-defined parameters and compatible with the characteristic acidity of this type of products.

EXPERIMENTAL

Pretreatment system formulation and application

Binder. The film forming material was an all acrylic emulsion prepared in the laboratory by semicontinuous emulsion polymerization. Analytical grade monomers (Fluka Chemika) were used as received. Methyl methacrylate (MMA) contained 25 ppm of hydroquinone. Ethylene glycol dimethacrylate (EGDMA), ethyl acrylate (EA) and methacrylic acid (MAA) contained hydroquinone monomethyl ether, 50, 100 and 200 ppm, respectively. The emulsifier, sodium lauryl sulfate (SLS), and the initiator, potassium persulfate (KPS), were of analytical grade and used without further purification. Distilled water (DW) was used throughout the synthesis of binder.

Polymerizations were carried out using a two-piece reactor composed of a conical-based glass vessel (capacity 1.30 dm^3, with a thermostatic jacket and sampling utility) and a five-necked cap. The cup was fitted with a reflux condenser, a stirrer (Teflon two-blade

propeller type), an inlet for inert gas (nitrogen), a thermocouple and an inlet for the pump. The agitation speed was about 200 rpm. The list of latex components is given in Table I.

Table I

Raw materials employed in latex synthesis

Reagents	Initial load (g)	Feed (g)
Ethyl acrylate	220.00	---
Methyl methacrylate	75.65	144.35
Ethylene glycol dimethacrylate	0.29	0.15
Methacrylic acid	---	8.80
Potassium persulfate	2.74	---
Sodium lauryl sulfate	2.96	1.53
Distilled water	355.65	53.15

The procedure for emulsion polymerization was as follows: the initial SLS was added to the water in the reactor followed by all the EA (the less reactive monomer) and a fraction of the MMA and EGMA (Table I), with stirring. Nitrogen was passed through the emulsion during 30 minutes while heating up to 60 °C. The initiator was dissolved in 30 mL of DW, preheated and then poured into the reactor chamber. The emulsion was allowed to react for ca. 15 min, during which *in situ* seed particles were formed; then the feed was started at ca. 2 g of emulsion per minute. The flow rate of emulsion was adequately adjusted to add the MAA in the last part of reaction. An emulsification apparatus was used to prepare the monomer emulsion by stirring at 1500 rpm. The emulsion was then placed in a dropping funnel and deaerated for 30 minutes.

After monomer addition the temperature was maintained at 80 °C for ca. 120 min to complete polymerization. The latex solid content was measured gravimetrically by taking a few grams sample from the reactor and drying it under reduced pressure at 50 °C.

Particle size was estimated by spectroturbidimetry **[19]**, and the glass transition temperature (T_g) was calculated using the Fox's equation. Surface tension was measured by means of the Du Noüy tensiometer (Table II). More experimental details on binder characterization are given in a previous paper **[20]**.

Table II

Latex Parameters

PARAMETER	
Solids content	47 %
Mean particle diameter	144 nm
pH	2.0
Density	1.08 g cm^{-3}
Surface Tension	31 mN m^{-1}
Glass Transition Temperature (T_g)	35 °C

Tannin. Chestnut tannin was selected for being more reactive than mimosa and quebracho tannins; as demonstrated in a previous research it exhibits the highest reaction rate with steel **[5].**

Primer manufacture. Typical preparation is as follows: 10 mL of a phosphoric acid solution (30% by weight) was added to a 6 g suspension of chestnut tannin in 40 mL of distilled water and treated according to a process to be patented to enhance its adhesive strength on steel **[21]**. The treated tannin was filtered off to eliminate insoluble matter and mixed with a 40% aqueous solution of the resin prepared as described above plus 2 mL of Texanol® and a flash rusting inhibitor **[21]**. The system was allowed to stand during 24 hours and filtered off again if necessary.

Application. The wash primer was brush applied on SAE 1010 steel panels (15.0x7.5x0.2 cm), previously degreased with toluene, up to a dry film thickness of 10 ± 2 µm. Test panels had a low surface roughness (average roughness 0.78 µm and a valley to peak distance of 4.96 µm) and a slight oxidation. This low surface roughness was selected to perform the tests in a disadvantageous condition with respect to the adherence of the first coat. Surface roughness was measured employing a Hommel tester Model T1000 magnetic device. Treated panels were kept in the laboratory atmosphere (RH $65 \pm 5\%$ and 20 ± 2°C) during 7 days. Then panels were covered with different paint systems as it can be seen in Table III. The anticorrosive paint was formulated with a medium solvent borne alkyd binder and contained zinc molybdenum phosphate; its anticorrosive performance was assessed in a previous research **[22]**. The topcoat was also an alkyd paint containing 20 % of resin (the same employed for the anticorrosive paint), 20 % of titanium dioxide and 60 % of solvent (white spirit). The solvent-borne coats were employed to make the painting scheme resistant to the salt fog test.

Table III

Tested paint systems

System	Tannin pretreatment	Anticorrosive paint	Topcoat
1	yes	---	60 µm
2	yes	60 µm	---
3	yes	30 µm	30 µm
4	---	35 µm	35 µm

NOTES: In all cases wash primer film thickness was 10 ± 2 µm. Anticorrosive paint was an alkyd pigmented with zinc molybdenum phosphate (30% by volume) and with a PVC/CPVC ratio equal to 0.8. Topcoat was alkyd paint pigmented with titanium oxide.

Laboratory tests

Accelerated tests, salt spray and humidity cabinet, were carried out to evaluate corrosion and water resistance of painted panels. Mechanical assays, such as flexibility and adhesion, were performed and it was expected that adhesion measurements could give an insight of metal-primer interaction. Finally, the anticorrosive behavior was monitored by direct current (d.c.) electrochemical measurements.

Salt spray test (ASTM B 117). A scratch line was made through the coating with a

sharp instrument so as to expose the underlying metal to the aggressive environment. After a 400 hours exposure, the panels were evaluated to establish the rusting degree (ASTM D 610) and failure at the scribe (ASTM D 1654). In all cases the experiences were carried out in triplicate, determining the mean value of the results obtained in the test. After visual examination, alkyd paints were removed by means of a hot 5 % sodium hydroxide solution (65°C ± 5 °C) to observe the film with a Nikkon binocular stereoscopic magnifier.

A set of primed panels was left under laboratory conditions during two years.

Humidity cabinet test (ASTM D 2247). Panels were exposed at 38 ± 1°C during 250 hours and the degree of blistering was evaluated according to the ASTM D 714-87 standard specification. Afterwards, as it was done in the case of the salt spray test, alkyd paints were removed and the remaining film was subjected to microscopic examination.

Flexibility (ASTM D 3111). The 3 mm mandrel was chosen to perform this test in the more disadvantageous condition.

Adhesion (ASTM D 4541). Adhesion measurements were carried out on treated panels and on panels covered with the paint systems mentioned in Table III.

Electrochemical tests on treated steel panels. The cells to measure the corrosion potential across the paint film-steel substrate interface with respect to the calomel electrode, were constructed by delimiting 3 cm^2 circular zones on the painted surface by means of a cylindrical open acrylic tube, with one flat end. The measurements were done employing a high impedance voltmeter.

The ionic resistance between the steel substrate and a platinum electrode was also measured employing the cells previously described and an ATI Orion, model 170, conductivity meter that operates at a 1000 Hz frequency. Similar measurements were performed on uncoated steel.

The polarization resistance of the painted specimens was determined as a function of time employing a similar cell but with three electrodes. Calomel was the reference electrode and the counterelectrode was a platinum grid. The voltage scan was ± 20 mV, starting from the corrosion potential and compensating the ohmic contribution. Measurements were done with an EG&G PAR Potentiostat/Galvanostat, Model 273A and the software SOFTCORR 352.

In every case, a 0.5 M sodium perchlorate solution was employed as supporting electrolyte and the time measurement was one week.

RESULTS AND DISCUSSION

Binder. The acid binder employed in this research had 47.7% of solids and average particle diameter of 144 nm. The complete set of latex parameters are presented in Table II. As stated above the binder has a good colloidal stability at low pH, due to a combined stabilization

mechanism of the sulfate from surfactant and the carboxylic groups from methacrylic acid.

Primer manufacture and application. Tannin is made more reactive towards steel by allowing it to combine with phosphoric acid through a chemical reaction yielding a product that resulted more acidic than phosphoric acid itself. The acid constant of this product was determined by potentiometric measurements according to a well-known analytical procedure **[23]** and it was found to be equal to $4.0x10^{-2}$ while the first acidic constant for phosphoric acid is $7.0x10^{-3}$.

Once the primer was applied on steel, the surface turned quickly to a black color because of the formation of an association compound known as "iron tannate". The tannate, is actually formed by chelation of ferric cations coming from oxide or from steel dissolution as a consequence of the pretreatment acidity. On this black iron tannate-acrylic resin film different systems were applied (Table III) to conduct accelerated tests and the adherence one.

Salt spray test (ASTM B 117). The pretreatment film applied on steel, without topcoating cannot be tested because it was destroyed after one-day exposure. Regardless of the zones adjacent to the scratch line, the paint systems numbered 1, 3 and 4 in Table III, showed an acceptable behavior during this test, according to ASTM D 610. On the other hand the system number 2 exhibited bad anticorrosive performance due to the high porosity of the anticorrosive paint (PVC/CPVC 0.8) and failed at the end of a 250 hours exposure period (Table IV).

Table IV

Evaluation of failures in the tested panels

System	Rusting degree in the salt fog chamber (ASTM D 610-85)	Failure at the scribe (ASTM D 1654-92)	Blistering in the humidity chamber (ASTM D 714-87)
1	8	7	8M*
2	3	5	8M*
3	9	9	6MD*
4	9	8	8F*

* M: medium, MD: medium dense, F: few

Microscopic examination after removing the alkyd paints (3.3X) revealed that the pretreatment film remained undamaged in the coated panel that corresponds to system 3 (Fig. 1). Some cracks were formed, in certain regions in its surface, probably, during the film redrying process after performing the test; however, no corrosion signs on the base metal were observed at the bottom of the cracks. The absence either of anticorrosive paint (system 1) or topcoat (system 2) led to a partial destruction of the primer and underfilm oxide growth (Fig. 2). Although panels coated with the anticorrosive paint and the topcoat primer (system 4) showed a good finishing after this test, the removal of the paint revealed the presence of red iron oxide spots on the substrate.

Fig. 1. Aspect of the ferric tannate film after 400 hours exposure in the salt spray test of a treated panel covered with an anticorrosive paint plus a topcoat (system 3, Table III).

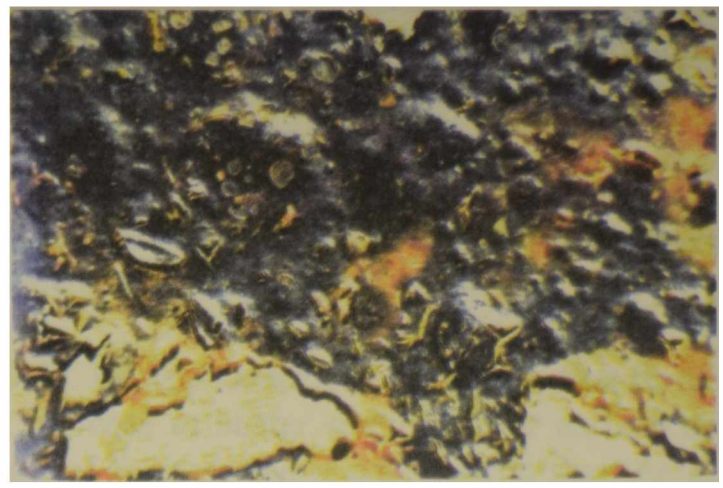

Fig. 2. - Aspect of the ferric tannate film after 400 hours exposure in the salt spray test of a treated panel covered with an anticorrosive paint without a topcoat (system 2, Table III).

Fig. 3. – Aspect of the ferric tannate film at the scratch line after 400 hours exposure in the salt spray test of a treated panel covered with an anticorrosive paint plus a topcoat (system 3, Table III).

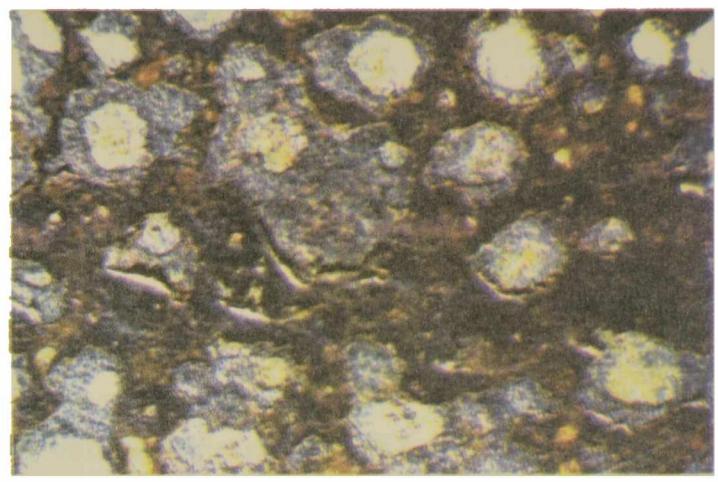

Fig. 4. - Aspect of the ferric tannate film after 250 hours exposure in the humidity chamber of a treated panel covered with an anticorrosive paint without a topcoat (system 2, Table III).

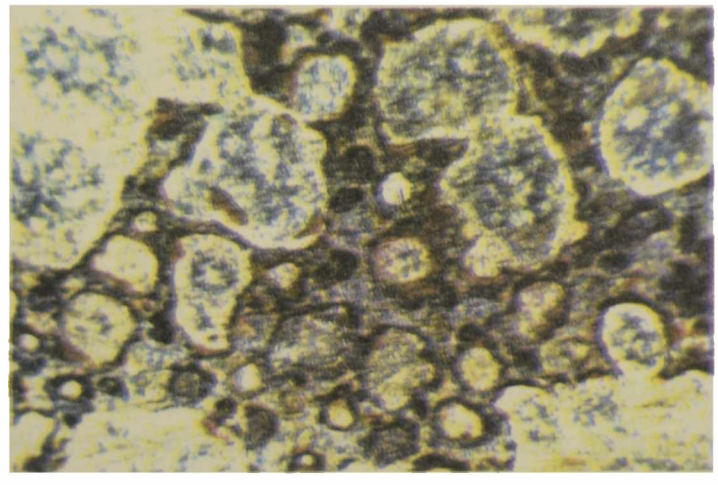

Fig. 5. - Aspect of the steel surface after 250 hours exposure in the humidity chamber of a panel covered with an anticorrosive paint plus a topcoat (system 4, Table III).

Treated panels (systems 1, 2 and 3) developed blisters in the zone adjacent to the scratch mark due to the loss of adherence between the pretreatment and the alkyd paint. Despite the corrosion process being more intense in this zone, not much oxide was observed in the scratch line because it was incorporated into the pretreatment film, which color turned from black to red (Fig. 3). Failure at the scribe was diminished by the presence of the tannin primer film (Table IV).

These results confirmed the well-known fact that tannin can be only employed in complete paint systems when subjected to severe exposures **[4, 9].**

Humidity cabinet test (ASTM D 2247). Blisters developed during the first three days of exposure. After this period no significant increase in blister size or blister surface density was observed. Blisters were broken at the end of the test and it was noticed that the loss of adherence had taken place firstly at the wash primer anticorrosive paint interface and then at the steel-wash primer film interface. No corrosion products were observed in the delaminated areas in the case of system 3. The absence of either anticorrosive paint (system 1) or topcoat (system 2) led to film destruction and oxide growth, as can be seen in Fig. 4, that corresponds to paint system 2. Pretreatment film absence also led to oxide development (Fig. 5). Table IV shows the results of different tests for the four paint systems.

Flexibility by mandrel bend test method (ASTM D 3111). The primer film containing tannin behaved satisfactorily in this test and no cracks were observed within the film after bending.

Adhesion (ASTM D 4541-89). The adhesion values obtained for panels covered with the primer alone are relatively high. After performing this test it was observed that some ferric tannate remained firmly adhered on the steel surface, pointing out that metal-pretreatment film interaction is responsible for the high adhesion values encountered. The values obtained in this test are lower in the case of complete paint systems recorded in Table V (systems 2-4) and it was noticed that film rupture was principally of the cohesive type in the alkyd paint, remaining a thin white film from the anticorrosive coating on the black pretreatment. Adhesion was reduced after the salt fog chamber test in the intercoat zone between the primer and the alkyd system.

Electrochemical tests on treated steel panels.

Corrosion potential measurements (Fig. 6) on treated panels showed that the primer protected the substrate because the corrosion potential remained more positive (+104 mV) with respect to the corrosion potential of bare steel after 7 days of immersion. This behavior is film thickness dependent, since when it diminished from 10 to 5 μm the anticorrosive behavior was lower as it may be deduced from the shifting in the corrosion potential. Formulations without tannin are claimed to have good anticorrosive properties **[24-26]**; however, it could be seen that corrosion potential decreased as a function of time, approaching the value corresponding to bare steel (-750 mV vs. SCE) as well as it was observed with lower film thickness. The initial protection achieved with the free tannin primer may be attributed to phosphoric acid which by itself is not able to produce an effective phosphatizing of the steel surface. White ferrous phosphate (vivianite) and some light brown ferric phosphate may appear

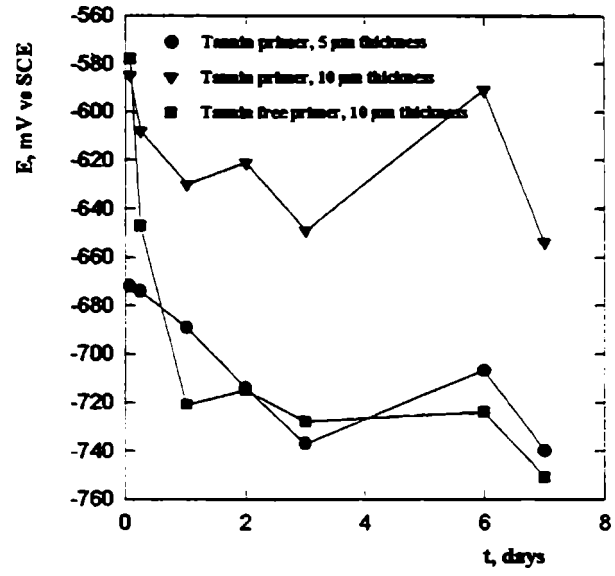

Fig. 6.- Corrosion potential of treated steel as a function of the exposure time in 0.5 M sodium perchlorate solution.

on the steel surface treated with phosphoric acid. In the presence of tannin these phosphates are readily converted into the more stable ferric tannate.

Table V

Adhesion (ASTM D 4541-89)

Systems	Adhesion ($kg.cm^{-2}$)	Adhesion after the salt fog chamber exposure ($kg.cm^{-2}$)
Pretreatment	20 ± 5	---
1	10 ± 5	5
2	9 ± 5	3
3	9 ± 5	6
4	10 ± 5	7

The measured ionic resistance (solution resistance and paint film resistance) is low and slightly higher than the solution resistance (70 $\Omega.cm^{-2}$); in this sense the pretreatment barrier effect to the electrolyte solution may be neglected (Fig. 7). The slight increase with time may be due to the sealing of pores having small and medium radii and to some oxide formation in the paint film **[26, 28]**. Polarization effects are negligible at the measuring frequency employed in this test.

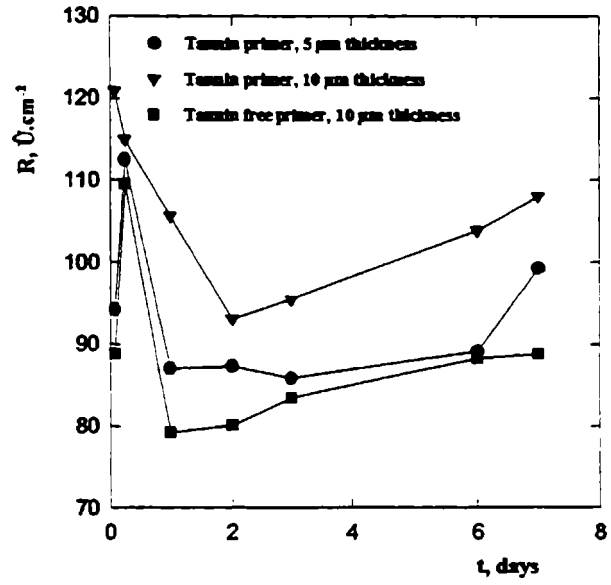

Fig. 7.- Ionic resistance of treated steel as a function of the exposure time in 0.5 M sodium perchlorate solution.

The polarization resistance (Fig. 8) of panels coated with the primer containing tannin decreased as film thickness increased. It is thought that as tannins have a great affinity for iron ions to form ferric tannate, steel corrosion increased **[5]** and polarization resistance diminished as tannin content increased within the film. However, polarization resistance is higher than the ionic resistance indicating that precipitated ferric tannate and the polymer of the binder blocked the active sites on the metallic surface protecting steel by a kinetic hindering mechanism [27]. In the case of the formulation tannin with lower film thickness, it is thought

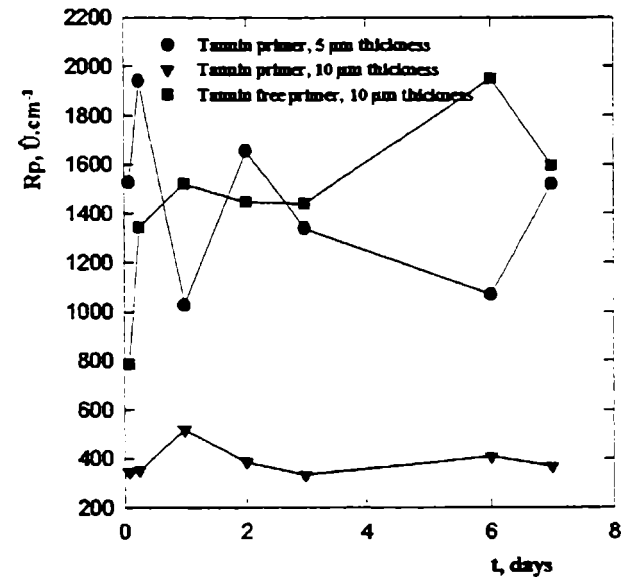

Fig. 8.- Polarization resistance of treated steel as a function of the exposure time in 0.5 M sodium perchlorate solution.

that tannate formation competed with oxide grow and the behavior approached that of the free tannin pretreatment for which polarization resistance increased as a consequence of oxide generation within the film. Fluctuations during the test are attributed to pore blocking and unblocking by corrosion products.

CONCLUSIONS

1. The pretreatment tested in this research protect adequately steel against corrosion in laboratory ambient. To achieve a good anticorrosive protection in aggressive environments an adequate paint system (anticorrosive + topcoat) must be applied.

2. The pretreatment system with tannin also gives an excellent protection against undercutting rusting.

3. The presence of tannins enhanced film adhesion to the substrate.

4. Tannins combine with ferric cation to yield an iron association compound ("ferric tannate"), which in combination with the polymer gives a film that inhibit further oxidation of the base metal by a kinetic hindering mechanism.

ACKNOWLEDGEMENTS

The authors wish to thank Comisión de Investigaciones Científicas de la Provincia de Buenos Aires and CONICET for financial support.

REFERENCES

[1] Ochoa, T.; Polianskaya, N.; Alvarez, Z.E.- **Memorias del II Congreso Iberoamericano de Corrosión y Protección,** 9-14 de Noviembre de 1986, Maracaibo, Venezuela, p. 259.
[2] Matamala, G.; Smeltzer, W.; Droguett, G.- **Corrosion, 50** (4), 270 (1994).
[3] M. Morcillo, M. Gracia, J. R. Gancedo, S. Feliú, **Memorias del II Congreso Iberoamericano de Corrosión y Protección,** 9-14 de Noviembre de 1986, Maracaibo, Venezuela, p. 221.
[4] Des Lauriers, P.J.- **Mat. Perf., 26** (11), 35 (1987).
[5] Vetere, V.F.; Romagnoli, R.- To be published in Surface Coatings International.
[6] Emeric, D.A.; Miller, C.E.- **Proc. ADV MAT/91** *(NACE, Houston)* 212, San Diego (1991).
[7] McConkey, B.H.- **Corros. Australas., 20**(5), 17 (1995).
[8] Bruzzoni, W.O.; Aznar, A.; Iñiguez Rodríguez, A.- **Rev. Iber. Corros. y Prot.**. **6** (2), 3 (1975).
[9] Seavell, A.J.- **J. Oil Col. Chem. Assoc., 61** (12), 439 (1978).
[10] Faure, M.; Landolt, D.- **Corros. Sci., 34**(9), 1484 (1993).
[11] González, M.I.; Abreu, A.- **Revistas de Ciencias Químicas de La Habana, 15** , 315 (1984).
[12] Ross, T.K.; Francis, R.A.- **Corr. Sci., 18**, 351 (1978).
[13] Joseph, G.; Vallejos, R.- **Rev. Iber. Corros. y Prot.**. **XIX**(6), 379 (1988).
[14] Nigam, A.M.; Tripathi, R.P.; Dhoot, K.- **Corr. Sci., 30** (8-9), 799 (1990).
[15] Almeida, E.; Pereira, D.; Waerenborg, J.; Cabral, J.M.P.- **Prog. Org. Coat., 21**, 327 (1993).
[16] Cerisola, G.; Barbucci, A.; Caretta, M.- **Prog. Org. Coat., 24,** 21 (1994).
[17] NIPPON OILS & FATS CO.- **Jap. Pat. Abs.** *92 (21) Gp G, 54. Patent Number 04/110357.*

[18] Alvarez, Z.E.; Callozo, I.; Valdés, D.- **Rev. Iber. Corros. y Prot., XVIII** (1), 35 (1987).
[19] Gledhill, R.J.- **J. Phys. Chem., 66**, 458, (1962).
[20] Amalvy, J.I.- **J. Appl. Polym. Sci., 59,** 339 (1996).
[21] Vetere, V.F.; Amalvy, J.I.; Romangoli, R.; Pardini, O.R.- To be patented.
[22] del Amo, B.; Romagnoli, R.; Vetere, V.F.- **Corrosion Reviews, 14** (1-2), 121 (1996).
[23] Kolthoff, I.M.; Furman, R.; Howell, N.- **Potentiometric Titrations. A theoretical and practical treatise**. Second Edition, John Wiley & Sons Inc., N.Y., 1947.
[24] Morcillo, M.; Feliú, S.; Simancas, J.; Bastidas, J.M.; Galvan, J.; Feliú (Jr.), S.; Almeida, E.M.-**Corrosion** *(NACE)* **48** (12), 1031 (1992).
[25] Guruviah, S.; Sundaram, M.- **Proc. Adv. Surf. Treatment Metals** 216, Bombay (1987).
[26] Lin, Ch.; Lin, P.; Hsiao, M.; Meldrum, D.A.; Martin, F.L.- **Ind. Eng. Chem. Res. 31** (1), 424 (1992).
[27] Szauer, T.- **Prog. Org. Coat., 10,** 157 (1982).
[28] Gust, J.; Bobrowicz, J.- **Corrosion** *(NACE),* **49** (1), 24 (1993).

PHOSPHORUS-BASED INTUMESCENT COATINGS

PINTURAS INTUMESCENTES BASADAS EN PRODUCTOS FOSFORADOS

J. C. Benítez[1], C.A. Giúdice[2]

SUMMARY

Fire is an energetic manifestation which carries undesirable consequences due to the problems that it originates. The conflagration is a disagreeable fact produced by fire.

The main objective of a fireproofing treatment is to make a material hardly flammable or autoextinguishable. An efficient fireproofing effect interrupts the combustion in one or more stadiums, leading the process to end in a reasonable period (preferably before ignition occurs).

Intumescent coatings, as a means of passive protection against fire, perform a fundamental role in this matter. Dry films of these paints, submitted to flame action, softens in a first stage and then swells due to an internal and partial loosing of non combustible gases, reaching up to 200 times of its original thickness. The charred coat, an incombustible spongy mass, protects the painted material, delays the temperature increase and avoids the access of air, and so the combustion. By means of intumescent coatings, different materials such as paper, wood, pasteboard, plastics, metals, etc. can be protected.

The objective of this paper was to study the influence of some formulation variables of phosphorus-based intumescent coatings, formulated and manufactured for this experiment. Chlorinated rubber coatings based on ammonium polyphosphate, pentaerythritol, melamine, 42 % chlorinated paraffin and an endothermic filler showed very high performance after ageing.

Keywords: *intumescence, intumescent coating, fire resistance, thermal protection*

INTRODUCTION

Fire loss is one of the major tragedies of modern civilization. Fire-resistant construction is an important factor since severe conflagrations have occurred in so-called fireproof buildings because highly combustible decorations and finishing materials have contributed to propagate the fire.

---

[1] Miembro de la Carrera del Investigador de la CIC
[2] Miembro de la Carrera del Investigador del CONICET; Profesor Adjunto, UTN

Taking into account the actual methods, it is important to mention that some of them show a performance independent of the human activity and besides that they are not conditioned by the adequate functioning of the installation. These methods are included in the generic concept of "passive protection against fire", so the decrease of material flammability performs a fundamental role.

Among these methods, the fire protection by intumescent coatings has an important place reserved. When heated, these coatings become plastic and produce non-flammable gases such as carbon dioxide and ammonia; the gases are trapped by the film converting it to a foam 50, 100 or in some cases 200 times thick in relation to the original coat film. At this stage the system solidifies, resulting in a thick, highly-insulating layer of carbon, which effectively protects the substrate from the fire.

Although, no building material is immune to the action of a fire of sufficient intensity and duration, the use of efficient fire-retardant coatings can reduce the severity of fire or delay its effects. On the other hand, the accumulation of multiple layers of conventional coatings can provide material to spread the fire.

As almost all the protecting methods, the employ of fire-retardant coatings was object at different moments of hardly controversial opinions by the protectionists since each one of these methods has both defenders and detractors. Intumescent coatings are a good example of that above mentioned; the fact of the existence of bad coatings or else of inadequate applications must not cause the disapproval. Continuous research work in this field has permitted to overcome some of these controversial aspects of the intumescent coatings.

The object of the present paper was to study the influence of some formulation variables of intumescent coatings and also to evaluate their fire-retardant properties after ageing.

FORMULATION OF INTUMESCENT COATINGS

The formulation of an intumescent coating is difficult because of its dual role in service; it must possess adequate decorative properties but in the case of a fire, the intumescent layer must swell up within seconds to give a protective barrier on the substrate. To produce that phenomenon of intumescence, the following components were selected:

A coal supplier or carboniferous agent. A carbonific or a source of carbon (sometimes termed char former) is generally chosen from polyfunctional alcohols. To be effective, it must contain hydroxyl groups and a high percentage of carbon.

The combustion of pure polyalcohols is generally of exothermic type; they decompose generating different carbon oxides, water vapor and incombustible remainders. Nevertheless, polyalcohols can react under the action of heat with certain inorganic acids producing phosphorated esters. In these circumstances the degradation is difficult considering that the reaction becomes endothermic, neither flame nor flammable residues are formed, and combustible gases formation is greatly reduced; thus, fire developing is limited.

The coal supplier, which forms the carbon skeleton of the intumescent layer, must be more thermally stable than the catalyst. In this paper, **pentaerythritol** was selected since it showed a very good performance in many studies carried out by several authors **[1-6]**.

A dehydrating agent. A catalyst or a source of phosphoric acid, which decomposes giving the necessary products so as to modify the pyrolysis of the coal supplier, is usually used for this purpose. The catalyst should contain a high phosphorus content and must decompose to yield phosphoric acid at a temperature below at which the carbonific does. Generally, phosphoric acid salts, polymers of these salts as well as organic compounds, derivatives or not of this acid, are used.

The dehydrating agent decomposes liberating phosphoric acid and forming esters with hydroxyl groups of the carboniferous agent, which then transform themselves in phosphoric esters showing the above mentioned characteristics against fire.

Monoammonium phosphate was initially employed as dehydrating agent according to the satisfactory results obtained in the intumescent-isolating coat formation. Moreover, in wet zones or exteriors, coatings based on monoammonium phosphate lose their swelling capacity with time, and also show an efflorescence that alters the paint film decorative characteristics; the high solubility of this salt, that facilitates its diffusion to the surface, is the responsible of the mentioned disadvantages.

Studies trying to obtain more insoluble dehydrating agents, by polymerization of products like ammonium phosphate or by elaborating of phosphorus compounds of organic type, are carried out since a long time. Two commercial **ammonium polyphosphates** (catalysts C1 and C2), previously characterized in laboratory tests, were employed in this paper.

Blowing agents. These are the source of the gases; they decompose by thermal action liberating non combustible gases that swell paint film. This additive is generally based on nitrogenous products, like melamine, dicianamine or organic compounds partially halogenated like chlorinated paraffins.

The three mentioned compounds can not be chosen in an arbitrary form; the dehydrating agent or the catalyst must have a decomposition temperature near to the blowing agent. For example, if the last one works at a temperature noticeable superior to the catalyst, a carbonaceous mass without expanding would be formed, without a spongy consistence and so would not have a low thermal conductivity; on the contrary, if the blowing agent decomposition temperature is too low, gases liberate before carbonaceous mass is formed. Two different generators of gases were included in this experiment so as to extend the period of volatile products: **melamine and 42 % chlorinated paraffin**. The last one also acts as plasticiser of the selected resin.

Regarding the other components, they were:

Resinous binder. The film forming material must be thermoplastic. Some convertible resins, such as drying oil alkyds can not be softened sufficiently by heat to allow the foam to expand.

In this experiment, **20 cP chlorinated rubber** was employed as binder. Dry films based on this resin show a noticeable thermal decomposition at approximately 130 °C and a complete charring (without melting) at about 200 °C. Chlorinated rubber also assists as a blowing agent and a source of carbon.

To select the mentioned binder, the following properties were taken into account: it softens and decomposes below the activation temperature of the intumescent agent and also it contributes during thermal activation to the stability of the intumescent foam produced by the agent. Besides, it is nonburning and self-extinguishing when exposed to a flame.

Pigment. The incorporation of a non-flammable pigment leads to a limited degree of fire protection. The pigment only dilutes the combustible organic binder to the extent that the flame spread is reduced or at least is not increased. On the other hand, unpigmented coatings often show a higher flame spread than the combustible substrate. In addition to the diluting effect before mentioned, some pigments perform a physical-chemical role to control the fire.

In this paper, **rutile titanium dioxide** was used in all formulations to achieve adequate hiding power. In some compositions, titanium dioxide was partially replaced by fillers: **alumine trihydrate** or **modified barium metaborate**.

From a quantitatively point of view, considerable technical effort is required to optimize the composition since intumescent coatings not only must show excellent fire retardant properties but also adequate decorative qualities. It is necessary to incorporate large amounts of active pigments to attain the best efficiency since the fire retardancy and degree of intumescence are directly affected; however, the high loading of solids in an intumescent coating can lead to poor serviceability, simply because the film is porous if the pigment volume concentration (PVC) is too far above its critical value (CPVC). In this paper, the considered PVC values were 60 and 65 %.

The composition of six intumescent coatings is included in Table I.

MANUFACTURE OF INTUMESCENT COATINGS

It was performed at laboratory scale in triplicate by employing a porcelain jar ball mill of 1.0 liter of total capacity. The operative conditions of the ball mill were specially considered with the aim to achieve an efficient pigment dispersion **[7]**.

First, a solution of binder in the solvent mixture was prepared under stirring. The ball mill was loaded with the mentioned solution and the pigments were added; these components were milled for 24 hours previous incorporation of a dispersant in the quantity indicated by the manufacturer. Finally, the viscosity was adjusted in the can.

LABORATORY TESTS

A great variety of test methods are known to evaluate the material behavior exposed to fire **[8-13]**. The main characteristic that distinguishes them is the way of determining the

performance of a phenomenon or situation, fire or conflagration, that does not adjust to preestablished laws and in which different variables have a great influence.

Table I

Intumescent coating composition*, % v/v

Component	I	II	III	IV	V	VI
Ammonium polyphosphate C1	51.5	--	51.5	--	51.5	--
Ammonium polyphosphate C2	--	51.5	--	51.5	--	51.5
Pentaerythritol	18.9	18.9	18.9	18.9	18.9	18.9
Melamine	18.2	18.2	18.2	18.2	18.2	18.2
Titanium dioxide	11.4	11.4	7.4	7.4	7.4	7.4
Modified barium metaborate	--	--	4.0	4.0	--	--
Alumina trihydrate	--	--	--	--	4.0	4.0
20 cP chlorinated rubber	62.8	62.8	62.8	62.8	62.8	62.8
42 % chlorinated paraffin	37.2	37.2	37.2	37.2	37.2	37.2

Note: Samples with PVC 60.0 % (1.I/VI) and with PVC 65.0 % (2.I/2.VI). Solvent and diluent, C9 aromatic hydrocarbon/ white spirit (4/1 ratio by weight). Additives, 2.3 and 2.4 % v/v on solids for samples 1.I/VI and 2.I/2.VI, respectively

Fire resistance can be determined by exposing the material to a small ignition or heat source. The reaction to fire embraces an extensive amount of possibilities according to test conditions, where material interaction, design and utility must be reflected.

1. Limiting Oxygen Index

SAE 1010 test panels (150 x 80 x 2 mm) were used. The surface (initial grade A) was sandblasted to Sa 2 ½ (SIS 05 59 00-67 Specification) attaining 20 μm maximum roughness and then degreased with toluene. The experimental intumescent coatings were brushapplied achieving about 260-280 μm dry film thickness in three coats; each coat was applied with a 48 hours period between them.

The coated panels remained at laboratory conditions for 10 days and then they were carried out to stove at 40/45 °C for 24 hours to eliminate the most quantity of the remaining solvent.

With the aim to study the intumescent coating behavior after exposure to a high humidity environment, panels were placed in an enclosed chamber containing a heated, saturated mixture of air and water vapor (100 % relative humidity chamber, ASTM D 2247-92) for 500 hours. Then the coated panels were kept in laboratory for 10 days for film drying before starting the test.

To carry out the Limiting Oxygen Index (LOI) test, the flow measuring system was calibrated by using a water-sealed rotating drum meter; the gas flow rate in the column was 4 $cm.s^{-1}$.

LOI test, carried out according to ASTM D 2863-87 Standard, determines the minimum concentration of oxygen, in a mixture with nitrogen, that will just support combustion of a material under equilibrium conditions of candle-like burning. It is important to mention that this method is not representative of the real behavior of a material in contact with fire but it is one method of preference in the development and improvement of fire retardant treatments due to it permits the obtainment of reproducible numerical values. This test was done in triplicate.

2. Intermittent Bunsen burner flame

The necessity of determining the efficiency of the formulated coatings led to the development of a comparative method. For this aim a combustible substrate was used (Araucaria angustifolia). Test panels of 200 x 100 x 3 mm were carefully sandpapered in both faces and edges. The selected panels remained at laboratory conditions for 6 months (free of knots and any other imperfections).

Intumescent coatings were applied by brush on the panels. The first coat was constituted by the selected sample previously diluted to 50 % by weight in order to fill surface pores; the film was let to dry at laboratory conditions for 24 hours and then another two coats were applied, with 48 hours between them, reaching to a final dry film thickness about 210-230 μm.

The conditions of film drying and exposure to 100 % relative humidity chamber were similar to those employed to determine LOI values.

The test panels were arranged in a Flame Chamber, whose characteristics are in according to UL 94 Underwriters Laboratories Standard. In this experiment, the coated panels were placed in such way that their longitudinal axes showed an inclination of 45 degrees with respect to the supporting level while their transversal axes were in a parallel position.

The test done in triplicate consisted of to submit the front bottom part of the panel to the intermittent flame of a Bunsen burner vertically disposed. Flame was adjusted so as to reach 10 mm height of blue cone. The exit hole of the burner was arranged at 15 mm of the testing surface.

The painted panel, fitted in the mentioned position, was submitted to flame action for 20 seconds, with resting periods of 10 seconds. The exposure fire/resting cycle was repeated until the flame persisted on the surface at least 5 seconds after removing the burner.

When the number of cycles with self-extinguishing behavior reached the value 30 (stage A), the flame action was extended to 50 seconds with 10 seconds of resting (stage B) and if the self-extinguishing continued after other 35 cycles in the cited conditions, the flame was kept in a constant way (stage C) until 30 minutes as maximum. The number of cycles with a self-extinguishing behavior was determined, qualifying each of them with 1 and 2 points for

stages A and B respectively and 5 points for each minute corresponding to stage C. Then, the whole amount of each panel and also the average results of the three panels were calculated.

3. Thermal conductivity test

It is very important for these coatings to determine the thermal conductivity of a coated panel exposed to a fire. It is possible to evaluate the thermal isolation degree produced by the intumescent coating registering the temperature decrease on the backface of the panel.

In this experiment SAE 1010 test panels (200 x 300 x 3 mm) were used. The test was carried out on panels prepared in a similar form than those used for evaluating the Limiting Oxygen Index. The samples were placed in the before mentioned UL 94 Flame Chamber avoiding air currents.

A bare panel selected as reference was fitted in horizontal position. The measuring system (thermoelectric couple) was fixed on the superior face of the panel. The Bunsen burner was vertically disposed at the inferior face; the flame was adjusted so as to reach 10 mm height of the blue cone and the exit hole of the burner was arranged at 15 mm from the surface.

Above mentioned panel was exposed to a fire regulating the flame intensity up to cover an area of 6-8 cm diameter bringing a constant temperature of 400 ± 05 °C at the backface. It is registered from the beginning the functionality of the temperature with time to develop the calibrating curve.

This operation was exactly repeated for each one of the coated panels registering the temperature evolution during 25 minutes.

For the three mentioned tests , that means for LOI, Intermittent Bunsen burner flame and thermal conductivity, a commercial alkyd paint was used as reference.

RESULTS AND DISCUSSION

Characterization of ammonium polyphosphates

In general, catalysts showed similar characteristics (Table II), particularly regarding high phosphorus content in their composition which could lead to a great release of phosphoric acid upon decomposition. However, the water solubility is markedly different: the ammonium polyphosphate C1 displayed the value 13.7 g/100 g at 25 °C, higher than that correspondent to catalyst C2 (4.2 g/100 g), at the same temperature.

Concerning thermogravimetric analysis (TGA), the curves obtained with the detector Shimadzu TGA-50 H (run under Argon at 10 °C/min, cell of alumina) are shown in Figures 1 and 2. Both catalysts demonstrated the highest thermal stability in the initial decomposition range (below about 200 °C); then they undergo a gradual weight loss, diminishing in rate to about 500 °C and in the limit of thermogravimetric analysis (temperature higher than 800 °C);

in this region the weight appears to be leveling off in the both cases. Moreover, in the entire temperature range of testing, the catalyst C2 showed a higher thermal stability than catalyst C1.

Table II

Characteristics of ammonium polyphosphates

Property	Catalyst C1	Catalyst C2
Form	White powder	White powder
Phosphorus, % P	30.6	31.4
Nitrogen, % N	14.1	14.3
Water solubility at 25 °C, %	13.7	4.2
pH of saturated solution	5.9	6.6
Specific gravity, $g.cm^{-3}$	1.82	1.72
Oil absorption, g/100 g	76	81
Diameter (50.0/50.0 %), μm	17.2	22.3

Figure 3 displays the theoretical chemical mechanism of two dehydrating agents during a conflagration; to simplify, the composition is expressed as $(NH_4)_2HPO_4$.

Thermal analysis of pigment

The determination of the endothermic and exothermic reaction temperatures for the inorganic pigments was performed by using the detector Shimadzu Differential Thermal Analyzer (DTA) at a programmed scanning of 10 °C/min under argon atmosphere. Moreover, thermogravimetric analysis (TGA) was also carried out on the pigment, in the before mentioned conditions for the catalysts.

Concerning hydrated aluminium oxide pigment, it is a white crystalline product of extremely fine and uniform particle size. Chemically, it is considered either as aluminium oxide combined with three molecules of water hydration or as aluminium hydroxide. Technically, the latter is correct since the hydrated alumina consists of three hydroxyl ions in co-ordination with an aluminium ion. However, since water molecules (34.6 % W/W) can be driver off at elevated temperatures, hydrated aluminium oxide is the commonly preferred name.

When hydrated alumina is heated to a high temperature, it releases its water of hydration that in turn acts to dissipate heat; it does not actually extinguish fire, but the heat absorbed during the release of the water of hydration increases flame resistance and retards heat build up **[14]**.

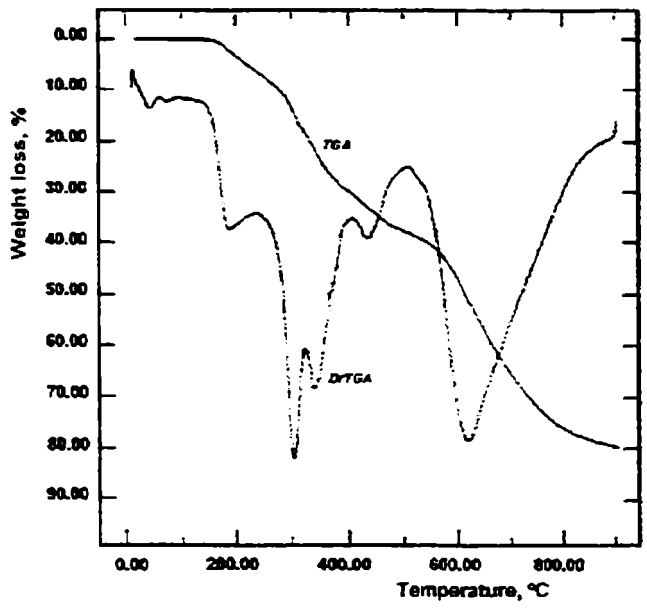

Fig. 1.- Thermogravimetric analysis (TGA) of ammonium polyphosphate C1 (heating rate 10°C/min; 30 ml Argon/min).

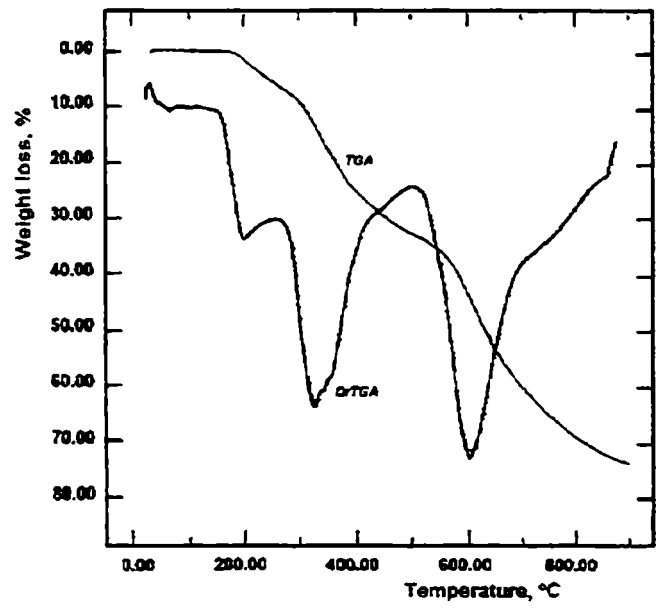

Fig. 2.- Thermogravimetric analysis (TGA) of ammonium polyphosphate C2 (heating rate 10°C/min; 30 ml Argon/min).

$$x\,(NH_4)_2HPO_4 \xrightarrow{\phi} HO\left[\begin{array}{l} O \\ | \\ P-O \\ | \\ OH \end{array}\right]_x H + 2\,x\,NH_3 + (x\text{-}1)\,H_2O$$

polyphosphoric acid

$$HO\left[\begin{array}{l} O \\ | \\ P-O \\ | \\ OH \end{array}\right]_x H + R\text{-}CH_2CH_2OH \xrightarrow{\phi} R\text{-}CH_2CH_2O\,PO_3H_2 + HO\left[\begin{array}{l} O \\ | \\ P-O \\ | \\ OH \end{array}\right]_{x-1} H$$

$$R\text{-}CH_2CH_2OPO_3H_2 \xrightarrow{\phi} R\text{-}CH=CH_2 + H_3PO_4$$

$$x\,H_3PO_4 \xrightarrow{\phi} HO\left[\begin{array}{l} O \\ | \\ P-O \\ | \\ OH \end{array}\right]_x H + (x\text{-}1)\,H_2O$$

Fig. 3.- Theoretical reactions between the catalyst and the coal supplier

The DTA and TGA curves of the hydrated aluminium oxide are shown in Figures 4 and 5, respectively. The Fig. 4 indicates three regions of endothermic activity; the first occurs at about 242 °C, the second appears from 250 to 350 °C with a maximum endothermic peak approximately at 311 °C and the other near to 538 °C. These results were confirmed by TGA which also shows a weight fraction of 64.5 % remaining at 800 °C for this endothermic filler.

In relation with barium metaborate used as filler in some intumescent coatings, its commercial form is a modified pigment that contains a minimum of 90 % of barium metaborate calculated as $BaB_2O_4.H_2O$. It acts as both a flame retardant and an afterglow inhibitor and has a mode of action typical of all boron compounds.

Figure 6 displays the differential thermal analysis of modified barium metaborate; it can be seen from the thermal profile obtained that this filler does not indicate a large exothermic or endothermic behavior in the desired temperature range.

Moreover, from thermogravimetric analysis of this pigment it is possible to conclude that it has good heat stability since it does not decompose at high temperatures. Figure 7 shows near to 9.0 % weight loss at 600 °C with a heating rate of 10 °C/min.

It is important to mention that both fillers, hydrated aluminium oxide and modified barium metaborate, have low water solubility and hence a great permanence in the film under exterior weathering conditions. Moreover, they do not produce toxic fumes when heated.

Finally, rutile titanium dioxide used as pigment in all the formulations can yield a high refractive index as well as chemical and physical stability. Its ability to opacity might be considered a major optical property. TGA indicates that titanium dioxide is extremely stable at high temperatures, Figure 8. This exceptional stability can be attributed to the strong bond between the tetravalent titanium ion and the bivalent oxygen ions. Moreover, it is water insoluble.

100 % relative humidity testing

The degree of blistering and film adhesion were assessed on coated metallic panels aged in a 100 % relative humidity chamber for 1500 hours. The mean values are indicated in Table III.

The degree of blistering was evaluated according to ASTM D 714-87. The blister size is qualified with reference standards from 10 to 0, where 10 represents no blistering, 8 is the smallest blister size easily seen by the unaided eye, 6, 4 and 2 indicate progressively larger sizes. The frequency is qualitatively defined as F (few), M (medium), MD (medium dense) and D (dense). Observed blistering corresponded to the osmotic phenomenon, that is the blistering exclusively developed by water diffusion through the paint film and not from rusting.

As expected, the blister resistance was significant due to the high permeability showed by the coatings formulated with high PVC values: in these films the water can readily escape to the outside surface without the loss of film adhesion.

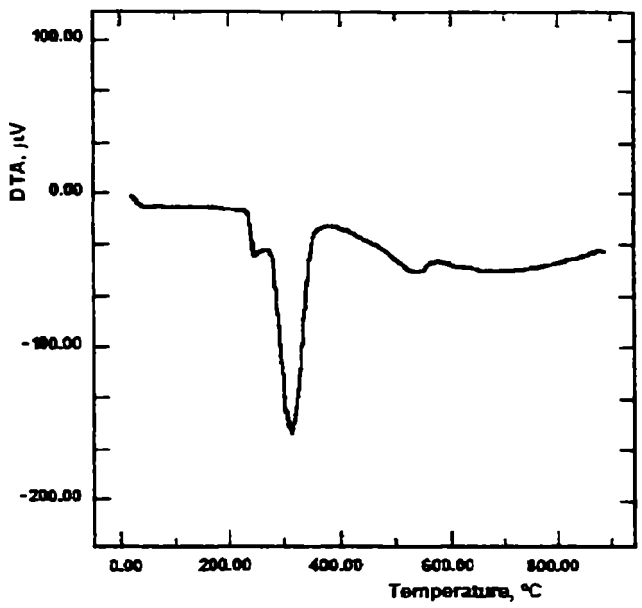

Fig. 4.- Differential thermal analysis (DTA) of hydrated aluminium oxide (heating rate 10 °C/min; 30 ml Argon/min; sample weight 20.25 mg).

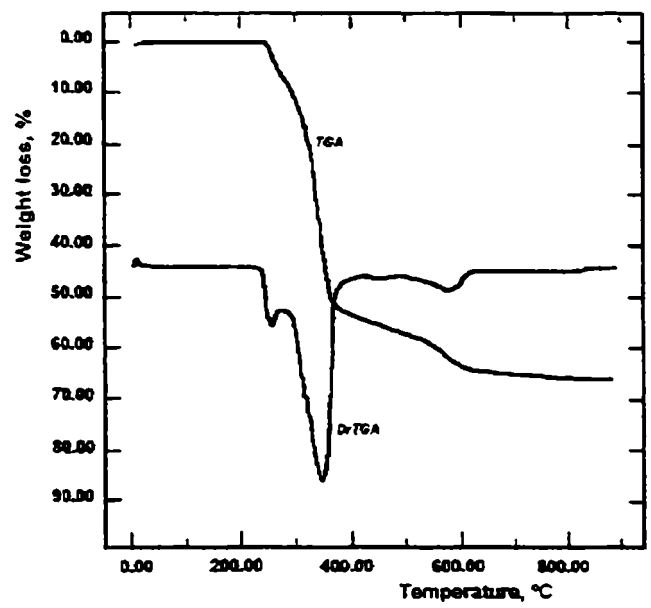

Fig. 5.- Thermogravimetric analysis (TGA) of hydrated aluminium (heating rate 10 °C/min; 30 ml Argon/min).

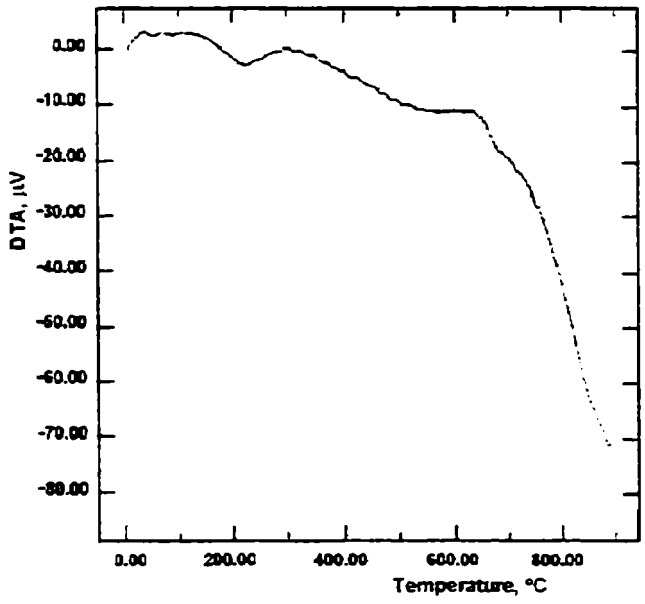

Fig. 6.- Differential thermal analysis (DTA) of modified barium metaborate (heating rate 10 °C/min; 30 ml Argon/min; sample weight 9.52 mg).

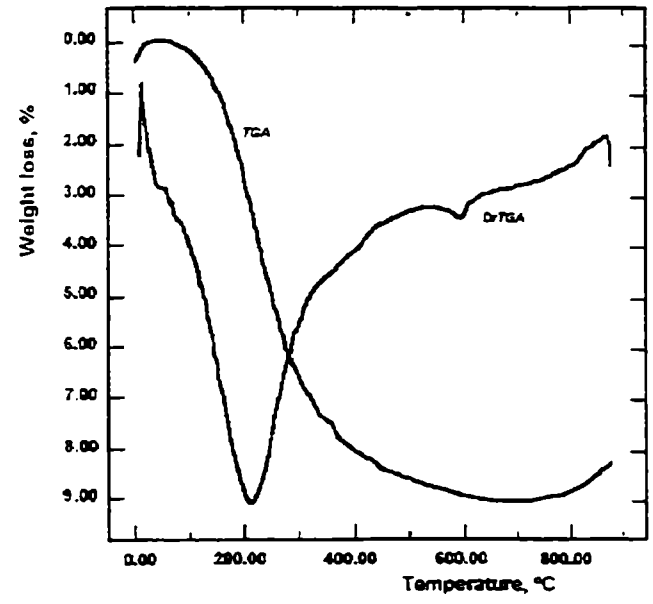

Fig. 7.- Thermogravimetric analysis (TGA) of modified barium metaborate (heating rate 10 °C/min; 30 ml Argon/min).

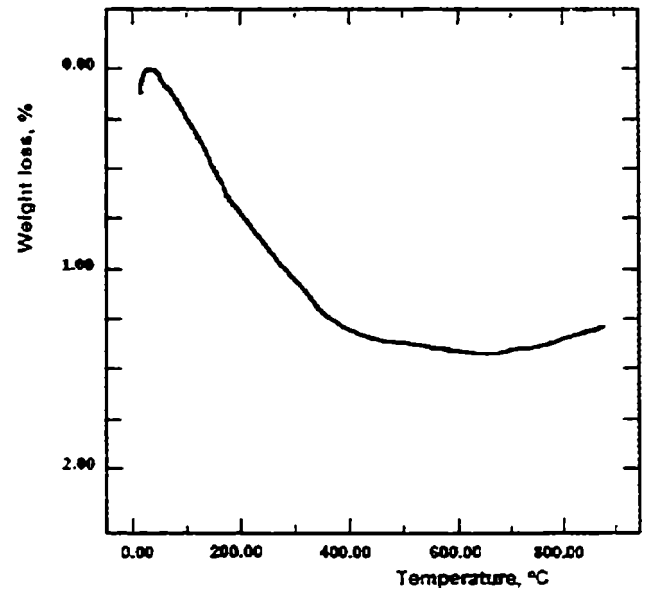

Fig. 8.- Thermogravimetric analysis (TGA) of titanium dioxide (heating rate 10 °C/min; 30 ml Argon/min).

To determine film adhesion, the Elcometer Tester Model 106 was used. The dolly bonded to the coating under test is subjected to progressively increasing stress at a constant rate until it fractures: dragging indicator retains the maximum pull of force reached. Near to 20 determinations at room temperature (20 ± 2 °C) were made for each intumescent coating to minimize the scattering of the results. The fracture values were expressed related to corresponding original coating (adimensional unit), Table III.

Table III

Degree of blistering and film adhesion
Limiting Oxygen Index

Coating	PVC, %	Degree of blistering (1)	Film adhesion (1, 2)	LOI **(3), %
1.I		9-F	0.7	> 50
1.II		9-F	0.9	> 50
1.III	60.0	10	0.8	> 50
1.IV		10	0.9	> 50
1.V		9-F	0.7	> 50
1.VI		10	0.9	> 50
2.I		10	0.8	> 50
2.II		10	0.9	> 50
2.III	65.0	10	0.7	> 50
2.IV		10	0.9	> 50
2.V		10	0.7	> 50
2.VI		10	1.0	> 50
Commercial alkyd paint		4-D	0.5	13

(1) 100 % relative humidity chamber (ASTM D 2247-92). 500 hours
(2) Relative to original coating (adimensional unit)
(3) Normal velocity. 4.0 cm.s^{-1}

Results display high values of film adhesion, since they range between 0.7 and 1.0, that is the coatings retained approximately from 70 to 100 % of the original fracture values after ageing.

Since all coated panels showed a reasonable behavior in the two tests carried out after ageing, the whole of them were selected for evaluating their fireproof capacity.

Limiting Oxygen Index

Experimental results corresponding to LOI test are also shown in Table III; all samples were tested in triplicate at about 20 °C and showed a self-extinguishing capability since their Limiting Oxygen Index was higher than that corresponding to the experimental limit for this type of chamber LOI 28 % **[3]**.

This test did not allow to establish the influence of the formulation variables considered in this study since all the intumescent coatings displayed a very good performance, LOI > 50 %.

Intermittent Bunsen burner flame

Coating qualification and classification was carried out according to Table IV. Average results of the exposures to the intermittent flame test are shown in Table V.

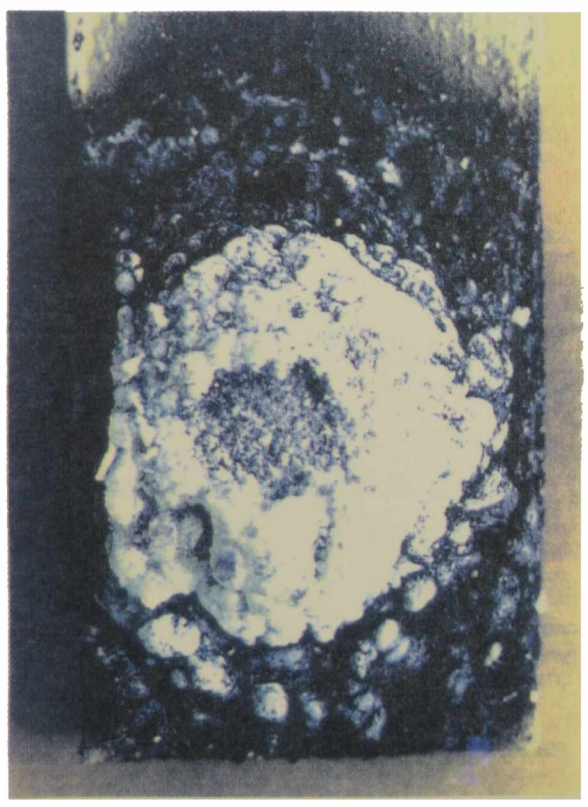

Fig. 9.- View of panel for testing. Coating 2.II after finishing Intermittent Bunsen burner flame.

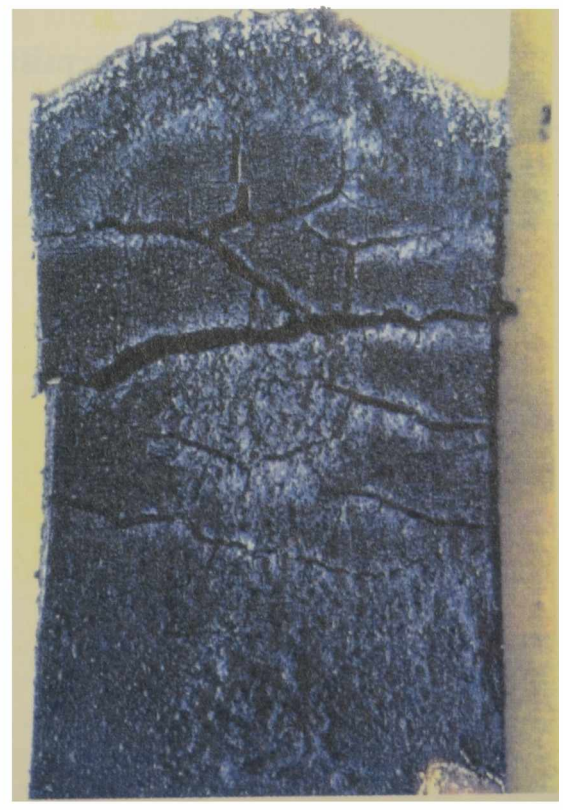

Fig. 10.- View of reference panel protected with commercial alkyd paint, Intermittent Bunsen burner flame test.

All the experimental coatings showed a significant intumescence and a quite uniform development. Only in a few cases a slightly depression attributable to the flame pressure was observed; the insulating layers remained firmly adhered to the substrate in all the panels.

Referring to average height of the intumescence, values ranged between 5 and 9 mm for coatings 1.I/1.VI (PVC 60.0 %) and between 11 and 16 mm for coatings 2.I/2.VI (PVC 65.0 %), Table V. Fig. 9 shows a panel protected with coating 2.II after finishing the test.

Table IV

Coating classification

Average rating in intermittent flame test	Coating Qualification	Coating classification
200 or more	Passed	Class A
100 to 199	Passed	Class B
70 to 99	Passed	Class C
30 to 69	Failed	Class D
29 or less	Failed	Class E

Pigment volume concentration had a definite effect both on flame retardant properties and on the height of the intumescence. Moreover, the type of catalyst showed a significant influence on fireproofing capacity of films exposed to adverse humidity conditions. Coatings with the best performance in this test were formulated with ammonium polyphosphate C2: the whole of them were classified as class A and in all cases their behavior as fire retardant was higher than samples with ammonium polyphosphate C1 in their composition.

Table V

Intermittent flame test results

Coating	Average value	Intumescence, mm	Coating qualification	Coating classification
1.I	140	5/6	Passed	Class B
1.II	205	8/9	Passed	Class A
1.III	175	6/7	Passed	Class B
1.IV	225	8/9	Passed	Class A
1.V	155	5/6	Passed	Class B
1.VI	245	8/9	Passed	Class A
2.I	180	12/13	Passed	Class B
2.II	>250	15/16	Passed	Class A
2.III	220	11/12	Passed	Class A
2.IV	>250	15/16	Passed	Class A
2.V	190	12/13	Passed	Class B
2.VI	>250	14/15	Passed	Class A
Reference*	2	0**	Failed	Class E

* Commercial alkyd paint
** No intumescence

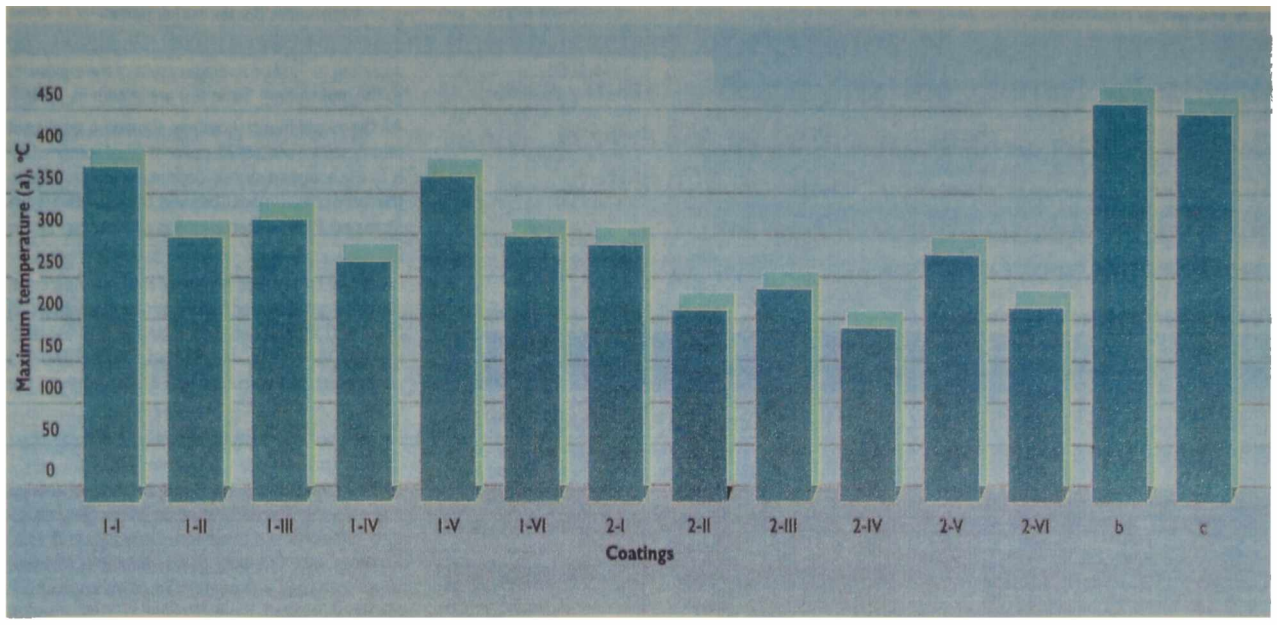

Fig. 11.- Thermal conductivity test.

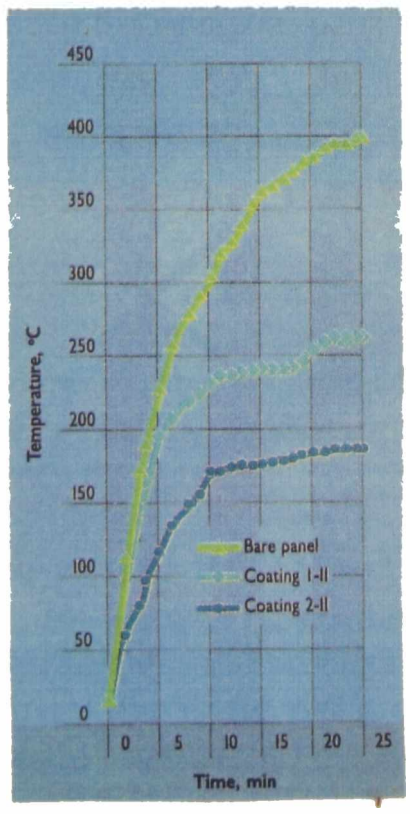

Fig. 12.- Influence of pigment volume concentration (PVC) on thermal conductivity.

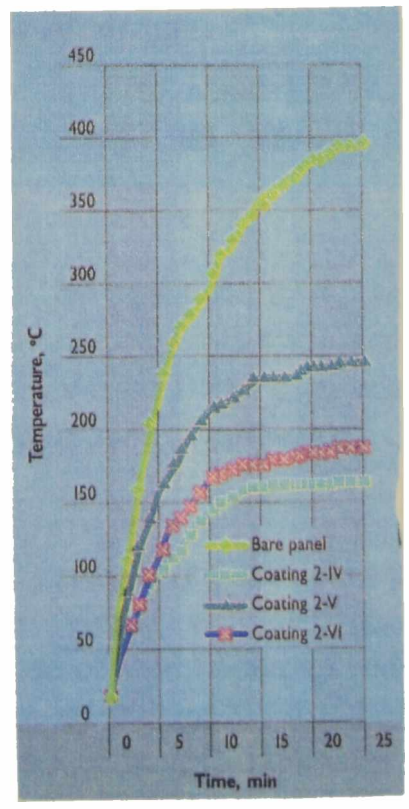

Fig. 13.- Influence of catalyst and filler types on thermal conductivity.

All coatings were classified as Class A or B and their performances were better than the commercial alkyd paint selected as reference: Class E, Fig. 10.

Without any doubt, an important consideration in the performance of the thermal protection coating is the ability to maintain their properties during exposure to the aggressive humidity or water. Film degradation due to leaching or extraction of the intumescent agent by water usually alters the expansion process, thereby destroying the thermal effectiveness of intumescent coatings. In spite of the similar properties of both dehydrating agents employed in this study, the very low water solubility of catalyst C2 compared to C1 makes it the preferred material for formulating coatings that must provide serviceability under humid or wet conditions.

However, the higher thermal stability of the ammonium polyphosphate C2 generates a thicker insulating layer and hence a more effective protection.

Thermal conductivity test

The following criteria for qualifying as successful the formulated intumescent was applied: the temperature registered by the thermocouple at the backface of the painted panels must not exceed 200 °C during the test (25 minutes). Results are displayed in Fig. 11, which indicates that in all cases the thermal insulation due to the charred coat formed after testing at the front of the panels led to temperatures at backface lower than those attained both with the bare material and the reference paint under the same conditions of testing.

From above mentioned viewpoint, some coatings with significant mean height of intumescence (Table V) fulfilled the requirement since they showed a maximum temperature at backside inferior to the fixed limit (200 °C).

The values obtained in these experiences corroborate the conclusions reached in the intermittent Bunsen burner flame test in relation with the influence of PVC and catalyst type. Fig. 12 indicates a better insulating behavior of coating 2.II (PVC 65.0 %) than coating 1.II (PVC 60.0 %) while Fig. 13 shows that the coating 2.VI (ammonium polyphosphate C2) had a higher efficiency than coating 2.V (catalyst C1).

Moreover, this test allowed to attain conclusions regarding the influence of fillers incorporated by partial replacement of titanium dioxide. Some coatings showed an improvement of the thermal protection by introducing into those compositions an endothermic filler like hydrated aluminium oxide; this pigment counter-balanced the natural exothermic heat of decomposition produced during intumescence in the pyrolysis zone. Coatings with hydrated aluminium oxide showed the best behavior in this experiment: the effect of endothermic filler should reduce the rate of the backface temperature rise of metallic substrates. On the other hand, no significant differences were observed in samples either with titanium dioxide or with titanium dioxide/modified barium metaborate as pigment: time-temperature data were not altered with this filler.

CONCLUSIONS

1. The performance of an intumescent coating depends on the ability to maintain their physical properties during exposure to humidity or water. The environment can deteriorate the film and besides leaches or extracts some components and consequently decrease the thermal effectiveness.

2. Laboratory tests demonstrated the effect of pigment volume concentration on fire retardancy. Results on intumescent coatings in which PVC was varied indicated that efficiency is higher at PVC 65.0 % than 60.0 %. Other PVC values above of the critical one were not considered since its influence on some key service properties of the coating is important.

3. Hydrated aluminium oxide has demonstrated an improved thermal control of a metallic substrate when exposed to fire action. Differential thermal analysis of this filler displays an endothermic behavior. On the other hand, modified barium metaborate used as filler did not show an altering in the thermal profile at least in the desired temperature region.

4. Owing to the highest thermal stability and the lowest water solubility, ammonium polyphosphate C2 is the preferred compound as catalyst.

ACKNOWLEDGEMENTS

The authors are grateful to CONICET (Consejo Nacional de Investigaciones Científicas y Técnicas) and to CIC (Comisión de Investigaciones Científicas de la Provincia de Buenos Aires) for their sponsorship for this research.

REFERENCES

[1] Bishop, D.M.; Bottomless, D.; Nobel, F.- **J. Oil Col. Chem. Assoc., 66** (12), 373, 1983.
[2] Dunk, J.V.- **J. Oil Col. Chem. Assoc.,72** (10), 413, 1989.
[3] Wake, L.V.- **J.Oil Col. Chem. Assoc., 71** (11), 378, 1988.
[4] Shaw, R.J.- **J.Oil Col. Chem. Assoc.,72** (5), 177, 1989.
[5] Roberts, A.F.; Moodie, K.- **J.Oil Col.Chem.Assoc.,72** (5) 192, 1989.
[6] Sawko, P.M.; Riccitiello S.R.- **J.Coat. Technol., 49** (627) 38,1977.
[7] del Amo, B.; Giúdice, C.; Rascio, V. - **J. Coat.Technol., 56** (719), 63 ,1984.
[8] British Standard 476 , Part 7 (1971) Surface spread of flame test for materials.
[9] ASTM E 84 (1980) Surface burning characteristics of building materials.
[10] ASTM D 1360 (1979) Fire retardancy of paints (cabinet method).
[11] ASTM D 2863 (1987) Flammability of plastics using the oxygen index method.
[12] ASTM E 162 (1987) Surface flammability of materials using a radiant heat energy source.
[13] ASTM D 1433 (1977) Rate of burning and/or extent and time of burning of flexible thin plastic sheeting supported on a 45 degree incline.
[14] Williams, J., Jr. - Pigment Handbook, vol. I, T. C. Patton Ed., p. 293, 1972.

EXTRACTION AND CHARACTERISATION OF QUEBRACHO (SCHINOPSIS SP.) TANNINS

EXTRACCION Y CARACTERIZACION DE TANINOS DE QUEBRACHO (SCHINOPSIS SP.)

M.L. Tonello[1], C.A. Giúdice[2], J.C. Benítez[3]

SUMMARY

Vegetables tannins are organic substances; when considering the great number of different tannins, it is possible to state certain properties which are common to all of them such as: a high molecular weight, causing colloidal solutions in which the particles of tannins are present in all forms of dispersions; a great number of free hydroxy phenolic groups, which are mainly responsible for the solubility of tannins in water; with few exceptions, all tannins are amorphous and no crystalline; a different degree of acidity resultant from the polarity of the hydroxy phenolic groups which in some cases is enhanced by free carboxyl groups; tannins formed by esterification of carboxyl groups usually exhibit a higher acidity than those made by condensation or polymerisation of components free from carboxyl groups; formation of intense precipitates in the presence of soluble iron (III) salts, etc.

This last property of the tannins, that is the capacity of forming chelates with the hexahydrated iron (III) ion, could be employed efficiently to modify the kinetic of oxidation of iron and steel substrata. In this paper, the extraction, the purification, the concentration and the characterisation of tannins obtained from quebracho (Schinopsis sp.) were performed, particularly with the objective of knowing some inherent properties to the reaction between the tannins and the iron.

Keywords: *tannins, quebracho, extraction, purification, concentration, characterisation, iron- tannins reaction.*

INTRODUCTION

The generic term tannins involves a group of compounds of high molecular complexity, widely distributed in the vegetable kingdom and with common characteristics. It is useful the employment of the word tannins in plural in view of the difficulty to define with precision their chemical composition.

---

[1] Becario de Perfeccionamiento de la CIC
[2] Miembro de la Carrera del Investigador del CONICET; Profesor Adjunto, UTN
[3] Miembro de la Carrera del Investigador de la CIC

In the last years, the chromatographic study of the tannins has permitted to establish the heterogeneity of the different extracts and also to determine the presence of small quantities of phenols, which generate by polymerisation different and complex compounds.

The classification of the vegetable tannins was evolving according to the state of the knowledge over these compounds. At first, since the chemical structure was unknown (only some products of hydrolysis or those obtained from destructive distillation were identified), the cause of their formation was taken into account. Afterwards, the behaviour against certain chemicals was studied and finally the composition was considered **[1-4]**.

Freudenberg classified the tannins according to the structure, in pyrogall tannins and catechol ones. In general, the vegetables supply extracts of mixed base.

The pyrogall tannins, which are also called hydrolyzable ones, are weakly polymerised and are soluble in water. They have a polyester structure and consequently hydrolyse with facility by the action of the acids in a sugar, a polyalcohol and a phenol carboxyl acid. Their bencenic nuclei are bonded through atoms of oxygen forming large complexes.

On the other hand, the catechol tannins are strongly polymerised and the bencenic group is bonded to the carbon atoms of the chain. They have low solubility in water at laboratory temperature; treated with acid solutions produce a progressive polymerisation to form amorphous tannins called flavatannins or red tannins. They are in consequence derived by condensation of flavanoid units, being also formed in a long time postmorten metabolic process **[5,6]**.

In spite of their heterogeneity, the vegetable tannins present a series of properties in common. Particularly in 0.4 % aqueous solutions, they produce an intense coloration with iron (III) salts: blue the pyrogall tannins and green the catechol ones. These tannins, in more concentrated solutions, generate an abundant blue black precipitate. This property of the tannins, that is the capacity of forming complex chelates with the iron (III) ion, could be employed to modify the kinetic of oxidation of iron and of steel substrata **[1,7]** . The aim of this paper was the optimisation of the operative conditions for the tannins extraction from the heartwood of quebracho (Schinopsis sp.) and later the determination of their properties, particularly those connected with the reaction of extracted tannins and the hexahydrated iron (III) ion.

EXPERIMENTAL AND RESULTS

1. Preparation of raw material. The sample of quebracho (Schinopsis Lorentzii, Province of Formosa, Argentina) was extracted from a live and healthy tree, discarding all those parts that did not satisfy the before mentioned conditions. Heartwood was only selected since the tannins find almost exclusively in that zone of the tree **[8]**. Observations by means of optical and electron microscopes as well as an histochemistry test were performed; the results indicate the following anatomical characteristics: diffuse-porous wood, solitary pores, simple perforation plates and scanty vasicentric paratracheal parenchyma. The presence of tannins in the heartwood is characterised by secretory radial canals (tanniniferous tubes) and by thickwalled cells caused by tannins impregnation, Fig. 1.

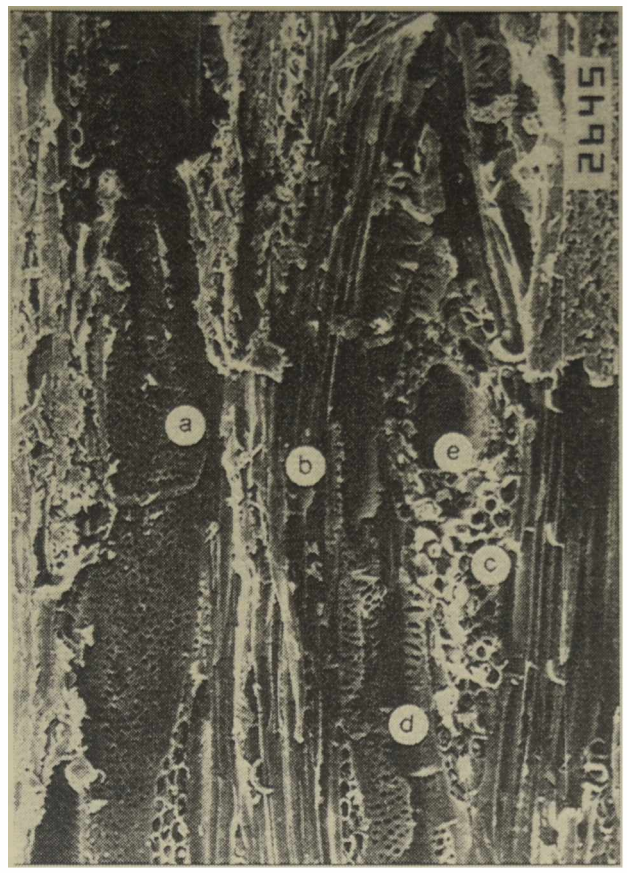

Fig. 1.- Quebracho wood, Schinopsis sp.: longitudinal tangential cross-section (SEM, 200 x). a) Vessel; b) fibres; c) heterogeneous rays; d) parenchyma cells and d) radial secretory canals.

However, other plants possess important quantities of tannins in blades, bark, etc. **[9,10]**.

The sample was cutted in parallel manner and also transversally to the fibrovascular bunches. Afterwards, it was dried in stove at 50 °C until 4-6 % humidity. The determination was performed in a glass dish over 10 g at 100-105 °C up to constant weight (approximately 10 hours).

Later, it was crushed in a hammers mill ; this mill has an axis that turns at great speed, mutually binding to a disk with articulate hammers in the form of cross. The rotor moves in the interior of a chassis supplied with a feeding hopper. Finally, the sample was sieved in 30 mesh.

2. Extraction of the tannins. This is fundamentally an osmotic process through the cellular membranes and was carried out in a high speed stirring disperser. The vertical vessel has a double jacket to permit the heating and to control the temperature. The following factors were taken into account:

2.1. Distilled water / heartwood ratio. The selected ratio was 3 / 1 in weight, since it permits to cover completely the sawdust of the quebracho wood. Major quantity of distilled water would present the inconvenient of diluting excessively the liquor, besides not to get to improve significantly the efficiency of the extraction.

2.2. Number of extractions. This variable influenced meaningfully the quantity of tannins extracted from the quebracho wood (Table I).

Table I

Influence of the number of extractions

	First extraction	Washing						
		1	2	3	4	5	6	Total
Tannins on wood, % in weight	8.9	5.6	2.9	1.8	1.3	1.1	0.8	22.4

Note: Humidity of the quebracho wood, 6.2 %. The content of tannins was determined by applying the method of Lowenthal.

In the first extraction, approximately the half of the water remained retained in the sawdust and the other half corresponded to the liquor. In this experiment, two subsequent washes were performed; in these cases the water employed was the 50 % of the former quantity.

2.3. Temperature. This variable influenced significantly the composition of the extract (Table II). The results indicate that the quantity of tannins extracted and the tannins/no tannins ratio increased with the temperature, reaching the major efficiency at 70-75 °C and 75-80 °C; first rank was selected to avoid the oxidation of the extract. The two final washes were performed at the same temperature.

Table II

Influence of the extraction water temperature

Temperature	Tannins, %	No tannins, %
30-35	57	80
40-45	68	82
50-55	79	85
60-65	88	90
70-75	100	100
75-80	100	100
80-85	91	100

Note :The results correspond to the extract composition at 70-75°C. The content of tannins was determined by applying the method of Lowenthal and the no tannins by difference between the soluble components and the level of tannins.

2.4. Time. To get a high yielding extraction of the tannins without overpassing the quoted temperature, the sawdust was let in macerating with distilled water for 3 hours at laboratory temperature and later 1 hour, with strong agitation, at 70-75 °C. The two subsequent washes were also carried out for 1 hour, in the before mentioned conditions.

The liquor presented a marked turbidity: the concentration was approximately 3° Bé (60 g solid extract/1000 ml liquor) and the pH 5.2. The wood and extract compositions are shown in Table III.

Table III

Composition, % in weight*

	Wood	Extract powder	Dry extract (by calculus)
Tannins**	22-23	60-62	72-74
No tannins***	2-3	6-7	7-8
Insoluble Components	67-70****	15-16	18-19
Humidity	6-7	15-18	----

* Six extractions were made (water/sawdust, 3/1 ratio in weight, 70-75 °C
** Method of Lowenthal
*** It was calculated by difference between the soluble components content and the level of tannins
**** Fibres of wood are included

3. Purification of the liquor. In the composition of the vegetable extracts, the following compounds are conventionally distinguished: tannins, no tannins, water insoluble substances and water **[11]**.

The no tannins are usually glucids, organic acids, phenols, salts, etc. while the water insoluble components (generally they are in suspension or forming sediments) are tannins of high degree of polymerisation (flavatannins or condensed tannins), incapable to keep dispersed due to the effect of remaining components and of hydrolysis products of pyrogall tannins, which are also water insoluble.

A series of dissolved substances like gums, resins, etc. and other of inert type influence the formation of precipitates and sediments which are difficult to separate by filtration due to their characteristics. The solubility of these substances increases with the temperature and also as the concentration does it.

To eliminate these gumresins and the water insoluble components from the liquor, which remained in the liquid in colloidal manner due to their small particle size, the original extract was cooled at 0-2 °C for 24 hours and afterwards centrifuged. The extract was separated in two defined layers, a superior which is clear and other inferior, whose turbidity increased from overhead toward down and that practically contained almost all the water

insoluble substances and the gumresins. These solids were finally washed several times with distilled water to recuperate the tannins retained in them.

4. Concentration of the liquor. To avoid the serious problems derived from the employment of elevated temperatures, which generates losses of tannins and produce darkness of the extract, a system of vacuum concentration (approximately 550- 600 mm Hg) was employed at a temperature inferior to 40 °C. The selected container is made from glass to avoid chemical reactions with the acids present in the liquor. The final extract had a 18-20 °Bé concentration (410- 450 g/1000 ml liquor) and also a clear aspect, that is turbidity free, with a pH remaining between 4.5 and 5.0. For practical effects, acid fermentation was not observed at laboratory conditions which allow to infer that the sugars content in the experimental liquor was reduced.

5. Quantitative determination of tannins: method of Lowenthal. It is based on fact that the tannins are oxidised in solution by potassium permanganate in presence of indigo carmine, which is employed as indicator of the final point **[12,13]**. Taking as reference the titration of a sample of tannic acid, the volume of potassium permanganate of known normality, consumed by the extract of quebracho, was assessed. Since the tannins in the liquor are accompanied by other reducing agents, the tannins were eliminated by coagulation with gelatine.

Afterwards, the content of the remaining reducing substances were evaluated and by difference of both determinations the content of tannins in every solution was calculated. The trials were performed in triplicate, taking the precaution of to carry out them in the same conditions that in the liquor, particularly in relation with addition, dilution and agitation time of chemicals. The results are indicated in Tables I/IV.

6. Characterisation of the tannins solutions. The quebracho wood is very hard and dense (approximately 1.3 $g.cm^{-3}$). Connected with the density of the purified extracts, the values ranged between 1.52 and 1.54 $g.cm^{-3}$, at an humidity of 6 % in weight.

Furthermore, the difference between pyrogall and catechol tannins present in the extracts was qualitatively established; an analytic solution of approximately 0.4 % tannins was employed. This solution, previously acidified with drops of acetic acid, showed abundant precipitation when bromine water is incorporated. This evidenced the presence of catechol tannins; on the other hand, with the addition of a lead acetate solution to the acidified liquor the precipitation was not meaningful, which indicated that the content of pyrogall tannins in the experimental extracts is not quantitatively significant.

7. Oxidation of the quebracho liquor. Chemical composition of the vegetable tannins points out that are condensed phenolic substances and consequently, susceptible to be oxidised **[12,13]**. The oxidation can be initiated in the same raw material, during the process of extraction and also in the liquor concentration. Numerous factors act as catalyst of this process, such as air, light, temperature, pH, etc.

Table IV

Oxidation of the quebracho liquor:
light and air exposure for 30 days, at laboratory temperature

pH		Tannins on dry solid extract			No tannins on dry solid extract			Insoluble components on dry solid extract		
Initial	Final	Wi	Wf	Δ	Wi	Wf	Δ	Wi	Wf	Δ
5.02	4.84	14.624	14.164	-2.16	0.731	0.569	-0.76	5.931	6.580	+3.05
5.73	5.41	15.975	14.929	-4.91	1.278	1.725	+2.10	4.047	4.914	+4.07
6.97	6.39	17.732	16.678	-4.96	1.419	2.093	+3.17	2.105	2.991	+4.17
8.03	7.21	17.783	16.134	-7.74	2.134	3.044	+4.27	1.388	2.639	+5.87
9.14	8.17	17.942	15.777	-10.17	2.871	4.089	+5.72	0.472	1.862	+6.53

Note: Initial pH was adjusted with 0.1 N Na H0 solution
Wi and Wf are, respectively, the initial and final weights in g/100 ml liquor
Δ is the percent variation, in weight on dry solid extract

In this particular case, it was studied the oxidation of the quebracho extract at different values of pH and a concentration of about 10 ° Bé, after 3 hours exposition to light and laboratory ambient.

The analysis of the results shown in Table IV permits to conclude that :

- The water solubility of the quebracho extract, which depends on tannins and no tannins content, increased as the pH increased in the range studied.

- The oxidation originated a considerable loss of tannins, which was more meaningful to higher values of pH.

- The decrease of tannic substances during the oxidation is attributable to their transformation in no tannins and insoluble compounds.

- The oxidation drove to the acidification of the liquor.

8. Iron/tannins reaction

In laboratory tests, several acidified tannins solutions were brushapplied on steel plates with an insufficient mechanical preparation to eliminate all the products of corrosion. Visual and microscopic observations allowed to establish the formation of a blue black layer due to the reaction of the tannins with the residual iron oxides and that furthermore no immediate reaction over the steel exempt from superficial oxides was registered. Consequently, the decision of studying some aspects of the reaction tannins/iron was taken **[1,7]**; the trial was carried out with concentrated extracts and employing different iron (III) salts solutions, at pH placed between 2 and 6. The formation of an abundant blue black precipitate was observed; from a quantitative point of view, the precipitate increased when acidity was reduced. The reaction between the hexahydrated iron (III) ions and the hydroxy phenolic groups gives insoluble chelates and liberates $[H_30]^+$ ions, which explains the major yield of the reaction as the pH increased; pH must be lower than 6 to avoid oxidation reactions (Table IV). A sodium acetate solution was employed to regulate the hydrogenionic concentration between the cited values.

Similar trials were carried out in parallel with iron (II) salts solutions instead of iron (III) ones showed also the formation of a blue black precipitate. Although the divalent cations do not form insoluble compounds with the hydroxy phenolic groups of the tannins, the iron (II) ions are rapidly oxidised to iron (III) ions, specially if the reaction is carried out under conditions in that there is access of oxygen to permit the oxidation and to reduced pH. The reaction of oxidation of the iron (II) ions takes place according to the following way:

$$4\ Fe^{2+} + 2\ H_20 + 0_2 \rightarrow 4\ Fe^{3+} + 4\ 0H^-$$

Considering that the totality of the extract solids are from tannic nature, increasing quantities of the quoted iron (III) salts were added to the solutions, at every pH studied and working under intense stirring, until reaching a maximum mass of the blue black precipitate,

which was determined after centrifuging, washing with distilled water and drying in stove at 50 °C.

The blue black chelates obtained at laboratory temperature showed an iron content, according to atomic absorption determinations, between 2.0 and 2.5 % in weight. The iron tannates are highly water insoluble and in consequence their redissolution is practically impossible; furthermore, they showed a colloidal aspect, that is particles extremely fine, which does not permit the total retention in the filter paper during the step of washing. As a result of that, the separation of precipitates was carried out by centrifuging.

9. Infrared spectrophotometry. The characterisation of the tannins was also performed working in the infrared spectrum, on account of which it was necessary to prepare pills of approximately 0.3 - 0.5 mm in diameter, with a content of 0.1 % of extract or else of tannic acid employed as reference; potassium bromide was used as dispersing agent.

The spectra did not show marked differences between the tested extracts, but demonstrated the presence of polyphenols due to bonds of hydrogen between the hydroxyl ions: maximum of absorption in the 3400-3200 cm^{-1} band were observed in all cases.

Regarding samples of iron tannates prepared at laboratory according to before mentioned conditions, the spectra confirmed a reduced absorption at 3400-3200 cm^{-1} indicating that the formation of iron tannates involves the chelation with the hydroxyl groups of the quebracho tannins structure. Figure 2 show the infrared spectrum corresponding to iron (III) tannates.

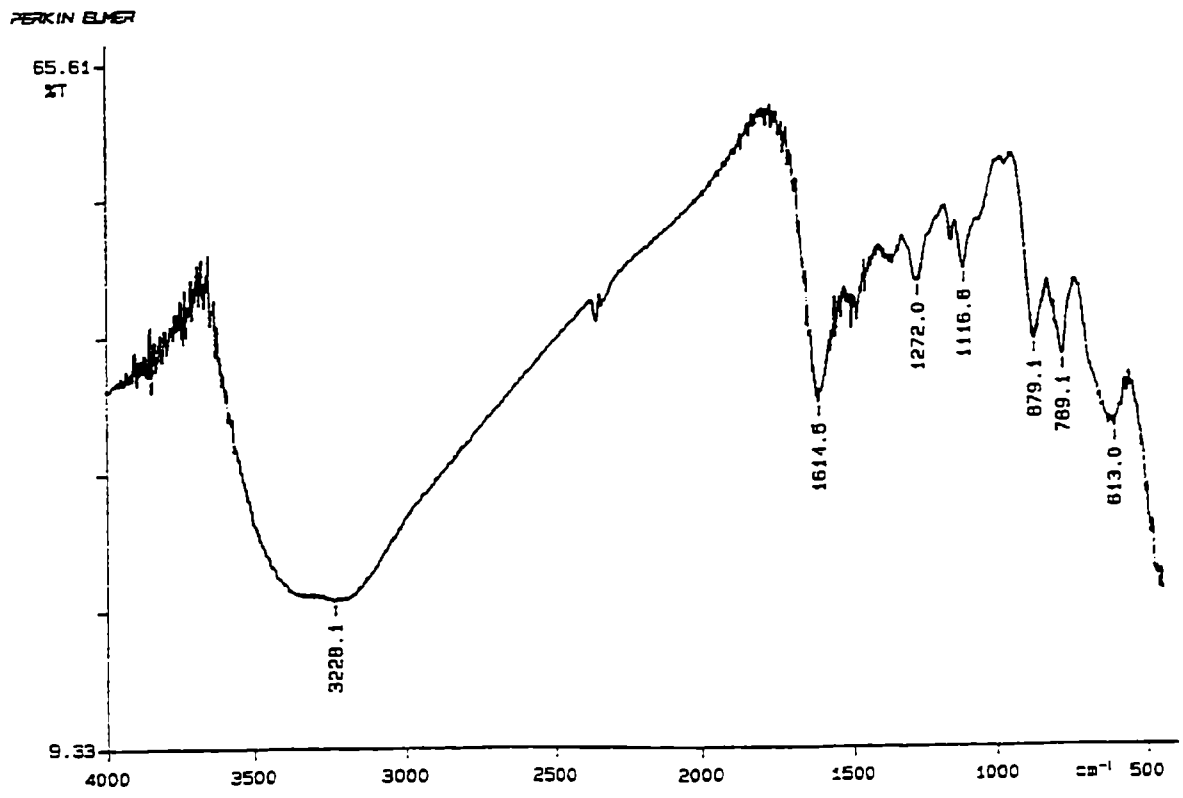

Fig. 2.- Infrared spectrum of iron tannates: the reduced absorption in 3400-3200 cm^{-1} band corresponds to the remaining hydroxy phenolic groups of the original tannins

Future works

In the last years, tannins chemistry has shown a high development and many and different compounds and their corresponding structures have been identified. In spite of the those progresses, the condensed tannins are widely distributed among the plants and, as a consequence, it is very important to carry out extensive researches on this subject and particularly, from corrosion and anticorrosion points of view, the conditions affecting the tannins/iron reactions and the properties of these compounds.

ACKNOWLEDGEMENTS

The authors are grateful to CIC (Comisión de Investigaciones Científicas de la Provincia de Buenos Aires) and to CONICET (Consejo Nacional de Investigaciones Científicas y Técnicas) for their sponsorship of this research and also to Eng. Zicarelli, S. by IR determinations.

REFERENCES

[1] Ohara, S. - **JARQ**, **28** (1), 70 (1994).
[2] Streit, W.; Fengel, D. - **Holzforschung**, **48**, 15 (1994).
[3] Kashiwada, Y.; Nonaka, G.I.; Nishioka, J. - **Chem. Pharm. Bull.**, **34**, 3208 (1986).
[4] Porter, L.J.; Foo, L. Y.; Furneaux, R.H. - **Phytochemistry**, **24**, 567 (1985).
[5] Foo, L.Y.; Karchesy, J.J.- **Chemistry and Significance of Condensed Tannins**, Ed. Hemingway, R.W. and Karchesy, J.J., Plenum Press, New York, 109-118 (1989).
[6] Sealy Fisher, V.J.; Pizzi, A. - **Holz Roh-Werkst**, **50**, 212 (1992).
[7] Yamaguchi, H.; Higuchi, M.; Sakata, J. - **Mokuzai Gakkaishi**, **37**, 942 (1991).
[8] Jane, F.W. - 2nd ed. Adam and Charles Black, London (1970).
[9] Makkar, H.P.S.; Becker, K. – **J. Agricultural and Food Chemistry**, **42**, 731-734 (1994).
[10] Neera, S.; Arakawa, H.; Ishimaru, K. - **Phytochemistry**, **32** (4), 921 (1993).
[11] Streit, W.; Fengel, D. - **Phytochemistry**, **36** (2), 481 (1994).
[12] Erickson, M.; Larsson, S.; Miksche, G.E. - **Acta Chem. Scand.**, **27**, 127 (1973).
[13] Gellerstedt, G.; Gustafsson, K. - **Wood Chem. Techn.**, **7**, 65 (1987).

MANUFACTURE AND TESTING OF WATER-BASED TANNIC PRETREATMENTS

ELABORACION Y ENSAYO DE IMPRIMACIONES TANICAS DE BASE ACUOSA

C. A. Giúdice[1], J. C. Benítez[2], M. L. Tonello[3]

SUMMARY

The anticorrosive efficiency of the different coating systems depends to a great extent on the initial state of the metallic surface, since the best paints do not insure a lengthy protection when they are applied over a structure that is not adequately prepared. In consequence, at present the treatment of the corroded surfaces continues being a great challenge in spite of the modern existing methods, specially when the conditions do very expensive the total removal of oxides or is not practicable by diverse motives.

In a previous work, the purification and the characterisation of tannins extracted from the heartwood of quebracho (Schinopsis sp.) were performed particularly with the objective of knowing some inherent properties of the reaction between the tannins and the iron oxides. In the present work, several water-based tannic pretreatments acidified with orthophosphoric acid were formulated and manufactured at laboratory scale; results of tests carried out allowed to conclude that the application of the quoted tannic solutions on a substratum with a mechanical preparation insufficient to eliminate the totality of the products of corrosion, increased the useful life of the applied coating system, delaying oxidation and in consequence the deterioration of the subsequent paint films.

Keywords: *rusted steel, pretreatment, tannins, coating system, practical adhesion, degree of rusting.*

INTRODUCTION

In the last years important developments in corrosion-inhibiting coatings were achieved, but the anticorrosive efficiency also depends significantly on the surface preparation, since the very good paints inclusive do not insure a lengthy protection if they are applied over a surface that is not totally free of iron oxides **[1,2]**.

The treatment of the corroded surfaces continues being a great challenge, in spite of the existing methods. In the case of a totally rusty metal, the cleanliness by sandblasting or

[1] Miembro de la Carrera del Investigador del CONICET; Profesor Adjunto, UTN
[2] Miembro de la Carrera del Investigador de la CIC
[3] Becario de Perfeccionamiento de la CIC

gritblasting generates a surface of excellent characteristics to apply the coating system; but in some cases, the blastcleaning can not be selected by the high cost, by operative problems of the structure to protect, by the difficulties in achieving an adequate coordination of the surface preparation/application of the first layer of the coating system or for ecological problems. Other mechanical treatments (brush and sandpaper cleaning, etc.) do not result efficient to eliminate completely corrosion products, particularly in pits generated by the metal dissolution as a consequence of the anodic reaction **[3-6]**.

Pretreatments based on different mineral acids present also serious limitations; salts formed in the metal/surface usually generates abundant osmotic blistering. Regarding solutions of orthophosphoric acid, they do not give a true passivity since the reaction with different layers of iron oxides is markedly heterogeneous **[7]**.

Researches carried out in many institutes of different countries employing natural products of high molecular weight to form stable complexes with the iron oxides purport to obtain an homogeneous reaction with the products of the metallic corrosion **[8-10]**. Particularly and owing to the commercial significance, tannins extracted from the quebracho wood have been object of numerous studies; these natural tannins react rapidly with the soluble iron salts forming intense blue black precipitates; the hexahydrated iron (III) ions and the hydroxy phenolic groups present in the condensed tannins gives insoluble chelates and liberates $[H_30]^+$ which explains the major yield of the reaction as the pH increases. It is not convenient to exceed the pH 6 due to meaningful loss of tannins by oxidation **[11-16]**. Regarding the iron (II) salts in solution, although they do not form insoluble compounds with the hydroxy phenolic groups of condensed tannins; the $[Fe\ (H_20)_6]^{2+}$ ions are rapidly oxidised to $[Fe\ (H_20)_6]^{3+}$, specially if the reaction is carried under conditions where there is an access of oxygen to permit the oxidation and to values of reduced pH. In consequence iron (II) salts solutions instead of iron (III) ones also show the formation of blue black precipitates.

In this work diverse formulation variables of aqueous pretreatments based on tannins extracted from heartwood of quebracho (Schinopsis sp.) were studied. These water-based tannins solutions were applied over steel plates with a mechanical preparation insufficient to eliminate completely the corrosion products with the objective of establishing the influence of that variable on the anticorrosive capacity of a coating system.

EXPERIMENTAL PART

1. Extraction and purification of the tannic liquor

The sample of quebracho (Province of Chaco, Argentina) was extracted from a live and healthy tree, selecting only heartwood **[17]**. The sample was cutted, dried in stove at 50 °C until 4-6 % humidity and finally crushed in a hammer mill, choosing the fraction that passes by the 30 mesh sieve.

The extraction was carried out in a vessel with a double jacket to permit the heating (70-75 °C), employing a 3/1 distilled water/heartwood ratio in weight and stirring intensely for 1 hour. The first extraction was performed in the quoted conditions while the two subsequent

washes were fulfilled in similar way but employing only the 50 % of water due to a half remains retained in the sawdust and the other one forms the liquor.

Afterwards the tannic liquor was purified to eliminate the gumresins and the insoluble components, which remain in the liquid in the colloidal state due to their small particle size. The original extract was cooled at 0-2 °C for 24 hours and then centrifuged, collecting the free-turbidity superior layer; the solids were finally washed several times with distilled water to recuperate the tannins retained.

Later, the concentration of the liquor was carried out employing a vacuum system (approximately 550-660 mm Hg at 40 °C) to avoid the serious inconveniences that generate the elevated temperatures (oxidation and loss of tannins). The final concentration was 18-20 °Be (410-450 g solid extract/1000 ml liquor) with a pH remaining between 4.5 and 5.0 according to the experiment.

An analytic solution of the purified liquor (0.4 % solids w/w) evidenced, previous acidification with drops of acetic acid, an abundant precipitate formation with the incorporation of bromine water, which indicated the presence of catechol tannins (structure strongly polymerised, with bencenic ring bonded by carbon chain); on the other hand, with the addition of a lead acetate solution to the acidified liquor, the precipitation was not significant which demonstrated that the content of pyrogall tannins (structure weakly polymerised, polyester type) is not quantitatively important in the extracts of the quebracho heartwood **[11]**.

The method of Lowenthal allowed to determine quantitatively the content of tannins in the purified liquor **[9]**; it is based on fact that the tannins are oxidised in solution by the potassium permanganate in presence of indigo carmine, which is employed as indicator of the final point. The results point out the presence of 17.5 g of tannins, over 100 g of wood with a humidity of 6.3 % (one extraction and two subsequent washes in the quoted conditions) or else approximately the 91.0 % in weight of tannins over the dry extract free of insoluble components.

2. Water-based tannic pretreatments

The pretreatments were prepared in aqueous solution with different concentrations of tannins, which ranged from 2.5 to 20.0 % in weight. The pH of the solutions was regulated with an orthophosphoric acid solution until reaching values between 1.5 and 4.5 with variations of 0.5 each time. Furthermore, a wetting agent at 0.2 % level in weight was employed; 56 samples in duplicate were elaborated (8 concentrations of tannins x 7 levels of pH).

3. Test panels

a) Surface preparation

SAE 1010 steelplates were chemically pickled and sandblasted to Sa 2 ½ degree (SIS 05 59 00/67 Standard, 32 μm maximum roughness) and then exposed to natural weathering in

the CIDEPINT experimental station (Table I), until reaching the total oxidation of the surface [5]. Later the corrosion products not adhered to the metallic base were eliminated by rubbing with sandpaper, observing a similar degree to C St 2 of quoted standard; afterwards the panels were washed with toluene in vapour phase.

Table I

CIDEPINT experimental station, La Plata (Argentina)

Geographic position	Latitude Longitude	34° 50' S 57° 53' W
Atmospheric conditions, 1994/1995	Mean temperature, °C Mean relative humidity, % Amount of rain, $mm.year^{-1}$ Mean sulphur dioxide, $mg.m^{-2}.day^{-1}$	16.7 78.8 1104 6.6
Corrosion rate, 1994/1995	Steel, $mg.dm^{-2}.day^{-1}$	5.44

b) Application of the tannic solution and the protective system

A coat of tannic pretreatments was brush applied in each case. The time of reaction (4 and 8 hours) was considered as operative variable, which elapsed in laboratory ambient (relative humidity, 62-65 %; temperature, 15-18 °C).

The coating system, also applied by brush, was constituted by one film of the corrosion-inhibitive coating (40 ± 5 μm dry film thickness), one of the intermediate coating or sealer (25 ± 5 μm) and finally two top coats (40 ± 5 μm). The coating composition is shown in Table II, carrying out the preparation in a ball mill with porcelain jars of 1.0 litre total capacity.

Moreover, two test panels were prepared to be used as reference by applying directly the coating system on the weathered-sanded metallic base, without tannic pretreatment. Other two test panels included as pretreatment a single coat of a 15 % orthophosphoric acid solution.

c) Experimental trials

The whole of the prepared panels were placed in a frame and then subjected to natural weathering for 24 months. The specimens were exposed at 45 ° facing to the north. On the aged panels, the following laboratory trials were performed:

Table II

Composition of coatings, % in weight on solids*

Component	Anticorrosive coat	Sealer	Top coat
Titanium dioxide	-	-	38.2
Zinc hydroxy phosphite	33.7	-	-
Micaceous iron oxide	-	41.9	-
Red iron oxide	16.7	-	-
Micronised barytes	-	6.1	-
Micronised talc	16.8	3.1	-
Chlorinated rubber grade 20	23.0	34.2	15.3
Medium oil alkyd resin **	-	-	45.9
42 % chlorinated paraffin	9.8	14.7	-
Driers	-	-	0.6
PVC, %	45.0	25.0	15.0

* Solvent mixture: Aromasol H/white spirit, 4/1 ratio in weight
** From soya bean oil (70 % solids)

d) Degree of rusting

A visual and microscopic judgement was carried out by employing the ASTM D 610 Standard, whose scale ranges from 0 (approximately 100 % of the surface rusted) to 10 (no rusting or less than 0.01 % of the surface rusted). The intermediate values are: 9, less than 0.03 % of surface rusted; 8, less than 0.1 % ; 7, less than 0.3 %; 6, less than 1 %; 5, approximately 3 % ; 4, approximately 10 % ; 3, approximately 1 / 6 of the surface rusted; 2, approximately 1 / 3 and finally 1, approximately 1 / 2 of surface rusted.

e) Practical adhesion

The evaluation of the film adhesion was carried out by employing an Elcometer Tester Model 106, according to ASTM D 4541 Standard. The instrument is direct reading and does not include the frictional forces of the nut and bearing assembly. It has a base support ring to avoid bending of thin substrata and a cutter to remove the excess of adhesive (twin-pack epoxy resin) from around the base of the dolly.

The dolly is bonded to the coating under test; when adhesive has cured, the adhesion Tester is placed over the dolly and the claw engaged. The dragging indicator is set to zero.

Bonded dolly is subjected to progressively increasing stress at a constant rate until it fractures: dragging indicator retains the maximum pull of force reached. About 10 determinations on every test panel were performed and then the mean values were calculated.

RESULTS AND DISCUSSION

Experimental values of rusting degree as well as of the practical adhesion obtained from test panels exposed to natural weathering for 24 months are presented, respectively, in Tables III and IV. These results were statistically treated according to factorial design of the 2 x 7 x 8 type, that is 112 different combinations; each combination was prepared and tested in duplicate (replicas).

The values shown in Tables III and IV were used to calculate the sum of squares and the degrees of freedom of each effect; by dividing each sum of squares by the corresponding degrees of freedom, the estimated variance was calculated. Hypothesis zero implying that all the main effects are equal to zero, is accepted. Thus all the variance estimations would be independent and would refer to the same estimated amount by means of the residual variance, that is the magnitude of the experimental error. If the variance of the cited sources is bigger than that based on the residual error (experimental), the F test indicates that it is little probable that the observed variances ratio occurred randomly. If the F test gives a positive result, the hypothesis zero fails. In such case, it will be evident that the variance does not simply arise from the experimental error, but also from an additional variance introduced by the fact that the design modification was meaningful.

The F test indicates that the influence of the main effects studied is significant. To interpret the experimental results, the sum of the main effects were considered, Table V. As a consequence, it is concluded that to reach the **best anticorrosive protection** it is necessary to take into account the concentration of orthophosphoric acid which leads to a value of pH 1.5, the level of 20.0 % in weight of tannins and finally regarding time of reaction, to let to elapse 8 hours in ambience of laboratory before application of the first layer of the coating system.

The results also indicate that the **incorporation of orthophosphoric acid** to the tannic solutions drove to pretreatments which showed an increased corrosion resistance and furthermore an improved film adhesion, which is in agreement with the conclusions attained in the statistical study. It is convenient to mention that the tests demonstrated that to reach a satisfactory stabilisation of the metallic oxides was more effective the employment like pretreatment of some tannic solution acidified with orthophosphoric acid instead of a 15 % orthophosphoric acid solution.

After application of the pretreatment, the phosphoric acid firstly reacts with the iron oxides, furthermore, in presence of oxygen and to a strongly acid pH, the iron (II) ions are oxidised rapidly to iron (III) ions. As the pH of the solution increases by the neutralisation reactions on the metal surface, the formation of a blue black insoluble layer of iron (III) tannates is favoured. This reticulated layer would delay the oxidation reactions on the metal and in consequence the deterioration of the protective system.

Table III

Degree of rusting (ASTM D 610)
24 months of natural weathering (La Plata Station)

1. Tannic primers (4 hours) and coating system

pH of tannic solution	Level of tannins, % in weight							
	2.5	5.0	7.5	10.0	12.5	15.0	17.5	20.0
1.5	4	5	5	5	6	6	7	7
2.0	4	5	6	6	6	6	6	7
2.5	4	4	5	5	5	5	5	6
3.0	4	4	4	4	5	5	5	6
3.5	4	4	4	5	5	4	5	6
4.0	3	4	4	5	4	4	5	5
4.5	3	4	4	4	4	4	5	5

2. Tannic primers (8 hours) and coating system

pH of tannic Solution	Level of tannins, % in weight							
	2.5	5.0	7.5	10.0	12.5	15.0	17.5	20.0
1.5	6	6	6	7	8	9	9	10
2.0	5	5	6	6	8	9	9	9
2.5	5	5	5	6	8	9	9	9
3.0	4	5	5	6	8	8	8	8
3.5	4	5	5	5	7	7	7	8
4.0	4	5	5	5	7	7	7	7
4.5	4	5	5	5	6	7	7	7

3. Coating system (15% orthophosphoric acid solution like pretreatment)
Degree of rusting = 5

4. Coating system (test of reference, without any pretreatment)
Degree of rusting = 4

Table IV

Practical adhesion, $kg.cm^{-2}$
24 months of natural weathering (La Plata Station)

1. Tannic primers (4 hours) and coating system

pH of tannic Solution	Level of tannins, % in weight							
	2.5	5.0	7.5	10.0	12.5	15.0	17.5	20.0
1.5	6	7	7	7	8	9	10	10
2.0	6	7	7	7	8	8	9	10
2.5	6	6	7	7	7	7	9	9
3.0	5	5	6	7	7	7	9	9
3.5	5	5	6	7	7	6	8	9
4.0	5	5	5	6	6	6	8	9
4.5	4	5	5	6	6	6	7	8

2. Tannic primers (8 hours) and coating system

pH of tannic solution	Level of tannins, % in weight							
	2.5	5.0	7.5	10.0	12.5	15.0	17.5	20.0
1.5	7	8	8	9	10	11	12	13
2.0	7	8	8	9	9	11	11	12
2.5	7	7	7	8	9	10	11	11
3.0	6	6	7	9	8	9	10	11
3.5	6	6	7	8	8	9	9	11
4.0	5	6	6	7	8	9	9	10
4.5	5	6	6	7	8	9	9	10

3. Coating system (15% orthophosphoric acid solution like pretreatment)

Practical adhesion* = 7 kg . cm^{-2} (24 month weathering)
Practical adhesion* = 11 kg . cm^{-2} (72 month drying)
* Type of failure: almost completely adhesive (90 %)

4. Coating system (test of reference, without any pretreatment)

Practical adhesion* = 6 kg . cm^{-2} (24 month weathering)
Practical adhesion* = 10 kg . cm^{-2} (72 month drying)
* Type of failure: completely adhesive (100 %)

Table V

Statistical results

Main effect		Sum of the main effects	
Type	Level	Degree of rusting	Practical adhesion
Tannins, %	2.5	58	80
	5.0	66	87
	7.5	69	92
	10.0	74	104
	12.5	87	109
	15.0	90	117
	17.5	94	131
	20.0	100	142
PH	1.5	106	142
	2.0	103	137
	2.5	95	128
	3.0	89	121
	3.5	85	117
	4.0	81	110
	4.5	79	107
Time of Reaction, hours	4	271	389
	8	367	473

Regarding the **concentration of tannins** in the water-based pretreatments formulated, this variable showed a great influence on the protective efficiency. Microscopic observations permitted to determine that a great quantity of iron oxides remained on the surface after finishing the cleanliness carried out with sandpaper, previous to the pretreatment application. The surface showed pits and many iron oxides were in the interior. The tannic solutions wetted those oxides and so a great quantity of iron tannates was observed in the places where the thickness of the layer of iron oxides was major. The solutions with high content of tannins presented a more homogeneous action on the surface, which would explain the best performance reached with 20 % tannins in solution acidified at pH 1.5: the blue black chelates obtained at room temperature showed an iron content, according to atomic absorption determinations, between 2.0 and 2.5 % in weight, which would explain the before mentioned.

In consequence, the initial condition of the metallic base (roughness of the surface and mainly the remaining quantity iron oxides previous to the application of the tannic solution) would be an important variable to be considered to define the optimum level of tannins in the pretreatment composition.

Concerning the **time of reaction**, the panels with a single coat of pretreatment showed the formation of the mentioned reticulated insoluble layers just after some hours. It was evident that the tannins had not reacted completely with the corroded surface after 4 hours in laboratory ambient since brown tannic solution without reacting existed in some areas more than the blue black iron tannates. After 8 hours in the cited conditions, the reaction was completed and areas of tannins without reacting were not observed.

However, tests carried out parallely to those included in this work indicated that the optimum reaction time depends on the relative humidity of the environment in that the panels are placed after application of the tannic solution. The specimens maintained at low relative humidity (15-18 °C) showed a low rate of dark chelate formation, while at high relative humidity (i.e. 80 %) complete changes were observed.

FINAL CONSIDERATIONS

1. The visual and microscopic observation permitted to conclude that the yellow/red colour corresponding to the layer of hydrated iron oxides, after application of a tannic pretreatment, evolved toward the blue black one, making it more intense as the time was elapsing. The pretreatments with very good corrosion inhibiting behaviour (minor degree of oxidation and major value of practical adhesion) registered the cited change of color in all the thickness of the layer of iron oxides, according to observations carried out in cross sections on pretreated panels.

2. The practical adhesion performed on aged panels showed that the employment of some no polluting water-based pretreatment formulated in addition to modify the absolute fracture values, influenced on the type of failure. In spite of the high scatter of values observed, some tannic pretreatments presented an almost completely adhesive failure (break between the paint film and the substratum), but as the anticorrosive efficiency increased the coating system failed in the adhesive/cohesive form, reaching a totally cohesive fracture (cracking of the film) with the best formulated pretreatment.

3. Reference panels, without any pretreatment, showed a similar behaviour to those in which no efficient acidified tannins solutions were applied. As a consequence, the low degree of rusting and the high practical adhesion registered with some of the tannic pretreatments formulated indicate that the molecules of the purified condensed tannins extracted from the heartwood of quebracho develop complex chelates with the iron oxides on the metallic surface in the form of reticulated insoluble layers which would improve the useful life of the subsequent coating system.

ACKNOWLEDGEMENTS

The authors are grateful to CIC (Comisión de Investigaciones Científicas de la Provincia de Buenos Aires) and to CONICET (Consejo Nacional de Investigaciones Científicas y Técnicas) for their sponsorship of this research.

REFERENCES

[1] Bagchi, D.- **Finish**, **1** (2), 25 (1994).
[2] Hare, C.H.- **J. of Prot. Coat. Linings**, **10** (1), 57 (1993).
[3] Matamala, G.; Smeltzer, W.; Droguett, G.- **J. Sci. Eng. Corros.**, **50** (4), 270 (1994).
[4] Feliú S.- **Corros. Sci.**, **35** (5-8), 1351 (1993).

[5] Pfefferkorn, J.- **Applica, 101** (20), 12 (1994).
[6] Feliú, S.; Morcillo, M.; Feliú Jr, S.- **Corros. Sci., 34** (3), 403 (1993).
[7] Jenal, L.- **Applica, 100** (21), 32 (1993).
[8] Morcillo M. et al.- **J. Sci. Eng. Corros., 48** (12), 1032 (1992).
[9] Des Lauriers, P.J.- **Materials Performance, 26** (11), 35 (1987).
[10] Favre, M.; Landolt, D.- **Corros. Sci., 34** (9), 1481 (1993).
[11] Pizzi, A.; Meikleham, N.- **J. Applied Polym. Sci., 55** (8), 1265 (1995).
[12] Pizzi, A.; Meikleham, N.; Stephanov, A.- **J. Appl. Polym. Sci., 55** (6), 929 (1995).
[13] Pizzi, A.; Stephanov, A.- **J. Appl. Polym. Sci., 50** (12), 2105 (1993).
[14] Pizzi, A.; Stephanov, A.- **J. Appl. Polym. Sci., 51** (13), 2109 (1994).
[15] Pizzi, A.; Stephanov, A.- **J. Appl. Polym. Sci., 51** (13), 2125 (1994).
[16] Baecker, A.; Schnippenkoetter, W.; Shelver G.; Scherer, U.- **Material und Organismen, 26** (4), 269 (1991).
[17] Streit, W.; Fengel, D. – **Phytochemistry, 36** (2), 481 (1994).

TIN TANNATES AND IRON TANNATES IN CORROSION-INHIBITING COATINGS

TANATOS DE ESTAÑO Y TANATOS DE HIERRO EMPLEADOS COMO PIGMENTOS INHIBIDORES EN PINTURAS ANTICORROSIVAS

C.A. Giúdice[1], J.C. Benítez[2], M.L. Tonello[3]

SUMMARY

The efficiency of the coating systems in the protection of metallic substrata depends fundamentally, in relation with formulation variables, on the type and content of corrosion-inhibitive pigment, the characteristics of the film forming material and the pigment / binder ratio in volume.

Concerning the pigment, there is not doubt that the use of some inhibitors in anticorrosive paints is actually an important source generating toxicity problems both for the worker and for the environment. This problem is extended to the applicator and also to the removal operation of old coatings.

In this research tin tannates and iron tannates were employed as inhibitive pigments in anticorrosive paints. The mentioned metallic tannates were prepared on laboratory scale under controlled operative conditions, carrying out the reaction between the metallic ions and the polyphenolic groups of condensed tannins extracted from "quebracho" heartwood (Schinopsis sp.)

Keywords: *corrosion, paint, pigment, inhibitor, iron tannates, tin tannates*

INTRODUCTION

The general term corrosion is commonly defined as the alteration of a material promoted by the environment. In considering the nature of the medium, metallic corrosion includes a chemical attack or an electrochemical one; environments that produce electrochemical process are characterised by their ionic conduction. As a consequence, iron and steel oxidation reaction is usually of an electrochemical type and very complex; it occurs not only on naked metallic substrata, but on those surfaces apparently covered by coatings. In the last years, the environmental pollution has led to enhance corrosion processes.

The function of an organic or inorganic film is to retard the phenomenon. From a physicochemical point of view, a coating is a system formed by dispersion of a solid or a mixture of solids (pigments) in a liquid medium called vehicle. Proper selection of the different

[1] Miembro de la Carrera del Investigador del CONICET; Profesor Adjunto, UTN
[2] Miembro de la Carrera del Investigador de la CIC
[3] Becario de Perfeccionamiento de la CIC

components for each formulation allows the required properties of a coating or coatings to be achieved. Anticorrosive paints usually contain compounds as pigments which are particularly hazardous and besides contribute to the mentioned pollution **[1,2]**.

Owing to the toxicity of conventional pigments and also to legal restrictions in force, many studies are carried out about non-toxic inhibitors **[3-11]**. Phosphates, ferrites, borates, molybdates and also silicates have been proposed; barrier pigments with lamellar structure as micaceous iron oxides were found to be effective for decreasing the corrosion rate of painted surfaces.

The aim of this paper was to carry out at laboratory conditions the elaboration of tin tannates and iron tannates to be used as non-toxic inhibitors, the assessment of their most important characteristics and finally the evaluation of the protective efficiency of formulated anticorrosive paints.

EXPERIMENTAL PART

1. Iron tannates and tin tannates preparation

1.1. Flavatannins extraction. The heartwood of "quebracho colorado" (Schinopsis sp., Province of Chaco, Argentina) was selected for carrying out the experiment; the sample was extracted from a live and healthy tree. The lixiviation of condensed tannins was performed according to the conditions mentioned in previous papers **[12,13]**. The method consisted of the crushing of the wood in a hammer mill previous drying in stove to 50 °C (4-6 % humidity), the maceration of the sawdust for 3 hours at room temperature and then for 1 hour at 70-75 °C under strong stirring (3/1 distilled water/sawdust ratio in weight), and finally the achievement of two subsequent washes to improve significantly the efficiency of the extraction.

The extracts presented marked turbidity, with a concentration of approximately 3 °Bé (60 g solid extract/1000 ml liquor) and a pH 5.2 . The composition of the extracts, expressed on dry solids, was 72-74% of tannins (method of Lowenthal), 7-8 % of no tannins (difference between the contents of the soluble components and the level of tannins) and finally 18-19 % of insoluble substances (without considering the fibres of the wood).

The extracts were purified to eliminate the gumresins and the water insoluble components, which remained in the liquid in colloidal form due to their small particle size; they were separated by centrifuging previous cooled at 0-2 °C for 24 hours. Finally, the extracts were concentrated by means of a system operating to vacuum (approximately 550-600 mm Hg), at a temperature inferior to 40 °C, reaching a final value of 18-20 °Bé (410-450 g / 100 ml liquor). These extracts showed a clear aspect, that is turbidity free, with a remaining pH between 4.5 and 5.0.

These final extracts were qualitatively characterised employing an analytic solution of 0.4 % tannins, previously acidified with drops of an acetic acid solution: abundant precipitation was observed with bromine water which indicated the presence of condensed tannins and

practically absence of precipitation with a lead acetate solution which permits to conclude that the concentration of pyrogall tannins is not meaningful from a quantitative viewpoint in the heartwood of "quebracho" employed in the experiment.

1.2. Inhibiting pigment preparation. The manufacture was carried out starting from concentrated extracts and heptahydrated iron sulphate or else dihydrated tin chloride at room temperature and under controlled conditions. The reaction between the cations and the hydroxy phenolic groups of the condensed tannins in both cases was immediate, generating a blue-black precipitate with the iron and a light brown one with the tin; the before mentioned precipitates were called iron tannates and tin tannates, respectively.

Metallic tannates were separated by centrifuging, washing with distilled water and finally drying at 50 °C until constant weight. Several trials were performed to determine the characteristics of the metallic tannates.

2. Paints formulation

2.1. Pigmentation. Experimental samples included either as inhibitor iron tannates or tin tannates manufactured according to the before described method. The zinc tetroxychromate was taken as reference pigment owing to the efficient behaviour showed up to now ; the current tendency is to proceed to its replacement due to carcinogenic action that it would present on the human being.

In all the cases, other two pigments were used together: red iron oxide and micronised talc, 50 / 50 ratio in volume. The inhibitor/inert pigment ratios were 30/70, 40/60 and 50/50 in volume.

2.2. Film forming material. The corrosion-inhibitive capacity of a paint depends, among several variables, on the active pigment as well as on the film forming material.

In this work the behaviour of paints pigmented with the quoted metallic tannates and based on an epoxy binder was studied. The epoxy binder consisted of a base with a weight per epoxide WPE about 450 and a polyamineamide hardener with an amine value in the 210-220 range. The solvent mixture, expressed as % w/w, was 42.7 % xylene, 14.6 % butanol and 42.7 % oxygenated hydrocarbon. Clay modified with gel-like amines was added as rheological agent after finishing the pigment dispersion (1 % w/w on the coating).

2.3. Pigment level. Generally, the corrosion-inhibiting paints are formulated with a pigment volume concentration lightly less than the critical pigment volume concentration (CPVC), where just sufficient binder is present to fill the voids between the pigment particles **[14]**.

CPVC was estimated by carrying out determinations of permeability of free films by applying the Gardner method **[15]**; the trials were made in triplicate, averaging the results

obtained. Afterwards, the experimental values were plotted in function of PVC considered, which ranged from 30.0 to 50.0 %, with increases in 5.0 % each time. To obtain CPVC the curves were adjusted to the polynomial equation $y = A + Bx + Cx^2 + Dx^3$ through a regression method and calculating the root of the second derivative (inflexion point). Experimental CPVC values ranged from 38 to 42 %. Finally, taking into account those results the PVC values were selected: 35.0 and 40.0 %.

3. Paint manufacture

It was performed at laboratory scale in triplicate by employing a porcelain jar ball mill of 1.0 liter of total capacity. Mill operative conditions were specially considered with the aim to achieve an efficient pigment dispersion **[16]**.

Firstly, a solution of epoxy resin in the solvent mixture was prepared with stirring. The ball mill was loaded with the mentioned vehicle and the pigments were added; these components were milled for 24 hours previous incorporation of a dispersant in the quantity indicated by the manufacturer. After pigment dispersion, the rheological agent was added by employing a high speed agitation equipment .

The hardener was mixed with the base of the paint in the ratio suggested by the manufacture (2/1 epoxy resin/hardener ratio in weight) before its application.

4. Experimental tests

SAE 1010 steel plates of 150 x 80 x 2 mm were used for the tests. The plates were previously sandblasted to **Sa** 2 ½ (SIS Specification 05 59 00/67), with a 40 μm maximum roughness (Rm); then they were cleaned and coated with the experimental paints by brushing. A dry film thickness of 80 ± 5 μm was obtained; paints were applied with an interval of 24 hours between coats. Tests were performed at 20 ± 2 °C, seven days after the application of paints for curing.

4.1. Salt spray (fog) testing. Painted plates were exposed in a salt spray chamber adjusted to ASTM B 117: temperature 35 °C, continuous spraying with 5 % sodium chloride solution of pH 6.5-7.2 **[17]**. All panels were assessed for 500, 1000 and 1500 hour testing: degree of rusting according to ASTM D 610 was determined. Tests were carried out in triplicate and then mean values were calculated.

4.2. Film adhesion. A great number of tests are often used in an attempt to measure film adhesion; different methods would give very dissimilar values: they would depend on substrate/film interface size and shape, force application rate, test temperature, etc. In spite of the mentioned difficulties, it is possible to select a method to determine adhesion performance and to obtain relatively precise data by controlling those factors which influence the results: a known variation would lead to establish differences in performance. The Elcometer Tester Model 106 (ASTM D 4541) was used to determine adhesion on coatings after 1500 hours in salt spray chamber. Ten determinations at room temperature (20 ± 2 °C) were made to minimise the results scattering. The fracture values of the studied paints were expressed with

respect to the aged binder after 1500 hours in salt spray chamber (80 ± 5 μm dry film thickness).

4.3. 100 % relative humidity chamber. Other series of panels were placed in an enclosed chamber containing a heated, saturated mixture of air and water vapour according to ASTM D 2247. The surfaces were observed at 500, 1000 and 1500 hours of testing. The degree of blistering was evaluated by using ASTM D 714; blistering corresponded to the osmotic phenomenon, that is the blistering exclusively promoted by water diffusion through the paint film and not from rusting. This test was also made in triplicate.

RESULTS AND DISCUSSION

Typical properties of metallic tannates

Atomic absorption determinations permitted to assess the capacity of forming complex of condensed tannins in the used conditions. The values ranged between 2.0 and 2.5 % for iron and between 4.5 and 4.8 % for tin, both of them in weight on the corresponding metallic tannates.

Particles of metallic tannates showed a small mean size and in consequence a large specific area, Table I. These characteristics agree with the visual conclusion: precipitates are extremely fine and so they can not be retained in their totality by filter paper. Furthermore, microscopic observations allowed to determine some hydrophobic characteristics of the pigments, that is that the particles of both metallic tannates are repelled by drops of water.

Table I

Typical properties of metallic tannates

Property	Iron tannates	Tin tannates
Colour	Blue black	Light brown
Density, $g.cm^{-3}$	1.52/1.54	1.54/1.56
Oil absorption, g/100 g	20.4	20.3
Particle size (50.0/50.0 %), μm	2.9	2.7
Specific surface area, $m^2.g^{-1}$	1.2	1.3
Fe, % by weight	2.0-2.5	-----
Sn, % by weight	-----	4.5-4.8
Na, % by weight	0.6	0.1

Other properties of iron tannates and tin tannates are assembled in Table I. Figures 1 and 2 show the infrared spectrums corresponding to tin tannates and iron tannates, respectively. In both cases, the reduced absorption in 3400-3200 cm^{-1} band corresponds to the remaining hydroxy phenolic groups of the original tannins.

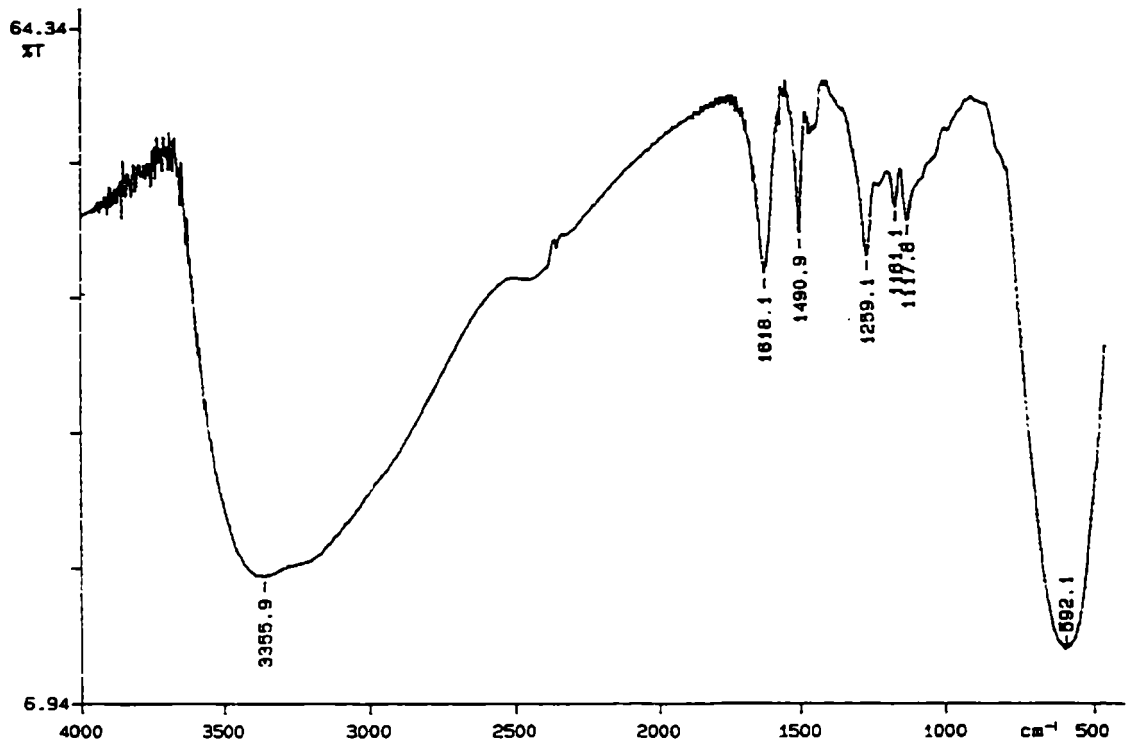

Fig. 1.- Infrared spectrum of tin tannates.

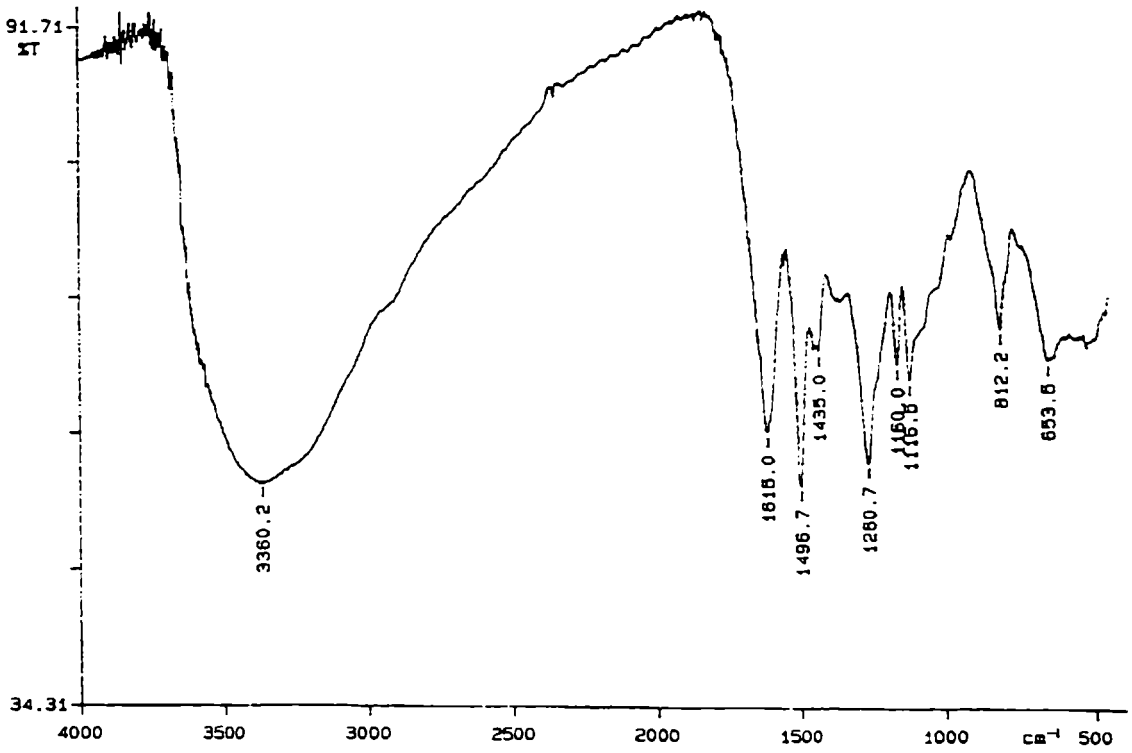

Fig. 2.- Infrared spectrum of iron tannates.

Degree of rusting and practical adhesion

The results obtained in salt spray testing (degree of rusting) and practical adhesion (tension of fracture) were statistically treated according to a factorial design of the 2 x 2 x 3 type (two pigments, two pigment volume concentrations and three inhibitive pigment/inert pigment ratios, that is 12 combinations); every combination included replicas. The values assembled in Tables II (degree of rusting) and III (practical adhesion) were used to calculate the estimated variance and afterwards the F test was carried out **[18]**. The tables mentioned **[19]** indicate that PVC and inhibitive pigment/inert pigment ratio (effects P and R, respectively) showed a meaningful influence on the paint behaviour while the type of inhibitive pigment (effect T) displayed an action devoid of significance.

Table II

Salt spray (fog) testing (ASTM B 117)
Degree of rusting (ASTM D 610)*

Inhibitive pigment	Inhibitive pigment/ inert pigment ratio	PVC, %	Time, hours		
			500	1000	1500
Iron tannates	30/70	35.0	9	7	6
	40/60		10	9	8
	50/50		9	9	8
	30/70	40.0	9	8	8
	40/60		10	10	9
	50/50		10	10	9
Tin tannates	30/70	35.0	8	8	7
	40/60		9	9	7
	50/50		10	9	8
	30/70	40.0	10	9	9
	40/60		10	10	9
	50/50		10	10	9
Zinc tetroxychromate	30/70	40.0	9	9	8

* Key of the table: rust grade 10, no rusting or less than 0.01 % of surface rusted; 9, less than 0.03 % of surface rusted; 8, less than 0.1 % of surface rusted; 7, less than 0.3 % of rusted; 6, less than 1.0 % of surface rusted.

Table III

Practical adhesion, 1500 hour salt fog testing (relative to aged binder)

Inhibitive pigment	Inhibitive pigment/ inert pigment ratio	PVC, %	Fracture value, adimensional unit
Iron tannates	30/70	35.0	1.43
	40/60		1.64
	50/50		1.71
	30/70	40.0	1.68
	40/60		1.79
	50/50		1.82
Tin tannates	30/70	35.0	1.53
	40/60		1.60
	50/50		1.72
	30/70	40.0	1.77
	40/60		1.85
	50/50		1.83
Zinc tetroxyhromate	30/70	40.0	1.69

Note: Practical adhesion for original binder/aged binder ratio was 1.65

To interpret the experimental results corresponding to painted panels, the main effects were considered; the mean values of trials carried out in triplicate are shown in Table IV. These values indicate that to reach the best performance in salt spray testing for 1500 hours, of both inhibitive pigments (tin tannates and iron tannates), the 50/50 inhibitive pigment/inert pigment ratio and the 40 % pigment volume concentration must be selected. Considering the R effect, in order of importance to the 50/50 ratio, it is possible to quote the 40/60 ratio (similar effectiveness) and finally the 30/70 ratio. Concerning the P effect, the concentration 35 % was located in the following level to 40 %.

Degree of blistering

The results obtained in 100 % relative humidity testing (degree of blistering) could not be interpreted by means of the before mentioned statistical method since frequency of blistering

is not qualified in a quantitative manner by ASTM D 714 Standard in contrast to the size of blistering which is described in an arbitrary numerical scale from 10 to 0. The mean values for 500, 1000 and 1500 hours are shown in Table V.

Table IV

Mean values of degree of rusting and practical adhesion (salt spray testing, 1500 hours)

	Type	Degree of rusting	Practical adhesion, adimensional unit
Inhibitive pigment	Iron tannates	8.00	1.68
	Tin tannates	8.17	2.73
Inhibitor/inert pigment ratio	30/70	7.50	1.60
	40/60	8.25	1.72
	50/50	8.50	1.77
Pigment volume concentration, PVC %	35	7.33	1.61
	40	8.33	1.79

Results corresponding to coated panels showed an apparent major tendency to blister in the composition in which the PVC value was 35 %; on the other hand, the blistering resistance improved at 40 % PVC with the both metallic tannates and for all the inhibitive pigment/inert pigment ratios selected.

The major tendency to blister at 35 % may be attributable to the inferior film permeability since this value increases as PVC also increases, particularly at pigmentation levels close to the critical one.

Regarding the type of metallic tannates and inhibitor/inert pigment ratios, no significant differences were observed.

CONCLUSIONS

• The testing results indicate that the iron tannates and tin tannates prepared at laboratory scale displayed a very good behaviour in accelerated tests like salt spray (fog) testing, 100 % relative humidity chamber (in both cases for 1500 hours) and practical adhesion on aged films (salt spray chamber, 1500 hours).

Furthermore, the quoted metallic tannates are not toxic and fulfil with the regulations in force in many countries over contamination and security.

• Both inhibitive pigments show a reduced solubility in water; the high blistering resistance corresponding to the osmotic phenomenon (that is not from rusting) could be attributable to this cause.

Besides, their low oil absorption (approximately 20 g/100 g) allows the incorporation of high levels of pigment in the formulation, with the advantage that this gives to this type of paints (simultaneous requirements of high rusting resistance, no blistering formation and adequate film practical adhesion).

Table V

100 % relative humidity chamber (ASTM D 2247)
Degree of blistering (ASTM D 714)*

Inhibitive pigment	Inhibitive pigment/ inert pigment ratio	PVC, %	Time, hours		
			500	1000	1500
Iron tannates	30/70	35.0	8-F	8-M	7-M
	40/60		7-M	6-M	6-M
	50/50		8-M	8-M	7-M
	30/70	40.0	10	9-F	9-M
	40/60		9-F	9-F	8-F
	50/50		10	10	9-F
Tin tannates	30/70	35.0	8-F	8-M	7-M
	40/60		7-MD	6-MD	6-MD
	50/50		7-M	6-M	6-M
	30/70	40.0	10	10	9-F
	40/60		9-F	9-F	9-M
	50/50		10	9-F	9-M
Zinc tetroxychromate	30/70	40.0	9-F	8-M	8-M

* Key of the table. Size: 10, no blistering; 8, smallest size blister easily seen by the unaided eye; 6, 4 and 2 represent progressively larger sizes. Frequency: F, few; M, medium; MD, medium dense; D, dense.

• The pigment volume concentration and the inhibitor/inert pigment ratio performed a meaningful influence over the corrosion-inhibitive efficiency of paints based on metallic tannates. For both PVC considered, an increase of the inhibitor/inert pigment ratio led to a major anticorrosive efficiency; 40 % PVC improved the protective capacity of coatings.

•In spite of the scattering of the experimental results, it is possible to conclude that paints with low pigment content (35 % PVC) showed cohesive and adhesive failures; with a higher pigment content (40 % PVC) the failure was usually of the adhesive type.

• Coatings of major efficiency were formulated with a 40 % PVC value and a 30/70 v/v metallic tannates/inert pigment ratio. These coatings showed either a similar or a light superior behaviour to the reference sample based on zinc tetroxychromate.

•For a 6 month storage, metallic tannates incorporated to the epoxy base showed a very low sedimentation and a suitable can stability. After adding the curing agent, the corrosion-inhibiting coatings could be easily applied with only a previous light stirring.

ACKNOWLEDGEMENTS

The authors are grateful to CIC (Comisión de Investigaciones Científicas) and to CONICET (Consejo Nacional de Investigaciones Científicas y Técnicas) for their sponsorship for this research.

REFERENCES

[1] Smith, L.M.- **J. Prot. Coat. Linings, 12** (7), 73 (1995).
[2] Fowler, H.- **Modern Paint Coat., 85** (6), 28 (1995).
[3] Rao A.V.; Khismatrao, P.K.- **Paintindia, 45** (3), 59 (1995).
[4] Morgan, N.R.- **Surface Coat. Int. (JOCCA), 78** (7), 300 (1995).
[5] Ericson, G.- **Am. Paint J., 80** (4), 53 (1995).
[6] Kopecny, F.; Srank, Z.- **Pitture e Vernici, 72** (8), 23 (1995).
[7] Amirudin, A.; Barreau, C.; Hellovin, R.; Thierry, D.- **Prog. Org. Coat., 25** (4), 339 (1995).
[8] Aldcroft, D.; Black, J.- **Surface Coat. Int. (JOCCA), 77** (12), 495 (1995).
[9] Giúdice, C.A.- **European Coatings Journal,** (5), 292 (1994).
[10] Giúdice, C.A.; Benítez, J., C.- **Pitture e Vernici, 70** (11), 33 (1994).
[11] Giúdice, C.A.; del Amo, B.- **European Coatings Journal,** (7-8), 490 (1994).
[12] Tonello, M.L.; Giúdice, C.A.; Benítez, J.C.- **Pitture e Vernici, 73** (14), 9 (1997).
[13] Giúdice, C.A.; Benítez, J.C.; Tonello, M.L.- **Pitture e Vernici, 73** (11), 10 (1997).
[14] Asbeck, W.K.; van Loo, M.- **Ind. Eng. Chem., 41**, 1470 (1949)
[15] Koleske, J.V..- **Paint Testing Manual.** Ed. Koleske J.V., ASTM STP 500, 252 (1995).
[16] del Amo, B.; Giúdice, C.; Rascio, V.- **J. Coat. Technology, 56** (719), 63 (1984).
[17] Funke, W.- **J. Oil Col. Chem. Assoc., 62** (3), 63 (1979).
[18] Giúdice, C.A.; del Amo, B. - **Rev. Iberoam. de Corrosión y Protección, XVII** (2), 141 (1986).
[19] Li, J.C.R.- **Statistical Inference**. Edwards Brothers, Michigan, USA (1964).

SEM STUDY OF INTERMETALLIC PHASES GROWTH IN A HOT-DIP GALVANIZING PROCESS

ESTUDIO POR SEM DEL CRECIMIENTO DE FASES INTERMETALICAS EN EL PROCESO DE GALVANIZADO POR INMERSION

P.R. Seré[1], J.D. Culcasi[2], C.I.Elsner[3], A.R. Di Sarli[4]

The influence of both the cooling rate and the base steel roughness upon the Al-rich phase was analized. For this, steel sheets were coated in a simulator of the hot-dip galvanized process working at 470 °C up to reaching an average roughness value of 1.30 or 0.90 μm; besides, either an air or water spray flow was used in order to obtain cooling rates between 7 and 22 °C s^{-1}, respectively. The galvanized plate surfaces were characterized by means of SEM and XRD analysis. From the experimental results the following conclusions could be drawn: a) the Al-rich phase growths as an intermetallic (Al_5Fe_2), that crystallizes forming an orthorombic lattice in which increasing cooling rates do not change the morphology but stop the growing of the crystals, and b) an increase of the steel roughness makes that outburst structures but not the Al-rich phase develops at the bottom of pits.

Keywords: *outburst, intermetallic growth, hot-dip galvanized steel, cooling rate, surface topography.*

INTRODUCTION

Affected by the chemical activity as well as by the diffusion and subsequent cooling processes, the complex structure of layers comprising a galvanized coating differs meaningfully not only in chemical composition but also in physical and mechanical properties. Furthermore, small differences in coating composition, bath temperature, immersion time, cooling rate and substrate characteristics give rise to significant changes in the coating appearance and properties **[1]**. An Al-rich layer is formed when a steel plate is brought into contact with a zinc bath containing more than 0.1% Al. This layer is thought to hinder the alloying between the steel sheet and molten zinc, reason by which is referred to as the inhibition layer, since it inhibits the formation of Fe-Zn phases (Γ, δ and ξ) **[2]**. The aim of the present work was to analize the influence of both the cooling rate and the base steel roughness upon the Al-rich phase growth.

---

[1] Becario de Perfeccionamiento de la CIC
[2] Profesor Adjunto, Departamento de Mecánica, Facultad de Ingenieria, UNLP
[3] Miembro de la Carrera del Investigador del CONICET; Profesor Adjunto, UNLP
[4] Miembro de la Carrera del Investigador de la CIC

(a)

(b)

Fig.1.- Micrographs of the cooling rate effect on the Al-phase growing.
a) 7°C s^{-1} (7700X); b) 22°C s^{-1} (7700X).

EXPERIMENTAL DETAILS

SAE 1004 steel plates were coated in a simulator of the hot-dip galvanized process at laboratory scale, containing a bath whose chemical composition was: Al, 0.2%; Fe, 0.02%; Sb, 0.09%. The remainder was zinc. The specimens surface topography was modified up to the average roughness values: 1.30 and 0.90 μm. The bath temperature and immersion time were kept constant at 470 °C and 30 s, respectively. Besides, either an air flux of 600 $l.min^{-1}$ or a water spray were used as cooling media, given cooling rates of 7 and 22°C s^{-1}, respectively.

For SEM studies, some galvanized plates were submitted to pickling with sulfuric acid, using aresenious anhydride as inhibitor so that, from the selective dissolution of Zn (dezincification), the aluminium-rich phase could be observed using a plant view **[3]**. The other samples were placed in slides and etched with nital 1%, then rinsed with distilled water and newly etched using this time a chromic acid solution in order to be observed by cross-section.

(a)

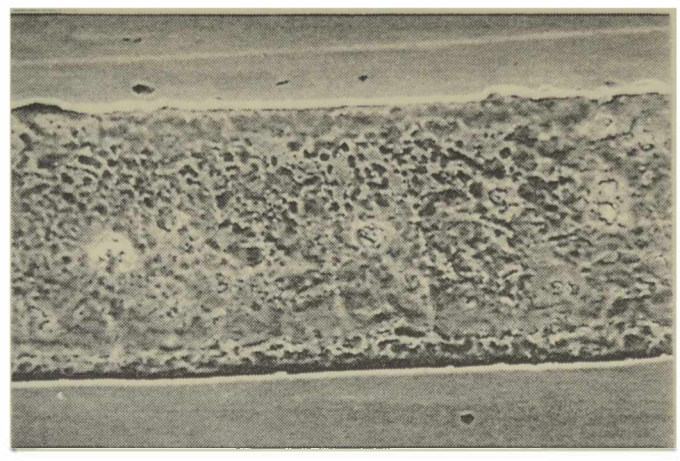

(b)

Fig.2.- Development of outburst structures as a function of the steel surface roughness; a) Ra = 1.30μm (1490X) and b) Ra = 0.90μm (500X).

RESULTS

Fig.1 shows the cooling rate effect on the aluminium-rich phase growing; the compound formed was identified as Al_5Fe_2 by XRD. This intermetallic phase crystallizes as an orthorombic lattice (a = 7.675, b = 6.403, c = 4.203) and develops through the nucleation-growing mechanism forming equiaxial crystals, Fig.1a. Its morphology is not changed by an increase of the cooling rate but these last stop the crystals growing, Fig.1b. Under such conditions, not only smaller crystals but also some of them showing a preferential development (heterogeneous growing) were obtained. Furthermore, a greater growing could be observed at the base steel boundary grains, where the higher surface energy causes the growing not only of this phase but also the Fe-Zn intermetallic derived from the same. The steel roughness would not affect the Al-rich phase morphology; nevertheless, when the roughness increases this phase cannot develop at the bottom of the pits, sites at which Zn diffuses through the Al_5Fe_2 and reacts with the Fe atoms giving rise to the development of Fe-Zn phases ("outburst

structures"), Fig.2a. On the other hand, on less rough steel surfaces this effect is either avoided or delayed, Fig.2b.

ACKNOWLEDGEMENTS

The authors gratefully acknowledge the Comisión de Investigaciones Científicas de la Provincia de Buenos Aires, the Consejo Nacional de Investigaciones Científicas y Técnicas (CONICET) and the Universidad Nacional de La Plata (UNLP) for their financial support to this research work.

REFERENCES

[1] ASMs Handbook.- Vol. 13, **Corrosion**, ASM International ed. (1992=.

[2] Lin, C.S.; Meshii, M.- **Galvatech'95 Conference Proc.**, p.335 (1995).

[3] Kiusalaas, R.; Engberg, G.;. Klang, H.;. Schedin, E.; Schan, L.- **Galvatech'89 Conference Proc.**, p.485 (1989).

FACTORES QUE AFECTAN LA ESTRUCTURA DE RECUBRIMIENTOS DE CINC OBTENIDOS POR INMERSIÓN

FACTORS AFFECTING THE HOT-DIP ZINC COATINGS STRUCTURE

P.R. Seré[1], J.D. Culcasi[2], C.L. Elsner[3], A.R. Di Sarli[4]

SUMMARY

Coating solidification during hot-dip galvanizing is very complex due to Al-Fe, Al-Fe-Zn and Fe-Zn intermetallic compounds development. Fe-Zn ones are brittle and detrimental for mechanical properties, while the diffusion towards the surface of a segregated insoluble alloying such as antimonium causes the sheet darkness. Steel sheets of different roughness were hot-dip galvanized under different operation conditions using a laboratory scale simulator. The effect of steel roughness and process parameters upon coating characteristics were analysed. Experimental results showed that the steel roughness affects the coating thickness, zinc grain size and texture as well as the out-bursts development, while the process parameters affects the Fe_2Al_5 morphology and antimonium segregation.

Keywords: ***Galvanized steel sheet, hot-dip galvanizing, microstructure, alloy layer, roughness, zinc coatings.***

INTRODUCCIÓN

Durante el proceso de galvanizado por inmersión, las reacciones químicas que tienen lugar entre el acero y el cinc líquido dan origen a la formación de diferentes fases. Así, sobre el sustrato crecen cuatro fases: Γ (18-31% Fe), Γ_1 (19-24% Fe), δ (8-13% Fe) y ζ (6-7% Fe). Por último, se forma una solución sólida de hierro en cinc (fase η), la cual disuelve alrededor de 0,04% de hierro **[1]**. Las mencionadas fases intermetálicas son duras y frágiles, razón por la cual el producto obtenido no es apto para el conformado ya que enevitablemente se produciría la fisuración y desprendimiento del recubrimiento. La adición al baño de 0,1-0,3% de aluminio conduce a la rápida formación de una fase Al-Fe que inhibe el crecimiento de los compuestos intermetálicos de Fe-Zn y, por lo tanto, mejora las propiedades mecánicas de la chapa galvanizada **[2]**. Esta fase intermetálica ha sido identificada por algunos autores como Fe_2Al_5 mientras que otros sugieren que se trata de un compuesto ternario de Fe-Al-Zn **[3]**. El carácter transitorio de esta película de inhibición tiene como consecuencia indeseable la nucleación y

---

[1] Becario de Perfeccionamiento de la CIC
[2] Profesor Adjunto, Departamento de Mecánica, Facultad de Ingeniería, UNLP
[3] Miembro de la Carrera del Investigador del CONICET; Profesor Adjunto, UNLP
[4] Miembro de la Carrera del Investigador de la CIC

crecimiento localizado de compuestos intermetálicos de Fe-Zn ("out-bursts"), los que emergen del acero base al romperse la capa de inhibición **[4, 5]**. La ocurrencia o no de este fenómeno depende de la temperatura y composición química del baño (fundamentalmente del contenido de Al), del tiempo de inmersión, de la velocidad de enfriamiento y de la condición superficial del sustrato **[3, 6]** la cual tiene, además, efecto sobre las características de la película de cinc. La orientación cristalográfica (textura) de los granos de cinc depende principalmente de factores externos tales como: velocidad de enfriamiento, gradiente térmico y condición superficial del acero durante el proceso de solidificación **[7]**. Este parámetro ejerce a su vez una marcada influencia sobre la resistencia a la corrosión, la pintabilidad y la conformabilidad de la chapa **[8, 9, 10]**.

En el presente trabajo se evaluó el efecto de la rugosidad del sustrato, de la temperatura del baño y de la velocidad de enfriamiento sobre la morfología de la capa de inhibición, la tendencia a la formación de "out-bursts" y la orientación cristalográfica de los granos de cinc. Asimismo, se investigó el efecto de la rugosidad del acero base sobre el tamaño de los cristales y el espesor de la película de cinc.

PARTE EXPERIMENTAL

Se galvanizaron flejes de acero, de 200x60x1 mm cuya composición química se muestra en la **Tabla I**. La rugosidad superficial de las muestras se modificó tratándolas con distintos abrasivos. Las condiciones operativas utilizadas fueron las siguientes: composición del baño (**Tabla II**); temperatura 470 ó 520°C; tiempo de inmersión 30 s; velocidad de enfriamiento entre 5 y 22°C s^{-1} (**Tabla III**).

Tabla I

Composición química del acero base (en p/p%)

C	Mn	P	S	Si	Al
0,060	0,250	0,015	0,015	0,020	0,040

Tabla II

Composición química del baño (en p/p%)

Sb	Al	Fe	Zn
0,09	0,20	0,04	99,67

La morfología y composición de las distintas fases se caracterizaron mediante microscopía electrónica de barrido (SEM), analizador EDAX y difracción de rayos X (XRS). Se realizaron observaciones metalográficas según dos planos: transversal y paralelo a la

superficie de la chapa. Las muestras para observación transversal se atacaron con Nital 1% + ácido crómico mientras que, en las paralelas a la superficie, la película de cinc fue disuelta en solución de ácido sulfúrico + inhibidor para evitar la disolución del intermetálico Fe-Al. Mediante XRS se determinó la intensidad de las reflexiones correspondientes a los planos cristalográficos de cinc y se las comparó con los valores dados por la carta ASTM 4-831, correspondiente a una muestra de polvos con orientación al azar. Para cada plano analizado se calculó la siguiente relación:

$$R_{(hk.l)} = (I_{(hk.l)} / \Sigma I_{(hiki.li)}) \times 100$$

donde $I_{(hk.l)}$ es la intensidad de la reflexión y $\Sigma I_{(hiki.li)}$ es la suma de las intensidades de todas las reflexiones analizadas. La misma relación se realizó a partir de los datos obtenidos de la carta ASTM 4-831 (muestra patrón, $R_{p(hk.l)}$).

Tabla III

Condiciones experimentales operativas

Muestra	Temperatura [°C]	Rugosidad R_a [μm]	Velocidad de enfriamiento [°C s^{-1}]
A	470	0,95	5,0
B	470	1,30	6,6
C	470	2,30	8,4
D	470	0,95	22,0
E	520	0,95	6,3
F	520	1,30	7,0
G	520	2,30	11,0

Por último se calculó el coeficiente de textura, $CT_{(hk.l)}$, definido como:

$$CT_{(hk.l)} = R_{(hk.l)} / R_{p(hk.l)}$$

Un $CT_{(hk.l)} > 1$ indica una orientación preferencial del plano correspondiente (hk.l) con respecto a la exhibida por la muestra patrón.

RESULTADOS Y DISCUSIÓN

1.- Topografía del sustrato

Para una temperatura del baño de 470°C, la disminución del tamaño de los cristales de cinc con el aumento de la rugosidad del acero mostrada en la Fig.1a se atribuye a que al aumentar la superficie específica también lo hace el número de sitios de nucleación, factor este último que conduce a la obtención de cristales de cinc más pequeños. Por otro lado, al ser mayor la cinética de la reacción entre el hierro y el cinc a 520°C que en el caso anterior, se

presume la existencia no sólo de una disolución más rápida en las zonas con mayor energía superficial (i.e., los picos superficiales del hierro) sino también que ésto conduciría a una disminución de la superficie específica y, por ende, del número de centros de nucleación y crecimiento. Tal presunción ha permitido explicar el motivo por el cual, a esta temperatura, el tamaño de grano del cinc depositado era similar al de las muestras de menor rugosidad ensayadas a 470°C; sin embargo, se continúa investigando con el objeto de encontrar mayor evidencia experimental que la apoye. Otro aspecto a tener en cuenta es que al incrementarse la altura y densidad de picos (i.e., la rugosidad) también aumenta el arrastre de cinc líquido y, en consecuencia, el espesor de la película de Zn (Fig.1b).

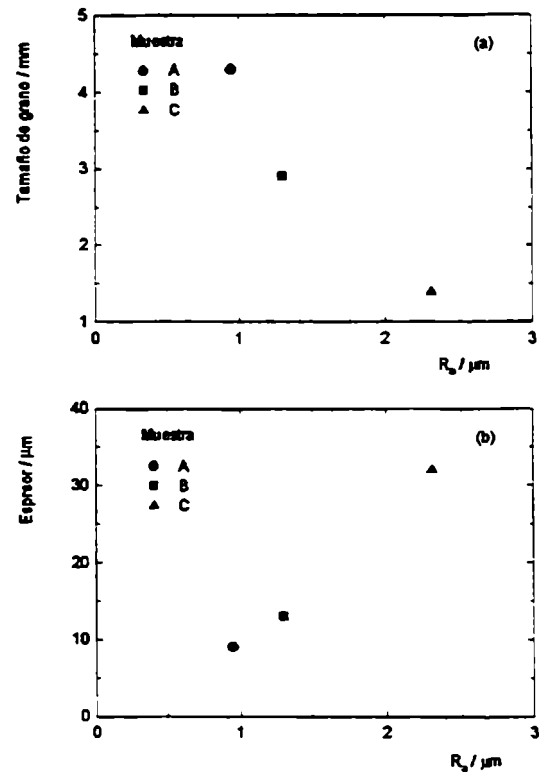

Fig. 1. Tamaño de los cristales a) y espesor b) del recubrimiento de cinc vs. rugosidad media del acero (Ra).

En cuanto a la influencia de la rugosidad del acero sobre la textura del recubrimiento, las muestras con mayor rugosidad presentaron un mayor coeficiente de textura para los planos (00.2), Fig.2, indicando que un aumento de la superficie específica promueve el desarrollo de planos basales paralelos al sustrato.

En concordancia con lo publicado por Shah et al **[11]**, a partir de comparar los resultados experimentales descriptos para los parámetros anteriores (espesor, textura y tamaño de grano) puede inferirse que la relación existente entre los mismos es: inversa entre el desarrollo de los planos basales y el tamaño de grano y directa entre aquél y el espesor del recubrimiento.

Con referencia a la formación de la capa de inhibición, identificada mediante XRS como Fe_2Al_5, no se detectaron diferencias en la morfología y tamaño de sus cristales al cambiar la rugosidad (Fig.3). Según Gutmman et al **[4]**, esta fase intermetálica está compuesta por dos subcapas; una de ellas, constituida por cristales equiáxicos de aproximadamente 60 nm de

diámetro, compacta y muy delgada en contacto con el sustrato mientras que la segunda, depositada sobre aquélla, es más gruesa y está formada por cristales aplastados de 300 a 600 nm de diámetro y aproximadamente 200 nm de espesor. La cinética del proceso de nucleación y crecimiento de la capa delgada es muy rápida, del orden de una fracción de segundo, en tanto que la de la superior, correspondiente a la segunda etapa de crecimiento, es mucho más lenta debido a que está controlada por la difusión del hierro a través de la ya solidificada capa adherida al acero. Por otro lado, mientras el mencionado proceso para la capa delgada está controlado por las características estructurales del acero, en la superior exhibe una morfología y orientación cristalográfica al azar. Este hecho explicaría la falta de correlación entre la rugosidad del sustrato y la morfología del intermetálico de Fe-Al. En lo que respecta a la formación de "out bursts", originada por la rotura localizada de la capa de inhibición, se encontró que el aumento de rugosidad estaría acompañado por una tendencia al crecimiento localizado de fases de Fe-Zn (Fig.4).

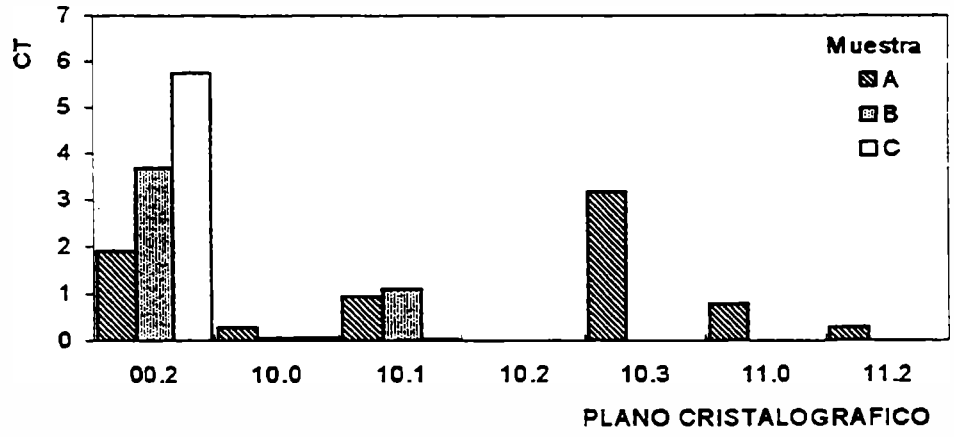

Fig. 2. Coeficiente de textura vs. Ra para las muestras: A (Ra = 0,95µm), B (Ra = 1,30µm) y C (Ra = 2,30µm).

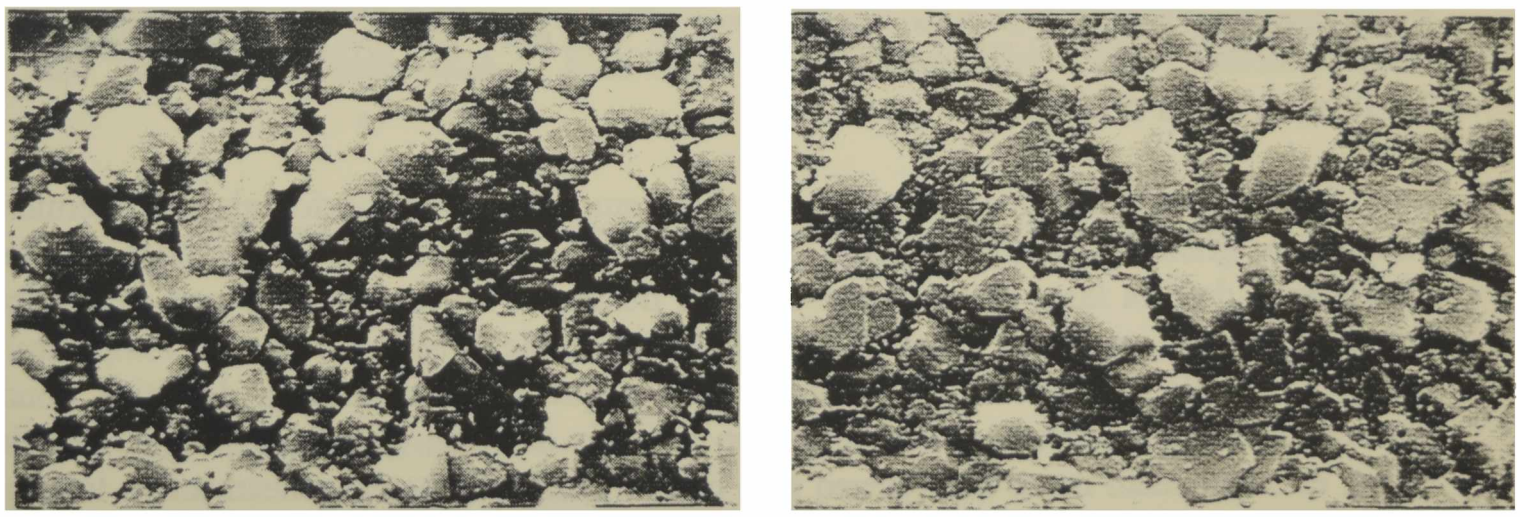

a) b)

Fig. 3. Morfología de la capa de inhibición vs. Ra para las muestras: a) E (Ra = 0,95µm, X 7700 y b) G (Ra = 2,30µm, X 7700).

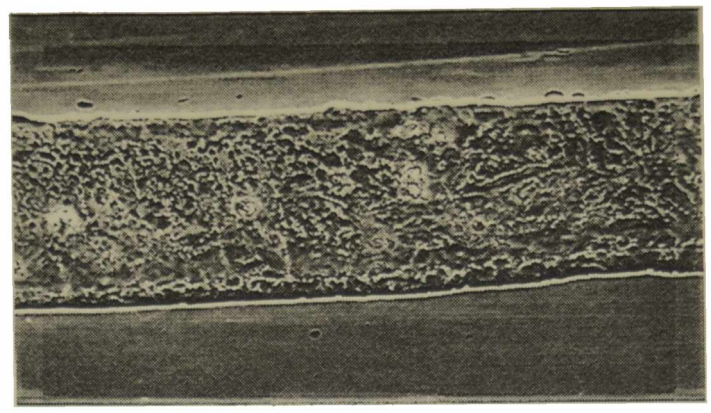

a)

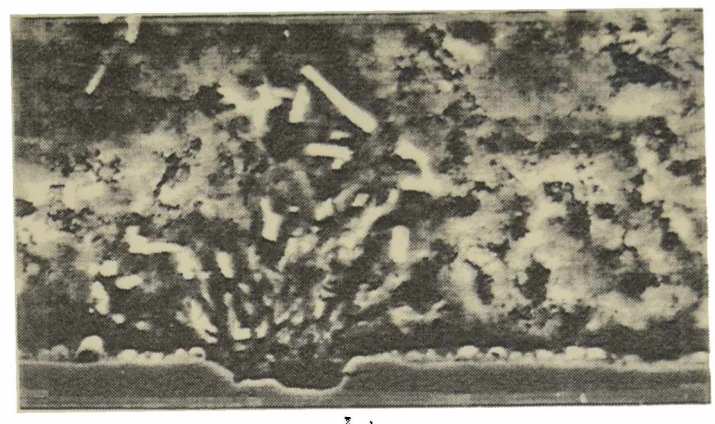

b)

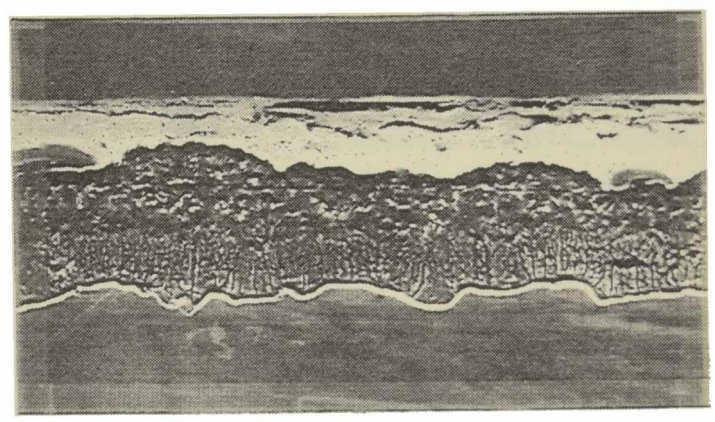

c)

Fig. 4. Desarrollo de "out-bursts" vs. Ra para las muestras: a) A (Ra = 0,95µm, X 500), b) B (Ra = 1,30µm, X 1490) y c) C (Ra = 2,30µm, X 500).

2.- Temperatura del baño

Si bien en los ensayos realizados a ambas temperaturas la morfología del intermetálico Fe_2Al_5 fue granular resultó evidente que, a mayor temperatura, se produce un mayor crecimiento de esta fase, alcanzándose un gran desarrollo de los cristales que se distribuyen homogéneamente en forma y tamaño sobre la superficie (Fig.5a); a menor temperatura se observó no sólo la presencia de cristales más pequeños sino también de sitios donde el intermetálico crece preferencialmente, hecho a partir del cual se infirió que, en su primera etapa, el crecimiento no es homogéneo sino que se desarrolla heterogéneamente a lo largo de la superficie (Fig 5b). Las muestras galvanizadas a 520°C mostraron un crecimiento de fases de Fe-Zn mientras que a 470°C no se detectó la presencia de "out-bursts".

Relacionado con a la orientación cristalográfica del recubrimiento, no se encontró ninguna dependencia entre la temperatura del baño y la textura.

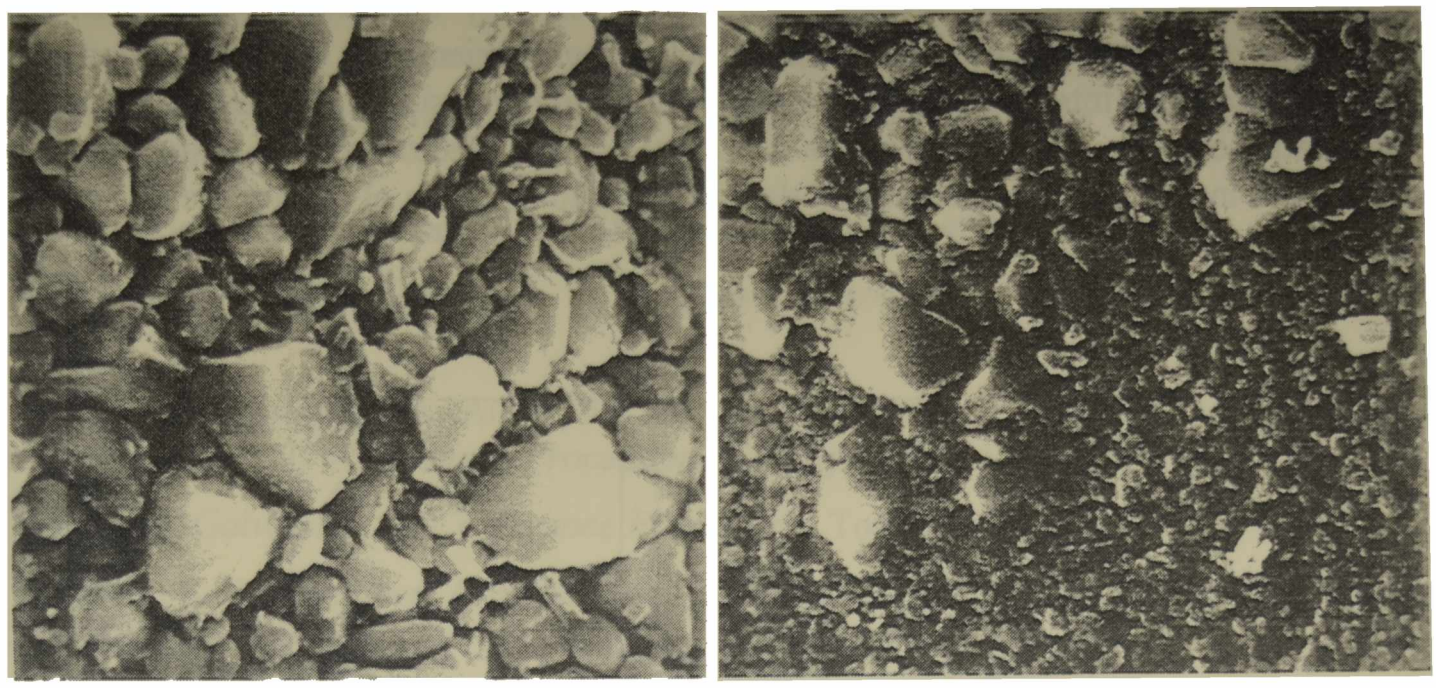

a) b)

Fig. 5. Morfología de la capa de inhibición en función de la temperatura del baño de cinc (T) para las muestras: a) E (T = 520°C, X 7700) y b) A (T = 470°C, X 7700).

a) b)

Fig. 6. Morfología de la capa de inhibición vs. velocidad de enfriamiento (v_e) para las muestras: a) A (v_e = 5°C seg^{-1}, X 2500) y b) D (v_e = 22°C seg^{-1}, X 2500).

3.- Velocidad de enfriamiento

La velocidad de enfriamiento tiene una marcada influencia sobre la formación del intermetálico Fe_2Al_5. Así, al aumentar ésta de 5 a 22°C s^{-1}, el tamaño de los cristales de la capa de inhibición disminuye (Fig.6a); además, los estudios de EDAX realizados en las muestras enfriadas a mayor velocidad detectaron, sobre el intermetálico, un agregado acicular formado

mayormente por antimonio, Fig.6b. Este hecho es muy importante ya que el antimonio segregado a la superficie es el responsable del ennegrecimiento de la chapa en cortos tiempos de exposición a la intemperie, perjuicio que podría evitarse si el antimonio segregara sobre el intermetálico y no sobre la superficie. Los estudios del efecto sobre la textura determinaron que con el incremento de la velocidad de enfriamiento aumenta el coeficiente de textura de los planos basales (Fig.7).

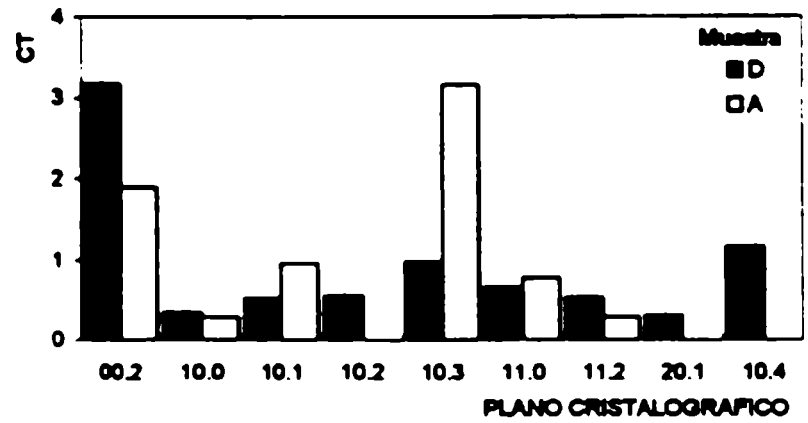

Fig. 7. Coeficiente de textura vs. v_r para las muestras: D (v_r = 22°C seg^{-1}) y A (v_r = 5°C seg^{-1}).

CONCLUSIONES

- La rugosidad del acero es un parámetro que influye significativamente las características del recubrimiento. En tal sentido, al aumentar dicha rugosidad se incrementa el espesor del recubrimiento, disminuye el tamaño de grano de cinc y se desarrolla una más definida textura basal. Existe, además, una mayor tendencia a la formación de "out-bursts".

- Altas temperaturas del baño producen un excesivo crecimiento de los cristales de la capa de inhibición y una gran tendencia a la formación de "out-bursts". No se encontró dependencia entre la temperatura del baño y la textura de los cristales de cinc.

- El empleo de un eficiente medio para extraer el calor de las muestras a la salida del baño (por ej., "spray" de agua) produce un aumento de la velocidad de enfriamiento y, como consecuencia de ello, no sólo una disminución del tamaño de los granos del intermetálico Fe_2Al_5 sino que, por esto último, también promueve la orientación cristalográfica de los planos basales paralelos al sustrato. Además, al aumentar la segregación de antimonio sobre el intermetálico disminuye el ennegrecimiento de la superficie de la chapa.

AGRADECIMIENTOS

Los autores del trabajo agradecen a la Comisión de Investigaciones Científicas de la Provincia de Buenos Aires (CIC), al Consejo Nacional de Investigaciones Científicas y Técnicas (CONICET) y a la Universidad Nacional de La Plata (UNLP) por el apoyo económico brindado para su ejecución.

REFERENCIAS

Desmond C., Cook and Richard G. Grant, *Galvatech '95 Conference Proceeding*, Chicago, USA, 1995: 497-508.

ASM Handbook, Ninth Edition, 13, Hot-Dip Coatings, 1992. 432.

C. S. Lin and M. Meshii, *Galvatech '95 Conference Proceeding*, Chicago, USA, 1995: 335-342.

M. Gutmman, Y. Leprêtre, A. Aubry, M. J. Roch, T. Moreau, P. Drillet, J. M. Mataigne, H. Baudin, *Galvatech '95 Conference Proceeding*, Chicago, USA, 1995: 295-307.

Y. Hisamatsu, *Galvatech '89 Conference Proceeding*, Tokyo, Japan, 1989: 3-12.

W. Maschek, S. P. Hayes and A. R. Marder, *Galvatech '95 Conference Proceeding*, Chicago, USA, 1995: 309-318.

S. Chang, J. C. Shin, *Corrosion Sci.*, **36**(8), 1994: 1425-1436.

J. L. Millán, *J.Material Engineering & Performance*, **1**(2), 1992. 275-283.

J. H. Lindsay, R. F. Paluch, H. D. Nine, V. R. Miller, T. J. O'Keefe, *Plating Surf. Finish.*, Mar., 1989. 62-69.

S. J. Shaffer, W. E. Nojima, P. N. Skalpelos, J. W. Morris, *TMS Symposium on Zinc-Based Steel Coating Systems Conference Procceding*, Detroit, USA, 1990. 251-261.

S. R. H. Shah, J. A. Dilewijns, R. D. Jones, *Galvatech '92 Conference Proceeding*, Amsterdam, Netherlands, 1992. 105-111.

INFLUENCE OF DIFFERENCES BETWEEN SAMPLE AND MOBILE PHASE VISCOSITIES ON THE SHAPE OF CHROMATOGRAPHIC ELUTION PROFILES

INFLUENCIA DE DIFERENCIAS ENTRE LAS VISCOSIDADES DE LA MUESTRA Y DE LA FASE MOVIL SOBRE LA FORMA DE LOS PERFILES DE ELUCION CROMATOGRAFICA

R.C. Castells[1], C.B. Castells[2], M.A. Castillo[3]

SUMMARY

The injection of samples whose viscosities are appreciably different from that of the mobile phase can result in highly distorted elution profiles, showing several maxima. The distortions are produced at the rear of the band when the viscosity of the sample solvent is higher than that of the mobile phase. It is shown that the distortion of the peaks produced on injecting arbutin in columns of aminopropyl silica, using water as mobile phase and mixtures of 2-propanol and water as the sample solvent, grows in importance when the sample size increases, when the viscosity of the sample solvent increases and when the flow rate is decreased. On the other side distortions at the band front are observed when arbutin dissolved in water or in acetonitrile + water mixtures is injected in a 2-propanol-water (50:50) mobile phase of higher viscosity. These trends are coincident with the predictions of a hydrodynamic instability criterion postulated several years ago and up to now almost entirely ignored in chromatography, except in relation with size exclusion chromatography

Keywords: *liquid chromatography; mobile phase viscosity; sample viscosity; elution profiles.*

INTRODUCTION

The injection of samples dissolved in solvents different from the mobile phase can result in severe peak distortions. The peak for a single component can show a front or a rear shoulder, and in extreme situations double or multiple peaks are generated. This is a surprising behaviour since it is shown for solutes that are easily soluble in the mobile phase and in the sample solvent and, furthermore, for eluents and solvents that are totally miscible.

Tseng and Rogers **[1]** observed that the dihydroxybenzenes gave simple symmetric peaks when water or methanol were used as sample solvent and as mobile phase; however each

[1] Miembro de la Carrera del Investigador del CONICET; Profesor Titular, UNLP
[2] División de Química Analítica, Facultad de Ciencias Exactas, Universidad Nacional de La Plata
[3] Becario del FOMEC, UNLP

isomer produced a double peak when their solutions in water were injected in methanol as the mobile phase, and peaks with front shoulders resulted when methanol was the sample solvent and water was the eluent. Similar distortions and/or multiplication of peaks were reported by Kirschbaum *et al.* **[2]**, Khachik *et al.* **[3]**, Hoffman *et al.* **[4]** and by Vukmanic and Chiba **[5]**. Some of the quoted authors suggested theoretical explanations based on differences between the solvent strengths of the mobile phase and of the injection solvent, and peak splitting was simulated by means of a model that taked into account changes in the capacity factor as the injection solvent moved through the column **[6]**. Zapata and Garrido **[7]** demostrated that this explanation was highly questionable: chlorophyls produced single symmetric peaks when methanol-water (95:5) was the injection solvent, but multiple peaks were obtained when solutions in acetone-water mixture (90:10) were injected in the same eluent. The solvent strengths of both sample solvents differed by only 7% in Snyder's scale **[8]** and, furthermore, multiple peaks were produced by employing a 69:31 acetone-water mixture whose solvent strength matches exactly that of the 95:5 methanol-water mixture.

A totally different approach to the relationship between peak shape and sample solvent composition was followed by Czok *et al.* **[9]**. Using a high-performance size exclusion chromatography column and an aqueous phosphate buffer as the mobile phase they observed that the shapes of the peaks produced by injecting uracil dissolved in several water-glycerol mixtures depended dramatically on glycerol concentration. A single, almost symmetric peak was obtained when 100% water was the injection solvent, but shoulders were generated at the rear of the peaks when solutions containing 10 and 17% glycerol were injected, and very broad peaks with several maxima were obtained for higher glycerol concentrations; all the chromatograms showed a maximum at a retention time coincident with that of the peak obtained by using the aqueous buffer as injection solvent. A single peak was obtained when a phosphate buffer containing 33% glycerol was the eluent and the sample solvent; peak deformations at the band front were produced by injecting uracil solutions containing less than 33% glycerol, and distortions at the band rear appeared for injection solvents with glycerol concentrations higher than 33%. The authors attributed this behaviour to hydrodynamic instabilities resulting from viscosity differences between the injected pulse and the mobile phase.

These effects have been known under the name of "fingering", and a criterion of stability has been established in terms of viscosity and density differences **[10, 11]**. The interface between two fluids that are moving vertically upwards within a packed bed with uniform velocity u shall be stable if

$$(\mu_2 - \mu_1)u / k - (\rho_2 - \rho_1)g > 0 \qquad (1)$$

and unstable otherwise. Suffix 1 refers to the upper fluid and suffix 2 to the lower; μ denotes viscosity, ρ the density, k is the permeability of the bed and g the acceleration due to gravity. When instability conditions are given and any packing fluctuation has caused the boundary to bulge in the flow direction, the bulge shall grow giving rise to "fingers" of the less viscous fluid (suffix 2) that penetrate into the leading fluid. This effect has long been known in connection with the displacement of immiscible fluids in porous media; mixing tends to relax the boundary, thus restricting the possibilities of occurence of fingering in systems composed of miscible fluids.

The displacement of a sample band through a chromatographic column shows some obvious peculiarities in connection with the phenomenon under discussion. In the first place the permeabilty of chromatographic beds is low, about 5 x 10^{-10} cm^2 for 5 μm spherical porous particles **[12]**; this makes the term in densities of (1) negligible beside the term in viscosities. Then, since there are two boundaries between a chromatographic band and the mobile phase, any band whose viscosity is different from that of the eluent would be in a condition as to become unstable; instabilities would occur at the band rear if the band is more viscous than the eluent, and at the band front in the opposite case. This would transform fingering into a rather ubiquituous phenomenon, present each time that a sample dissolved in a solvent different from the mobile phase is injected; the facts do not agree with this prediction. The reason is that the injected pulse suffers a rapid dilution process as it moves through the first section of the column and, since mixing acts in the direction of removing the conditions for the onset of fingering, the occurrence of the phenomenon shall depend not only on viscosity differences but on the velocity of the dilution process also. It can be predicted that sample size and flow rate shall have a profound influence. Another experimental condition under which the phenomenon can pass unnoticed is when a very fast separation between solute and sample solvent occurs in the very first portions of the column and the solute has a long retention time.

Multiple peaks and shoulders quoted in references 1-5 may be considered as distortions of the single, unperturbed peak obtained by using mobile phase as the injection solvent; furthermore, it can be shown that these distortions are formed at the side of the sample band that could be predicted on the basis of eluent and sample solvent viscosities. For example, when Tseng and Rogers [1] injected any of the three dihydroxybenzenes dissolved in water (μ = 0.90 cp) using methanol (μ = 0.51 cp) as mobile phase, the retention time of the first peak was coincident with that of the only peak produced when methanol was the sample solvent, and a second, partially resolved peak appeared at band rear (the pulse, with a larger viscosity, is penetrated by the mobile phase on its rear portion). On the other side a front shoulder was produced when the roles of methanol and water were inverted (the pulse, with a lower viscosity, penetrates the mobile phase).

The incidence of sample viscosity on peaks shape has only been mentioned in the chromatographic literature in connection with the injection of highly viscous samples in size exclusion columns. The objective of the present paper is to demonstrate that under some conditions fingering can complicate or spoil results obtained in other forms of HPLC, and to study the effects of sample size, solvent composition and flow rate on the phenomenon. Arbutin dissolved in water or in 2-propanol-water mixtures of different compositions is injected into an aminopropyl silica column using water as the mobile phase at several flow rates. The viscosity of 2-propanol at 30°C is more than twice that of water, and the viscosity of 2-propanol-water mixtures shows a maximum close to the 50:50 composition. Some experiments were performed using this highly viscous mixture as the mobile phase.

EXPERIMENTAL

Equipment

The HPLC experiments were performed with a Shimadzu LC-10A System, which consisted of a DGU-2A helium degassing unit, an LC-10AD pump, a Sil-10A autoinjector

(50 µl loop), an SPD-M10A diode array detector and a CLASS-LC10 workstation. Detection of arbutin was performed at 285 nm.

Columns and reagents

All the chromatographic runs were performed with a Supelcosil LC-NH2, 5 µm spherical particles, 25 cm x 4.6 mm I.D. column. The column was placed in a jacket through which water at 30°C was circulated. 2-Propanol and acetonitrile were purchased from E. M. Science, and arbutin was from Sigma. Water was obtained by means of a Milli-Q Waters Purification System (Millipore).

Viscosity measurements

Densities and kinematic viscosities of 2-propanol + water mixtures at 30°C were measured by means of 5 ml pycnometer and of a No. 50 Cannon-Fenske viscometer, respectively. Relative viscosities, μ / μ_{water}, are plotted against composition in Figure 1.

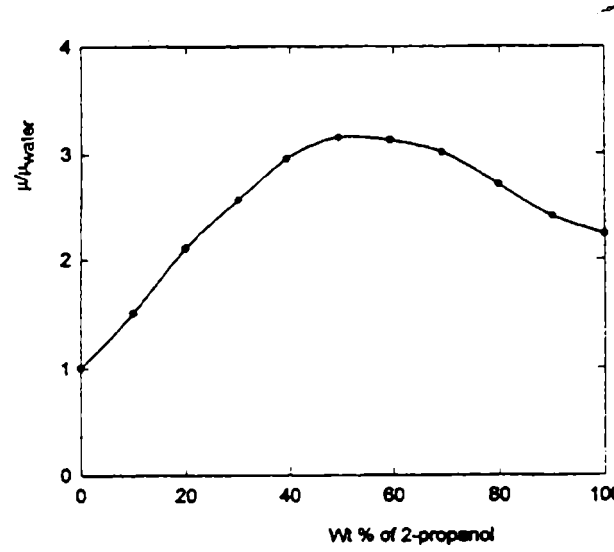

Fig. 1.-Relative viscosities of 2-propanol - water mixtures at 30 °C against composition.

RESULTS AND DISCUSSION

Figure 2 is a typical manifestation of fingering: arbutin, that elutes as a single symmetrical peak when the mobile phase is used as injection solvent, produces a peak with two maxima when a solution in a 2-propanol-water mixture is injected. The retention time of the most important peak in profile B is coincident with that of the peak in A; since the viscosity of the injection solvent in B is 3.2 times that of water, the rear of the band is fingered by the eluent. Several conditions for the manifestation of fingering are combined in this system: a) a large viscosity difference between the sample solvent and the mobile phase; b) solute and sample solvent elute almost together (see peak C for pure 2-propanol); c) since the solute has a short retention time, the possibilities of blurring the distortions in its concentration profile as a consequence of the several dispersion processes are minimized.

An important characteristic of the elution profiles produced by injecting arbutin dissolved in 2-propanol-water mixtures, with sufficient alcohol concentration, using water as mobile phase, is that all of them show a maximum in common. It is the first maximum of the

profile and its retention time coincides with that of the symmetrical peak obtained by injecting arbutin dissolved in the mobile phase; however, it is not necessarily the most important maximum. This is the only repetitive characteristic and, in the cases of manifest instability, the rest of the profile is completely unpredictable. Furthermore, totally different elution profiles may be obtained under identical experimental conditions; the two chromatograms shown in Figure 3 were obtained by two successive injections separated by a 10 min interval at 2 ml/min. These characteristics of the phenomenon are a clear indication of its origins; one could expect repeatibility in case peak distortions were produced by differences between the sample solvent and the mobile phase solvent strengths.

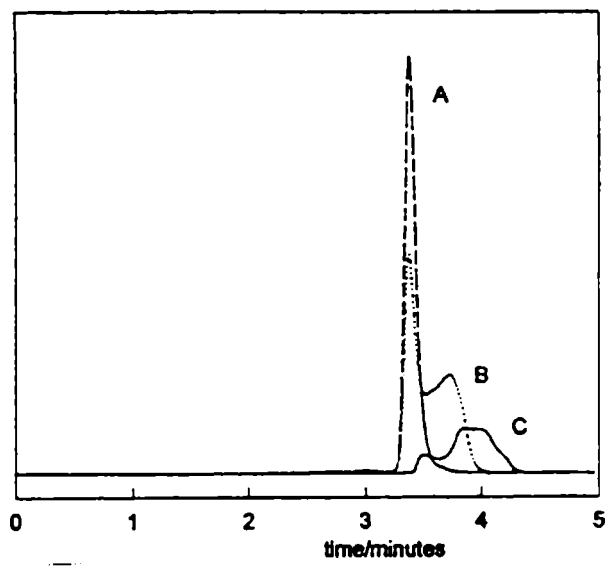

Fig. 2.- Elution profiles of arbutin dissolved in two different solvents and of pure 2-propanol. A: arbutin dissolved in Water (1.3 mg/ml), 5 µl; detection at 285 nm. B: arbutin Dissolved in 2-propanol-water mixture (67:33; 1.5 mg/ml), 5 µl; detection at 285 nm. C: 2-propanol, 10 µl; detection at 200 nm. Mobile phase: water, 1.0 ml/min.

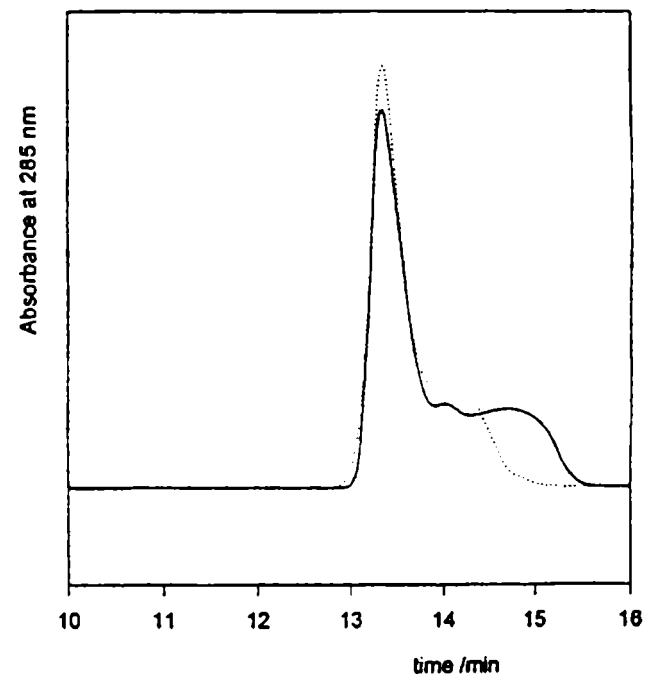

Fig. 3.-Unrepeatibility of elution profiles.Two successive injections of 5 µl of a solution of arbutin (1.6 mg/mL) in 2-propanol-water (65:35) mixture. Mobile phase: water, 0.25 ml/min

The unrepeatibility of the elution profiles obtained under instability conditions restricts the possibilities of studying the phenomenon. The effects of flow rate, of sample size, and of injecting a constant mass of arbutin dissolved in 2-propanol-water mixtures of different compositions were studied in the present work.

Sample size and flow rate effects when water is used as mobile phase are summarized in Table 1 where results obtained by injecting different volumes of a solution containing 1.6 mg/mL of arbutin in a 65:35 2-propanol-water mixture are gathered. Normal peaks are produced at small sample size and high flow rate; the shapes of the elution profiles become more complicated as the injected volume is increased and/or the flow rate is decreased and, at adequate values of these two parameters, very complex profiles, showing several maxima are obtained. The behaviour is well represented in Figure 4, where the results obtained for 5 µl samples are shown. It should be stressed that the product (peak are x flow rate) is constant within experimental error for the elution profiles shown in Figure 4; the coefficient of variation is only 2.2%, a very small value on account of the errors in integrating the irregular peaks obtained at the smaller flow rates. Therefore, the shapes of the profiles cannot be attributed to solute degradation or to any other chemical artifact occurrig within the column.

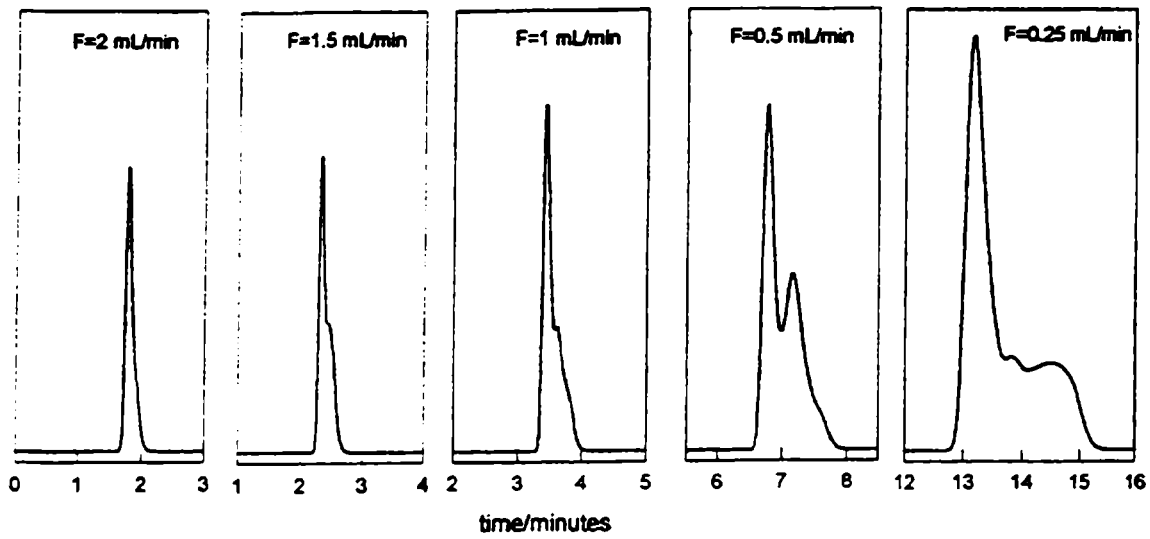

Fig. 4.- Effects of flow rate. Elution profiles for 5 µl of a solution of arbutin (1.6 mg/mL) in 2-propanol-water (65:35) mixture. Mobile phase: water, at the flow rates indicated in the figure.

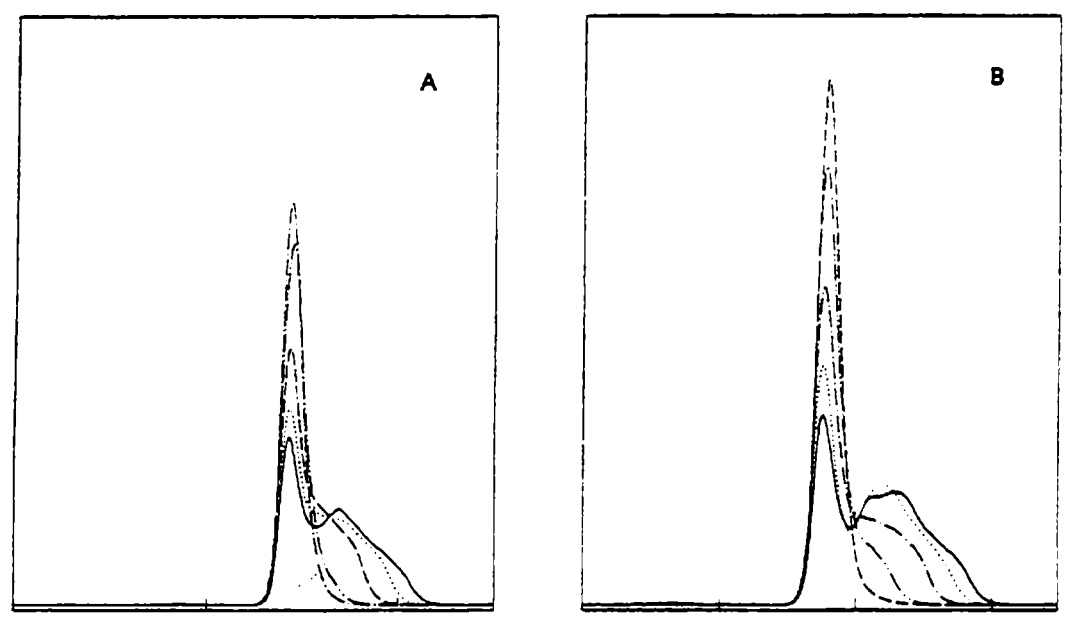

Fig. 5.- Effect of sample solvent composition. Injected solutions: arbutin, 1.4 mg/mL, dissolved in 2-propanol-water mixtures containig (from top to down) 10, 20, 40, 50 and 60 % v/v 2-propanol in water. Sample size: 10 µL. Mobile phase: water, at 1 mL/min in A and at 0.5 mL/min in B.

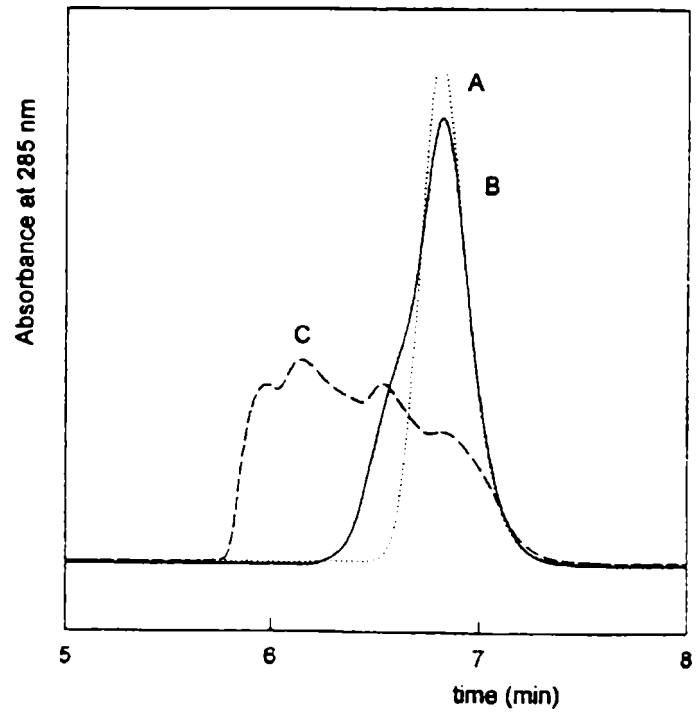

Fig. 6.-Elution profiles obtained by using a 50:50 2-propanol-water mobile phase at 0.50 mL/min. A:1.1 mg/mL arbutin in mobile phase. B: 1.3 mg/mL arbutin in water. C: 1.5 mg/mL arbutin in 90:10 acetonitrile-water mixture.

Table 1

Sample size and flow rate effects on the elution profiles of arbutin using water as mobile phase.

	Flow rate / (mL / min)				
Sample size /μl[a]	2.0	1.5	1.0	0.5	0.25
1	NF	NF	NF	NF	NF
2	NF	NF	NF	NF	NF
4	NF	NF	F	F	F
5	NF	F	F	F	F
10	F	F	F	F	F
15	F	F	F	F	F

[a] The solution injected contained 1.6 mg/mL of arbutin in a 65:35 2-propanol-water solvent.
NF: Fingering not manifested
F : Fingering manifested

A series of experiments was performed in order to detect relationships between peak shape and sample solvent composition at constant quantity of arbutin injected. All the chromatograms appearing in Figure 5 were obtained by injecting 10 μL of solutions of arbutin containing 1.4 mg/mL; sample solvents contained from 10 to 60% v/v 2-propanol in water. Parts A and B were run at 1.0 mL/min and at 0.5 mL/min, respectively. The chromatograms clearly show the constancy of the retention time of the first maximum, as well as the increase of sample pulse penetration by the mobile phase as the sample viscosity increases. The areas under the peaks are again constant, with coefficients of variation smaller than 2% at both flow rates.

Up to this point only systems in which the sample is more viscous than the mobile phase were considered; therefore only chromatograms showing constancy in the retention time of the first maximum and fingering of the mobile phase into the rear of the sample pulse have been shown. The chromatograms shown in Figure 6 were run using a 50:50 2-propanol-water mobile phase (μ = 2.50 cp at 30°C) at 0.5 mL/min. The three chromatograms correspond to the injection of 10 μL of solutions containing similar (although not exactly equal) concentrations of arbutin. The sample solvents were mobile phase in A, water (μ = 0.79 cp) in B, and a 90:10 mixture acetonitrile-water (μ = 0.43 cp) in C. The fingering of the less viscous pulses into the mobile phase is evident in B, and more notoriously in C. In this last case a maximum with a retention time coincident with that of peak A can be noticed; however profile C shows thar when viscosity differences are very large other peaks of larger height can be produced. The chromatograms in Figure 6 confirm the predictions of unequality (1).

CONCLUSION

Fingering, a phenomenon originated in hydrodynamic instabilities in the boundary between two moving fluids of different viscosity, can produce important distortions in the shape of the chromatographic peaks. This constitutes a new artifact to be taken into account during the design, development and analysis of chromatographic separations since its effects

can easily be mistaken with unexpected components in the sample, can mask expected peaks or otherwise spoil chromatographic results. It constitutes another reason to obey the long practiced rule of chromatographers of using the mobile phase as the injection solvent, as far as this practice is feasible.

ACKNOWLEDGEMENTS

This work was sponsored by CONICET (Consejo Nacional de Investigaciones Científicas y Técnicas de la Rep. Argentina) and by CICPBA (Comisión de Investigaciones Científicas de la Prov. de Buenos Aires.

REFERENCES

[1] Tseng, P.K.; Rogers, L.B.- **J. Chromatogr. Sci., 16,** 436 (1978).
[2] Kirschbaum, J.; Perlman, S.; Poet, R.B.- **J. Chromatogr. Sci., 20**, 336 (1982).
[3] Khachik, F.; Beecher, G.R.; Vanderslice, J.T.; Furrow, G.- **Anal. Chem., 60**, 807 (1988).
[4] Hoffman, N.E.; Pan, S.; Rustum, A.M.- **J. Chromatogr., 465**, 189 (1989).
[5] Vukmanic, D.; Chiba, M.- **J. Chromatogr., 483**, 189 (1989).
[6] Ng, T.L.; Ng, S.- **J. Chromatogr., 329**, 13 (1985).
[7] Zapata, M.; Garrido, J.L.- **Chromatographia, 31**, 589 (1991).
[8] Snyder, L.R.; Dolan, J.W.; Gant, J.R.- **J. Chromatogr., 165,** 3 (1979).
[9] Czok, M.; Katti, A.M.; Guiochon, G.- **J. Chromatogr., 550,** 705 (1991).
[10] Hill, S.- **Chem. Eng. Sci., 1,** 247 (1952).
[11] Saffman, P.G.; Taylor, G.- **Proc. R. Soc. London, Ser.** ***A*** **245,** 312 (1958).
[12] Snyder, L.R.; Kirkland, J.J.- ***Introduction to Modern Liquid Chromatography***, Wiley, New York, 2nd. ed., p. 37 (1979).
[13] Flodin, P.- **J. Chromatogr., 5,** 103 (1961).

CONCURRENT SOLUTION AND ADSORPTION OF HYDROCARBONS IN GAS CHROMATOGRAPHIC COLUMNS PACKED WITH DIFFERENT LOADINGS OF 3-METHYLSYDNONE ON CHROMOSORB P

ADSORCION Y DISOLUCION SIMULTANEA DE HIDROCARBUROS EN COLUMNAS DE CROMATOGRAFIA GASEOSA RELLENAS CON DIFERENTES CARGAS DE 3-METILSYDNONA SOBRE CHROMOSORB P

R.C. Castells[1], L.M. Romero[2], A.M. Nardillo[3]

SUMMARY

Thermodynamic properties of solution in 3-methylsydnone (3MS) and of adsorption at the nitrogen/3MS interface were gas chromatographically measured for a group of fifteen hydrocarbons at infinite dilution conditions. Retention volumes were measured at five temperatures within the range 37-52°C in six columns containing different loadings of 3MS on Chromosorb P AW. Partition and adsorption coefficients were calculated and from their temperature dependence the corresponding enthalpies were obtained, although with considerable error; infinite dilution activity coefficients of the hydrocarbons in the bulk and in the surface phases demonstrated an strong correlation. Bulk activity coefficients in 3MS were very much smaller than those previously measured for the same solutes in formamide (FA) and in ethyleneglycol (EG), and were also smaller than what could be predicted on account of 3MS cohesive energy density as estimated from the quotient $\sigma/v^{1/3}$ (σ: surface tension; v: molar volume). There was not such a large difference between the surface activity coefficients in the three solvents; furthermore, the quotients (surface activity coefficient/bulk activity coefficient) for a given solute in 3MS were twice as large as in FA and about three times larger than in EG. These results make evident the difficulties inherent in the prediction of surface phase properties from those in the bulk, and cast doubts on the pertinency of employing the surface tension to compare cohesive energy densities of polar solvents with important chemical differences.

Keywords: *3-methylsydnone; adsorption; solution activity coefficients; surface activity coefficients; gas chromatography; chromatography thermodynamics .*

INTRODUCTION

3-Methylsydnone (3MS) is a polar solvent with some interesting properties; conspicuous among these are the large values of its dielectric constant and of its dipole

[1] Miembro de la Carrera del Investigador del CONICET; Profesor Titular, UNLP
[2] División de Química Analítica, Facultad de Ciencias Exactas, Universidad Nacional de La Plata
[3] Miembro de la Carrera del Investigador del CONICET; Profesor Asociado, UNLP

moment. Some of its physical properties are given in Table 1 together with the corresponding values for formamide (FA) and ethyleneglycol (EG), two solvents that shall be compared with 3MS in the present paper. While FA and EG are highly associated liquids, 3MS is aprotic and the value of its Kirkwood *g* factor is 1.1 **[1]**, indicating a random distribution of the molecular dipoles. However the cohesive energy density (c.e.d) of 3MS measured by the quotient $\sigma/v^{1/3}$, as proposed by Gordon **[2]**, is apparently very high and intermediate between those of FA and EG.

Table 1

Physical Properties of Solvents

	EG, 25°C	FA, 25°C	3MS, 40°C
Dielectric Constant, ε	37.7[a]	105.[a]	144[c]
Dipole Moment, μ (D)	2.28[a]	3.73[a]	7.3[d]
Surface Tension, σ (dyn/cm)	46.[b]	57.9[b]	57.[e]
Refractive Index, n^D	1.4306[b]	1.4468[b]	1.5150[c]
Viscosity, η (cp)	16.2[a]	3.30[a]	5.50[c]
Molar Volume, v (cm^3/mol)	55.92[b]	39.89[b]	76.49[c]
$\sigma/v^{1/3}$ (dyn/cm^2)	12.0	16.9	13.4

[a] "Handbook of Chemistry and Physics", 68th. ed. The Chemical Rubber Co., Cleveland, OH, 1988.
[b] Riddick, J. A., and Bunger, W. B. "Organic Solvents". Wiley-Interscience, New York, 1970.
[c] Reference (1)
[d] Schmid, G. H., *J. Mol. Struct.* 5, 236 (1970).
[e] Reference (3).

On account of its high dielectric constant and c.e.d., 3MS was a good candidate to promote amphiphilic aggregation. But Evans and collaborators **[3]** were unable to detect formation of micelles in this solvent, a fact that these authors associated with the absence of hydrogen bonding in 3MS. This made the measurement of free energies of solution of hydrocarbons in 3MS interesting since, as Evans pointed out, they are intimately related to the driving force for surfactants aggregation. This interest was reinforced by the lack of information about the solvent properties of 3MS.

Gas chromatography, using 3MS as the stationary phase, offers a series of advantages for these measurements. In the first place because chromatographic measurements can be effectively done at infinite dilution of the solute in the stationary phase. In the second place because a considerable gas-liquid interface is generated when the stationary phase is coated on a porous solid; for a polar liquid like 3MS, in which the hydrocarbons shall display important positive deviations from the ideal solution behavior, a mixed retention mechanism can be predicted: partition in the bulk liquid and adsorption on the gas-liquid interface **[4-6]**. Using adequate conditions the thermodynamic parameters characteristic of both processes can be simultaneously determined. Finally the measurements can be performed over a range of temperatures, and partition and adsorption enthalpies may be evaluated **[7]**, although with considerable uncertainties because of the indirect nature of the calculation

The retention behavior of fifteen hydrocarbons representative of different families was measured in the present work at five temperatures equally spaced within the range 37-52°C, in six columns containing different concentrations of 3MS in their packings. Experimental results are treated according with well established theoretical chromatographic principles.

MATERIALS AND METHODS

3MS was synthesized from N-methylglycine by the method of Vasil'eva and Yashunskii **[8]**. N-nitroso-N-methylglycine was extracted with ether, during 36 h, in a liquid-liquid extraction apparatus; the extract was dried with magnesium sulfate and the ether was vacuum distilled. The intermediate was then reacted with acetic anhydride (5.5 moles per mole of N-methylglycine) for ten days in the dark at room temperature. Excess acetic anhydride was removed under vacuum using toluene to remove the last traces, and 3MS was distilled twice under vacuum (145°C / 0.25 Torr), a 20 cm Vigreaux column being intercalated in the second opportunity. The product thus obtained was lightly yellow, melted at about 36°C and its IR spectrum was coincident with that appearing in ref. 3. Hydrocarbon solutes of different origins, all of them more than 99% pure, were used as received; their names can be read in Table 2.

Table 2

Thermodynamic functions of partition and adsorption of hydrocarbons at infinite dilution in 3-Methylsydnone at 40°C

SOLUTE	$K_L \pm \sigma(K_L)$	$-\Delta H_L^\circ$ (KJ/mol)	$K_A \pm \sigma(K_A)$ (x 10^4 cm)	$-\Delta H_A^\circ$ (KJ/mol)
n-Heptane	9.98 ± 0.22	25.7 ± 2.6	3.46 ± 0.01	33.9 ± 1.3
n-Octane	19.8 ± 0.47	30.4 ± 3.5	9.11 ± 0.02	38.8 ± 1.7
n-Nonane	41.3 ± 2.02	37.8 ± 7.6	24.0 ± 0.11	42.8 ± 2.3
n-Decane	108. ± 12.0	44.9 ±18.5	61.0 ± 0.63	46.8 ± 3.0
2,2,4-Trimethylpentane	9.75 ± 0.39	29.4 ± 4.4	4.43 ± 0.02	33.5 ± 1.3
Methylcyclohexane	21.5 ± 0.20	21.9 ± 1.3	2.58 ± 0.01	31.6 ± 1.1
Ethylcyclohexane	46.0 ± 0.96	27.0 ± 2.7	6.66 ± 0.05	34.8 ± 1.9
1-Heptene	18.6 ± 0.30	23.7 ± 2.0	4.02 ± 0.01	35.0 ± 1.3
1-Octene	35.4 ± 0.90	29.1 ± 3.9	10.7 ± 0.05	38.8 ± 2.2
1-Nonene	73.3 ± 2.40	39.5 ± 5.7	27.6 ± 0.12	42.3 ± 2.2
Benzene	237. ± 0.83	29.3 ± 1.2	2.61 ± 0.04	30.3 ± 2.6
Toluene	455. ± 1.95	32.4 ± 1.2	7.86 ± 0.10	36.4 ± 2.3
Ethylbenzene	746. ± 4.92	34.5 ± 1.8	20.2 ± 0.26	40.4 ± 2.9
m-Xylene	875. ± 6.23	35.5 ± 2.1	22.7 ± 0.32	40.9 ± 3.4
p-Xylene	829. ± 5.25	35.3 ± 2.0	22.1 ± 0.27	41.2 ± 3.1

Chromatographic packings were prepared by coating 3MS on Chromosorb P AW 60/80 (Johns-Manville pink diatomaceous earth support) in a rotary evaporator, under a nitrogen stream and gentle heating, using chloroform as the volatile solvent. Six different packings, containing 5.11_3, 7.02_6, 9.05_1, 11.53_8, 15.74_6 and 19.51_0 % by weight of 3MS were

prepared. Coated supports were packed into 0.53 cm I.D. stainless steel tubes, 0.50 or 1.0 m in length.

Column temperature was controlled to better than ±0.05°C by immersion in a water bath. Nitrogen was used as carrier gas; it was successively passed through a molecular sieves trap (Davidson 5A), a Brooks 8606 pressure regulator, a Brooks 8743 flow controller and a 2 m x 1/8 in O.D. coiled copper tube immersed in the column bath. Inlet pressures were measured with a mercury manometer at a point between the copper coil and a Swagelock 1/4 in s.s. "T"; one branch of the latter was provided with a septum through which solute vapors were injected by means of Hamilton microsyringes; the column was connected to the remaining branch. Detection was performed with a Hewlett-Packard 5750 FID and electrometer whose signals were fed to a Hewlett-Packard 3396A integrator.

Sample sizes were of the smallest size compatible with instrumental noise (about 10 nmol); solute vapors and a small methane sample were simultaneously injected, and adjusted retention times were measured to 10^{-3} min between the maxima of the solute and the methane peaks. Specific retention volumes (V_g°) and net retention volumes per gram of packing (V_N°) were calculated in the usual form **[9]** from adjusted retention times and values of the experimental variables.

RESULTS AND DISCUSSION

Specific retention volumes measured in a given column were fitted to the equation

$$\ln V_g^\circ = -\Delta H_S^\circ / RT + \text{constant} \qquad (1)$$

where ΔH_S°, the heat of sorption, may signify different things depending on the retention mechanism(s). Differences between V_g° values calculated by means of Eq. (1) and experimental values were smaller than 0.3%; interpolation was thus very accurate and data obtained in different columns at slightly different temperatures could be corrected to a common temperature to enable further elaboration of results. Within experimental error (between ± 1% and ± 4% at a 95% confidence level) the heats of sorption were found to be independent of stationary phase loading.

In Figure 1 V_N° values at 43°C for a group of selected hydrocarbons, representative of different families, have been plotted against the percentage by weight of 3MS in the packing, w. There are notorious differences between the solutes and in none of the cases the retention can be explained exclusively in terms of solution in the stationary phase, since straight lines through the origin should be expected in that case; the existence of more than one retention mechanism is made evident. Conder *et al.* **[5]** proposed a model that takes realistically into account the most important possible contributions to solute retention; their model may be summarized in the equation

$$V_N^\circ = K_L V_L + K_A A_L + K_S A_S \qquad (2)$$

where K_L is the liquid-gas partition coefficient, K_A and K_S are the adsorption coefficients at the gas-liquid and at the liquid-solid interfaces, respectively, and V_L, A_L and A_S represent the stationary phase volume, the gas-liquid interfacial area and the solid-liquid interfacial area, all of them expressed per gram of packing. Adsorption on uncovered portions of the solid support, not included in Eq. (2), needs not to be considered when more than 2-3% by weight of a polar stationary phase is coated on the polar surface of Chromosorb P, whose specific surface area is about 4 m^2g^{-1}. Furthermore, it is highly improbable that 3MS molecules, highly polar and in enormous excess, might be displaced from their positions on the solid surface by hydrocarbon molecules. These considerations indicate that for the systems and experimental conditions of this work K_L and K_A can be evaluated by fitting V_N° to Eq. (2) with $K_S = 0$.

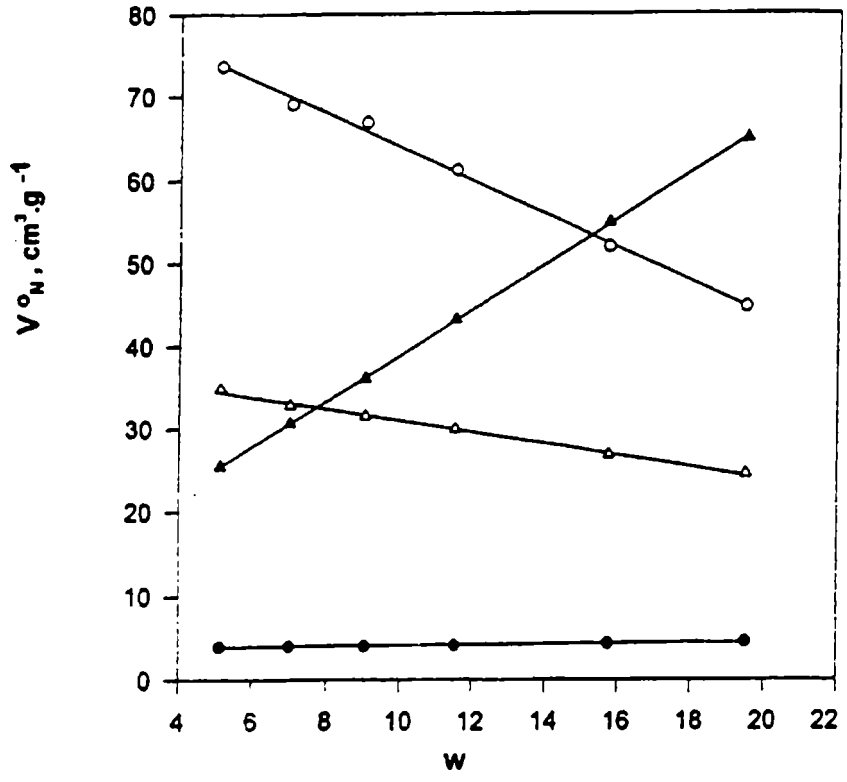

Fig. 1.- Retention volume per gram of packing at 43 °C, V_N°, against percentage by weight of 3MS in the packing, w. O: n-Decane; Δ: 1-nonene; ●: methylcyclohexane; ▲: toluene.

In order to use the reduced form of Eq. (2) the areas A_L remain to be evaluated; this was done by following the proposal of Martire *et al.* **[10]**, *i.e.* combining statically measured values of K_L and K_A for benzene and cyclohexane in β,β'-thiodipropionitrile (TDPN) with retention volumes obtained for both solutes in columns containing different loadings of TDPN on Chromosorb P and assuming that at the same loading of TDPN or 3MS calculated on a per volume basis both liquids have equal exposed surface areas. Thus obtained surface areas drop almost lineally with w for packings containing more than about 4 mL of stationary phase per 100 g of packing; this is why the plots of V_N° against w are straight lines with negative slopes for solutes whose retention is strongly adsorption dominated, as normal decane (see Figure 1).

Calculations performed by the same authors **[10]** indicate that the apparent liquid film thickness on Chromosorb P when w = 5% is about 30nm, and 200 nm when w = 20%. A volume of 1.3×10^{-22} cm^3/molecule can be calculated for 3MS in the liquid state at 40°C. If it is assumed that each molecule moves freely within a spherical cell with diameter d, a value of d = 0.6 nm can be calculated; this means that a stationary phase film 50 molecules thick could be calculated for the more lightly loaded packing in the present work. It is difficult to ascertain if support influence can be felt at the gas-liquid interface of such a film, and what fraction of the liquid is under true bulk conditions. This is an old and unresolved discussion between

chromatographers; probably the best answer is given by the results in Figure 1, that shows that V_N° values obtained with the lower loadings fall in line with those measured with the higher ones, for which films of up to 330 molecules can be calculated.

Values of K_L (intercepts) and K_A (slopes) were obtained from the linear regression of V_N° / V_L against A_L / V_L; the equation of 3MS density versus temperature given by Lemire and Sears **[1]** was employed. Correlation coefficients were always larger than 0.999, and in many cases larger than 0.9999.

Standard enthalpies of solution were computed with the equation

$$\Delta H_L^\circ = -R[\partial \ln K_L / \partial(1/T)] - RT(1-\alpha_1 T) \qquad (3)$$

where α_1 is the thermal expansion coefficient of 3MS, computed by means of the equation of Lemire and Sears. ΔH_L° corresponds to the transfer of one mole of solute from an ideal vapor phase at a pressure of 1 atm to an hypothetical solution where it is at unitary molar fraction with behavior extrapolated from infinite dilution **[11]**. On applying Eq.(3) a constant enthalpy of solution through the experimental temperature range was assumed, and non-idealities of the vapor phase were neglected. Both assumptions are justified by the unavoidably large errors in the measurement of ΔH_L° by combining data obtained in several columns.

Standard enthalpies of adsorption were calculated by means of the equation

$$\Delta H_A^\circ = R[\partial \ln K_A / \partial(1/T)] \qquad (4)$$

and correspond to the transfer of one mole of solute from the ideal vapor phase at 1 atm to an ideal adsorbed state where adsorbate molecules interact with the surface only **[12]**. Again, temperature independence of ΔH_A° and an ideal vapor phase was assumed in the calculations.

Solution and adsorption properties for the fifteen hydrocarbons in 3MS at 40°C were gathered in Table 2. Uncertainties given for K_L and for K_A are the standard deviations for the intercepts, σ (K_L), and for the slopes, σ (K_A), respectively, obtained in the regression of V_N° / V_L against A_L/V_L. The confidence ranges for ΔH_L° and ΔH_A° at the 95% level were calculated taking into consideration that two successive regressions are necessary to calculate the enthalpy values **[7]**.

The percent contribution of adsorption to the retention volume for four representative hydrocarbons in the columns containing extreme 3MS loadings, calculated using K_L and K_A values, are given in Table 3. In the first place these results give us an idea of the enormous errors that the neglect of adsorption would introduce in the study of the solution process; in the second, they explain the large errors made on computing ΔH_L° for paraffins. In the case of n-decane, a solute whose percent adsorption retention is 95% at the 5.11_3 % loading and 70%at the 19.51_0% loading, that error amounts to 41% of ΔH_L°

In order to investigate any correlation between solution and adsorption properties values of K_A at 40°C have been plotted against those of K_L in Figure 2. Points corresponding to solutes belonging to a given family fall on a common straight line, but there is not a general

correlation involving hydrocarbons of different families. A similar behavior can be detected in the plot of ΔH_A° against ΔH_L° in Figure 3, although the trends are not so clear in this case as a consequence of the large errors involved in the measurement of the enthalpies.

Table 3

Percent contribution of adsorption to the retention volume for extreme loadings at 45°C

SOLUTE	5.11_3 % w/w	19.51_0 % w/w
n-Heptane	91.9	58.3
1-Heptene	87.4	46.1
Methylcyclohexane	56.4	32.4
Toluene	36.7	6.7

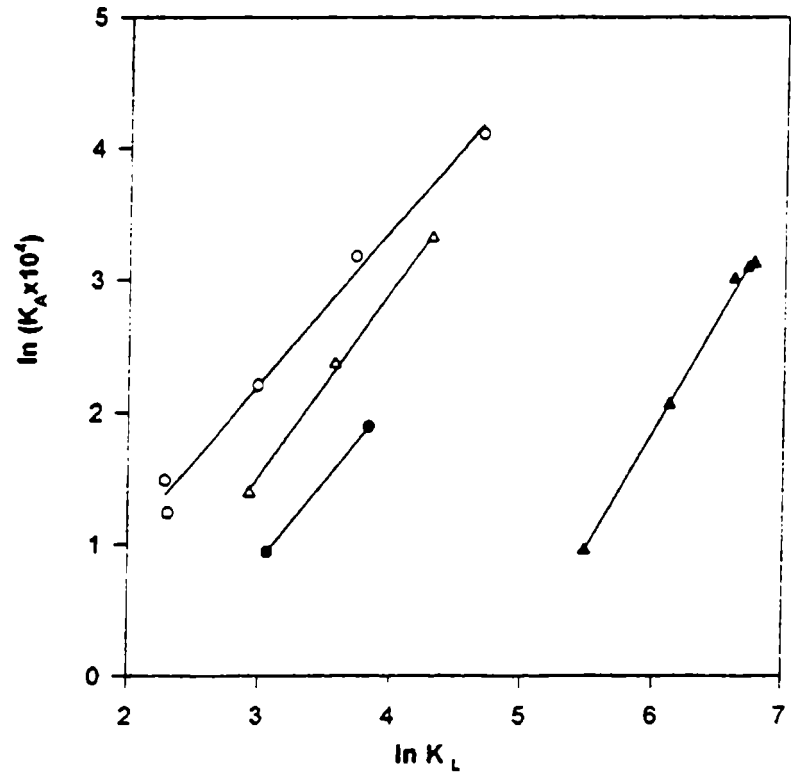

Fig. 2.- Relationship between adsoption and partition coefficients at 40 °C. O: Alkanes; Δ: 1-alkenes; ●: cycloalkanes; ▲: aromatics.

Bulk phase activity coefficients at infinite dilution, $\gamma_2^{b,\infty}$, were calculated by means of the equation

$$\gamma_2^{b,\infty} = RT / p_2^\circ K_L v_1^\circ \qquad (5)$$

where p_2° is the solute vapor pressure and v_1° the stationary phase molar volume **[6]**. Results obtained in 3MS at 40°C can be read on Table 4, and compared with the results obtained at 25°C in FA **[13]** and in EG **[14]**. The smallest values are obtained when 3MS is the solvent; differences with EG and FA are very important, and cannot be explained by the temperature difference. This trend is in coincidence with the absence of surfactant self-aggregation processes in 3MS found by Evans *et al.* **[3]**. It is important to stress that if positive deviations from the ideal behavior depend mainly on solute-solvent c.e.d. differences, and if the solvents

c.e.d.'s are correctly gauged by the $\sigma/v^{1/3}$ quotients, the values of the activity coefficients in 3MS should be intermediate between those in FA and EG.

Table 4

Bulk liquid and gas-liquid interface activity coefficients of hydrocarbons in polar solvents

	FA, 25°C		EG, 25°C		3MS, 40°C	
SOLUTE	$\gamma_2^{b,\infty}$	$\gamma_2^{s,\infty}$	$\gamma_2^{b,\infty}$	$\gamma_2^{s,\infty}$	$\gamma_2^{b,\infty}$	$\gamma_2^{s,\infty}$
n-Heptane	2220	110	1020	29.6	277	26.7
n-Octane	3880	163	1730	39.2	415	31.1
n-Nonane	6410	230	2850	53.5	585	39.3
n-Decane					650	51.1
2,2,4trimethylpentane	2280	134	1150	32.8	269	29.9
Methylcyclohexane	914	79.1	542	21.5	130	15.7
Ethylcyclohexane	1710	118	773	29.7	199	23.0
1-Heptene	1010	70.4	507	21.6	122	16.6
1-Octene	1850	103	914	28.6	191	21.6
1-Nonene					272	29.0
Benzene	52.3	15.2	32.3	5.64	5.89	2.49
Toluene	102	22.0	61.7	7.90	9.48	3.50
Ethylbenzene	196	32.0	112	10.3	15.9	4.63
m-Xylene	214	33.6	124	11.2	15.4	4.88
p-Xylene	208	33.9	123	11.2	15.5	4.98

Surface activity coefficients at infinite dilution, $\gamma_2^{s,\infty}$, were calculated with the equation deduced by Eon and Guiochon **[15]** for a monolayer model:

$$\gamma_2^{s,\infty} = [RT / p_2^\circ (K_L v_1^\circ + K_A a_1^\circ)] \exp[a_2^\circ (\sigma_1^\circ - \sigma_2^\circ) / RT] \qquad (6)$$

where σ_1° and σ_2° represent the stationary phase and the solute surface tensions in the pure state, respectively; a_1° and a_2° are the corresponding molar surface areas, approximated by the relation $a_i^\circ = 1.2N^{1/3}(v_i^\circ)^{2/3}$, where N is Avogadro's constant. This last is a rough approximation, only valid for spherical molecules; a more exact calculation would demand to take into account not only the molecular shape but also to know how the molecule settles on the surface. The results obtained for adsorption on 3MS at 40°C have been gathered in Table 4, together with the results taken from former papers for FA and EG at 25°C **[16]**.

In contrast to the trends observed in Figure 2, points corresponding to hydrocarbons of different families fall on a common straight line in Figure 4, where logarithms of activity coefficients in the surface phase are plotted against the corresponding values in the bulk phase; the correlation coefficient is 0.997, and a similar behavior is observed for the results in FA and in EG **[16]**. For systems with strong adsorption $K_A a_1^\circ >> K_L v_1^\circ$, and from Eq. (5) and Eq. (6)

$$K_A / K_L \cong (\gamma_2^{b,\infty} v_1^\circ / \gamma_2^{s,\infty} a_1^\circ) \exp[a_2^\circ (\sigma_2^\circ - \sigma_1^\circ) / RT] \qquad (7)$$

that indicates that the different trends displayed in both figures can be attributed to the very unlike surface tensions exhibited by hydrocarbons of different families in the pure state.

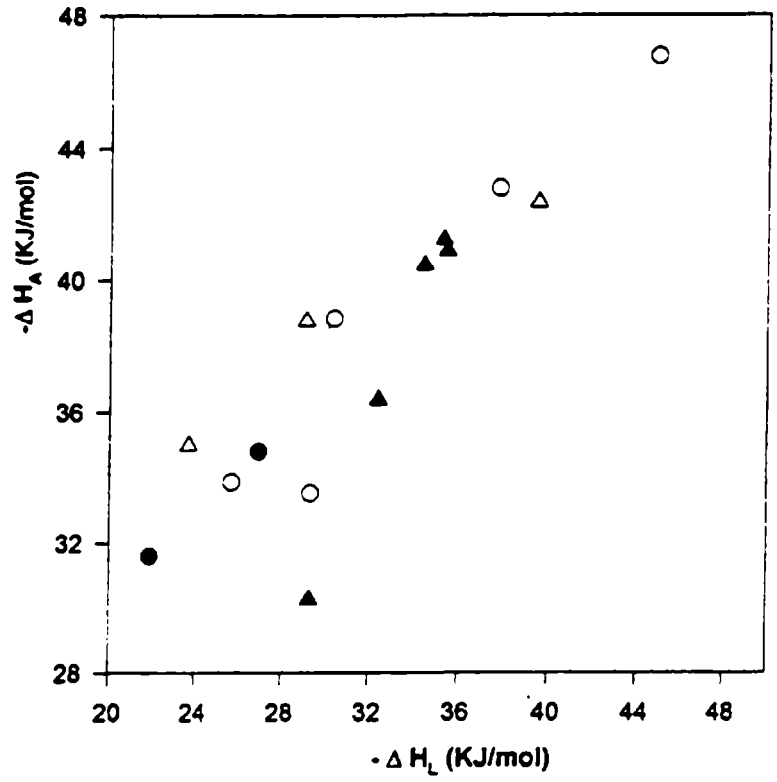

Fig. 3.- Relationship between adsorption and partition enthalpies. Symbols as in Figure 2.

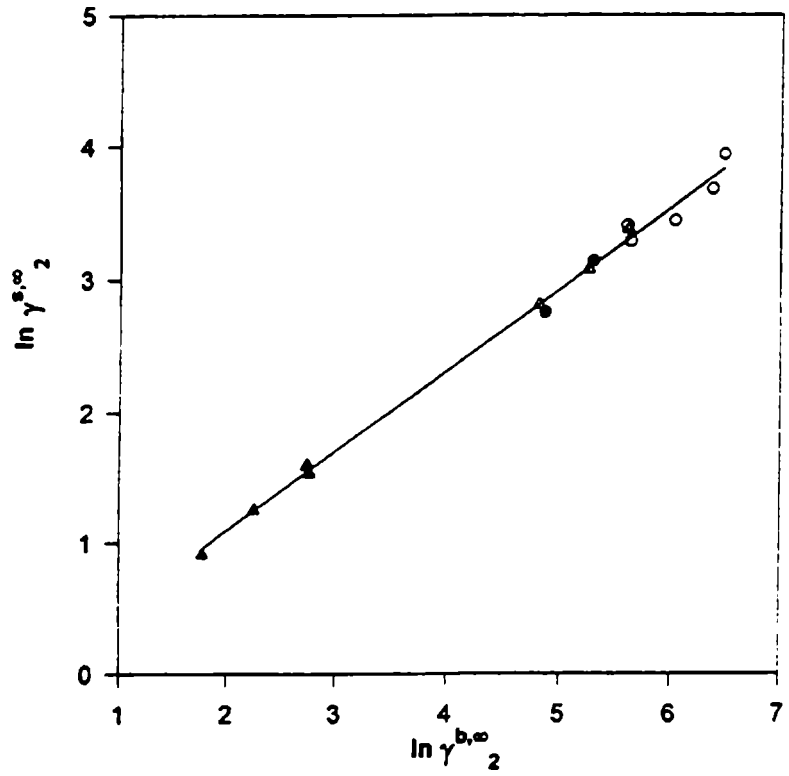

Fig. 4.- Relationship between gas-liquid interface and bulk liquid infinite dilution activity coefficients at 40°C. Symbols as in Figure 2.

For all the studied systems surface activity coefficients are smaller than their bulk counterparts. This is the trend that could be expected: since the number of nearest neighbors is smaller at the surface than in bulk solution, nonideality effects are expected to be lower at the surface. However when the values obtained in both phases of the three solvents are compared it can be seen that the activity coefficients on the 3MS surface are larger than what could be predicted on the basis of the values of the activity coefficients in the bulk phase; alkanes surface activity coefficients in 3MS, for instance, are almost equal to those in EG, in spite of very large differences between the bulk activity coefficients in both solvents. These trends are

made evident in Figure 5, where the quotients ($\gamma_2^{s,\infty} / \gamma_2^{b,\infty}$) in 3MS have been plotted against the corresponding quotients in FA or EG.

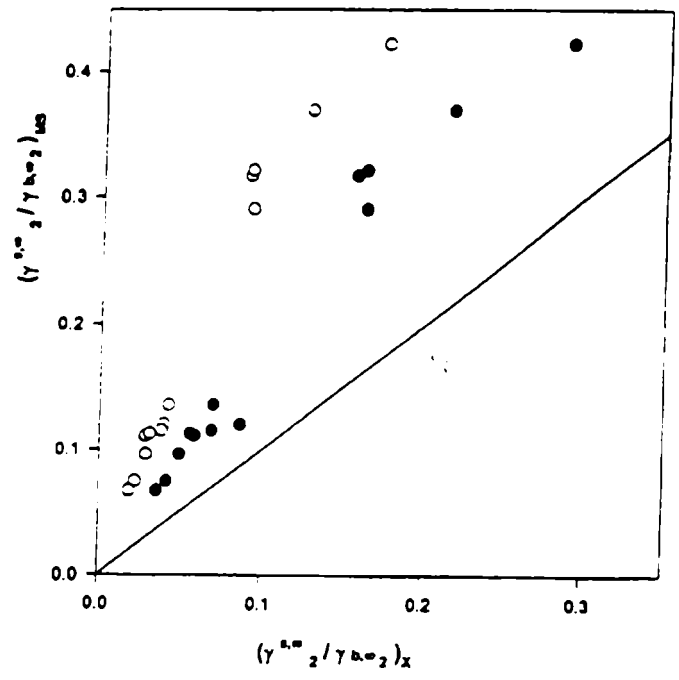

Fig. 5.- Relationship between the quotients ($\gamma_2^{s,\infty} / \gamma_2^{b,\infty}$) in 3MS and in the stationary phase X. o: X = EG; o: X = FA. The line corresponds to equal values in both stationary phases.

This figure tells us that the relationship between surface and bulk properties can be very different for different solvents, and about the unpredictability of surface properties exclusively on the basis of bulk properties and vice versa. This may be attributed to structural rearrangements of solvent molecules at the surface, through processes that can be very different in a given solvent than in another. From this point of view, the surface tension of 3MS can be the result of an intense dipoles orientation process at the liquid surface, that keeps very little relation with the random distribution in the bulk suggested by the value of its *g* factor.

In order to further test this possibility the dispersion contributions to the surface tension, σ_1^d, of FA, EG and 3MS were calculated by two methods:

I. The proposal of Hauxwell and Ottewill **[17]**, as applied by Hartkopf **[18]** to gas chromatographic data: a plot of $K_A p_2^\circ$ against σ_2° for saturated hydrocarbons (alkanes or cycloalkanes) results in a straight line that intersects the abscissa at $\sigma = \sigma_1^d$.

II. By Dorris and Gray proposal (19), according to which

$$\sigma_1^d = (\Delta G_{CH_2} / 2 N a_{CH_2})^{1/2} \sigma_{CH_2}^{-1} \qquad (8)$$

where N is Avogadro number, a_{CH_2} is the cross-sectional area of $-CH_2-$ groups (0.06 nm^2), σ_{CH_2} is the surface free energy of a surface made up of only $-CH_2-$ groups (35 dyn/cm, as calculated for poly(ethylene)), and ΔG_{CH_2} is given by

$$\Delta G_{CH_2} = RT \ln(K_{A,n-1} / K_{A,n}) \qquad (9)$$

where $K_{A,n+1}$ and $K_{A,n}$ are the adsorption coefficients for normal alkanes with n+1 and n carbon atoms, respectively. The results have been gathered in Table 5, that shows that both methods are only in a moderate agreement. Both methods indicate important polar contributions, σ_1^h, to the surface tension of 3MS (as calculated by the difference $\sigma_1^h = \sigma_1^\circ - \sigma_1^d$), not very different from those corresponding to FA and EG.

Table 5

Dispersion contributions to the surface tension of solvents calculated by two different methods

SOLVENT	METHOD I[a]	METHOD II[b]
FA	29.6	28.8
EG	30.2	28.6
3MS	28.3	32.0

Units: dyn/cm
[a] Ref. 17 and 18. [b] Ref. 19

These results reflect important differences between the surface (as given by σ_1^h) and the bulk (according to its Kirkwood g factor) properties of 3MS. Under these circumstances the prediction of its c.e.d. through the quotient $\sigma/v^{1/3}$ can result in a serious overestimation, and this can be the origin of its incapacity for forming micelles and of the relatively small positive deviations from Raoult's law displayed by hydrocarbons.

ACKNOWLEDGEMENTS

This work was sponsored by CONICET (Consejo Nacional de Investigaciones Científicas y Técnicas de la Rep. Argentina) and by CICPBA (Comisión de Investigaciones Científicas de la Prov. de Buenos Aires).

REFERENCES

[1] Lemire, R.J.; Sears, P. G.- **J. Chem. Eng. Data, 22**, 376 (1977).
[2] Gordon, J.E.- ***The Organic Chemistry of Electrolyte solutions***. Wiley, New York (1975).
[3] Beesley, A.H.; Evans, D.F.; Laughlin, R.G.- **J. Phys. Chem., 92**, 791 (1988).
[4] Martire, D.E.-, In ***Progress in Gas Chromatography*** (J. H. Purnell, Ed.), Chap. 2. Wiley-Interscience, New York (1968).
[5] Conder, J.R.; Locke, D.C.; Purnell, J.H.- **J. Phys. Chem., 73**, 700 (1969).
[6] Conder, J.P.; Young, C.L.- ***Physicochemical Measurement by Gas Chromatography***, Chap. 11, Wiley, New York (1979).
[7] Castells, R.C.- **J. Chromatogr., 111**, 1 (1975).
[8] Vasil'eva, V.F.; Yashunskii, V.G.- **J. Gen . Chem. USSR** (Engl. Transl.) **32**, 2845 (1962).
[9] Laub, R.J.; Pecsok, R.L.- ***Physicochemical Applications of Gas Chromatography***. Wiley-Interscience, New York (1978).
[10] Martire, D.E.; Pecsok, R.L.; Purnell, J.H.- **Trans. Faraday Soc., 61**, 2496 (1965).

[11] Castells, R.C.- **J. Chromatogr.**, **350**, 339 (1985).
[12] Meyer, E.F.- **J. Chem. Educ.**, **57**, 120 (1980).
[13] Castells, R.C.- **An. Asoc. Quim. Argent.**, **64**, 155 (1976).
[14] Arancibia, E.L.; Catoggio, J.A.- **J. Chromatogr.**, **238**, 281 (1982).
[15] Eon, C.; Guiochon, G.- **J. Colloid Interface Sci.**, **45,** 521 (1973).
[16] Castells, R.C.; Arancibia, E.L.; Nardillo, A.M.- **J. Colloid Interface Sci.**, **90**, 532 (1982).
[17] Hauxwell, F.; Ottewill, R.H.- **J. Colloid Interface Sci.**, **34**, 473 (1970).
[18] Hartkopf, A.- **J. Colloid Interface Sci.**, **40**, 313 (1972).
[19] Dorris, C.M.; Gray, D.G.- **J. Colloid Interface Sci.**, **77**, 353 (1980).

THEORETICAL AND PRACTICAL ASPECTS OF FLOW CONTROL IN PROGRAMMED-TEMPERATURE GAS CHROMATOGRAPHY

ASPECTOS TEORICOS Y PRACTICOS DEL CONTROL DE FLUJO EN CROMATOGRAFIA GASEOSA A TEMPERATURA PROGRAMADA

F.R. González[1], A.M. Nardillo[2]

SUMMARY

Behavior patterns for the temperature dependence of column head pressure and outlet volumetric flow rate are analyzed for some particular configurations of chromatograph's flow control system. Quantitative prediction of this behavior, and specially it's effect on gas hold up time, is evaluated. The attention is centered on the application to PTGC retention simulation.

Keywords: *temperature programming; flow control; hold-up time.*

INTRODUCTION

The current methodology for programmed temperature (PT) retention estimation through isothermal data was settled in the early 60's **[1-5]**. The starting point is the differential equation of band migration. From general isothermal chromatographic theory:

$$\frac{dz}{dt} = \frac{v(z)}{(1+k)} \qquad (1)$$

Where z is the axial variable of cylindrical coordinates which describes the position of solute's peak in the column at time t from injection, dz/dt is the migration rate of solute's peak at z position, k the capacity factor of the column and v(z) is the local carrier gas velocity. Assuming valid D'Arcy's equation as the differential equation of motion for the carrier gas, and the ideal gas equation of state, v(z) can be related to it's isothermal average along the column $\bar{v}$ by (see for example **[6]**) :

$$v(z) = \frac{\bar{v}}{Q(z)} \qquad (2)$$

---

[1] División Química Analítica, Facultad de Ciencias Exactas, Universidad Nacional de La Plata
[2] Miembro de la Carrera del Investigador del CONICET; Profesor Asociado, UNLP

Where the local velocity factor Q(z) is:

$$Q(z) = (3/2)\frac{(P^2-1)}{(P^3-1)}[P^2-(z/L)(P^2-1)]^{1/2} \qquad (3)$$

P is column's inlet/outlet pressure ratio, P_i / P_o.

So far, we were involved with isothermal conditions, being (z,t) the variables of differential eq. (1). In programmed temperature there is a defined relationship between variable t and the absolute temperature T, fixed by the operator as an explicit function: $T = f(t)$. We shall use the notation: $dT/dt = f'(T)$ .The configuration of the flow control system will define how column's head pressure will evolve with temperature, namely defining a certain P(T). The characteristics of this function for some types of flow control is a central topic of this paper. So, in PT eq. (3) shows that Q is dependent as Q(z,T). Obviously, $\bar{v}$ is a function only of P(T) for a given column.

Changing variable t by T, replacing v(z) in (1), and attending that gas hold-up time is $t_0(T) = L / \bar{v}(T)$, where L is column's length, the differential eq. of peak motion in PTGC becomes:

$$\frac{dz}{dT} = \frac{L}{f'(T)\, Q(z,T)\, t_{M0}(T)\, [1+k(T)]} \qquad (4)$$

As shown, estimation of retention parameters in PTGC means dealing with two general aspects: with thermodynamics as T affects k(T), and fluid dynamics, involving the behavior of P(T), and so conditioned by the gas flow control. Two special types of flow control have been most commonly treated in the literature related to PTGC retention: constant mass flow **[2,4]**, and constant pressure drop along the column **[4,6]**. Less attention has been given to other widely applied flow control devices, such as mechanical controllers consisting in a needle valve and diaphragm operated valve in serial array, and more recently developed electronic head pressure programmable chromatographs.

Integration of eq. (4)can be carried out considering this a summation of sequential isothermal states, or in other words, assuming thermal equilibrium for each integrating point (*Thermal equilibrium during practical temperature programming has been questioned* **[7,8]**). This is the fundamental hypothesis of the theory in addition to those implicit in (1) and (3). It can be shown **[9]** from eq. (4) that:

$$1 = \int_{T^0}^{T_R} \frac{dT}{f'(T)\, t_0(T)\, [1+k(T)]} \qquad (5)$$

Where T^0 and T_R are the initial temperature of the program and solute's retention temperature, respectively. Solving (5) for a certain system implies that $t_0(P(T))$ and k(T) should be attainable for this. The ultimate goal of this work is to develop, for the studied systems, analytical expressions of $t_0(T)$, as function of accessible parameters so the integrand of eq.(5) can be explicited .

The endeavor of taking approximations of different nature, with the aim to simplify the solution of the integral equation, has been a constant that signed PTGC simulation development from it's beginnings **[1-3, 10, 11]**. Present universally available computation facilities makes many of them now unnecessary. Nevertheless, a contemporary common practice among simulation procedures is to linearize the temperature dependence of t_0 **[6,11]**, approximation that would be suitable only for special situations, as will be shown. In other cases t_0 has been approximated as constant with temperature **[12-14]**.

EFFECTS OF TEMPERATURE ON GAS HOLD-UP TIME

The objective of this section is to settle a general expression of t_0 as a function of P(T), valid for capillary or packed columns.

Integrating D'Arcy's equation along the column and by applying Continuity equation **[15,16]** to the ideal gas, the following relationship may be stated between the volumetric flow rate at the outlet of the column $F_o(T)$, viscosity of the carrier gas $\eta(T)$ and P(T), all measured at column's temperature T **[15]**:

$$2\frac{L}{A\,B\,P_o}\,F_o(T)\,\eta(T) = [P^2(T)-1] \tag{6}$$

where A is the cross sectional area of the empty column and B the permeability (see for example **[17,18]**). Thermal expansion of materials is known to exert a very small effect and for practical purposes the factor L/(AB) may be taken as constant with temperature. The verisimilitude of this assumption is discussed in the following section. Then, if eq. (6) is divided by the same expression applied to a initial or reference condition and P_o is held constant :

$$\frac{F_o(T)\,\eta(T)}{F_o^0\,\eta^0} = \frac{[P^2(T)-1]}{[P^{o2}-1]} \tag{7}$$

where F_o^0 is the outlet volume flow rate at reference condition (T^0,P^0). From here forth, the superindex 0 will denote reference or initial condition for any variable. The temperature dependence of gas viscosity, in the range of chromatographic interest, can be written as **[15,19]**:

$$\eta(T) = C_G T^N \tag{8}$$

Exponent N is 0.725 for nitrogen, 0.646 for helium and 0.680 for hydrogen **[19]**. By applying (8), (7) turns to:

$$F_o(T) = (C_C\,T^{-N}P_o)\;[P^2(T)-1] \tag{9}$$

where column's "flow rate constant" C_C is:

$$C_C = \frac{F_o^0 T^{0N}}{(P^{0^2} - 1)\, P_o} \tag{10}$$

Replacing $F_o^0 / (P^{0^2} - 1)$ as given by (6) and T^{0N} by (8), reveals the physical meaning of the constant:

$$C_C = \frac{A\, B}{2\, L\, C_G} \tag{11}$$

For a given packed column at constant temperature and mass-flow B / C_G is inversely proportional to Blake-Kozeny's friction coefficient which is a factor that determines the irreversible conversion of mechanical energy into heat, the so called frictional loss **[16]**. The constant is a flow property of combined column and gas .

If temperature and outlet pressure are held constant, according to eq.(9) F_o should be a straight line passing through the origin when plotted against the adimensional variable $(P^2 - 1)$, being the slope $(C_C T^{-N} P_o)$. This is actually a procedure that can be followed to obtain C_C, as an alternative to the application of eq.(10).

Equation (9) is applicable either to packed or capillary columns connected to any kind of flow control, as it was derived considering the column individually. Thus, if flow parameters are measured at a reference or initial condition, as routinely do chromatographers, is imperative to know how P evolves with temperature to enable the prediction of flow rate as a function of temperature, and viceversa. The evolution of P(T) will depend upon the configuration of the system upstream the column.

A similar reasoning can be followed for t_0. According to the classical isothermal chromatographic theory, the dead volume of the column at temperature T can be evaluated by: $V_0(T) = F_o(T)\, j(T)\, t_0(T)$. Applying this to a reference condition, dividing both expressions, neglecting thermal dependence of void volume and eliminating flow rate by using (9), leads to the final expression we were seeking:

$$t_0(T) = (C_t\, T^{-N} P_o)^{-1}\, \frac{[P^3(T) - 1]}{[P^2(T) - 1]^2} \tag{12}$$

where the "dead time constant" is:

$$C_t^{-1} = t_0^0\, \frac{(P^{0^2} - 1)^2 P_o}{(P^{0^3} - 1)\;\; T^{0N}} \tag{13}$$

The relationship between column's constants, can be derived by applying the solution (32) from reference **[20]**:

$$C_t = \frac{3\, C_C}{2\, V_0} \tag{14}$$

The same considerations of (9) can be formulated for (12), standing out the fact that the only hypothesis added, to those already accounted for (4), is the insignificance of changes in column's geometric parameters L/AB and V_0 due to thermal expansion.

THERMAL EXPANSION EFFECTS

For a packed column can be shown, from basic definitions **[18,21]**, considering negligible the contribution of liquid phase respect to solid support, that thermal expansion will generate a relative change in total porosity ε according to:

$$\frac{1-\varepsilon(T)}{1-\varepsilon^0}=\left[\frac{1+3\alpha_S(T-T^0)}{1+3\alpha_W(T-T^0)}\right]\equiv D \qquad (15)$$

being α_W tube's wall linear thermal expansion coefficient , and α_S that of solid support. Assuming that the interparticle porosity ε_u is a constant fraction u of total porosity, and calculating the permeability B of the packed column through Carman-Kozeny's equation:

$$\frac{B(T)}{B^0}=[1+\alpha_S(T-T^0)]^2\left[\frac{1-D\,(1-\varepsilon^0)}{\varepsilon^0}\right]^3\left[\frac{1-u\varepsilon^0}{1-u\,[1-D\,(1-\varepsilon^0)]}\right]^2 \qquad (16)$$

With assumptions so far displayed, relative temperature changes in column's interstitial void volume, the space where convective gas transport occurs, is evaluable by:

$$\frac{V_0}{V_0^0}=\left[\frac{1-D(1-\varepsilon^0)}{\varepsilon^0}\right][1+3\alpha_W(T-T^0)] \qquad (17)$$

We must be bewared that, although eqs.(15-17) are applicable to global quantities, if thermal expansion effects would be significant in packed columns, the homogeneity of this must be affected. If the wall expands much more than the packing, the "extent of wall region" **[22]**, that is the region where homogeneousness of the packing is disturbed by the presence of the wall, should be increased. Channeling near the wall could be expected and a consequent anomalous behavior of the column, with a diminished pressure drop respect to a well packed one. The most disadvantageous condition, where thermal expansion coefficients differ significantly, is that when tube's wall is metallic, being the packing usually a siliceous material. In Table 1 are shown relative values of porosity, permeability, (L/AB) ratio and interparticle void volumes as a function of the temperature interval, calculated using eqs.(15-17) with reported values of expansion coefficients, specified initial porosity and u, assuming that the wall is made of stainless-steel.

Expected effect of thermal expansion on the described parameters is very poor, at a point that would be difficult to evaluate experimentally. An early attempt of estimation was conducted through volumetric measurements **[15]**, but what can be stated a priori is that the experimental error would be within the order of the greatest changes in the parameters to be monitored.

Table 1

Relative change of column geometric parameters as a function of temperature interval according to Eqs. (15-17) considering a porous solid support packing

$(T - T^0)$	$\varepsilon / \varepsilon^0$	B / B^0	(L/AB) rel.	V_0/V^0_0
50	1.0002	1.0020	0.9971	1.0027
100	1.0005	1.0041	0.9943	1.0054
150	1.0007	1.0061	0.9915	1.0081
200	1.0010	1.0081	0.9887	1.0108
250	1.0012	1.0101	0.9859	1.0135

If flow in a capillary column is approximated by Hagen-Poiseulle's equation (valid for incompressible fluids) the permeability may be estimated as: $B = d_c^2 / 32$, where d_c is the internal diameter of the column **[18]**. With this consideration can be shown that expected thermal effects on L/AB and V_0 in a capillary are even lower than those taking place in a packed column.

FLOW CONTROL

In this section we shall analyze the behavior of $t_0(T)$ in four different types of flow control, contrasting predicted curves with experimental data .

Experimental

All system's common monitored physical observables are:

a) Column's outlet absolute pressure P_o. Here will be invariably the atmospheric pressure measured with a Fortin's design barometer.

b) Column's manometric inlet pressure P_i. This was measured by a mercurial column manometer , in the case of low pressure drop columns, and with a Bourdon's tube needle manometer for high ones.

From this two data the absolute head pressure P_i and P was readily acquainted for any column temperature.

c) Column's outlet volume flow-rate. This was measured at ambient temperature with a bubble flowmeter. Gas reaching ambient temperature was ensured interposing between the detector's outlet and the flowmeter a 6 m long 1/4" coiled copper tube as a heat exchanger. Pressure drop along the exchanger was calculated through standard procedures **[16]** and found to be in the order 10^{-2} mmHg, being completely negligible. Measured flow rate was corrected by water vapor saturation at the flowmeter and by temperature according to:

$$F_0(T) = F_{meas.} \frac{T}{T^0} \frac{(P_o - P_w)}{P_o}$$

where P_w is water vapor pressure at ambient temperature T^0.

d) Gas hold-up time $t_0(T)$. This was determined using methane as the unretained solute. As different chromatographs were employed, data are given with two different precision levels of 10^{-2} and 10^{-3} min.. Detection was carried out with FID detectors in all cases.

The oven, temperature control and record/integrator of two chromatographs were used alternatively, a Hewlett Packard 5880 and a Konik 3000 .The original flow control from the chromatograph was disassembled in order to rebuild it according to each studied configuration.

Nitrogen was used as the carrier and test gas in all cases.

Further experimental details will be given for each studied system.

The needle valve flow control

Needle valve in itself does not have much importance as a flow control device. The importance stems from the fact that it's theoretical description is necessary for treating more complicated mechanisms, since it is a basic accessory of pneumatic systems. Probably for a long time the most widely applied devices have been the mechanical flow controllers consisting in a needle valve in serial array with a diaphragm operated valve, all machined in the same body **[23]**. In a forthcoming paper we shall intend an evaluation of systems containing it. For doing that, the first step to take is the description of thermal evolution of a system containing only one isothermal restriction (valve) connected to a temperature variable resistance to flow (column), as we do in this section. The needle valve system is the simplest device to provide a predictable non-linear head pressure program, as will be shown.

The configuration of flow control to be analyzed is the one contained in the scheme of Figure 1. The first device present in the gas stream is the pressure regulator A, currently connected directly to the high pressure supply tank. It's function is to ensure a constant selectable absolute pressure P_1 at the inlet of needle valve B. The chosen reference condition, for sake of simplicity, will be when all the system, included the oven, is at ambient temperature T^0.

1. ***Valve's equation***. The first task will be to obtain a relationship between the flow rate at plane "2", F_2, when the oven is at temperature T, and the actual pressure drop in valve B. For doing that we shall apply the Macroscopic Mechanical Energy Balance **[16]** to planes "1" and "2", making the following hypothesis :1) Steady state. 2) Laminar flow. 3) Ideal gas. 4) Velocity profiles across tubing connections can be approximated by solution of Navier-Stokes eq. **[16]**, considering that pressure drops along them are small, compared to those in the valve and column ; in this case the cross sectional averages of gas velocity hold the relationship: $< v^3 > / < v >= 2 < v >^2$. 5) Fanning's friction coefficient is calculated applying the arithmetic averages, between valve's inlet and outlet, to parameters present in Reynold's

number. 6) Considering negligible, in current chromatographic conditions, the kinetic energy difference per unit mass-flow term, respect to the other terms of the macroscopic mechanical energy balance. 7) Applying Continuity equation of the ideal gas to arithmetic average quantities in the valve and plane "2": $\overline{P}\,\overline{<v>} = P_2 <v>_2$.

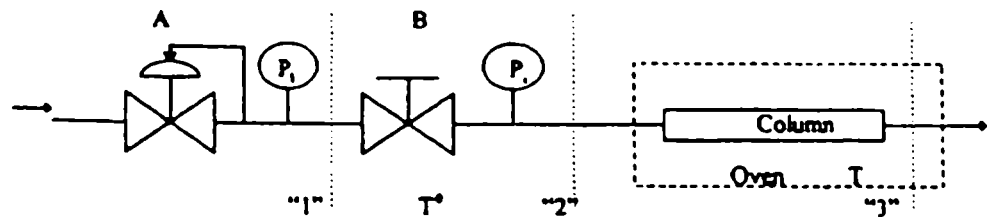

Fig. 1.- Scheme of the studied needle valve flow control system. A is a pressure regulator and B is the needle valve. Valve inlet pressure is P_1.

With the described hypothesis, the macroscopic balance leads to:

$$F_2 = (C_v\, T^{0\text{-}N} P_2)\left[\left(\frac{P_1}{P_2}\right)+1\right]^2 \ln(P_1 / P_2) \qquad (18)$$

where T^0 is valve's temperature (ambient), selected as reference, and $C_V = C / C_G$ .This is the valve equation. The constant C_V depends not only on the design and opening of the valve, through geometric parameters contained in C, but with the constant C_G of the carrier gas being used. Eq.(18) is of the same type of (9) and (12), although it was derived from a different formalism than the integration of D'Arcy's eq., valve constant plays an equivalent role as column's constant C_C.

We must be bewared that as pressure drop in the valve increases, velocity and pressure profiles bends along it, departing the arithmetic averages (hypothesis 5) from the correct ones calculated through the hypothetical exact fluid dynamic solution. In chromatographic conditions the inlet / outlet pressure ratio in the valve would rarely exceed 2 or 3.

*2. **Systems equation***. The second task is to study the system as a whole, to determine how it will evolve varying the temperature of the oven. When the column is connected to the valve in the chromatograph's flow control system, as was illustrated in the scheme of Figure 1, then $P_i(T) \equiv P_2(T)$. For a given oven temperature the flow rate at "2", F_2, can be related to the flow rate at plane "3", i.e. $F_o(T)$, accounting that mass flow is constant in steady state. Consequently, using Continuity eq. and the Ideal Gas eq.:

$$F_o(T) = \left(\frac{T}{T^0}\right)\left(\frac{P_i}{P_o}\right) F_2 \qquad (19)$$

$F_o(T)$ can be described also by column's eq.(9). Replacing (9) and (18) in (19) and rearranging:

$$\frac{\left(\frac{P_i}{P_o}\right)^2 - 1}{\left(\frac{P_i}{P_o}\right)^2 \left[\left(\frac{P_1}{P_i}\right)+1\right]^2 \ln(P_1 / P_i)} - C_S \left(\frac{T}{T^0}\right)^{1+N} = 0 \qquad (20)$$

where the constant of the system is: $C_S = C_V / C_C$ .Contrary to column's and valve's constants, C_S results independent of the parameter of the gas, depending only on geometric parameters of valve and column.

If selected P_1 and P_o remain constant through programmed temperature, then eq. (20) defines a implicit function of P_i in terms of C_S and the actual reduced temperature: $G(P_i, T) = 0$. This can be solved numerically by a trial and error algorithm of iterative approximations. System's constant can be evaluated from initial head pressure applying (20):

$$C_S = \frac{P^{02} - 1}{P^{02}\left[\left(\frac{P_1}{P_i^0}\right)+1\right]^2 \ln(P_1 / P_i^0)}$$

3. ***Experimental corroboration of valve's equation***. This implies testing the valve individually, separated from the column. If eq.(18) correctly describes the flow rate at the outlet of the valve, this plotted as a function of the adimensional variable $[(P_1 / P_2)+1]^2 \ln(P_1 / P_2)$ should provide a straight line passing through the origin with slope $(C_v T^{-N} P_2)$, when valve's temperature and outlet pressure remain constant .In Figure 2, curve 1, is presented the experimental behavior of a Brooks Instrument's needle valve (model 8504A) at constant ambient temperature. The outlet was connected directly to the flowmeter at the atmospheric pressure, so: $P_2 = P_o = \text{const}$. The inlet was connected to a pressure regulator. Note that the flow range longly exceeds that normally encountered in GC .

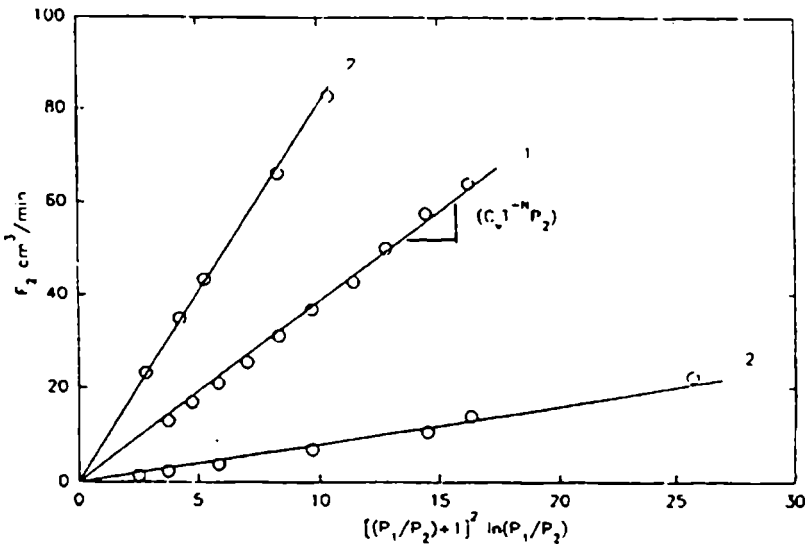

Fig. 2.- Outlet nitrogen flow-rate of a needle valve (plot 1) and a seat valve (plots 2) as a function of absolute inlet pressure. Range of P_1: 1120 to 2200 mmHg (abs.). Data interpreted by Eq. (18), measured at ambient temperature (T=26°C) and outlet atmospheric pressure (P_2=765 mmHg). Upper plot 2 belongs to an incremented opening, less than 5° knob turn with respect to lower plot 2.

In order to test the valve eq. with a different design, in the same figure are presented two curves, both identified by number 2, belonging to a almost closed seat valve. Valve's openings differ only in about a 5° turn between them .

As a matter of fact, the macroscopic balance (18) would be applicable to any restriction to the flowing gas meeting the basic hypothesis, as it only determines punctual values, making no inference about profiles between control planes. For example, it could be applied to two valves in serial array, or even to a packed bed, considering that the friction factor given by Blake-Kozeny's equation is for our purposes of the same nature of Fanning's factor **[16]**. As a curiosity in Figure 3 are plotted flow rate measurements for a 200 cm long column with 2 mm i.d.., filled with Chromosorb W 80/100 mesh, tested in the same conditions that were valves of Figure 2. Simultaneously are presented the same data interpreted according to integrated D'Arcy's eq. (9). Departures from linearity takes place at about 40 c.c./min in both representations and deviations are pondered differently. The origin of this phenomena may be conjecturally assigned to an uncontrolled heat build-up due to rising frictional losses, considering that frictional losses per unit mass-flow are in the order 10^8 cm^2/s^2, and the fact that is indifferent to the interpretation formalism. Measurements were taken at ambient temperature without a thermostatic bath.

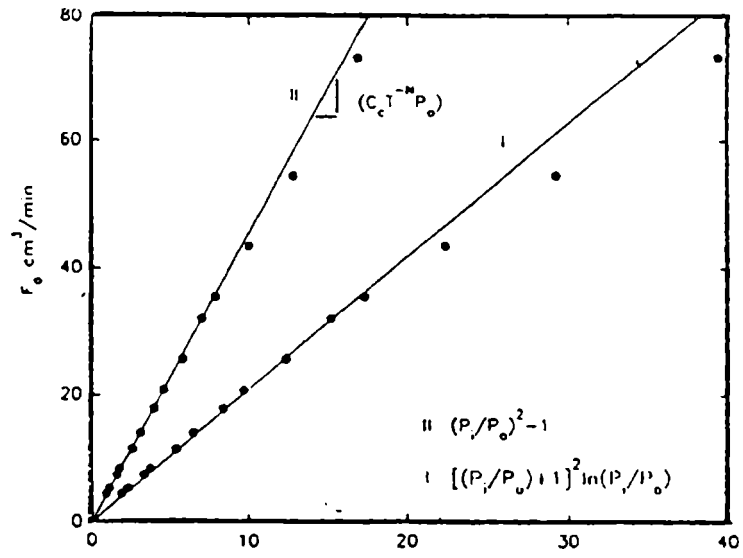

Fig. 3.- Same test as in Fig. 1 with a column 200 cm long, 2 mm I.D., filled with Chromosorb 80/100 mesh, 5% OV-101. T=27°C and P_o=760 mmHg. Plot I: data interpreted by Eq. (18), adimensional abscissa is $[P+1]^2$ ln P. Plot II: data interpreted by Eq. (9), adimensional abscissa is (P^2-1).

4. Experimental corroboration of system's equation. Experimental isothermal determinations of volume flow rate were performed at different temperatures with the flow control system illustrated in the scheme of Figure 1, using the needle valve mentioned before. Afterwards, fixing the same initial reference condition (P_i^0, T^0, F_0^0), chromatograph's FID detector was turned on and $t_0(T)$ were measured. A 2 m long packed column with OV-101 stationary phase was used. Figure 4A shows the experimental evolution of $P_i(T)$, starting from reference at 26° C, up to 240. Filled line was calculated by a Basic computer program solving equation (20). As column temperature rises, resistance to flow increases due to rising gas viscosity and P_i grows steeply. But since selected P_1 is constant, pressure drop in valve B is continuously diminishing, reducing consequently the gas supply as indicated by (18).

In Figure 4B calculated and experimental flow rates $F_o(T)$ are represented. The predicted behavior obtained by solving equations (20) and (9) is a initial increase, then going through a maximum, and later decay. This is what actually takes place as shown by

experimental data. In Figure 4C are represented experimental and theoretical behavior of $t_0(T)$ (equations (20) and (12)) for the column and conditions mentioned above. One should be alerted that this is not the unique behavior pattern of gas hold-up time for this flow control configuration. Theoretically, if initial conditions are selected adequately, $t_0(T)$ can go through a slight minimum, or be a almost linear monotonically increasing function.

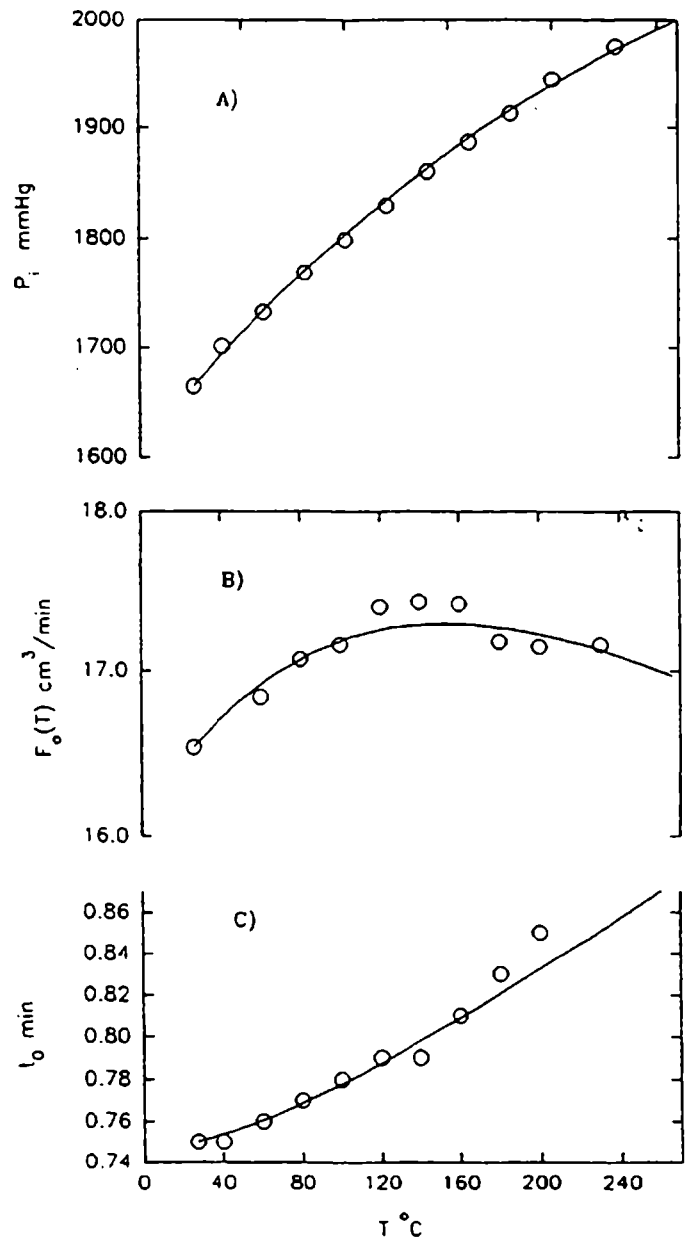

Fig. 4.- Flow functions for the needle valve control system. (A) $P_i(T)$ function. Column as in Fig. 3. P_o=766, P_1=2390 and P_i^0=1665 mmHg, T^0=26°C. Filled line calculated by using a Basic program solving Eq. (20). (B) $F_o(T)$ function, conditions as in (A) and F_0^0=16.54 cm^3/min. Filled line calculated by the same program, Eqs. (9,10,20). (C) t_0 function, conditions as in (A) and t_0^0=0.75 min. Filled line calculated by Basic program, Eqs. (12,13,20).

The constant head pressure control

A configuration of mechanical devices generating a constant head pressure on the column is schematically indicated in Figure 5. Pressure regulator A makes a coarse pressure reduction, smoothing operation conditions for the fine tuning regulator B, this one assures constant inlet pressure P_i through temperature program.

This is a rather trivial case already considered **[4, 6]**. If column's outlet pressure is held constant too, from eqs. (9,10) and (12,13) will result:

$$F_o(T) = F_o^0 \left(\frac{T}{T^0}\right)^{-N} \tag{21}$$

$$t_0(T) = t_0^0 \left(\frac{T}{T^0}\right)^{N} \tag{22}$$

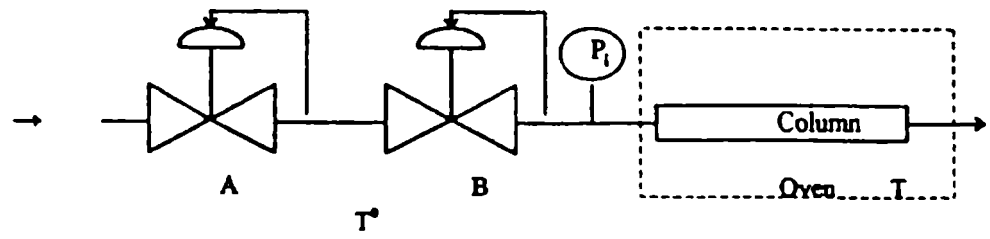

Fig. 5.- Scheme of the applied control for generating a column constant inlet pressure.

Figure 6 shows the behavior pattern expected for this flow control system. In the particular condition described here one could linearize $t_0(T)$ for practical purposes without committing an appreciable error. A 120 cm column with 5% OV-17 stationary phase and Gas Chrom Q 80/100 mesh was used in this case .

The constant mass flow control

We shall consider an idealized device capable to hold constant mass flow during a temperature program .This could be, for example, a electronic microprocessor sensing gas delivery at a constant reference temperature T^0 by means of a differential hot wire anemometer and commanding a solenoid valve in such a way that flow will remain constant whatever is column's temperature. Electronically drived mechanisms have been described in the literature **[24]**. If such commitment is attained, then F_o measured at T^0 in a running will be constant and equal to that at initial conditions. Then:

$$F_o(T) = F_o^0 \frac{T}{T^0}.$$

Replacing in (9):

$$P(T) = \left[1 + (P^{0^2} - 1)\left(\frac{T}{T^0}\right)^{1+N}\right]^{1/2} \tag{23}$$

And from (12):

$$t_0(T) = t_0^0 \left(\frac{T}{T^0}\right)^{-(2+N)} \frac{\left\{\left[1 + (P^0 - 1)\left(\frac{T}{T^0}\right)^{(1+N)}\right]^{\beta/2} - 1\right\}}{(P^{0^3} - 1)} \tag{24}$$

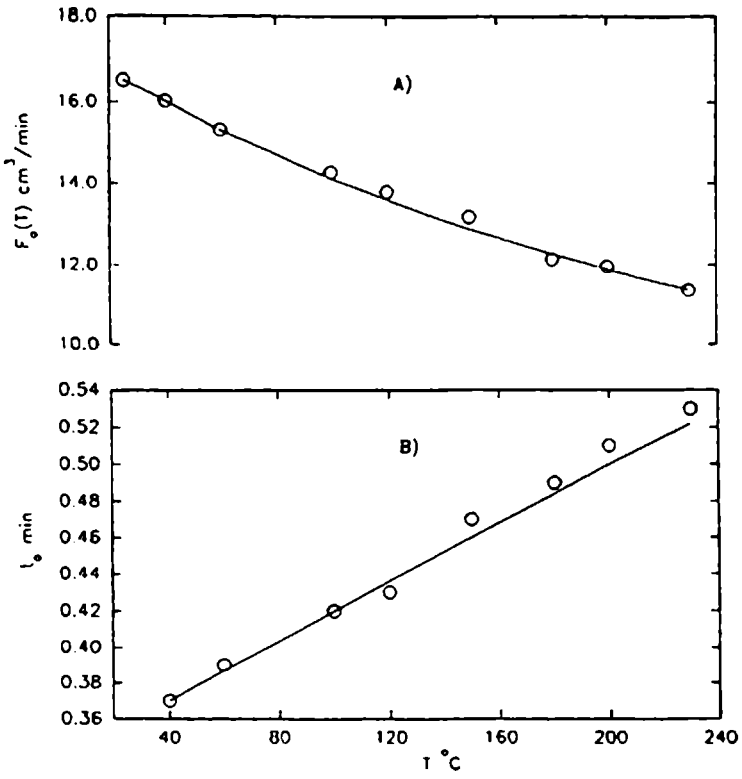

Fig. 6.- Flow functions for the constant head pressure control. (A) $F_0(T)$ function. Column 120 cm x 2 mm I.D., filled with Gas Chrom Q 80/100 mesh, 5% OV-17. P_i=1140 and P_0=760 mmHg, F_0^0=16.52 cm^3/min, T^0=25°C. Filled line calculated using Eq. (21). (B) $t_0(T)$ function. Conditions as in (A), T^0=40°C and t_0^0=0.37 min. Filled line calculated using Eq. (22).

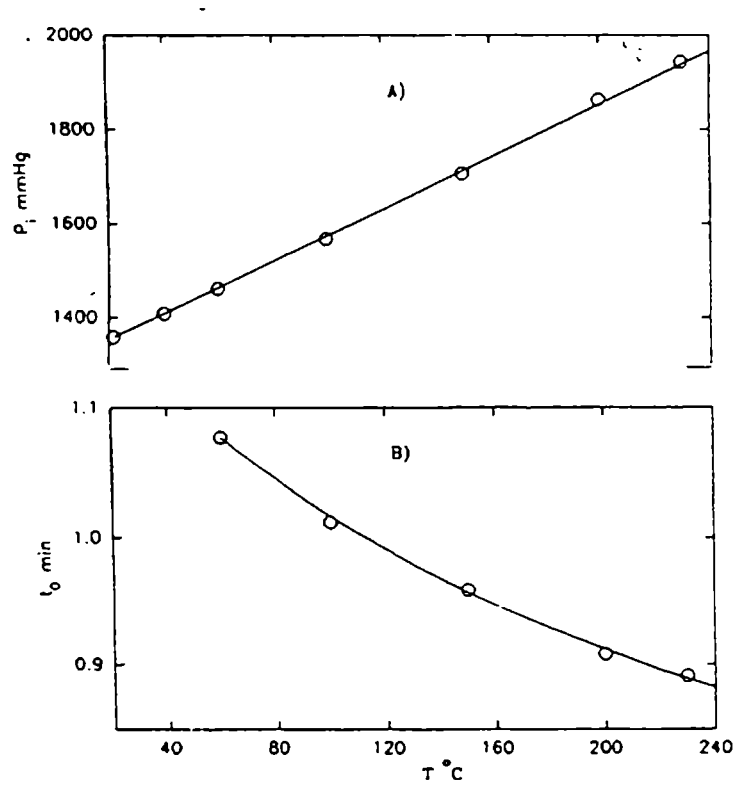

Fig. 7.- Flow functions for the constant mass flow control. (A) $P_i(T)$ function. Column 140 cm x 2 mm I.D., filled with Chromosorb W 80/100, 5% OV-17. F_0=10.27 cm^3/min, T^0=21.5°C and P_i^0=1358 mmHg. Filled line calculated using Eq. (23). (B) $t_0(T)$ function, column as in (A), T^0=60°C, t_0^0=1.077 min and P_i^0=1462 mmHg. Filled line calculated using Eq. (24).

Figure 7 shows the expected behavior pattern and the experimental results in this case. A electronic flow controller was not available, so a standard mechanical flow controller consisting in a needle valve/diaphragm operated valve combination , was employed. The Hewlett Packard 5880 chromatograph with the original controller was used with a 140 cm column filled with Chromosorb W 80/100 and 5% OV-101. Conditions were selected to allow the system resemble the postulated behavior. Even with the relative low pressure drop column used and with flow rates as low as 10 c.c./min, the best performance would have a 5% flow rate drift in a temperature interval of 200° C. Obviously, with a higher pressure drop column or

a higher flow rate demand the device was not able to comply with the duty. Shown experimental data were corrected for the observed flow rate drift.

The programmable head pressure

Recent advances in computer controlled head pressure have been described with some detail **[25].** The performance of commercially available linear programmable head pressure chromatographs has been evaluated **[26]**.

Pressure program is coupled to temperature program to obtain the desired optimized performance. Both programs are given by the respective explicit functions :T= f(t), and P=E(t). Then:

$$\frac{dP}{dT} = \frac{E'}{f'}$$

Integrating between the initial values of the programs and a generic point:

$$P(T) = P^0 + \int_{T^0}^{T} \frac{E'dT}{f'} \tag{25}$$

For example, if temperature and pressure programs are linear and P_o is held constant, namely:

$$T = T^0 + r_T\, t$$

$$P_i = P_i^0 + r_P\, t$$

Then using (25):

$$P_i(T) = P_i^0 + \frac{r_P}{r_T}(T - T^0) \tag{26}$$

In this case eq.(9) delivers:

$$F_o(T) = F_o^0 \left(\frac{T}{T^0}\right)^{-N} \frac{\left\{\left[P_i^0 + \frac{r_P}{r_T}(T - T^0)\right]^2 - P_o^2\right\}}{(P_i^{0^2} - P_o^2)} \tag{27}$$

and from (12):

$$t_0(T) = t_0^0 \frac{(P_i^{0^2} - P_o^2)^2}{(P_i^{0^3} - P_o^3)} \left(\frac{T}{T^0}\right)^{N} \frac{\left\{\left[P_i^0 + \frac{r_P}{r_T}(T - T^0)\right]^3 - P_o^3\right\}}{\left\{\left[P_i^0 + \frac{r_P}{r_T}(T - T^0)\right]^2 - P_o^2\right\}^2} \tag{28}$$

A programmable pressure control system was not available but it's function could be simulated by fixing the column's inlet pressure manually at each temperature, using the system described in section *"The needle valve flow control"*, increasing pressure at a rate of $r_p / r_T = 1.5$ mmHg / C. In Figure 8 are represented the experimental data and the calculated curves by means of eqs. (27) and (28).

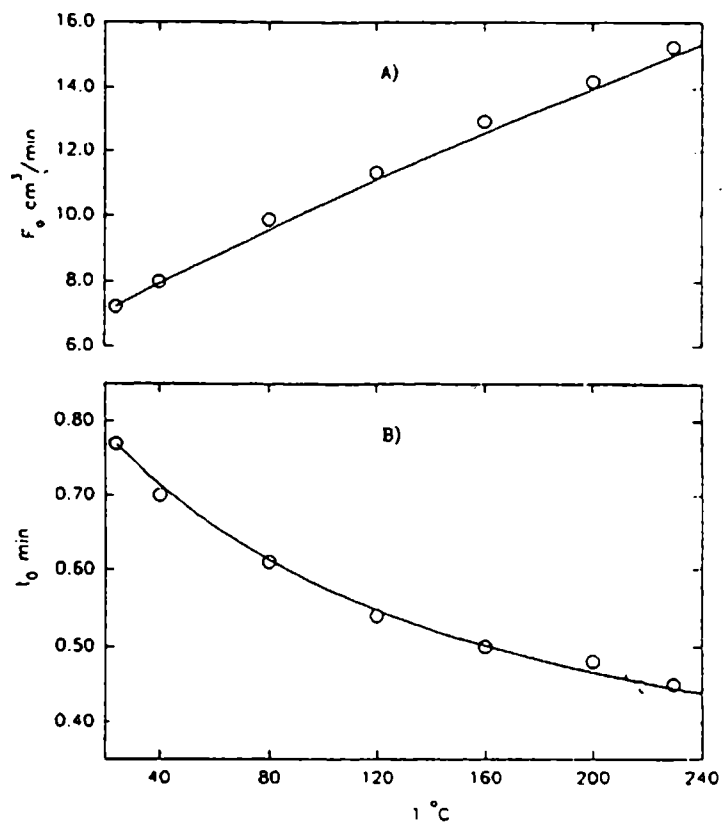

Fig. 8.- Flow functions for a linear head pressure program. (A) $F_0(T)$ function. R_p/r_T=1.5 mmHg/°C, T^0=24°C, P_i^0=956 mmHg and F_0^0=7.23 cm^3/min. Filled line calculated using Eq. (27). (B) $t_0(T)$ function. Conditions as in (A) and t_0^0=0.77 min. Filled line calculated using Eq. (28).

CONCLUSIONS

Analytical expressions of $t_0(T)$ have been displayed for four flow control modes : needle valve system, constant inlet pressure, constant mass flow and linear programmed head pressure. All are applicable to packed or capillary columns. The method being used assumes that geometric parameters V_0 and L/AB remain constant with temperature, hypothesis that as shown in section 3 would not have major consequences under practical chromatographic conditions. In this paper $t_0(T)$ was determined always by estimating column's constant C_t from a single point (from initial dead time, inlet and outlet pressure, and temperature, using eq.(13)), which a priori could be appreciated as a inaccurate procedure. One may fairly think that a more precise estimation of column's constant should be conducted, e.g. by linear regression applying eq. (12). Contrasting calculated and experimental data showed that the applied procedure suffices for predicting $t_0(T)$ with reasonable precision for practical purposes as retention simulation in PTGC. This, obviously, is consequence of the fact that the parameters P_i^0, P_o, T^0 and t_0^0 can be measured accurately. The application of the expressions of $t_0(T)$ to retention simulation is a matter of a related work **[27]**.

ACKNOWLEDGEMENT

This work was sponsored by the Consejo Nacional de Investigaciones Científicas y Técnicas and the Comisión de Investigaciones Científicas de la Provincia de Buenos Aires.

REFERENCES

[1] Giddings, J.C.- **J. Chromatogr., 4**, 11 (1960).
[2] Dal Nogare, S.; Langlois, W.E.- **Anal. Chem., 32**, 767 (1960).
[3] Habgood, H.W.; Harris, W.E.- **Anal. Chem., 32**, 450 (1960).
[4] Habgood, H.W.; Harris, W.E.- ***Programmed Temperature Gas Chromatography***, J. Wiley and Sons, N.Y. (1966).
[5] Rowan, R.- **Anal. Chem., 33**, 510 (1961).
[6] Zhang, J.Y.; Wang, G.M.; Quian, R.- **J. Chromatogr., 521**, 71 (1990).
[7] Shrotri, P.Y.; Mokashi, A.; Mukesh D.- **J. Chromatogr., 387**, 399 (1987).
[8] Conder, J.R.- **J. Chromatogr., 248**, 1 (1982).
[9] F.R. González and A.M. Nardillo, unpublished.
[10] Grant, D.W.; Hollis, M.G.- **J. Chromatogr., 158**, 3 (1978).
[11] Curvers, J.; Rijks, J.; Cramers, C.; Knauss, K.; Larson, P.- **J. High. Resolut. Chromatogr. Chromatogr. Commun., 8**, 607 (1985).
[12] Bautz, D.E.; Dolan, J.W.; Snyder, L.R.- **J. Chromatogr., 541**, 1 (1991).
[13] Gerbino, T.C.; Castello, G., Pettinati, U.- **J. Chromatogr., 634**, 338 (1993).
[14] Castello, G.; Moretti, P.; Vezzani, S.- **J. Chromatogr., 635**, 103 (1993).
[15] Horlick, G.; Harris, W.E.; Habgood, H.W.- **Anal. Chem., 38**, 7 (1966).
[16] Bird, R.B.; Stewart, W.E.; Lightfoot, E.N.- ***Transport Phenomena***, J. Wiley and Sons, N.Y. (1964).
[17] Guiochon, G.- **Chromatogr. Rev., 8**, 1 (1966).
[18] Cramers, C.; Rijks, J.; Schutjes, C.P.M.- **Chromatographia, 14**, 439 (1981).
[19] Ettre, L.S.- **Chromatographia, 18**, 243 (1984).
[20] Blumberg, L.M.- **Chromatographia, 41**, 15 (1995).
[21] Touloukian, Y.S.- ***Thermophysical Properties of Matter***, Vol. 12, IFI, Plenum, N.Y. (1975).
[22] Knox, J.H.- **J. Chromatogr. Sci., 15**, 352 (1977).
[23] Cowper, C.J.; De Rose, A.J.- ***The Analysis of Gases by Chromatography***, Pergamon Press, N.Y. (1985).
[24] Wicar, S.- **J. Chromatogr., 295**, 395 (1984).
[25] Hinshaw, J.V.- **LC GC, 13**, 792 (1995).
[26] Hermann, B.W.; Freed, L.M.; Thompson, M.Q.; Phillips, RJ; Klein, K.J.; Snyder, W.D.- **J. High. Res. Chromatogr. Instrum., 13**, 361 (1990).
[27] González, F.R.; Nardillo, A.M.- Submitted for publication.

RETENTION IN MULTISTEP PROGRAMMED-TEMPERATURE GAS CHROMATOGRAPHY AND FLOW CONTROL. LINEAR HEAD PRESSURE PROGRAMS

RETENCION EN CROMATOGRAFIA GASEOSA CON TEMPERATURA PROGRAMADA EN ETAPAS MULTIPLES Y CONTROL DE FLUJO. PROGRAMAS CON GRADIENTE LINEAL DE PRESION DE ENTRADA

F. R. González[1], A. M. Nardillo[2]

SUMMARY

A comparative study of retention in different systems of flow control, that provide linear dependence with temperature of column's head pressure, is performed by numerical simulation considering multistep (or multiramp) PTGC as the most general situation. Calculation algorithms for each flow control mode are developed on the basis of general retention equation and the only additional hypothesis that certain geometric parameters of the column remain practically constant along the program. Procedures are individually contrasted with experiment, prior to application. The comparative view indicates that simple correlations cannot be obtained between retention times and temperatures in two different pressure controls or pressure programs. It seems that numerical procedures are unavoidable when it is required the conversion of retention data from one chromatographic system to another with the same stationary phase.

Keywords: *temperature programming; head pressure; flow control systems.*

INTRODUCTION

The velocity of the carrier gas is a function of pressure drop along the column, and the way the later changes with temperature is conditioned by the employed flow control system, thus retention is primarily affected by the function *P(T)* generated by the chromatograph (*T* is the absolute temperature and *P* is the inlet/outlet absolute pressure ratio in the column: $P = p_i / p_o$). Each *P(T)* function has associated a gas hold-up time function $t_M(T)$ biunivocally related by column's and carrier gas flow properties. Consequently, at the time of reporting PTGC retention data, also *P(T)* ought to be informed, by itself or the associated $t_M(T)$.

For a few years ago the most widely applied devices for setting the carrier gas velocity (or the *P(T)* function) were the mechanical flow controllers **[1]** consisting in a needle valve in

[1] División Química Analítica, Facultad de Ciencias Exactas, Universidad Nacional de La Plata
[2] Miembro de la Carrera del Investigador del CONICET; Profesor Asociado, UNLP

serial array with a diaphragm operated valve. Although these were employed with the intention to keep a constant mass flow, their capacity to respond adequately to changing flow conditions along wide temperature intervals becomes rapidly overwhelmed **[2]**. In consequence, their behavior under actual temperature programming turns unpredictable from a practical standpoint. With the development of electronically driven mechanisms reliable mass flow control is possible for PTGC **[1,3,4]**. On the other hand, the constant inlet pressure condition is easily accomplished, even with mechanical devices, but presents a monotonously decreasing outlet volume flow rate with rising temperature **[1,2]**, i. e. going in the opposite way to temperature programming in respect to the analysis time. With the advent of computer controlled head pressure numerous possibilities **[1]** are opened to pressure programming in PTGC.

Much attention has been given in recent years to the estimation of retention in programmed temperature from thermodynamic parameters, involving not only a single step temperature programming, but also including the choice of different heating rates steps, or isothermal steps **[5-10]**. Simultaneously, effort has been devoted to searching some sort of correlation of PTGC retention data for different columns using the same stationary phase through a programmed temperature retention index **[9,11-15].** Less attention was dedicated to the study of the interrelations between programmed temperature retention resulting from different *P(T)* functions. We believe these relations are important as different types of flow control are currently used, not existing a common standarization of *P(T)*. The nature of the retention equation in PTGC, in which the unknown variable (the retention time t_R) is an integration limit, does not permit to settle a priori a quantitative approach to the problem without making any explicit calculation.

GENERAL

The statement of the applied algorithms of calculation in this paper is based on two related works where the fundamental theory can be found **[2,16].**

The differential equation of peak motion in isothermal chromatography is:

$$\frac{dz}{dt} = \frac{u(z)}{(1+k)} \tag{1}$$

where z is the axial variable of cylindrical coordinates that describes peak position in the column at time t, $u(z)$ is the local carrier gas velocity, k column's capacity factor and dz/dt is the migration rate of the peak at z position. The local gas velocity $u(z)$ may be substituted by: $u(z) = \bar{u} / Q(z)$, where $\bar{u}$ is the average linear velocity along the column, which can be replaced in turn by L / t_M, being L the length of the column, and $Q(z) = \bar{u} / u(z)$ is the local velocity factor. For example, if D'Arcy's equation and the ideal gas equation of state are used for describing the motion of the gas, Q is **[2]**:

$$Q(z) = (3/2)\frac{(P^2-1)}{(P^3-1)}[P^2 - (z/L)(P^2-1)]^{1/2} \tag{2}$$

From eq. (1), the movement of the band along the column during any isothermal step of a given global temperature program would be given by:

$$\int_{z_i}^{z_f} Q(z)\, dz = \frac{L}{(1+k)} \int_{t_i}^{t_f} \frac{dt}{t_M} \tag{3}$$

where (z_i , z_f) are the initial and the final positions of peak along the step, and (t_i , t_f) are the corresponding times. Q and t_M are functions of P. In the case of chromatographs where the flow control system responds to column's varying flow conditions, e. g. mechanical controllers and needle valve systems **[2]**, P remains constant during isothermal steps. The same holds for the constant mass-flow control. P would only change during an isothermal interval when it is programmed to do so, being in this case a function of time. For this reason t_M was included inside the integral in eq. (3), as the most general condition.

The differential equation of peak motion in programmed temperature (PT) can be written as **[2]**:

$$\frac{dz}{dT} = \frac{L}{f'(T)\, Q(z,T)\, t_M(T)\, [1+k(T)]} \tag{4}$$

$T = f(t)$ is the function that relates time and temperature representing the chosen temperature program ($f' = dT/dt$). Now t_M is a function of $P(T)$. Hence, for any PT step of the general program, we can write:

$$\int_{z_i}^{z_f} Q(z,T)\, dz = L \int_{T_i}^{T_f} \frac{dT}{f'(T)\, t_M(T)\, [1+k(T)]} \tag{5}$$

and for the part of the global program that covers the complete elution of the band **[16]:**

$$1 = \int_0^L (Q/L)\, dz = \sum_{all\ steps}^{peak\ emerg.} \left[\underbrace{\frac{1}{(1+k)} \int_{t_i}^{t_f} \frac{dt}{t_M}}_{\text{isoth. steps}} + \underbrace{\int_{T_i}^{T_f} \frac{dT}{f'(T)\, t_M(T)\, [1+k(T)]}}_{\text{PT steps}} \right] \tag{6}$$

The sum is performed over all the steps of the global program involved from injection until solute's peak emerges at the end of the column. In the first step $t_i = 0$, if it is isothermal; otherwise $T_i = T_0$ if it is a PT one, being T_0 the initial temperature of the program. In the final step involved in peak elution: $t_f = t_R$, or $T_f = T_R$, depending on the case. The initial and final steps with their particular limits are not indicated explicitly in eq. (6) with the intention of keeping the expression as brief as admissible, considering that there are four possibilities in placing the limits. As it follows, all multistep retention expressions will be resumed in the same way. Although the retention time/temp. will not be indicated there, it will be assumed as implicitly present in the last step.

Currently, the capacity factor, given by eq. (7), is evaluated neglecting the variation of the enthalpy and entropy of solution with temperature and pressure.

$$k = \frac{a}{\beta} e^{-\Delta H_S / RT} \tag{7}$$

ΔH_S is the molar enthalpy of solution, a the entropic factor, β the phase ratio of the column and R the universal gas constant.

The dependence of t_M with P, for packed or capillary columns **[2]**, is given by:

$$t_M = (C_t\, T^{-N}\; p_o)^{-1}\; \frac{(P^3 - 1)}{(P^2 - 1)^2} \tag{8}$$

The "dead time constant" C_t is a flow property of the column/carrier gas couple that may be estimated by several methods:

From a single point. *(from initial conditions).* An operation position of the flow control system is selected, to be used during the PTGC running, e. g. setting a fixed numer of knob turns of a mechanical flow controller, or initial setting in a electronic pressure control. At the initial temperature T_0 and head pressure p_i^0, the initial gas hold-up time t_M^0 is measured in such isothermal-isobaric reference condition. Then, the constant is estimated by **[2]**:

$$C_t^{-1} = \frac{t_M^0\, (P^{0\,2} - 1)^2\, p_o}{(P^{0\,3} - 1)\, T_0^{\,N}} \tag{9}$$

From t_M measured as a function of P. Setting different inlet pressures to the column at a fixed temperature and outlet pressure, $t_M(p_i)$ is measured. Plotting the dead time as a function of the adimensional variable $(P^3 - 1)/(P^2 - 1)^2$, C_t can be estimated from the resultant slope (eq. (8)).

From volumetric flow rate measurements. The relationship between "column's flow rate constant" C_c and C_t is **[2]:**

$$C_t = \frac{3}{2} \frac{C_c}{V_d} \tag{10}$$

The dead volume of the column V_d is usually estimated from the isothermal elution volumes of two or more n-alkanes **[17]**. C_c can be estimated from volume flow rate measurements performed at constant temperature and outlet pressure **[2]**.

From column's geometric parameters and gas constant. According to eq. (10), the physical meaning of the "dead time constant" is interpreted by the following equation:

$$C_t = \frac{3}{4} \frac{B}{L^2\, \varepsilon_u\, C_G} \tag{11}$$

C_G is a constant of the carrier gas and ε_u is the interparticle porosity. For capillary columns ε_u=1. In the evaluation of the permeability B additional hypothesis are to be hold. If gas flow in the capillary is approximated by Hagen-Poiseulle's equation, which is valid only for incompressible fluids, $B = d_c^2 / 32$; then:

$$C_t = \frac{3}{128\, C_G}\left(\frac{d_c}{L}\right)^2 \tag{12}$$

Here we will estimate C_t, for all retention expressions, from eq. (9) exclusively, defining T_0, p_i^0 and t_M^0 as the initial values of the program measured before starting the PTGC running.

Finally, making use of eq. (8), retention eq. (6) can be written explicitly in terms of $P(T)$ or the head pressure function generated by the chromatograph:

$$C_t^{-1} = \sum_{all\ steps}^{peak\ emerg.} \left[\underbrace{\frac{1}{(1+k)\,T^N} \int_{t_i}^{t_f} \frac{(p_i^2 - p_o^2)^2\, dt}{(p_i^3 - p_o^3)}}_{\text{Isoth. steps}} + \underbrace{\int_{T_i}^{T_f} \frac{(p_i^2 - p_o^2)^2\, dT}{f'(T)\,(p_i^3 - p_o^3)\,(1+k)\,T^N}}_{\text{PT steps}} \right] \tag{13}$$

Once C_t of the column is determinated by one of the described possible procedures, and the head pressure program $p_i(T)$ is defined, the numerical estimation of retention from solute's thermodynamic parameters through eq. (13) is obtainable.

EXPERIMENTAL

A Hewlett-Packard 5890 Series II Plus chromatograph, connected to a HP 3395 integrator, was used in three selectable operation modes: constant head pressure (CP), constant mass flow (CMF) and linear pressure programming (PP). Only a 30 m long, 0. 25 mm i. d. with 0. 25 μm film width, AT-1, catalogue AllTech 13638 (Polydimethylsiloxane), capillary column was employed throughout this work, using nitrogen as the carrier gas. Detailed information about chromatograph's flow control configurations, main features of the electronic pressure control, as well as some aspects of response performance can be obtained from the paper by Hermann et al. **[4]**. Injection was carried out with a split ratio ranging from 30:1 to 70:1, depending on the case, with FID detection. Methane was used as the unretained solute for t_M^0 estimation. Eight hydrocarbons were employed individually and as solutions to undertake two tasks. First, for thermodynamic parameter determination, solutions of two or three solutes with similar boiling points were used running isothermal chromatograms at temperature intervals of 20 C, ranging 40-80 C around each solute's T_R from temperature program 1, Table 2. These runnings were made in the constant mass flow mode of pressure control. The entropic and enthalpic terms of k were estimated from mean square linear regression of $\ln(t_R' / t_M)$ - $1/T$ data, being t_R' the adjusted retention time. Results are presented in Table 1 indicating the thermal interval where these were evaluated and the correlation coefficient. The temperature-head pressure programs defined in Table 2 were ran injecting a mixture of the eight substances. Chloroform was the solvent for naphthalene. In those cases

where the initial isothermal-isobaric dead time t_M^0 was not determinable from the same chromatogram (programs 1 and 4), it was evaluated previously by two or three methane injections at program's initial conditions (T_0, p_i^0). In program 1 t_M^0 is longer than the isothermal-isobaric initial step, and in program 4 pressure varies from the beginning. Experimental retention times from temperature-pressure programs are presented in Table 3 under "exp" headings, indicating the corresponding initial conditions, data required for the numerical simulation.

Table 1

Entropic and enthalpic parameters of k .

Solute	$-\Delta H_s^0/R$ (K)	$(a/\beta)x10^6$	Temp.Interval C	Correl.coeff.
n-Octane	4175	5.533	50-120	0.99990
p-Xilene	4262	6.924	50-120	0.99979
1,3,5 Trimethylbenzene	4661	4.417	70-120	0.99998
1-Undecene	5313	1.729	100-160	0.99978
Naphthalene	5107	4.623	120-180	0.99986
n-Dodecane	5559	1.695	140-180	-
n-Tetradecane	5990	1.545	200-220	-
n-Hexadecane	6760	0.635	160-220	1.00000

Table 2

Description of applied T-P programs

Designation	Temperature Program	Pressure Program
1	[I: 1 min]→[PT: 10 C/min to 200 C]	CMF
2	[I: 2.5 min]→[PT: 5 C/min to 80C]→ →[I:0.5 min]→[PT: 10 C/min to 250]	CMF
3	same as 2	[CP:2.5 min]→[PP: 21.7 Torr/min to 1412 Torr]→[CP: 0.5 min]→[PP: 43.4 Torr/min]
4	same as 2	[PP: 51.715 Torr/min]
5	same as 2	CP

Initial temperature is T_0 = 50 C for every program , (p_o, p_i^0) are: (765,1277) Torr in 1 and 2 , (770,1282) Torr in 3 and 4 , (770,1546) Torr in 5 . Symbols: I-isoth. step , PT-lin.programmed temp. step , CMF-constant mass flow , CP-constant inlet pressure , PP-lin.progr.inlet pressure .

Table 3

Experimental and calculated retention times in different temperature-pressure programs

Solute	Retention Times (min)									
	Progr.1 CMF mode		Progr.2 CMF mode		Progr.3 PP mode		Progr.4 PP mode		Progr.5 CP mode	
	exp.	calc.	exp.	calc	exp.	calc.	exp.	calc.	exp.	calc.
n-Octane	4.879	4.880	6.169	6.189	6.032	6.070	5.153	5.230	4.562	4.590
p-Xilene	5.777	5.778	7.685	7.769	7.450	7.559	6.359	6.490	5.974	6.030
1,3,5Trimethylbenzene	7.296	7.270	10.539	10.560	10.154	10.200	8.710	8.790	8.865	8.850
1-Undecene	9.285	9.260	13.644	13.580	13.081	13.070	11.831	11.830	12.601	12.540
Naphthalene	10.445	10.360	14.990	14.860	14.317	14.250	13.066	12.990	14.094	13.950
n-Dodecane	10.931	10.800	15.641	15.450	14.952	14.820	13.800	13.640	14.924	14.700
n-Tetradecane	13.585	13.350	18.570	18.500	17.720	17.440	16.672	16.330	18.246	17.870
n-Hexadecane	15.975	15.830	20.983	20.800	20.025	19.890	19.050	18.860	20.962	20.770
Mean error %	0.66		0.68		0.76		1.15		1.01	
t_M^0 (min)	2.224		2.224		2.215		2.214		1.489	
p_i^0 (Torr)	1277		1277		1282		1282		1546	
p_o (Torr)	765		765		770		770		770	

Programs from Table 2 . Mean error % defined as : $[(t_R^{exp.} - t_R^{calc.}) / t_R^{calc.}]$ 100 (same definition as in Table 4 and reference [10]) .

THE CONSTANT HEAD PRESSURE MODE

We will assume this mode as a special case of a linear head pressure programming with zero compression rate and we shall employ it as a reference. The ramps are restricted to linear temperature programs with heating rates r_T C/min ($f'(T) = r_T = const.$).

Being $p_i = p_i^0 = const.$, by using eq. (9), eq. (13) reduces to:

$$\frac{t_M^0}{T_0^N} = \sum_{all\ steps}^{peak\ emerg.} \left[\underbrace{\frac{1}{(1+k)\,T^N} \int_{t_i}^{t_f} dt}_{\text{isoth. Steps}} + \underbrace{\frac{1}{r_T} \int_{T_i}^{T_f} \frac{dT}{(1+k)\,T^N}}_{\text{PT steps}} \right] \qquad (14)$$

For the evaluation of retention through eq. (14) the only information to be entered into the calculation, besides selected program's parameters, are the initial isothermal dead time and the initial temperature, the thermodynamic parameters for $k(T)$ and the constant N of the carrier gas. Applying eq. (14) to a single ramp reduces to the expression derived by Messadi **[15].**

In Table 3, program 5, the experimental retention data belonging to the eight hydrocarbons, measured in the isobaric condition (CP) indicated in the lower lines, are listed under the heading "exp. ". In the same table the results, rendered by the numerical solution of eq. (14) through a Basic computer program, are shown under the "calc. " heading. Measured values of the initial temperature and dead time, the parameters of k given in Table 1 and the constant N for nitrogen (0. 725, **[18]**)were entered to the computer program. The mean error

of predicted retention is in the order of 1%, as indicated in the table. The applied time and temperature increments in the computer program were 0. 01 min and 0. 1 K, respectively.

In the same way, Table 4 shows calculated retention times using the reported thermodynamic parameters and the isobaric multistep temperature programs indicated in reference **[10]**. Results are compared simultaneously with experimental and calculated data listed in table 11 in the paper of Snijders, Janssen and Cramers. Differences between the algorithms followed by the cited and present authors deserves a brief comment.

In reference **[10]** the geometric parameters of the column L and d_c are introduced with two purposes. First, L is the integration limit of variable z, as consequence that the carrier gas local velocity is evaluated for each coordinate and temperature increment. In reference **[16]** is shown that procedures including the explicit calculation of the local velocity at each temperature are equivalent to that used here, where L becomes irrelevant. Second, the length and diameter of the column were necessary in ref. **[10]** for determining the head pressure through an expression equivalent to the combination of eqs. (8) and (12), i. e. calculating p_i from the measured value of t_M^0. The head pressure is present in the estimation of the local velocity. In spite of the number of operations included in the algorithms, with additional input of parameters, that from ref. **[10]** and present procedure are formally equivalent **[16]**, involving the same basic chromatographic hypothesis. Only two minor differences are to be considered. In the present work C_t is evaluated by eq. (9) and the procedure followed by Snijders et al. corresponds to the evaluation of C_t from eq. (12), which assumes valid Poiseulle's equation. The other aspect is that we approximated the temperature dependence of gas viscosity as a temperature power law. N=0. 646 was entered for He as the carrier gas **[18]**. Small numerical differences between calculated retention times in Table 4 arise, principally, from: a) machine roundup associated with the number of operations performed by the computer, b) the values given to the increments in the sumation and c) the intrinsic error of the L input **[16]**.

The outstanding characteristic of the constant pressure mode in multistep PTGC, that becomes even more evident from eq. (14), is that retention is parametrically dependent on the head pressure or chromatograph's gas control design (implicitly through t_M^0). This is just what occurs in isothermal chromatography, where the influence of the flow conditions can be eliminated reporting the retention data in a standarized way relative to the retention framework of n-alkanes, by means of Kovats retention index. This unique characteristic of parametrical dependence of retention on chromatograph's fluid dynamics is not accounted for systems where $p_i(T)$ is allowed to evolve during the temperature program, depending the retention on this function (eq. (13)). The simplicity of the retention expression, more precisely the missing influence of $p_i(T)$, makes the constant pressure mode an appropriate reference for the comparison of retention measured under different flow control systems.

THE CONSTANT MASS-FLOW MODE

During a temperature program running, with constant mass flow of the carrier gas, the evolution of $P(T)$ can be described by **[2]**:

$$P(T)=\left[1+(P^{0^2}-1)\left(\frac{T}{T_0}\right)^{1+N}\right]^{1/2}$$

or

$$p_i(T)=\left[p_o^2+(p_i^{0^2}-p_o^2)\left(\frac{T}{T_0}\right)^{1+N}\right]^{1/2} \qquad (15)$$

This equation presumes valid the same hypothesis that are inherent to eq. (8), already mentioned in the section General (D'Arcy, ideal gas, thermal invariance of column's geometric parameters and gas viscosity factorization). Although it does not strictly defines a linear pressure increase with rising temperature, in practical chromatographic conditions it behaves like a linear head pressure program (see for example fig. 4 from refence **[1]** and fig. 5 from ref. **[2]**). If the initial value of P is $P^0 = 2$, and T_0 = 323 K, deviations from linearity would become significant beyond 600 K. The number of comparisons to undertake in this study are simplified due to the property that this flow control mode presents, having the same $P(T)$ of a linear pressure programmable device, although restricted to a fixed compression rate and isobaric behavior at isothermal steps.

Now, the calculation of the retention time of a solute will require the numerical solution of eq. (13) with $p_i(T)$ given by eq. (15). In addition to the input information necessary in the CP mode, the initial inlet and the oulet pressures of the column (p_i^0, p_o) must be entered. A computer program solving the system of equations, applying the same time and temperature increments reported previously, was employed for retention estimation. In Table 3, programs 1 and 2, experimental and calculated retentions are compared for the solutes under constant mass flow (CMF). Errors are in the same order of program 5 or Table 4 (CP mode).

LINEAR PROGRAMMED INLET PRESSURE

Electronic pressure control adds the possibility of changing the rate of pressure increase at column's head, and also to vary p_i along isothermal steps. In this later specific situation, considering linear programming:

$$p_i(t) = p_i^0 + r_P\, t \qquad (16)$$

where r_P is the compression rate (e. g. Torr/min).

We may also write for a initial PT ramp **[2]**:

$$p_i(T) = p_i^0 + \frac{r_P}{r_T}\,(T - T_0) \qquad (17)$$

The same holds for any intermediat step replacing $(T_0\ , p_i^0)$ by the correspondent initial temperature and pressure of the interval. Now the calculation algorithm requires the

introducton of eq. (16) in the isothermal cycle and (17) in the PT cycle. Furthermore, the computation program has to incorporate the necessary data input sentences for pressure program's parameters.

Table 3, programs 3 and 4, presents the calculated retentions for two multistep pressure-temperature programs. Program 3 is an example of isobaric condition for the isothermal steps and Program 4 includes variable pressure during the isothermal intervals. Again, the contrast with experimental data reveals a close accuracy in respect to programs described previously.

COMPARISON OF RETENTION UNDER DIFFERENT PRESSURE PROGRAMS

With the intention of avoiding redundant examinations we must recall two aspects commented previously. First, comparisons can be conducted using the CP mode as a reference, as it can be assumed to be a special case of linear pressure programming with $r_P = 0$. Second, the CMF mode might be considered a particular linear PP with a fixed r_P, having the restriction of invariable pressure isothermal intervals, thus representing only another example of the linear PP mode with these two characteristics.

The first duty to face is to select some appropriate combination of parameters that would allow a wide overview of retention behavior with temperature-pressure programming. We will start considering the simplest choice, consisting of T and p_i single ramps, excluding isothermal intervals. The relationship between retention time and temperature is:

$$t_R = \frac{T_R - T_0}{r_T} \tag{18}$$

Then, we may write for any pair of eluted substances x and y:

$$\frac{(t_{R_x} - t_{R_y})^{PP}}{(T_{R_x} - T_{R_y})^{PP}} = \frac{1}{r_T} \tag{19}$$

And, by analogy, in the isobaric mode having the same heating rate:

$$\frac{(t_{R_x} - t_{R_y})^{CP}}{(T_{R_x} - T_{R_y})^{CP}} = \frac{1}{r_T} \tag{20}$$

Taking the difference between the last two expressions and rearranging:

$$\frac{(t_{R_x} - t_{R_y})^{PP}}{(t_{R_x} - t_{R_y})^{CP}} = \frac{(T_{R_x} - T_{R_y})^{PP}}{(T_{R_x} - T_{R_y})^{CP}} \tag{21}$$

So, when comparing retention differences of pairs between the PP and CP modes, or between different PP, with the parameter defined by eq. (21), the use of retention times or temperatures

results indistinguishable. Of course, equality (21) does not hold for multistep temperature programs, being valid, in this later case, only under some particular conditions.

Table 5 presents calculated values of the parameter for the eight solutes of this study, under the program defined by ramps: r_T=15 C/min and r_P=15 Torr/min, and specified initial temperature T_0, initial head pressure p_i^0, isothermal-isobaric initial gas hold-up time t_M^0, and outlet pressure p_o. Residence times of the unretained solute were calculated entering k=0 to the CP and PP computer programs, yielding t_M^{CP} and t_M^{PP}, respectively. At first glance it arises that eq. (21) parameter has a very low variation along the table, roughly decreasing from left to right and from top to bottom. There is an exceptional abnormal high value, respect to surrounding values, for the naphthalene/n-dodecane pair. This exception was also observed in the other three T-P ramps reported in Table 6, and it is related to the fact that the elution of this pair has an isothermal retention cross-over in the temperature interval of the program. We shall intend to approach this problem in a forthcoming paper.

Table 5

Variations of eq.(21) parameter for different pairs of solutes (x,y)

y \ x	n-Octane	p-Xilene	1,3,5 TMBenzene	1-Undecene	Naphthalene	n-Dodecane	n-Tetradecane	n-Hexadecane
Unretained	0.934	0.932	0.930	0.927	0.923	0.924	0.922	0.921
n-Octane		0.930	0.928	0.924	0.918	0.920	0.918	0.918
p-Xilene			0.926	0.922	0.916	0.919	0.917	0.917
1,3,5TMBenzene				0.919	0.912	0.916	0.915	0.915
1-Undecene					0.900	0.912	0.913	0.914
Naphthalene						0.951	0.918	0.917
n-Dodecane							0.914	0.915
n-Tetradecane								0.916

The T-P program is defined by: r_P=15 Torr/min , r_T =15 C/min , T_0=50 C , p_i^0 =1282 Torr , p_o =770 Torr and t_M^0 =2.224 min .

The mean value of the eq.(21) parameter is : $\overline{X}$ =0.920 and the standard deviation is σ = 0.0083 .

Table 6 is an arrangement of characteristic data from four different tables of the same type of Table 5. The later is designated as "A" in Table 6. The data has been ordered by increasing r_P ramps. E is a multiramp program. Reported $\overline{X}$value is the average retention time parameter of eq. (21) . Variations, accounted by the standard deviation σ of eq. (21) parameter, are amplified by increasing the compression rate r_P, expanding under multiramp programs. In the sixth column the parameters for the least retained pair (n-octane/unretained) are tabulated. This pair provides a near limiting value of the parameter in the table (not considering the crossing couple). The next column presents the value of $(t_M^{PP} / t_M^{CP})^2$, which is found to be very close to the limiting value of the least retained couple. However, the nature of this apparent correlation is not justified, being a mere empirism. In case of corroboration, a simple thumb rule could be settled for non-crossing solutes, or solutes of similar structure, under single T/P ramps with discrete compression rates:

$$\frac{(t_{R_x} - t_{R_y})^{PP}}{(t_{R_x} - t_{R_y})^{CP}} = \frac{(T_{R_x} - T_{R_y})^{PP}}{(T_{R_x} - T_{R_y})^{CP}} \approx const. \approx \left(\frac{t_M^{PP}}{t_M^{CP}}\right)^2 \qquad (22)$$

Table 6

Behavior of eq.(21) parameter under different T-P programs

Designation	Temp.Progr. r_T (C/min)	Press.Progr. r_P (Torr/min)	$\overline{X}$	σ	n-Oct/Unret.	$(t_M^{PP}/t_M^{CP})^2$
A	15	15	0.920	0.0083	0.934	0.938
B	10	CMF (equiv. to 22.5 Torr/min)	0.881	0.0103	0.910	0.906
C	10	51.715	0.805	0.0185	0.820	0.817
D	5	60	0.810	0.0196	0.873	0.897
E	Progr.3 Table 2	Progr.3 Table 2	0.860	0.0300	0.941	——

In consequence, for a gross estimation of the effect on retention by changing the pressure control mode (in a given temperature program), the unavailability of thermodynamic parameters would not be crucial. The dead times are readily acquainted by entering k=0 to the respective computer programs. Equation (22) could also be applied to two PP with different r_P.

In the case of multiramp programs this approximation does not fit and, in this way, useful information cannot be obtained, being necessary the complete numerical simulation.

CONCLUSIONS

All three applied calculation algorithms for the CP, CMF and linear PP modes are supported on the same basic chromatographic hypothesis **[16]**, so the fact that all yield close accuracy of prediction (Table 3) was expected a priori. The order of the mean error of calculated retentions is lower than the retention differences between studied T-P programs, so the reliability of the procedure applied in the comparative study is assured.

Multistep T-P programs are actually globally non-linear programs, and retention behavior, even for homologues substances, is very complex, leaving no other way than the estimation through numerical simulation from thermodynamic parameters. In the only case where changing the pressure program has a uniform effect on the whole chromatogram is that of single T-P ramps applied to solutes of similar nature (eq. (22)). For example, rising r_P means that the chromatogram is going to be uniformly compressed.

Other empirical combinations of retention parameters were used along the development of this work seeking for some general correlation of retention under different pressure single ramps, leading to discouraging results.

ACKNOWLEDGEMENT

This work was sponsored by the Consejo Nacional de Investigaciones Científicas y Técnicas and the Comisión de Investigaciones Científicas de la Provincia de Buenos Aires. The authors are very grateful to Prof. Dr. L.F.R. Cafferata, who provided the chromatographic facilities.

REFERENCES

[1] Hinshaw, J.V.- **LC-GC**, **13**, 792 (1995).
[2] Gonzalez, F.R.; Nardillo, A.M.- **J. Chromatogr. A** , **757**, 109 (1997) .
[3] Wicar, S.- **J. Chromatogr.**, **295**, 395 (1984).
[4] Hermann, B.W.; Freed, L.M.; Thompson, M.Q.; Phillips, R. J.; Klein, K.J.; Snyder, W.D.- **J. High Res. Chromatogr., Instrum.**, **13**, 361 (1990).
[5] Akporhonor, E.F.; Le Vent, S.; Taylor, D.R.- **J. Chromatogr.**, **405**, 67 (1987).
[6] Dose, E.V.- **Anal. Chem.**, **59**, 2414 (1987).
[7] Bautz, D.E.; Dolan, J.W.; Snyder, L.R.- **J. Chromatogr.**, **541**, 1 (1991).
[8] Gerbino, T.C.; Castello, G.; Pettinati, U.- **J. Chromatogr.**, **634**, 338 (1993); **635**, 338 (1993).
[9] Gerbino, T.C.; Petit Bon, P.- **Ann. Chimica**, **84**, 305 (1994).
[10] Snijders, H.; Janssen, H.G.; Cramers, C.- **J. Chromatogr. A**, **718**, 339 (1995).
[11] Curvers, J.; Rijks, J.; Cramers, C.; Knauss, K.; Larson, P.- **J. High. Res. Chromatogr., Chromatogr. Commun**, **8**, 607, 611 (1985).
[12] Guan, Y.; Kiraly, J.; Rijks, J.A.- **J. Chomatogr**, **472**, 129 (1989).
[13] Fernández-Sánchez, E.; García-Domínguez, J.A.; Menéndez, V.; Santiuste, J.M.- **J. Chromatogr.**, **498**, 1 (1990).
[14] Said, A.S.; Jarallah, A.M.; Al-Ameeri, R.S.- **J. High Res. Chromatogr., Chromatogr. Commun**, **9**, 1 (1986).
[15] Messadi, D.; Ali-Mukhnache, S.- **Chromatographia**, **37**, 64 (1993).
[16] Gonzalez, F.R.; Nardillo, A.M.- **J. Chromatogr. A**, **766**, 147 (1997).
[17] Al-Thamir, W.K.; Purnell, J.H.; Wellington, C.A.; Laub, R.J.- **J. Chromatogr**, 173 , 388 (1979).
[18] Ettre, L.S.- **Chromatographia**, 18, 15 (1984).

INTEGRATION OF THE EQUATION OF PEAK MOTION IN PROGRAMMED-PRESSURE AND –TEMPERATURE GAS CHROMATOGRAPHY

INTEGRACION DE LA ECUACION DE MOVIMIENTO DE PICO EN CROMATOGRAFIA GASEOSA CON PRESION Y TEMPERATURA PROGRAMADAS

F.R. González[1], A.M. Nardillo[2]

SUMMARY

Numerical procedures for the estimation of the retention are compared considering the simultaneous programming of temperature and column head pressure , embracing issues from the mathematical basis to the practical aspects in the simulation of the chromatographic process by computer.

Keywords: *programmed-pressure and –temperature gas chromatography; retention models; computer simulation; alkanes; hydrocarbons.*

INTRODUCTION

The equation of peak motion in programmed pressure and temperature gas chromatography (PPTGC) may be written in terms of four well defined and accessible functions **[1]**:

$$\frac{dz}{dT} = \frac{L}{f'(T)\, Q(z,T)\, t_M(T)\, [1+k(T)]} \qquad (1)$$

where the variables of the equation (z,T) are the axial position of the peak in the column and the absolute temperature. The parameter L is the length of the column . The function $f'(T)$ is the first derivative of the relationship between time and temperature, $T=f(t)$, that describes the temperature program selected by the chromatographer. This relationship is an external restraint imposed to the system , fixing how the temperature will evolve in time. In the most general situation f' may be a function of T. In the particular case of linear temperature programs is a parameter : the heating rate r_T. Another restraint is the head pressure program $p_i(t)$ or $P(t)$ (where $P = p_i / p_o$). It can also be expressed as a function of T **[1]**, $P=P(T)$. The outlet pressure of the column p_o is usually a constant. The pressure program $P(T)$ cannot always be selected voluntarily. In chromatographs without pressure programming capabilities, $p_i(T)$ is a

[1] División Química Analítica, Facultad de Ciencias Exactas, Universidad Nacional de La Plata
[2] Miembro de la Carrera del Investigador del CONICET; Profesor Asociado, UNLP

characteristic function of the flow control system **[1]**. Therefore, as a matter of fact, all chromatographs have some intrinsic sort of pressure programming.

In the denominator of Eq.(1), $Q(z,T)$ function is the local velocity factor. This is the ratio between the average carrier gas velocity along the column at temperature T, $\bar{u}(T)$, and the local velocity of the carrier gas at position z , $u(z,T)$[3]: $Q(z,T) = \dfrac{\bar{u}(T)}{u(z,T)}$. If the isothermal motion of the carrier gas is described by the differential form of Hagen- Poiseulle Equation, in the case of capillary columns ; or by D'Arcy's Equation in packed columns, then :

$$u(z) = -\frac{B}{\eta}\frac{dp}{dz} \tag{2}$$

where η is the viscosity of the gas and p the absolute local pressure at z position. B can be assumed to be a constant of the system **[1]**. From Eq. (2) we derive the following expression for Q (see for example reference **[2]**):

$$Q = \frac{3}{2}\frac{(P^2-1)}{(P^3-1)}\left[P^2 - \frac{z}{L}(P^2-1)\right]^{1/2} \tag{3}$$

The current theory of programmed temperature assimilates the chromatographic process to a sequence of consecutive isothermal states, so P will be the pressure program $P(T)$ and Q will depend definitely as $Q(z,T)$. This basic hypothesis of the theory also implies that the process is assumed to be a summation of sequential steady state flows at successive temperatures , with an existing thermal equilibrium at each point .

The third function present in the denominator of Eq.(1) is the isothermal gas hold-up time $t_M(T)$. Resembling Q , $t_M(T)$ is also a function of the pressure program $P(T)$; and in the same way, from Eq. (2) we can derive the expression for this function **[1]**:

$$t_M(T) = \frac{T^N}{C_t P_o}\,\frac{[P^3(T)-1]}{[P^2(T)-1]^2} \tag{4}$$

where C_t is another constant of the system .

Finally, the fourth function present in the denominator of Eq.(1) is the capacity factor $k(T)$ describing the thermodynamics of the process:

$$k = \frac{1}{\beta}\,exp\left[-\frac{\Delta G^{\circ}(T)}{RT}\right] \tag{5}$$

---

[3] The local velocity of the carrier gas u ,as usually is indicated in GC , is the crossectional average of the radial profile of the axial velocity v_z in the column: $u = \langle v_z \rangle$ (see for example ref.[3]).

The standard partial molar free energy of solution ΔG° is a function of T and p. The dependence on pressure can be neglected in chromatographic conditions. The phase ratio of the column β may be considered a constant if the thermal expansion of column materials is neglected too , hypothesis that was necessary for accepting B and C_t as constants.

Equation (1) is the differential equation governing the motion of the band. This motion is the resultant from the combination of a fluid dynamic effect, the transportation of the band by means of the gas stream, and the thermodynamics of interaction between the solute and the stationary phase. As shown, the fluid dynamics of the chromatographic process is defined by functions $Q(z,T)$ and $t_M(T)$; depending naturally on both: the pressure program and the temperature program. The differential equation can be solved by direct variable separation only when P is constant, as consequence of the function Q depending simultaneously on z and T if P changes with temperature. When using the constant inlet pressure mode of flow control, the integration of the equation after direct variable separation leads to the well known relationship for linear temperature programs **[4]**:

$$r_T = \int_{T_0}^{T_R} \frac{dT}{t_M(T)\ [1+k(T)]} \tag{6}$$

where T_0 and T_R are the initial and the retention temperature, respectively. Otherwise , by changing to the variable t, the equivalent expression is **[5]**:

$$1 = \int_{0}^{t_R} \frac{dt}{t_M\ (1+k)} \tag{7}$$

where t_R is the retention time of the solute.

Historically, in conditions of variable pressure drops with temperature, rigorous retention estimation initiated from general Eq. (1) has been carried out avoiding the mathematical difficulty of the simultaneous dependence of Q on z and T by means of a defined numerical procedure of calculation. The classical example is the strict treatment developed by Dal Nogare and Langlois **[6]**, specifically for the constant mass flow mode of carrier gas control[4], although it has general applicability. We shall identify the algorithm with the general expression **[6]**:

$$t_R = \int_{0}^{L} \frac{[1+k(T)]\,dz}{u(z,T)} \tag{8}$$

In this algorithm the local velocity $u(z,T)$ has to be calculated at each incremented value of z. A stepwise numerical integration of eq.(8) begins when $z=0$ and $T = T_0$, then the local velocity can be calculated at the initial position by means of the general equation:

[4] In current chromatographic conditions , this mode of flow control behaves like a special case of linear head pressure programming [7] .

$$u(z,T) = \frac{L}{Q(z,T)\, t_M(T)} \tag{9}$$

Incrementing z in dz leads to an incremented elapsed time (from injection) given by the stepwise integration of Eq.(8), (determining k by using the initial temperature in Eq.(5) for the first cycle of calculation):

$$t = \int_0^z \frac{[1+k(T)]\, dz}{u(z,T)} \tag{10}$$

The sum is performed up to the actual position z. Now the effective temperature at the incremented z can be obtained from the temperature program $T=f(t)$. With this temperature another cycle of calculation is possible: incrementing z, determining u and k from Eqs. (9,5), actual t from Eq.(10) and actual T from $f(t)$. The cycle is repeated until the incremented z reaches the value of L, as it is indicated in Eq. (8). Then the time elapsed at this point is the retention time t_R, and $T=f(t_R)$ is the retention temperature T_R. These are the unknown parameters, object of the calculation. If desired, the procedure allows listing T as a function of z, or vice versa. Therefore, it makes the solution of Eq. (1) attainable, which is a curve in the plane z-T or z-t (the integral curve). Notwithstanding, the chromatographic interest is only centred on obtaining t_R . In Fig. 1 are shown integral curves belonging to the solute *n*-dodecane, calculated through the described procedure with conditions indicated in Table 1. The influence of the temperature program parameter on the solution of Eq. (1) is illustrated (in other words, the influence of the $T=f(t)$ function on the movement of the band).

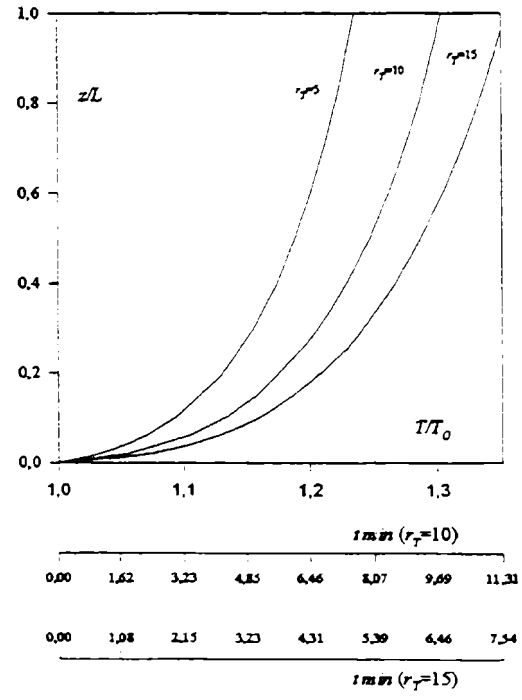

Fig. 1.- Peak position as a function of column temperature (reduced variables) or time (min). The integral curves belong to *n*-dodecane in the chromatographic conditions indicated in Table 1 and [7]. These were calculated through the classical algorithm of [6].

Table 1

Comparison of calculated retention times using constant mass flow mode of carrier gas control

Solute	1. t_R (min) Eq.(11)	2. t_R (min) algthm. Ref.[6]	3. $\int_0^L Q/L\,dz$ algthm. Ref.[6]
n-Octane	4.310	4.303	0.9974
p-Xilene	5.090	5.084	0.9968
1,3,5 Trimethylbenzene	6.430	6.424	0.9960
1-Undecene	8.320	8.313	0.9955
Naphthalene	9.400	9.391	0.9950
n-Dodecane	9.820	9.819	0.9952
n-Tetradecane	12.350	12.356	0.9951
n-Hexadecane	14.830	14.860	0.9957

Column 1: retention times estimated through Eq. (11).
Column 2: results calculated according to the classical algorithm [6].
Column 3: numerical integration of Q/L along z applying the same procedure of column 2.
Temperature program is a single ramp with r_T = 10 °C/min. , $T_0 = 50\ °C$, L=30 m (reported by the supplier), $p_o = 765$ Torr , initial p_i=1277 Torr . Applied $P(T)$, $t_M(T)$ and $k(T)$ functions , from Reference [7].

A recent example of programmed temperature retention simulation , involving the described stepwise calculation of the local velocity , is the work by Snijders, Janssen and Cramers **[8]**, which uses a procedure essentially equivalent to that followed in reference **[6]**, but applied to constant inlet pressure.

The objective of the present work is to demonstrate the validity of equations (6) and (7) under variable P(T) flow conditions, or more generally, the validity of the following retention expression for programmed pressure and temperature gas chromatography:

$$1 = \int_{T_0}^{T_R} \frac{dT}{f'(T)\, t_M(T)\, [1 + k(T)]} \tag{11}$$

The consequences of chromatographic interest, the advantages and limitations of this relationship, with respect to the procedure identified by Eq. (8), will be discussed .

DEMONSTRATION

General Eq.(1) can be rearranged to:

$$\frac{Q(z,T)}{L}\,dz \;-\; \frac{1}{f'(T)\,t_M(T)\,[1+k(T)]}\,dT = 0 \tag{12}$$

which fits the generic form of :

$$M(x,y)\,dx \;+\; N(x,y)\,dy = 0 \tag{13}$$

The necessary and sufficient condition allowing Eq.(13) to be a exact differential is:

$$\frac{\partial M}{\partial y} = \frac{\partial N}{\partial x} \tag{14}$$

The general solution of the exact equation is (see for example **[9,10]**):

$$\int M\,\partial x \;+\; \int\left(N - \frac{\partial\left(\int M\,\partial x\right)}{\partial y}\right)dy = C \tag{15}$$

where C is an integration constant.

In our specific case: $dx \equiv dz$, $dy \equiv dT$, $M(z,T) \equiv Q(z,T)/L$, and

$$N(T) \equiv -\frac{1}{f'(T)\,t_M(T)\,[1+k(T)]}$$

Equation (12) is not in general an exact differential, since:

$$\frac{\partial N(T)}{\partial z} = 0 \neq \frac{\partial M(z,T)}{\partial T}$$

We want to determine if Eq.(12) becomes a exact equation when $z \to L$, considering that we are only interested in the particular solution with boundary condition: $(z=L\ ,\ T=T_R)$. Out of the limits $0 \le z \le L$ the equation has no physical meaning. Invariably, the integration begins at $z=0$, this being a condition *sinequa non*. It should be noted that the initiation of the integration at a point different to $z=0$ has not any physical meaning either .

As derivation and integration are inverse operations, we know that:

$$\frac{\partial M}{\partial T} = \frac{\partial\left[\dfrac{\partial\left(\int M\,\partial z\right)}{\partial z}\right]}{\partial T} \tag{16}$$

In the limit when $z \rightarrow L$, the primitive of M in the numerator of the right member of Eq. (16) is equal to:

$$j(T) = \frac{3\,[P^2(T)-1]}{2\,[P^3(T)-1]}$$

Then, its partial derivative respect to z is zero, and from Eq. (16) we see that in the proximity of $z=L$ is verified that $(\partial M / \partial T) = 0$. So, the condition of Eq. (14) is satisfied when $z \rightarrow L$, the equation of peak motion becoming a exact equation. Therefore, for the particular solution of chromatographic interest, Eq.(15) yields:

$$\int_0^L M\,\partial z + \int_{T_o}^{T_R}\left[N - \frac{\partial\left(\int_0^L M\,\partial z\right)}{\partial T}\right] dT = 0 \tag{17}$$

The integral $\int_0^L M\,\partial z$ can be solved analytically by substitution, with a result equal to unity.

Thus, Eq. (17) is reduced to Eq.(11), being our demonstration concluded .

The statement on the validity of Eq. (11) for variable $P(T)$ can also be demonstrated with a rather more limited formalism. The sufficient condition for Eq. (13) to be a exact differential is the existence of a function V such that: $\frac{\partial V}{\partial x} = M$ and $\frac{\partial V}{\partial y} = N$ (see for example **[10]**). The existence of V for the equation of peak motion (12) can be proven when $z \rightarrow L$.

CONSEQUENCES AND CORROBORATION

Numerical corroboration on the validity of Eq. (11) with variable $P(T)$ chromatographic conditions can be carried out from its consequences. Some of these are of fundamental importance with respect to the retention numerical simulation in programmed pressure and temperature gas chromatography.

Retention simulations through the algorithm resumed in Eq.* (8) *and by the numerical integration of Eq.* (11) *are equivalent

The statement is supported by the fact that both procedures concern the same basic chromatographic hypothesis relative to Eq. (1), not involving additional mathematical assumptions, approximations or simplifications, one with respect to the other, as demonstrated in the preceding section. Corroboration of this statement can be easily achieved by comparing numerical results obtained through both procedures. These should arrive to the same values under variable *P(T)* conditions. In Table 1 are shown calculated retention data for the constant mass flow control mode, following the respective procedures. The expressions of the applied functions and the conditions in the calculations for each solute can be found in Reference **[7]**. One of the reasons why they do not yield *exactly* the same values is the discrepancy in the number of operations performed by the computer. In the case of Eq. (11) less operations must be performed. However, this would be a minor contribution to the observed differences, taking into account that machine round-up has a minimal incidence in the numerical results. Furthermore , the forms of the integrands in equations (8) and (11) are quite dissimilar, generating different errors along the numerical integration, even if the same integration method is applied to both. Probably, the most important contribution to the observed differences is the existence of the additional parameter L in the algorithm of Eq. (8), not present in Eq. (11). The contribution of the error of L may be significant if nominal values are entered into the calculation. Besides, there might be inconsistency between measured values of L and gas hold-up time. It should be noted that there is a functional interrelation between them that should be fulfilled .

Parameter L is irrelevant for retention estimation from $t_M(T)$ and k(T)

L becomes irrelevant for the retention calculation through Eq. (11), instead, for simulation by the algorithm of Eq. (8) is a necessary input. Note that the effect of column's length is already accounted for by the function t_M(T). If Eq. (11) is strictly applicable to variable *P(T)* , then in these conditions L should be irrelevant too. This fact was corroborated by present authors running programs according to Eq. (11) for different *P(T)* functions and comparing calculated retentions with the experimental values **[7]**, concluding that the errors are in the same order respect to algorithms that include L as a significant parameter .

The following equality is verified:

$$\int_0^L \frac{Q(z,T)\,dz}{L} = \int_0^L \frac{Q(z,T)}{L}\,\partial z = 1 \qquad (18)$$

The integral in the left member represents the sum performed with algorithm of Eq. (8), a stepwise numerical integration with simultaneous variation of z and T. The integral on the right is the analytical one keeping T constant, which is equal to unity. This statement derives directly from the demonstration of section 2 and the statement 1 from this section. Equation (18) represents a special property of the fluid dynamics of the GC system. It was first observed by Said and Stenberg as it is mentioned in **[11]** (p. 105). This relationship displays the reason why

L becomes irrelevant. In Table 1 are shown calculated values of the integral on the left, introducing the respective sentences in the computer program used for calculating the retention times and the integral curves. The discrepancies respect to unity show clearly the errors associated to the numerical integration and to the introduction of L, as was mentioned previously .

There are some precedents in the literature concerning the application of Eqs. (6) or (7) to chromatographic conditions pertaining to variable $P(T)$. For example, in the paper by Dose **[12]** the reported $t_M(T)$ function cannot be associated to a constant head pressure condition **[1]**.

CONCLUSIONS

The equation of peak motion only becomes a exact equation when $z \rightarrow L$, i.e. in the proximity of the particular solution of chromatographic interest ($z=L$) being applicable Eq. (15) only if the integration is performed along the whole domain of z. So, Eq. (11) would not yield correct results if it is applied to an integration to intermediate values of z. In other words, the strict mathematical solution of Eq. (1) (i.e. relating z as a function of T or t) is not possible with this procedure. Nevertheless, the chromatographic interest is centred exclusively on the value of t_R or T_R, and not in obtaining the integral curve T vs. z. Therefore, this could be appreciated as a minor limitation of the procedure. On the other hand, there is a neat advantage in not needing to enter the value of the parameter L with its intrinsic error. Furthermore, having few operations to be done results in simpler and faster computer programs , with a reduced amount of sentences. The most outstanding characteristic of Eq. (11) is that it can be written explicitly in terms of the pressure program $P(T)$, this being crucial for a simplified treatment in PPTGC **[7]**.

REFERENCES

[1] González, F.R.; Nardillo, A.M.- **J. Chromatogr. A, 757**, 97 (1997).

[2] Zhang, J.Y.; Wang, G.M.; Quian, R.- **J. Chromatogr., 521**, 71 (1990).

[3] Bird, R.B.; Stewart, W.E.; Lightfott, E.N.- ***Transport Phenomena***, Wiley, New York (1964).

[4] Curvers, J.; Rijks, R.; Cramers, C.; Knauss, K.; Larson, P.- **J. High Resolut. Chromatogr., Chromatogr. Commun., 8**, 607 (1985).

[5] Akporhonor, E.F.; Le Vent, S.; Taylor, D.R.- **J. Chromatogr., 405**, 67 (1987).

[6] Dal Nogare, S.; Langlois, W.E.- **Anal. Chem., 32**, 767 (1960).

[7] Gonzalez, F.R.; Nardillo, A.M.- **J. Chromatogr. A, 757**, 109 (1997).

[8] Snijders, H.; Janssen, H.G.; Cramers, C.- **J. Chromatogr. A, 718**, 339 (1995).

[9] ***Handbook of Chemistry and Physics***.- CRC Press, Boston, 72th ed. (1992).

[10] Ford, L.R.- ***Differential equations***, McGraw-Hill, New York, 2nd ed. (1955).

[11] Habgood, W.; Harris, W.E.- ***Programmed Temperature Gas Chromatography***, Wiley, New York (1966).

[12] Dose, E.V.- **Anal. Chem., 59**, 2414 (1987).

COMUNIDADES INCRUSTANTES DE AREAS COSTERAS NATURALES DEL SUR DE LA PROVINCIA DE BUENOS AIRES (ARGENTINA)

STUDY OF MARINE FOULING COMMUNITIES FROM SOUTHERN AREAS OF THE BUENOS AIRES PROVINCE (ARGENTINA)

R. Bastida[1], J.P. Martin[2], E. Ieno[2]

SUMMARY

This work deals with the study of marine fouling communities of two coastal localities of Buenos Aires Province. Sampling programme was carried out using artificial sampling substrates which were placed vertically on the intertidal and subtidal zone of Reta and Monte Hermoso shores. Both localities showed the dominance of the small mussel ***Brachidontes rodriguezi****. Density of this species decreases towards the subtidal levels, while associated fauna density fluctuates with increasing depth.*

The studied localities show differences in some of their specific components and differ notably from fouling communities described for harbour areas of the Buenos Aires Province.

Associations between fouling samples are based on specific components and enviromental factors related with tidal levels.

Keywords: *Fouling communities, ecology, intertidal and subtidal.*

INTRODUCCION

Los estudios ecológicos sobre las comunidades incrustantes de las costas argentinas fueron iniciados en la década del 60 (Bastida, 1968, 1971a). La mayor parte de estos estudios fueron realizados por el CIDEPINT e instituciones asociadas a dicho centro.

Los trabajos publicados hasta el presente pueden ser clasificados en tres líneas principales, una de ellas de tipo básico descriptivo, tendiente a conocer las características ambientales de los principales puertos de la provincia de Buenos Aires y la composición, estructura y dinámica de sus comunidades incrustantes (Bastida 1968, 1971, 1973; Bastida y Torti, 1973; Bastida *et al.*, 1974a, 1974b; Bastida y Lichtschein, 1978; Bastida y Brankevich, 1980, 1981, 1982, 1984; Martinez *et al.*, 1984). Otra línea, consecuencia de la primera y del resultado de los ensayos de pinturas, ha estado vinculada con la biología y

---

[1] Investigador Principal del CONICET, Director Científico de la Fundación Mundo Marino y Profesor de la Universidad Nacional de Mar del Plata

[2] Becario de Perfeccionamiento del CONICET, Fundación Mundo Marino y Universidad Nacional de Mar del Plata

ecología de aquellas especies más agresivas del fouling (Bastida, 1995; Spivak, 1975). La tercer línea es básicamente de tipo experimental, de carácter generalmente interdisciplinario y vinculada con los sistemas de protección anticorrosiva y antifouling (Bastida *et al.*, 1970, 1976; Rascio *et al.*, 1969a, 1969b, 1970, 1972, 1973a, 1973b, 1974, 1976a, 1976b, 1977, 1978, 1979, 1990; Giúdice *et al.*, 1980, 1983, 1984, 1986, 1987, 1988a, 1988b; del Amo *et al.*, 1986; Benítez *et al.*, 1990).

Durante las últimas décadas fueron relevadas la totalidad de las áreas portuarias bonaerenses, por lo cual, era de interés poder completar el panorama con el estudio de las comunidades bentónicas asentadas sobre sustratos artificiales en áreas costeras naturales. De esta forma sería posible completar el inventario de biofouling de las costas argentinas, a la vez de constituir nuevos estudios ecológicos de base, de gran utilidad ante la eventual construcción de nuevas áreas portuarias en la zona.

Con el presente estudio se cubren dos nuevas localidades costeras del sur de la Provincia de Buenos Aires (Reta y Monte Hermoso). Estas nuevas investigaciones, unidas al conocimiento previo de los puertos de Mar del Plata, Quequén, Puerto Belgrano e Ingeniero White, han permitido lograr un amplio panorama del biofouling del sector sur de la costa bonaerense.

Actualmente se están desarrollando estudios en el extremo norte de la provincia, con influencia estuarial, con lo cual se completaría todo el panorama del biofouling bonaerense.

AREA DE ESTUDIO

Los estudios fueron realizados en las localidades de Reta y Monte Hermoso, ubicadas en el sudeste de la costa de la Provincia de Buenos Aires **(Fig. 1)**. Este sector de la costa se extiende en sentido este-oeste y se caracteriza por la presencia de amplias playas arenosas de granulometría mediana-fina y de pendiente suave. Corresponden a costas en claros procesos de erosión marina, las cuales se encuentran acompañadas en casi toda su extensión por un cordón de dunas costeras semifijas y relativamente elevadas que, en algunos sitios, cubren barrancas erosionadas por el mar (Teruggi *et al.*, 1959; Mouzo y Garza, 1974; Bremec, 1986).

El sector de playa arenosa se encuentra interrumpido por restingas de sustratos consolidados de naturaleza limo-arcillosos y que afloran tanto en el intermareal como en el submareal. Dichas restingas, si bien de escasa importancia, constituyen el sustrato natural de las asociaciones faunísticas de las cuales provienen las especies integrantes del biofouling local.

Todo el sector sur de la costa bonaerense posee, comparativamente, menor proporción de sustratos duros que el área central de Mar del Plata y Miramar, donde además de las plataformas de rocas limo-loessoides están presentes rocas cuarcíticas, afloramientos que corresponden al sistema de Tandilia. De todas maneras, desde el punto de vista biogeográfico, el sector norte y sur de la costa de la provincia de Buenos Aires constituyen una unidad, cuyas variaciones sólo se deben a condiciones ambientales locales.

En cuanto a las características hidrológicas, este sector de la costa se encuentra bañado por una masa de agua de segundo orden ubicada entre el continente y la corriente de Malvinas, y cuyo origen es subantártico. La dirección del movimiento netamente preponderante es hacia el norte, pero a veces los vientos y las mareas pueden cambiarla esporádica y localmente. Estas aguas reciben la influencia local de varios ríos y arroyos que desembocan directamente en el mar. La temperatura superficial del agua en la zona de Monte Hermoso es de aproximadamente 9 °C en invierno, pudiendo llegar a 23,5 °C en verano y la salinidad oscila entre 33 y 34 ‰ (Bremec, 1986).

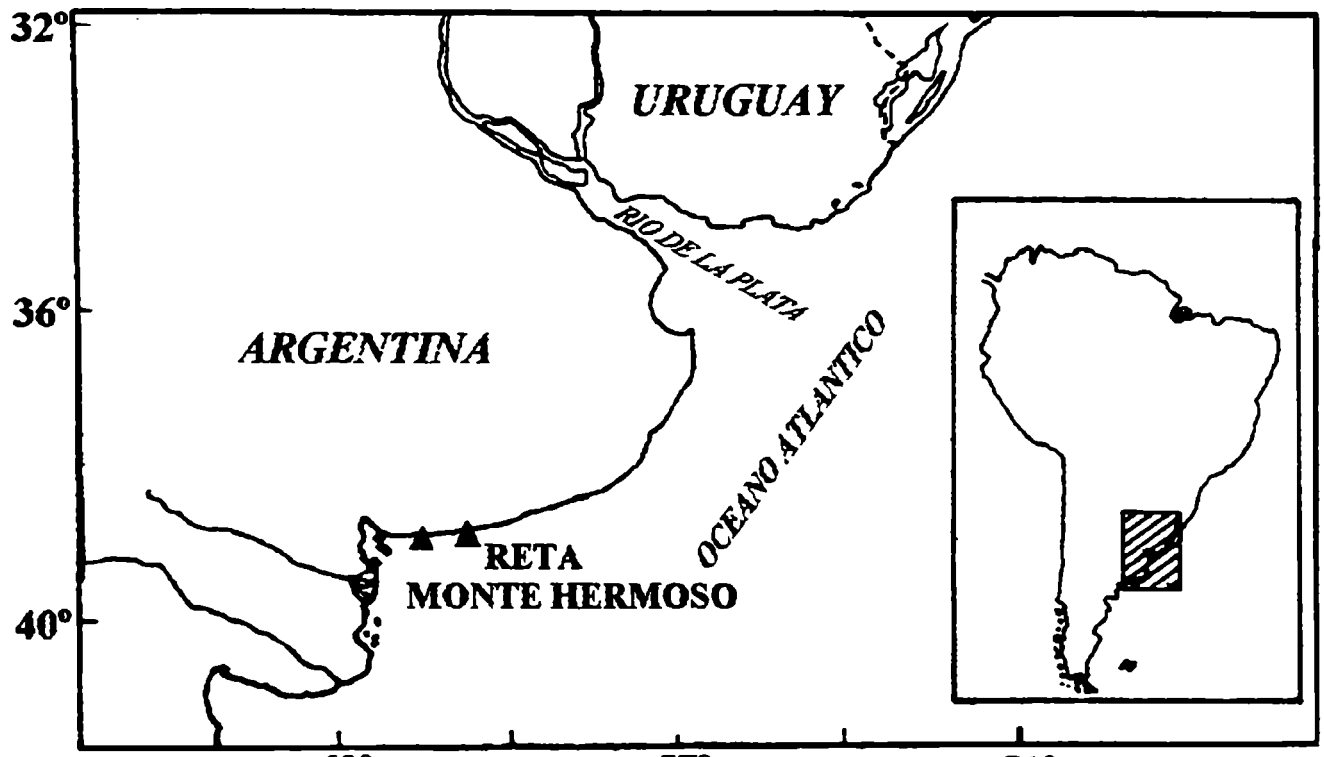

Fig. 1. Area de estudio.

MATERIALES Y METODOS

En marzo de 1989 se realizó un muestreo de la comunidades incrustantes asentadas sobre sustratos artificiales verticales, ubicados en las zonas intermareales de las localidades de Reta y Monte Hermoso. En Reta el sustrato muestreado fue el casco de hierro de un buque varado en la zona desde épocas remotas, en tanto que en Monte Hermoso el sustrato de estudio fue uno de los pilotes de un muelle construido de hormigón armado. En la primera localidad se tomaron siete niveles de muestreo correspondientes al piso mediolitoral. En Monte Hermoso se tomaron 4 niveles en el mediolitoral y 5 en el piso infralitoral. Las muestras, de una superficie de 49 cm^2 cada una, fueron tomadas utilizando una espátula metálica.

Los organismos obtenidos fueron fijados en formol neutralizado al 5% y posteriormente identificados y contados en el laboratorio utilizando una lupa binocular. Los datos obtenidos fueron procesados estadísticamente, aplicando el índice de asociación DICE y confeccionando los correspondientes diagramas de afinidad (Stirn, 1981).

Del sedimento intersticial de cada muestra se tomaron tres submuestras con pipeta, para analizar el microfouling utilizando microscopio binocular. Para determinar la abundancia de los distintos componentes del microfouling se utilizó una escala de abundancia relativa basada en cuatro categorías: **Abundante (A), Frecuente (F), Escasa (E)** y **Rara (R)**. Esta metodología ya ha sido utilizada en trabajos anteriores (Bastida et al., 1971a).

Para el estudio de los procesos de epibiosis, las frecuencias de los diferentes casos se obtuvieron analizando cada muestra y computando en cada una de ellas la aparición de una relación de epibiosis determinada y no la cantidad de veces en que la misma se presentaba (Bastida *et al.*, 1978).

Para el análisis de la estructura poblacional de *Brachidontes rodriguezi* se realizaron histogramas de frecuencia de tallas, para cada nivel en particular, utilizando clases de talla con un rango de 3 mm.

RESULTADOS Y DISCUSION

Descripción del macrofouling

Las comunidades asentadas sobre los sustratos artificiales estudiados, muestran una clara dominancia del mitílido *Brachidontes rodriguezi*. Las especies acompañantes son diferentes de un sitio a otro y variables con la profundidad del nivel muestreado.

A continuación se describen las características de la comunidad, en cuanto a sus componentes específicos principales, en cada uno de los lugares de estudiados.

RETA

En esta localidad, los siete niveles muestreados en el piso mediolitoral (niveles 1 a 7) presentan un mejillinar con una densidad de *Brachidontes rodriguezi* entre 9,35 y 3,08 ind./cm^2, la cual desciende al aumentar la profundidad, estabilizándose a partir del nivel 4. La elevada densidad de *B. rodriguezi* le da al mejillinar una estructura compacta a manera de tapiz.

La diversidad específica de las muestras es baja, debido a la amplia dominancia de *Brachidontes rodriguezi* y al reducido número de especies acompañantes. Sin embargo, el aumento de la riqueza específica y la disminución en la frecuencia relativa de *B. rodriguezi* con respecto a las especies acompañantes, provoca un aumento en la diversidad de la comunidad en los niveles de muestreo más profundos **(Fig. 2)**.

Los organismos acompañantes más importantes en los dos primeros niveles de muestreo son los platelmintos policládidos y los nemertinos. Los policládidos se hallan presentes en todos los niveles de muestreo, pero alcanzan su mayor densidad en el nivel 2, en tanto que los nemertinos sólo se encuentran en los niveles superiores.

A partir del nivel de profundidad 2 se observa la presencia del poliqueto *Syllis* sp., especie que va ganando importancia a medida que aumenta la profundidad. La misma llega a su máxima densidad (2,71 ind/cm^2) en el nivel 7, convirtiéndose en el organismo más importante de la comunidad luego de *Brachidontes rodriguezi*.

Entre los moluscos se encuentran presentes pequeños ejemplares de los bivalvos *Pododesmus rudis* y *Hiatella solida*. Si bien ambas especies se hallan en casi todos los niveles de profundidad estudiados, su densidad en las muestras es muy baja. El gastrópodo pulmonado *Siphonaria lessoni* sólo se halla en el nivel 1 y en muy baja densidad. Entre los ejemplares de *Brachidontes rodriguezi* se intercalan escasos ejemplares de *Mytilus edulis platensis* de talla reducida. Los mismos adquieren su mayor importancia en los niveles superiores.

Los hidrozoos se hallan representados por *Bougainvillia ramosa* y por *Clytia gracilis*. Ambas especies alcanza su mayor abundancia y grado de desarrollo en el nivel 5.

Entre los picnogónidos se encuentran ejemplares adultos y juveniles de *Anoplodactylus petiolatus* y *Tanystylum orbiculare*. El primero es el más importante en las muestras y su abundancia va acompañando a la de *Bougainvillia ramosa*, posiblemente por alimentarse de ella y/o por precisarla para su reproducción.

Los crustáceos se hallan representados por el anfípodo *Caprella* sp. y el decápodo *Pachycheles haigae*, ambos se presentan en la comunidad a partir del nivel 5.

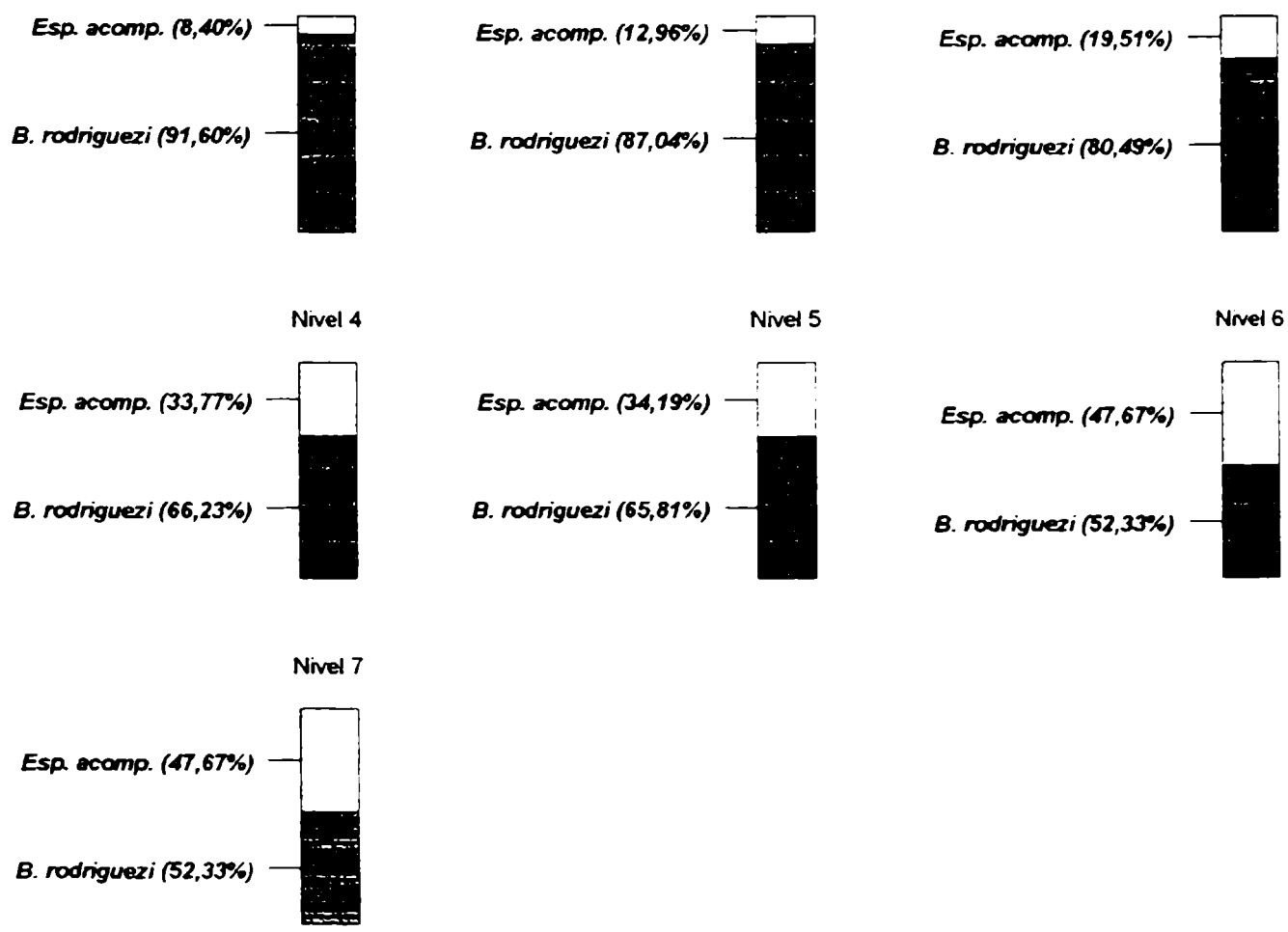

Fig. 2. Frecuencia de *Brachidontes rodriguezi* y especies acompañantes en la localidad de Reta.

Las algas están casi ausentes en las muestras, sólo se halla la clorofita *Ulothrix* sp. en los niveles superiores y la rodofita *Ceramium* sp. en el nivel 7, sin embargo ambas son muy escasas.

Tabla I

Principales organismos del macrofouling de Reta

	DENSIDAD DE EJEMPLARES (ind/cm^2) O ABUNDANCIA RELATIVA*						
PRINCIPALES ESPECIES REGISTRADAS	Nivel 1	Nivel 2	Nivel 3	Nivel 4	Nivel 5	Nivel 6	Nivel 7
Algas							
Ulothrix sp.	R	R	R	—	—	—	—
Ceramium sp.	—	—	—	—	—	—	E
Celenterados							
Bougainvillia ramosa	R	E	E	R	F	R	—
Clytia gracilis	—	—	R	—	E	R	—
Platelmintos							
Policládidos (indet.)	0,24	0,29	0,10	0,14	0,18	0,04	0,04
Nemertinos (indet.)	0,24	0,18	—	0,12	—	—	—
Anélidos							
Syllis sp.	—	0,04	0,59	1,14	0,69	1,84	2,71
Sabellaria wilsoni	—	—	—	—	0,04	—	—
Moluscos							
Brachidontes rodriguezi	9,35	5,35	4,04	3,08	3,14	3,24	3,67
Mytilus edulis platensis	0,24	0,22	0,18	0,10	0,02	0,04	0,02
Pododesmus rudis	—	0,08	—	0,02	0,14	—	0,08
Hiatella solida	0,04	0,08	0,06	0,02	0,08	0,06	0,47
Siphonaria lessoni	0,08	—	—	—	—	—	—
Crustáceos							
Caprella sp.	—	—	—	—	0,06	—	0,02
Pachycheles haigae	—	—	—	—	0,18	0,02	—
Picnogónidos							
Anoplodactylus petiolatus	—	0,08	0,02	0,02	0,22	—	—
Tanystylum orbiculare	—	—	0,02	—	—	—	—
Briozoos							
Membranipora puelcha	—	—	—	—	—	—	R

* A: abundante; F: frecuente; E: escaso; R: raro

MONTE HERMOSO

En la localidad de Monte Hermoso fueron muestreados cuatro niveles pertenecientes al piso mediolitoral (niveles 1 a 4) y cinco al infralitoral (niveles 5 a 9). En todos ellos se

observa una comunidad dominada por *Brachidontes rodriguezi*, el cual se encuentra en densidades que varían entre 9,02 y 3,28 ind/cm^2. También aquí la densidad de *B. rodriguezi* tiende a disminuir con el aumento de la profundidad. La riqueza específica de las muestras es superior a la hallada en la localidad de Reta. La diversidad es baja en las muestras de los niveles superiores y va aumentando con la profundidad, como resultado de la disminución en la densidad de *Brachidontes rodriguezi* y el aumento en el número de especies acompañantes **(Fig. 3)**.

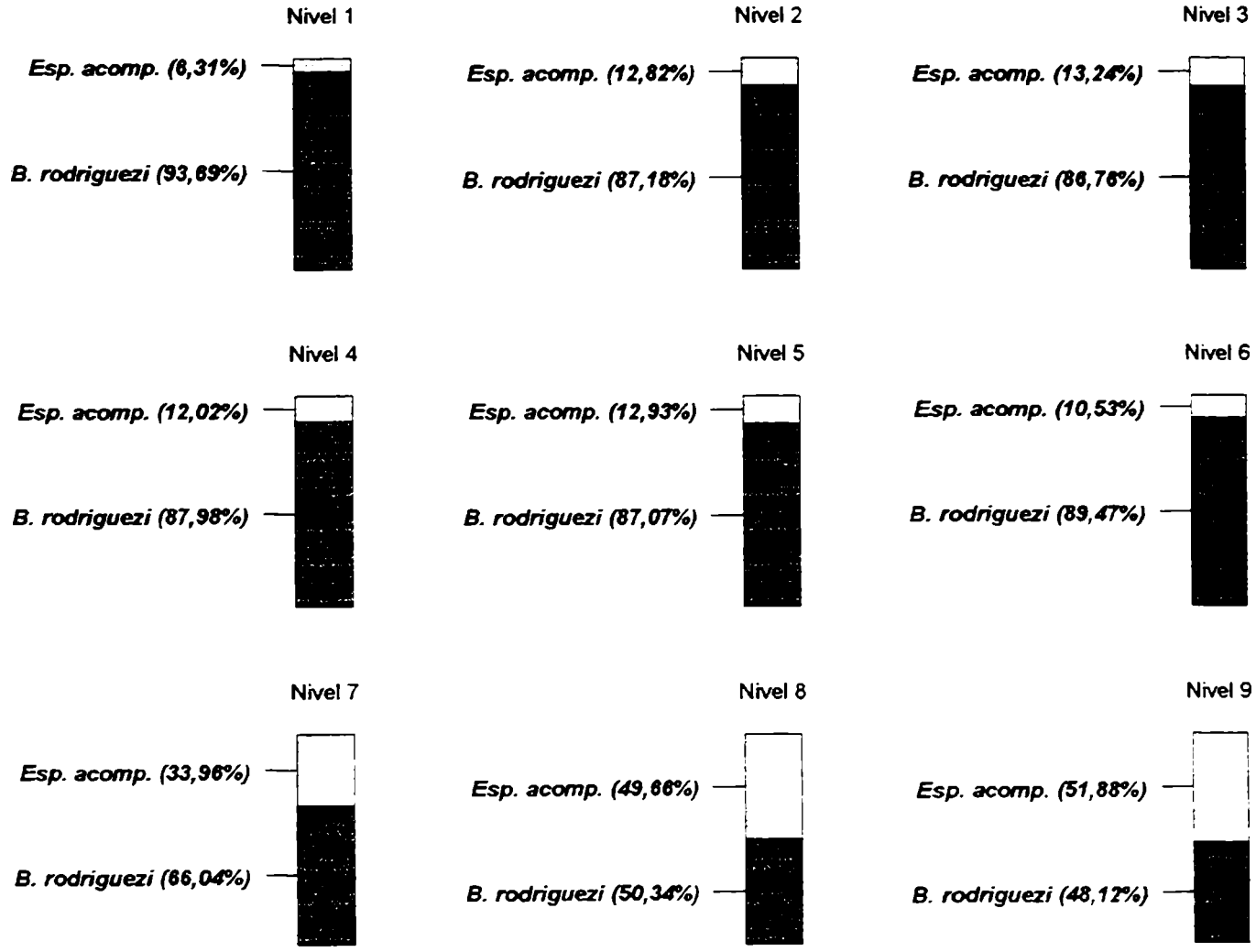

Fig. 3. Frecuencia de *Brachidontes rodriguezi* y especies acompañantes en la localidad de Monte Hermoso.

Los organismos acompañantes más importantes varían según el nivel de profundidad estudiado. En el nivel 1 predominan las larvas de insectos Chironomidae, con una densidad de 0,39 ind/cm^2. En el nivel 2, las mismas son reemplazadas por los nemertinos, los cuales si bien se encuentran presentes en los niveles 1 a 5, alcanzan en el nivel 2 su densidad máxima. El poliqueto *Syllis* sp. es la especie acompañante más importante en los niveles 3 a 5, si bien su densidad máxima (1,29 ind/cm^2) es alcanzada en el nivel 9. En el nivel 6 predomina *Pachycheles haigae*, especie que alcanza su abundancia máxima también en el nivel 9, con una densidad de 0,49 ind/cm^2. Este decápodo se halla representado por ejemplares de talla pequeña. Los ofiuros Amphiuridae son el grupo subdominante en el nivel 7, y se encuentran representados por ejemplares juveniles de tamaño pequeño. En los niveles 8 y 9, el organismo acompañante más importante en la comunidad, es el anfípodo *Caprella* sp., con densidades de 1,14 y 6,86 ind/cm^2 respectivamente. Posiblemente se trate de las especies *Caprella equilibra* y *C. penantis*, ya citadas para el biofouling de Puerto Belgrano y para las comunidades naturales

infralitorales de la zona, sin embargo no pudieron ser determinados en esta oportunidad por tratarse de ejemplares juveniles (Bastida *et al.*, 1974a; Bremec, 1986).

Entre los moluscos se encuentran, además de las especies ya mencionadas, *Pododesmus rudis* y *Hiatella solida*, ambas se hallan representadas en todos los niveles por ejemplares de pequeño tamaño y alcanzan su máxima abundancia en los niveles más profundos. *Mytilus edulis platensis* está prácticamente ausente en esta localidad, presentándose tan sólo en los niveles 2 y 3 con una densidad muy baja.

Los poliquetos se encuentran en esta comunidad más diversificados que en Reta, estando presentes, además de *Syllis* sp., *Sabellaria wilsoni* y *Dodecaceria* sp. en los niveles del mediolitoral, y *Halosydnella australis* y *Serpula* sp. en los niveles del infralitoral.

Entre los crustáceos se encuentran, además de los ya mencionados, los decápodos *Cyrtograpsus altimanus*, en los niveles 2 y 3, y *Coenophtalmus tridentatus* en los niveles 4, 7 y 9. El isópodo *Jaeropsis dubia* alcanza gran importancia en los niveles más profundos, llegando a una densidad de 0,67 ind/cm^2 en el nivel 8.

Los cnidarios se encuentran representados por los hidrozoos *Bougainvillia ramosa*, *Sarsia sarsii*, *Clytia gracilis*, *Obelia* sp. y *Plumularia setacea* y por la pequeña anémona *Tricnidactis errans*.

El picnogónido *Anoplodactylus petiolatus* se encuentra presente en los niveles intermedios (niveles 3 a 6), en tanto que *Tanystylum orbiculare* se encuentra en los niveles más profundos (7 a 9).

El briozoo *Membranipora puelcha* es particularmente abundante en el nivel 9.

Las algas están prácticamente ausentes, salvo por la escasa presencia de *Ulothrix* sp. y la rara presencia de *Ulva lactuca* en el nivel 1 y de *Ceramium* sp. en el 7.

Analisis de afinidad entre niveles de muestreo

En ambas localidades estudiadas, los diagramas de afinidad realizados en base a las especies integrantes del macrofouling, evidencian claros agrupamientos de los distintos niveles de muestreo, en función de sus componentes específicos **(Fig. 4)**.

RETA

En esta localidad, las muestras se reúnen formando dos agrupamientos de afinidad principales. Un grupo involucra los cuatro primeros niveles de muestreo (1 a 4), caracterizados por la presencia de nemertinos, el picnogónido *Anoplodactylus petiolatus* y el alga *Ulothrix* sp. y la ausencia de la mayor parte de los organismos presentes en los niveles más profundos. La presencia exclusiva en el nivel 1 de *Siphonaria lessoni* y la ausencia de muchos de los organismos que se encuentran presentes en los otros tres niveles que integran este grupo, hacen que este nivel se separe del resto, por lo cual posiblemente corresponda al horizonte inferior del piso supralitoral, en tanto que los niveles 2, 3 y 4 corresponden al mediolitoral superior.

Tabla II

Principales organismos del macrofouling de Monte Hermoso

	DENSIDAD DE EJEMPLARES (ind/cm^2) O ABUNDANCIA RELATIVA*								
PRINCIPALES ESPECIES REGISTRADAS	Nivel 1	Nivel 2	Nivel 3	Nivel 4	Nivel 5	Nivel 6	Nivel 7	Nivel 8	Nivel 9
Algas									
Ulothrix sp.	E	R	—	—	F	—	—	—	—
Ulva lactuca	R	—	—	—	—	—	—	—	—
Ceramium sp.	—	—	—	—	—	—	R	—	—
Celenterados									
Bougainvillia ramosa	—	R	E	—	E	E	R	R	R
Clytia gracilis	—	—	—	—	—	—	—	R	E
Sarsia sarsii	—	—	—	F	F	—	—	—	—
Obelia sp.	—	—	—	—	—	E	R	E	E
Plumularia setacea	—	—	—	—	—	—	R	R	R
Tricnidactis errans	—	E	R	R	R	R	E	F	R
Platelmintos									
Policládidos (indet.)	—	0,14	0,18	—	0,04	—	0,02	0,02	—
Nemertinos (indet.)	0,06	0,8	0,02	0,02	0,06	—	—	—	—
Anélidos									
Syllis sp.	—	0,12	0,33	0,33	0,27	0,06	0,59	0,86	1,29
Halosydnella australis	—	0,02	—	0,04	—	0,02	0,16	0,12	—
Serpula sp.	—	—	—	—	—	0,02	0,04	—	—
Sabellaria wilsoni	—	0,02	0,12	—	—	—	—	—	—
Dodecaceria sp.	—	—	—	0,02	—	—	—	—	—
Lumbrinereis sp.	—	—	—	—	—	—	—	—	0,10
Moluscos									
Brachidontes rodriguezi	7,57	9,02	5,08	3,29	5,63	4,16	5,00	4,57	8,35
Mytilus edulis platensis	—	0,02	0,02	—	—	—	—	—	—
Pododesmus rudis	0,02	0,08	0,16	0,33	0,33	0,35	0,16	0,45	0,66
Hiatella solida	0,02	0,02	—	—	0,04	0,02	0,06	0,04	0,04
Crustáceos									
Caprella sp.	—	—	—	—	0,06	0,04	0,06	1,14	6,86
Jaeropsis dubia	—	—	—	—	0,14	0,04	0,33	0,67	0,16
Pachycheles haigae	—	0,04	—	—	0,12	0,20	0,35	0,22	0,45
Cyrtograpsus altimanus	—	0,02	0,04	—	—	—	—	—	—
Coenophtalmus tridentatus	—	—	—	0,02	—	—	0,02	—	0,04
Balanus glandula	0,04	—	—	—	—	—	—	—	—
Picnogónidos									
Anoplodactylus petiolatus	—	—	0,04	0,02	0,02	0,02	—	—	—
Tanystylum orbiculare	—	—	—	—	—	—	0,06	0,04	0,04
Insectos									
Chironomidae (larvas)	0,39	0,10	—	—	—	—	—	—	—
Briozoos									
Membranipora puelcha	R	—	R	—	R	E	E	E	A
Equinodermos									
Amphiuridae (indet.)	—	—	—	—	—	0,02	0,82	0,22	0,02

* A: abundante; F: frecuente; E: escaso; R: raro

El otro grupo de afinidad se encuentra integrado por los niveles de muestreo 5, 6 y 7, pertenecientes al horizonte mesolitoral inferior y caracterizados por la presencia de *Sabellaria wilsoni*, *Clytia gracilis*, *Membranipora puelcha*, *Pachycheles haigae*, *Caprella* sp. y el alga *Ceramium* sp. Estas especies se encuentran ausentes en los niveles 1, 2, 3 y 4.

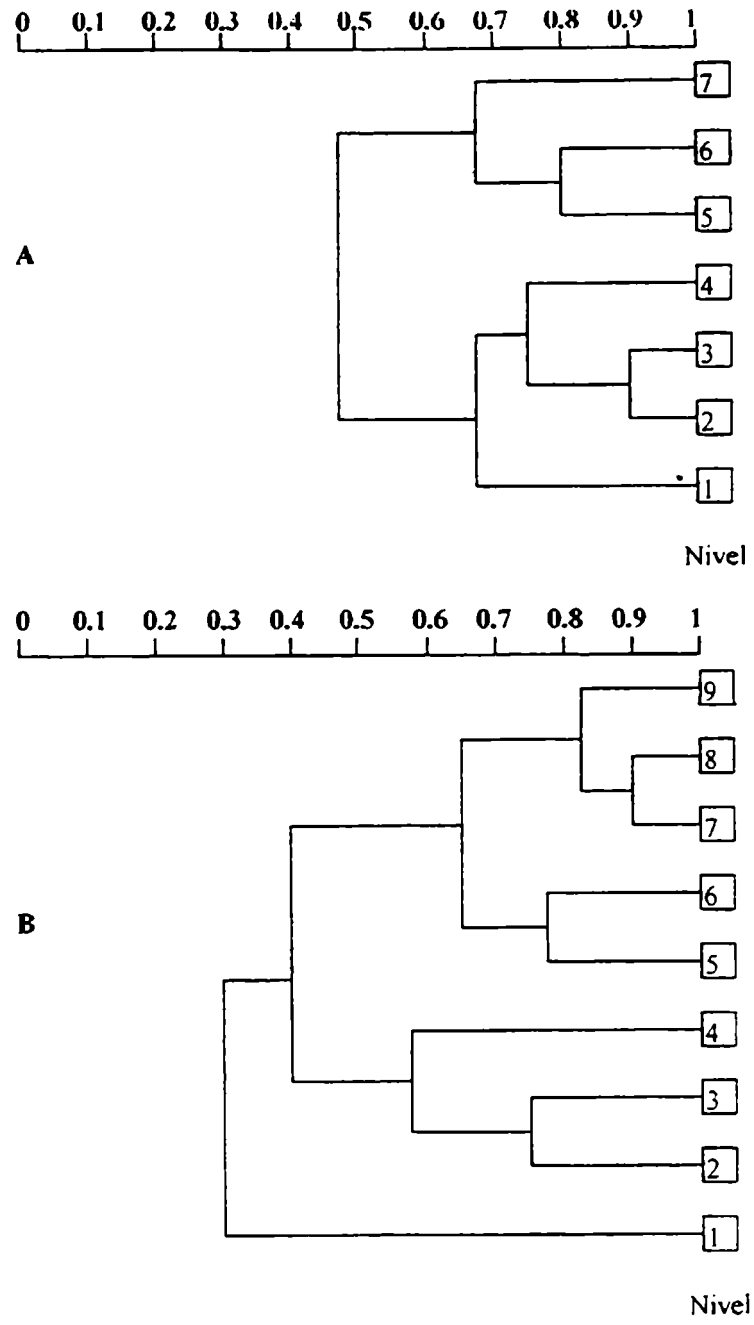

Fig. 4. Diagramas de afinidad entre los niveles de muestreo. A. Reta, B. Monte Hermoso.

Brachidontes rodriguezi, Mytilus edulis platensis, Pododesmus rudis, Hiatella solida, Syllis sp., platelmintos policládidos y *Bougainvillia ramosa* se hallan presentes en todos los niveles de muestreo, si bien con abundancias variables.

MONTE HERMOSO

El análisis de afinidad permite agrupar a las muestras de los diferentes niveles estudiados en dos grupos principales. Un grupo se encuentra integrado por las muestras de los niveles 2, 3 y 4, pertenecientes al piso mediolitoral y caracterizadas por la presencia de *Mytilus edulis platensis*, Nemertinos, *Sabellaria wilsoni* y *Cyrtograpsus altimanus y Anoplodactylus petiolatus* y la ausencia de la mayoría de los organismos presentes en los niveles más profundos.

El otro grupo reúne a aquellas muestras de los niveles de estudio 5, 6, 7, 8 y 9, caracterizados por una mayor riqueza específica y la presencia de Amphiuridae, *Caprella* sp., *Tanystylum orbiculare, Jaeropsis dubia, Pachycheles haigae, Plumularia setacea, Obelia sp.* y *Clytia gracilis*, especies que se encuentran mayormente vinculadas a los niveles inferiores del piso mediolitoral y superiores del piso infralitoral.

El nivel 1 se separa de los dos grupos anteriores por la alta abundancia de larvas de insectos *Chironomidae*, la presencia exclusiva de *Balanus glandula* y *Ulva lactuca* y por la ausencia de la mayoría de las especies presentes en los niveles restante, por lo cual posiblemente corresponda al horizonte inferior del piso supralitoral.

Especies como *Brachidontes rodriguezi* , *Pododesmus rudis, Hiatella solida, Syllis* sp., platelmintos policládidos, *Bougainvillia ramosa, Tricnidactis errans* y *Membranipora puelcha*, se hallan presentes en todos los niveles de muestreo con abundancias variables.

Procesos de epibiosis del macrofouling

Resultó de interés durante estos estudios, hacer un análisis de los procesos de epibiosis del macrofouling, dado que es uno de los mecanismos frecuentes que adoptan los organismos de comunidades incrustantes, ante la falta de sustrato adecuado o ante el exceso de contingentes colonizadores. De esta forma suelen producirse claros fenómenos de competencia espacial inter e intraespecífica por el sustrato de fijación.

A su vez, la comparación de estos procesos de epibiosis en áreas naturales con los observados en áreas portuarias, tal vez sirvan para aclarar aspectos referidos a la estructuración de la comunidad de biofouling.

Los procesos de epibiosis suelen constituir estrategias biológicas exitosas ante los sistemas de control antifouling, como lo son las pinturas tóxicas.

RETA

Los procesos de epibiosis no son muy importantes en esta localidad, lo cual es consecuencia de la baja diversidad que presenta la comunidad.

Como es lógico en una comunidad de este tipo, caracterizada por la amplia dominancia del mitílido *Brachidontes rodriguezi*, es este organismo el principal sustrato de fijación sobre el cual se establecen los organismos sésiles. En esta localidad, *B. rodriguezi* constituye el único sustrato vivo de fijación, no observándose casos de epibiosis de segundo grado.

La escasez de sutrato abiótico y el grado de aglomeración de la comunidad, provocan que el principal epibionte sea el mismo *B. rodriguezi*, observándose en general la presencia de los ejemplares más pequeños de la población fijos sobre los de tamaños mayores. Este tipo de epibosis constituye aproximadamente el 30% de los casos observados **(Fig. 5)**.

El segundo epibionte más importante de *Brachidontes rodriguezi* lo constituyen los hidrozoos. *Bougainvillia ramosa* representa el 25 % de los casos hallados, correspondiéndole el 16 % a *Clitya gracilis.*

Pododesmus rudis ocupa el cuarto lugar entre los epibiontes, correspondiéndole el 12 % de frecuencia en los casos de epibiosis registrados.

El porcentaje restante de casos de epibiosis corresponde al briozoo incrustante *Membranipora puelcha*, al poliqueto *Sabellaria wilsoni* y a las algas *Ulothrix* sp. y *Ceramium* sp.

En cuanto a la abundancia de los procesos de epibiosis en cada muestra, se observa una tendencia al aumento hacia los niveles más profundos. La misma alcanza su máxima intensidad en el nivel 5, donde la comunidad muestra su mayor diversidad y complejidad. Es en este nivel donde las colonias de *B. ramosa* presentan su mayor abundancia y grado de desarrollo.

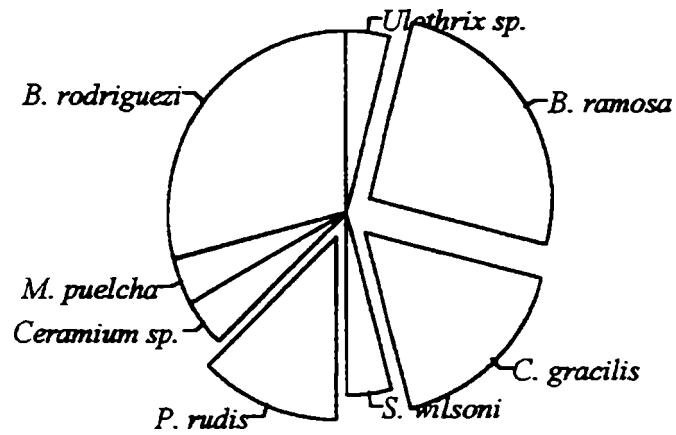

Fig. 5. Frecuencia de los casos de epibiosis sobre *B. rodriguezi* en la localidad de Reta.

MONTE HERMOSO

En esta localidad los procesos de epibiosis alcanzan una mayor importancia y grado de complejidad que en Reta. Los mismos son el resultado de la mayor diversidad que presenta el mejillinar en Monte Hermoso, llegando a observarse epibiosis de hasta tercer grado.

Si bien el principal sustrato vivo de fijación es *Brachidontes rodriguezi*, este rol es compartido con otros organismos de la communidad. Así, *Membranipora puelcha*, *Pododesmus rudis*, *Plumularia setacea* y *Balanus glandula* también actúan como sustrato de fijación de diversos epibiontes **(Fig. 6)**.

Brachidontes rodriguezi actúa como sustrato de fijación en el 76 % de los casos hallados. Sus principales epibiontes son, en orden de importancia, *B. rodriguezi*, *Tricnidactis errans*, *Pododesmus rudis*, *Membranipora puelcha* y *Bougainvillia ramosa* **(Fig. 7)**.

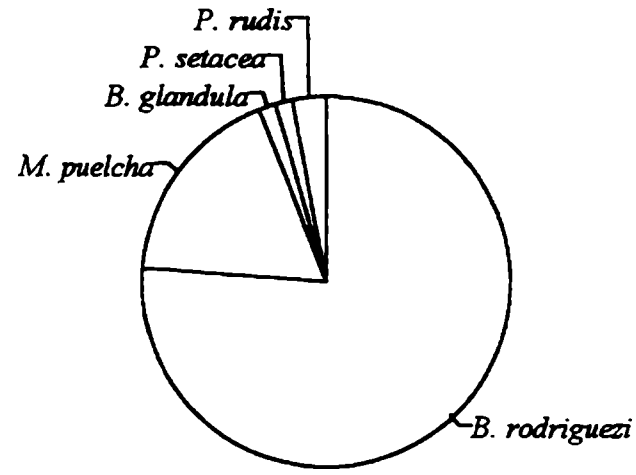

Fig. 6. Frecuencia de organismos que actúan como sustrato de fijación en la localidad de Monte Hermoso.

Otros epibiontes de *B. rodriguezi*, si bien con una frecuencia inferior a los ya mencionados son, en orden de importancia: los hidrozoos *Plumularia setacea, Obelia sp., Clytia gracilis* y *Sarsia sarsii*; los poliquetos *Serpula* sp. y *Sabellaria wilsoni,* y el alga rodofita *Ceramium* sp.

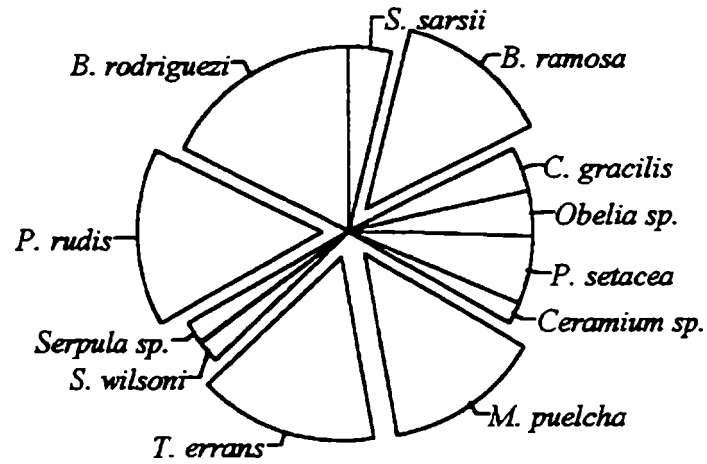

Fig. 7.Frecuencia de los casos de epibiosis sobre *B. rodriguezi* en la localidad de Monte Hermoso.

Membranipora puelcha constituye el segundo sustrato de importancia en esta comunidad, siendo *Obelia sp.* su principal epibionte, seguida en orden de importancia por *Clytia gracilis* y *Pododesmus rudis*. El porcentaje restante de casos corresponde a los epibiontes *Sarsia sarsii, Bougainvillia ramosa, Plumularia setacea* y *Tricnidactis errans* **(Fig. 8)**.

Pododesmus rudis es el tercer sustrato vivo, en orden de importancia, en esta comunidad. Entre sus epibiontes se han registrado el hidrozoo *Sarsia sarsii* y la anémona *Tricnidactis errans*.

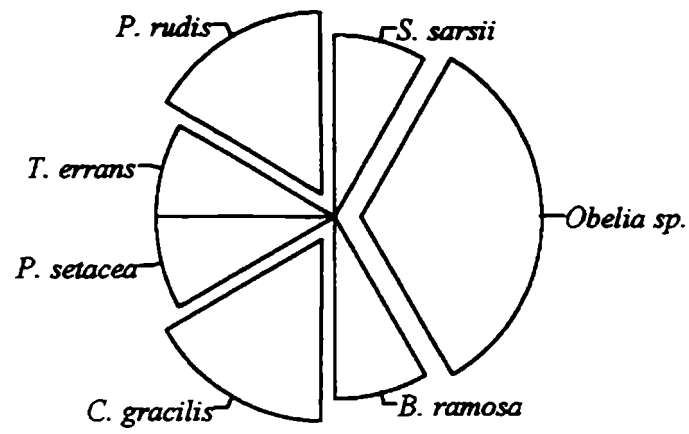

Fig. 8. Frecuencia de los casos de epibiosis sobre *Membranipora puelcha*.

Balanus glandula se presenta únicamente en el primer nivel de muestreo, donde actúa como sustrato de pequeños ejemplares de la clorofita *Ulva lactuca*.

La complejidad de este tipo de interacción entre los diferentes organismos de la comunidad, aumenta con la profundidad del nivel estudiado y con la diversidad de la muestra.

Una asociación interesante

Las relaciones de parasitismo entre picnogónidos e hidrozoos, son procesos biológicos ampliamente difundidos en otras partes de mundo. Existen muchos registros de la presencia de larvas de picnogónidos (protonymphon) encapsuladas dentro de los hidrantes de diferentes especies de hidrozoos. Sin embargo, este tipo de relación no había sido registrada hasta el presente para las costas argentinas (Genzano, com. pers.).

En la comunidad de biofouling de la localidad de Reta, se observa la presencia de colonias del hidrozoo atecado *Bougainvillia ramosa*, cuyos hidrantes albergan en su interior larvas de picnogónido, aparentemente *Anoplodactylus petiolatus*. Varios de los hidrantes de *B. ramosa* presentan estructuras en forma de cápsula ligeramente alargada, con una o más larvas en desarrollo en su interior. Este tipo de asociación se ha observado en el nivel 5, donde las colonias de *B. ramosa* alcanzan su mayor abundancia y desarrollo y *A. petiolatus* es más frecuente.

Existen diferentes teorías para explicar la forma en que la larva del picnogónido parasita al hidrozoo, según Hodge (1862), quien observó el parasitismo de *Phoxichilidium coccineum* sobre *Sarsia eximia*, la larva del picnogónido es ingerida por el hidrozoo y transportada a través de la colonia hasta localizarse y enquistarse en un hidrante en desarrollo. La larva se enquista en el perisarco del hidrocaulo y se alimenta del hidrante en desarrollo. Al finalizar el período de enquistamiento, el picnogónido en desarrollo rompe el perisarco y emerge para comenzar la fase libre de su ciclo de vida.

Análisis del microfouling

RETA

Las muestras de los diferentes niveles analizados se caracterizan en general por la presencia de escaso sedimento intersticial, formado por abundante detrito orgánico particulado y por arena fina. La proporción de esta última aumenta hacia los niveles más profundos, seguramente como consecuencia de su cercanía al fondo arenoso.

El análisis microscópico del sedimento intersticial revela la presencia de diversas diatomeas, en su mayoría de hábitos bentónicos.

Entre las diatomeas pennadas se destaca en los niveles superiores *Achnanthes longipes*, la cual es **abundante** en el nivel 2 **(Fig. 9)**. Esta diatomea se encuentra formando cadenas cortas de 2 a 4 células unidas a un estípite que le permite fijarse al sustrato. Posiblemente esta especie forme cadenas más largas, las cuales se rompen con el manipuleo de las muestras.

El género *Navicula*, principalmente representado por *Navicula grevillei*, se halla presente en todos los niveles, sin embargo, su abundancia es mayor en los inferiores **(Fig. 9)**.

Grammatophora spp., de la cual se diferencian por lo menos dos especies distintas, se destaca en los niveles intermedios (3 a 6) donde su presencia es **frecuente (Fig. 9).**

El género *Licmophora* repite el mismo patrón batimétrico de distribución que *Grammatophora*, si bien su máxima abundancia es alcanzada en los niveles 5 y 6 **(Fig. 9)**.

Otras de las diatomeas presentes en las muestras con presencia **escasa** son: *Synedra* spp., *Thalassiothrix* spp. y *Rhabdonema* sp.

Entre los géneros de diatomeas pennadas de importancia menor a los ya citados se encuentran *Raphoneis*, *Amphora*, *Cocconeis* y *Pleurosigma*.

Entre las diatomeas céntricas, *Melosira* es el género más abundante. Esta diatomea se halla en todos los niveles del muestreo, alcanzando su máxima abundancia (**escasa**) en los niveles 2 a 5.

Las diatomeas de los géneros *Coscinodiscus*, *Biddulphia*, *Actinoptychus*, *Cyclotella* y *Triceratium* son **raras** en las muestras. La última se halla representada por *Triceratium antediluvianum*.

Hay que destacar la presencia en las muestras de todos los niveles de profundidad del dinoflagelado *Dinophysis* sp., aunque con abundancia **rara**. Posiblemente, este dinoflagelado, componente común del fitoplancton local en esta época del año, llegue al bentos por sedimentación en la columna de agua.

En los niveles superiores del muestreo se encuentran talos del alga clorofícea *Ulothrix* sp. de escaso desarrollo.

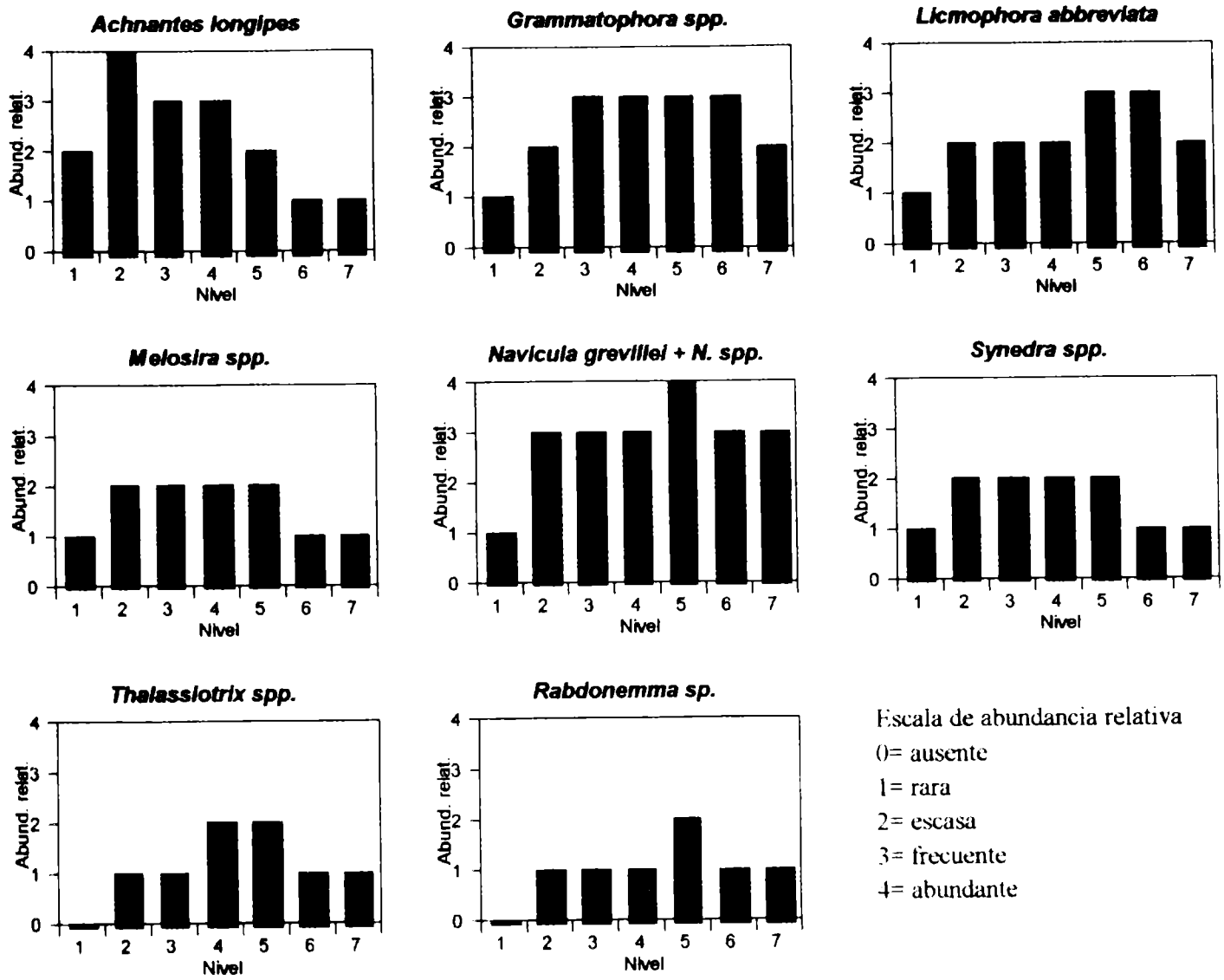

Fig. 9. Abundancia relativa por niveles, de las principales diatomeas de Reta.

Entre los organismos del zoobentos se encuentran copépodos harpaticoideos adultos y en estadios larvales, si bien su presencia es **rara**. La presencia de nematodes es frecuente en todos los niveles. Es llamativa la ausencia de algas cianoficeas y la baja presencia de protozoos en las muestras analizadas. Entre estos últimos se hallan Suctorios, con baja abundancia en las muestras.

MONTE HERMOSO

El sedimento intersticial es escaso en los niveles superiores y más abundante en los inferiores. El mismo está constituido por arena fina y detrito orgánico particulado. La proporción de arena es mayor en las muestras más profundas, como consecuencia de su cercanía al fondo arenoso.

Entre las diatomeas pennadas se destaca la presencia, en los niveles superiores del muestreo, de *Achnanthes longipes* y *Navicula* spp. **(Fig. 10)**.

Achnanthes longipes alcanza su abundancia máxima (**abundante**) en los niveles 3 y 4, siendo su presencia **rara** en los niveles más profundos.

Navicula spp. alcanza su abundancia máxima en el nivel 4, disminuyendo su presencia en los niveles más profundos.

Las diatomeas *Grammatophora* spp., *Synedra* spp., *Thalassiothrix* spp. y *Amphora* sp. son más abundantes en los niveles inferiores del muestreo. Todas ellas presentan abundancias bajas en los niveles superiores y se encuentran ausentes en el nivel 1 **(Fig. 10)**.

Las especies *Pleurosigma* sp., *Cocconeis* sp. y *Raphoneis* sp. se hallan presentes en todos los niveles de profundidad estudiados, sin embargo sus abundancias son bajas.

Entre las diatomeas céntricas se encuentran *Actinoptychus* sp., *Coscinodiscus* spp., *Melosira* spp. *y Biddulphia* spp.. Estos géneros se hallan presentes en casi todos los niveles de muestreo, sin embargo con baja abundancia. *Triceratium* sp. sólo se encuentra en el nivel más profundo y con presencia **rara**.

El dinoflagelado *Dinophysis* sp. se presenta en todos los niveles de profundidad, si bien con abundancia **rara.**

En los niveles superiores se hallan pequeños talos de la cloroficea *Ulothrix* sp..

Entre los organismos del zoobentos, los nematodes son frecuentes en todos los niveles de profundidad, en tanto que los copépodos harpaticoideos, tanto adultos como en estadios larvales, son **raros** en las muestras.

Es llamativo, al igual que en Reta, la escasez de protozoos y la ausencia de algas cianoficeas en todos los niveles muestreados. La abundancia de Suctorios en esta localidad es mayor que en Reta, sin embargo su densidad en las muestras es baja. Estos protozoos adquieren mayor importancia en las muestras de los niveles más profundos.

Comparación entre las comunidades incrustantes de diferentes áreas estudiadas

Las comunidades incrustantes de Reta y Monte Hermoso, presentan entre sí diferencias en algunos de sus componentes específicos y una marcada disimilitud con las comunidades de áreas portuarias de la Provincia de Buenos Aires.

La comunidad de fouling de Monte Hermoso presenta una riqueza específica notablemente superior a la de Reta, sin embargo el estudio realizado en la primera involucra niveles del infralitoral no considerados en la última. Es así como en la comunidad de Monte Hermoso se encuentran componentes como *Serpula* sp., *Lumbrinereis* sp., *Obelia* sp., *Plumularia setacea*, *Jaeropsis dubia* y Amphiuridae, que se encuentran vinculadas a los niveles del infralitoral y se hallan ausentes en las muestras de Reta.

En los niveles superiores de la localidad de Monte Hermoso se encuentran ejemplares de *Balanus glandula* y larvas de Chironomidae, los cuales están ausentes en Reta, en tanto que los poliquetos e hidrozoos se hallan más diversificados en la primera.

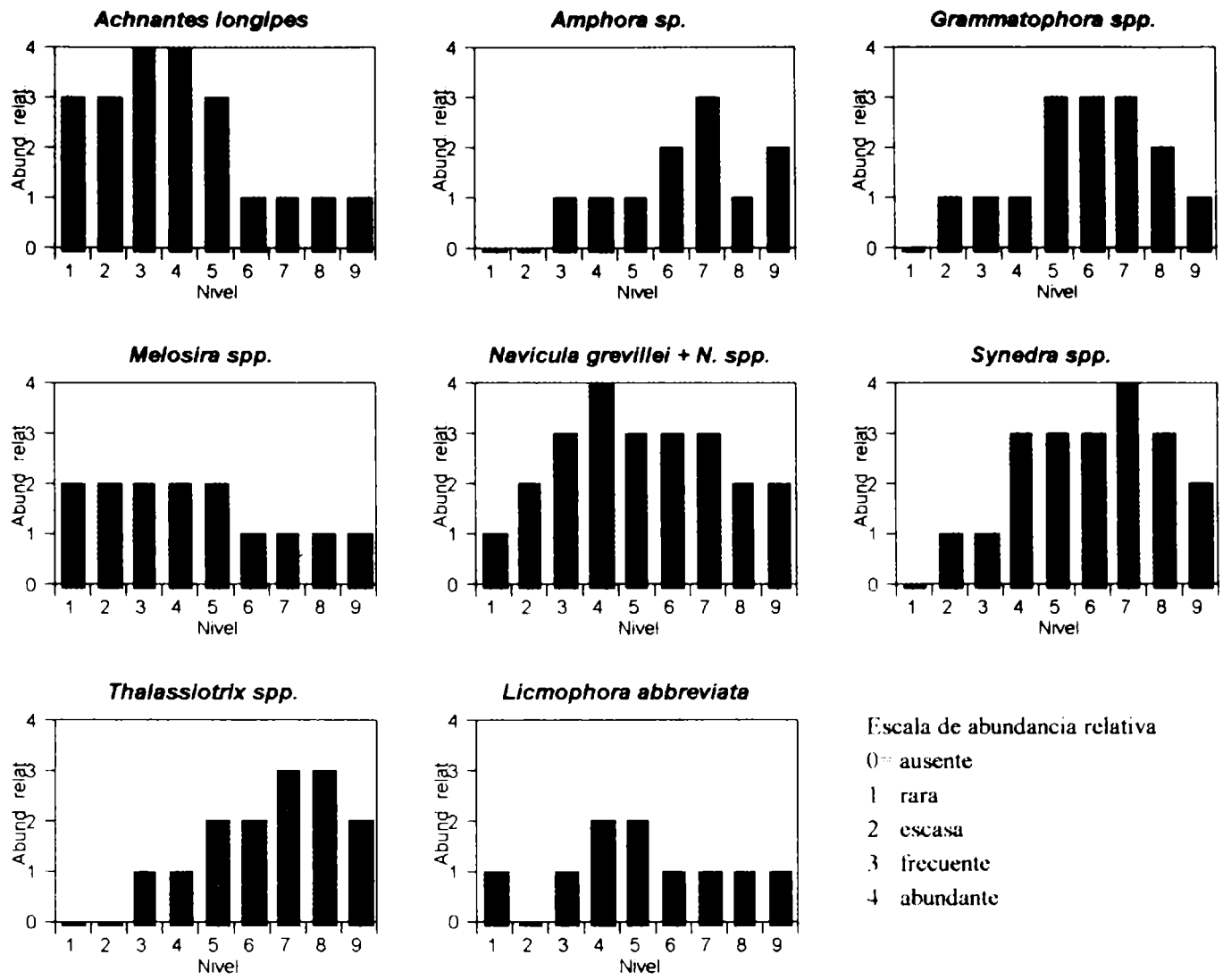

Fig. 10. Abundancia relativa por niveles de las principales diatomeas de Monte Hermoso.

En ambas localidades las comunidades de fouling se encuentran dominadas ampliamente por el mitílido *Brachidontes rodriguezi*, lo cual constituye una de las principales diferencias con respecto a las comunidades de áreas portuarias. Este organismo es un miembro típico de las comunidades mediolitorales e infralitorales de áreas rocosas naturales, sin embargo, ha sido detectado con muy baja frecuencia en los estudios realizado en los puertos bonaerenses. Esto se debe a la dificultad de *B. rodriguezi* para colonizar la superficie de los paneles experimentales utilizados en el estudio de las comunidades portuarias, en virtud de trabajarse con sistemas artificiales flotantes (balsas experimentales) y por problemas de contaminación.

En cuanto a otros organismos importantes en las comunidades estudiadas, los anfípodos caprélidos, particularmente abundantes en los niveles inferiores de Monte Hermoso, constituyen un grupo muy conspicuo en Puerto Belgrano (Bastida *et al.*, 1974a), lo cual no ocurre en el puerto de Mar del Plata, donde su presencia es esporádica. *Caprella* sp. a sido hallado casi siempre en relación con colonias de *Plumularia setacea*.

De los poliquetos, *Syllis* sp. es el más importante en ambas localidades. Esto mismo ocurre en el fouling de Puerto Belgrano (Bastida y Torti, 1973; Bastida *et al.*,1974a) no siendo así para los puertos de Mar del Plata y Quequén.

Lista de las especies halladas en el microfouling de Reta

Diatomeas:
Actinoptychus sp.
Achnanthes longipes
Amphora sp.
Biddulphia sp.
Cocconeis sp.
Coscinodiscus spp.
Cyclotella striata
Cyclotella sp.
Grammatophora marina
Grammatophora sp.
Licmophora abbreviata
Melosira sulcata
Melosira sp.
Navicula grevillei
Navicula spp.
Pleurosigma spp.
Raphoneis sp
Rhabdonema sp.
Synedra sp.
Thalassiothrix spp.
Triceratium antediluvianum
Triceratium sp.
Dinoflagelados:
Dinophysis sp.
Protozoos:
Suctorios (indet.)
Nematodes (indet.)
Crustáceos:
Copépodos harpaticoideos

Lista de las especies halladas en el microfouling de Monte Hermoso

Diatomeas:
Actinoptychus sp.
Achnanthes longipes
Amphora sp.
Biddulphia sp.
Cocconeis sp.
Coscinodiscus spp.
Grammatophora marina
Grammatophora sp.
Licmophora abbreviata
Melosira sulcata
Melosira sp.
Navicula grevillei
Navicula spp.
Pleurosigma spp.
Raphoneis sp
Synedra sp.
Thalassiothrix spp.
Triceratium antediluvianum
Triceratium sp.
Dinoflagelados:
Dinophysis sp.
Protozoos:
Suctorios (indet.)
Nematodes (indet.)
Crustáceos:
Copépodos harpaticoideos

Entre los cnidarios, *Tricnidactis errans* constituye un nuevo registro para la zona. Si bien esta pequeña anémona no ha sido hallada en el fouling de áreas portuarias, se encuentra presente en las comunidades del intermareal rocoso del Atlántico Sudoccidental, siendo su registro más austral en el área de Mar del Plata (Excoffon y Zamponi, 1993). *Clytia gracilis* y *Plumularia setacea* han sido también registradas en el fouling de Puerto Belgrano, pero no en el puerto de Mar del Plata y Puerto Quequén. Estas especies se suelen presentar asociadas en los niveles más profundos de esta localidad (Bastida y Torti, 1973).

A diferencia del fouling de los puertos bonaerenses, se destaca la presencia en los niveles infralitorales de Monte Hermoso de ofiuros Amphiuridae, si bien, se trata de ejemplares juveniles de pequeña talla. Su presencia en la comunidad del fouling es llamativa, posiblemente estos organismos completen su desarrollo refugiados en el mejillinar para luego migrar hacia niveles más profundos de fondos arenosos.

La presencia de larvas de insectos Chironomidae es común en los niveles superiores del fouling de puertos.

Entre los moluscos, *Pododesmus rudis* se encuentra también presente en el fouling de Puerto Belgrano, pero no ha sido registrada en el puerto de Mar del Plata.

Los briozoos se encuentran en ambas localidades representados únicamente por *Membranipora puelcha*. Este grupo se halla mucho más diversificado en las comunidades incrustantes portuarias, siendo particularmente importantes en puerto Belgrano, donde se han registrado hasta siete especies diferentes. *Conopeum reticulum* junto a *Cryptosula* cf. *pallasiana* son las especies más frecuentes en Puerto Belgrano (Bastida y Torti, 1973).

Por último, en ambas localidades, se encuentran ausentes los componentes cosmopolitas que alcanzan altas frecuencias en las áreas portuarias, muchas de las cuales son transportadas en los cascos de los buques. Tal es el caso de *Balanus amphitrite*, *Tubularia crocea*, el isópodo *Sphaeroma serratum*, los tunicados como *Ciona intestinalis* y *Molgula* spp. y el alga *Enteromorpha intestinalis*. La ausencia de estas especies indica un bajo grado de impacto antrópico en las áreas estudiadas.

Los procesos de epibiosis son más complejos en la comunidad de Monte Hermoso que en la de Reta, lo cual se debe fundamentalmente a la mayor riqueza específica de la primera y por consiguiente, al mayor número de organismos sustrato. Sin embargo, la diversidad de los procesos de epibiosis aquí registrados, es muy inferior a la observada en comunidades de fouling de áreas portuarias, donde se observan casos de epibiosis de mayor grado de complejidad. El organismo sustrato más importante en las comunidades de Reta y Monte Hermoso es *Brachidontes rodriguezi*, en tanto que en el fouling de puertos este rol es jugado por otros organismos, dada la baja abundancia del mitílido en áreas portuarias. En el puerto de Mar del Plata los cirripedios del género *Balanus* spp. (*Balanus amphitrite* + *B. trigonus*) son los organismos que con mayor frecuencia actúan como sustrato de organismos del macrofouling. Sobre ellos se fijan principalmente hidrozoos Campanulariidae y el poliqueto *Polydora ligni* (Trivi de Mandri *et al.*, 1984). En puerto Belgrano, *Bugula neritica, Cryptosula pallasiana, Ciona intestinalis, Botryllus schlosseri* y *Conopeum reticulum* constituyen los principales organismos sustrato (Bastida y Lichtschein de Bastida, 1978).

La constitución del microfouling es muy similar en ambas localidades analizadas en el presente estudio, constituyendo una característica común la ausencia de algas cianoficeas y la escasez de protozoos. Ambos grupos se encuentran bien representados en el fouling de áreas portuarias, siendo más abundantes en ambientes contaminados, principalmente como resultado de la contaminación orgánica.

En cuanto a las diatomeas, la especie más importante en los niveles superiores de Reta y Monte Hermoso es *Achnanthes longipes*, en tanto que *Navicula* spp. es la especie más abundante en niveles un poco más profundos. Las especies secundarias varían de una localidad a otra, mientras en Reta *Grammatophora* spp. y *Licmophora abbreviata* siguen en importancia a las ya mencionadas, en Monte Hermoso encontramos como especies secundarias más importantes a *Synedra* spp., *Thalassiothrix* spp. y *Grammatophora* spp. El género *Navicula* es el más importante en el fouling de puertos, en los cuales se halla representado principalmente por *Navicula grevillei*. Esta diatomea se encuentra acompañada por *Synedra* sp. y *Licmophora abbreviata* en el puerto de Mar del Plata y por

Achnantes longipes, *Melosira moniliformis* y *Synedra* spp., en Puerto Quequén (Bastida *et al.*, 1980; Brankevich *et al.*, 1984), lo cual nos indica la poca variación entre las especies integrantes del fouling de puertos y las halladas en las comunidades de áreas naturales.

Si bien existen diferencias marcadas entre las comunidades analizadas en el presente estudio y las comunidades de áreas portuarias, se puede observar en general, una mayor semejanza de las primeras con las comunidades de Puerto Belgrano que con las del puerto de Mar del Plata y Puerto Quequén.

Estructura poblacional de *Brachidontes rodriguezi*

Dado que *Brachidontes rodriguezi* es el organismo dominante y por ende estructurante de las comunidades incrustantes estudiadas, se realizó un análisis más detallado de la estructura poblacional de este mitílido y de su variación con la profundidad. Para concretar este propósito con la mayor claridad posible, se realizaron histogramas de frecuencia de tallas para los individuos cuya talla es superior a los 2 mm de largo.

RETA

En líneas generales se observa que la densidad de ejemplares de *B. rodriguezi* desciende a medida que aumenta la profundidad del nivel estudiado, en tanto que la talla máxima de los ejemplares hallados tiende a aumentar, llegando a presentar ejemplares de hasta 38 mm en los niveles más profundos. Sin embargo, la baja frecuencia de estos últimos en las muestras y el aumento de la frecuencia de las tallas inferiores, provocan que la talla media, la cual aumenta hacia los niveles intermedios del muestreo, descienda en los niveles más profundos **(Fig. 11)**.

Las clases de talla mejor representadas son las inferiores e intermedias, encontrándose presentes con baja frecuencia las tallas superiores a los 20 mm. La presencia de un modo en las clases 2-4,9 y 5-7,9 evidencia la presencia de reclutamiento, el cual alcanza su mayor importancia en los niveles 1, desciende en los niveles intermedios y aumenta nuevamente hacia los niveles más profundos **(Fig. 12)**.

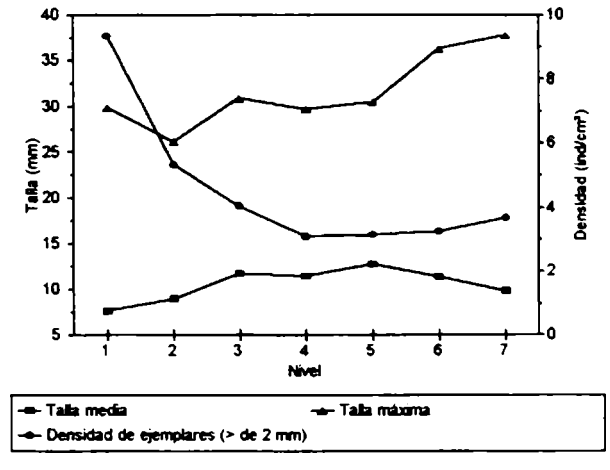

Fig. 11. Talla media , talla máxima y densidad de *Brachidotes rodriguezi* en los diferentes niveles. Reta.

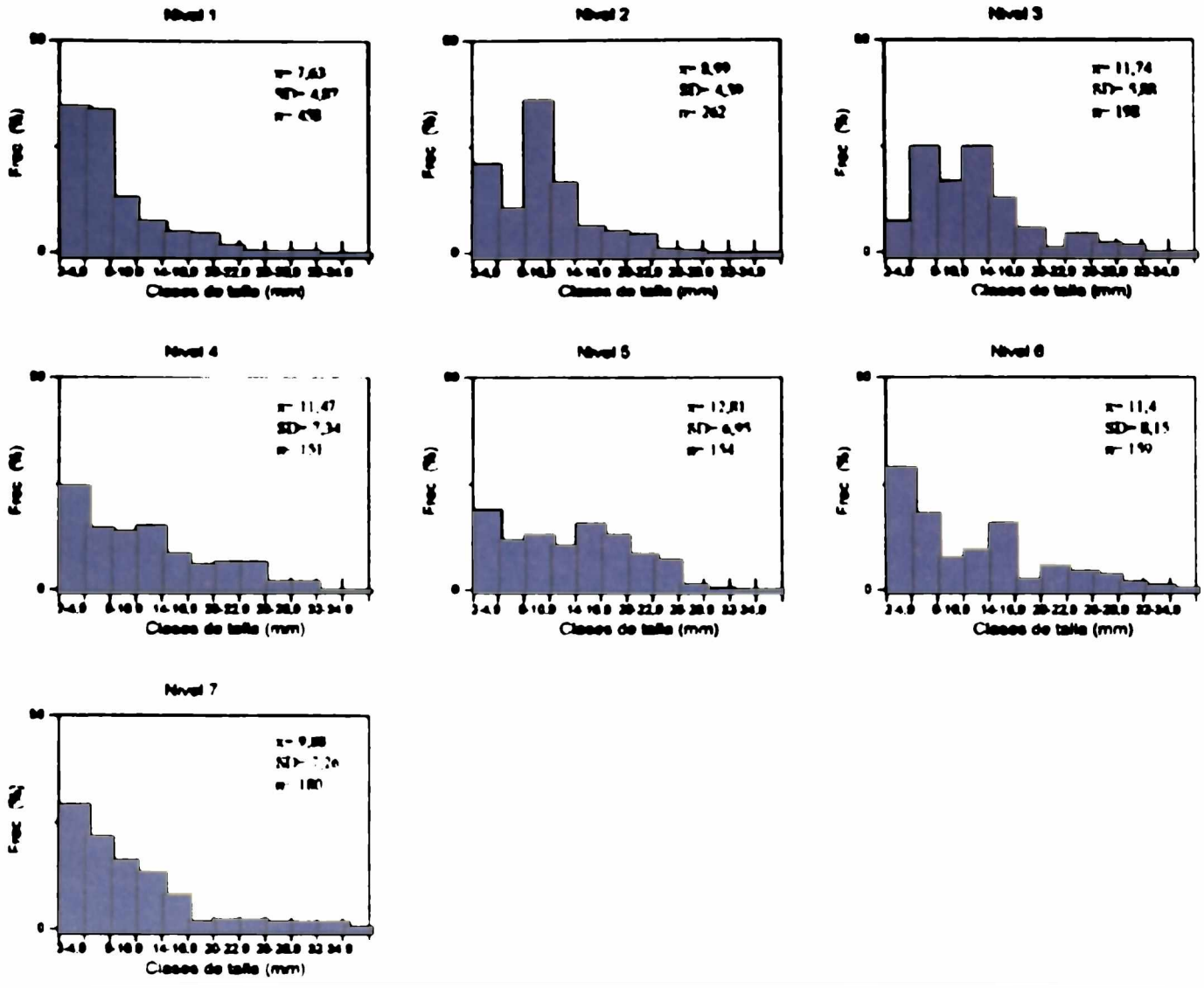

Fig. 12. Estructura poblacional de *Brachidontes rodriguezi* en los distintos niveles. Reta.

MONTE HERMOSO

La densidad de ejemplares de *Brachidontes rodriguezi* disminuye al aumentar la profundidad, sin embargo en el nivel 9 se observa un brusco aumento como resultado de una gran abundancia de ejemplares de las tallas menores (reclutas). La talla máxima registrada en cada muestra aumenta hacia los niveles más profundos, y alcanza su máximo en el nivel 6, donde se hallan ejemplares de hasta 45 mm **(Fig. 13)**.

En el nivel 4 se observan los valores más bajos de densidad y talla máxima. El bajo número de ejemplares y la ausencia de las clases de talla mayores de 23 mm en esta muestra puede ser el resultado del desprendimiento de parte del mejillinar a causa del embate de las olas.

La talla media de los ejemplares tiende a aumentar ligeramente hacia los niveles inferiores, sin embargo desciende bruscamente en el nivel 9 como resultado de la alta representación de las tallas más pequeñas **(Fig.13)**.

Las clases de talla mejor representadas son las pequeñas e intermedias. Estas últimas, entre los 8 y 20 mm, son las tallas más frecuentes en los niveles 3, 4, y 5, en tanto que los individuos entre los 2 y 8 mm son los más frecuentes en los niveles 1, 2 y 9 **(Fig. 14)**.

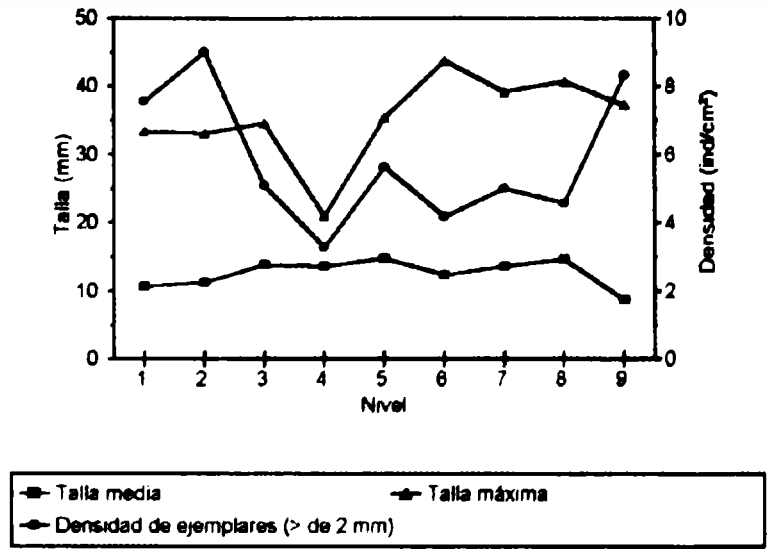

Fig. 13. Talla media , talla máxima y densidad de *Brachidotes rodriguezi* en los diferentes niveles. Monte Hermoso.

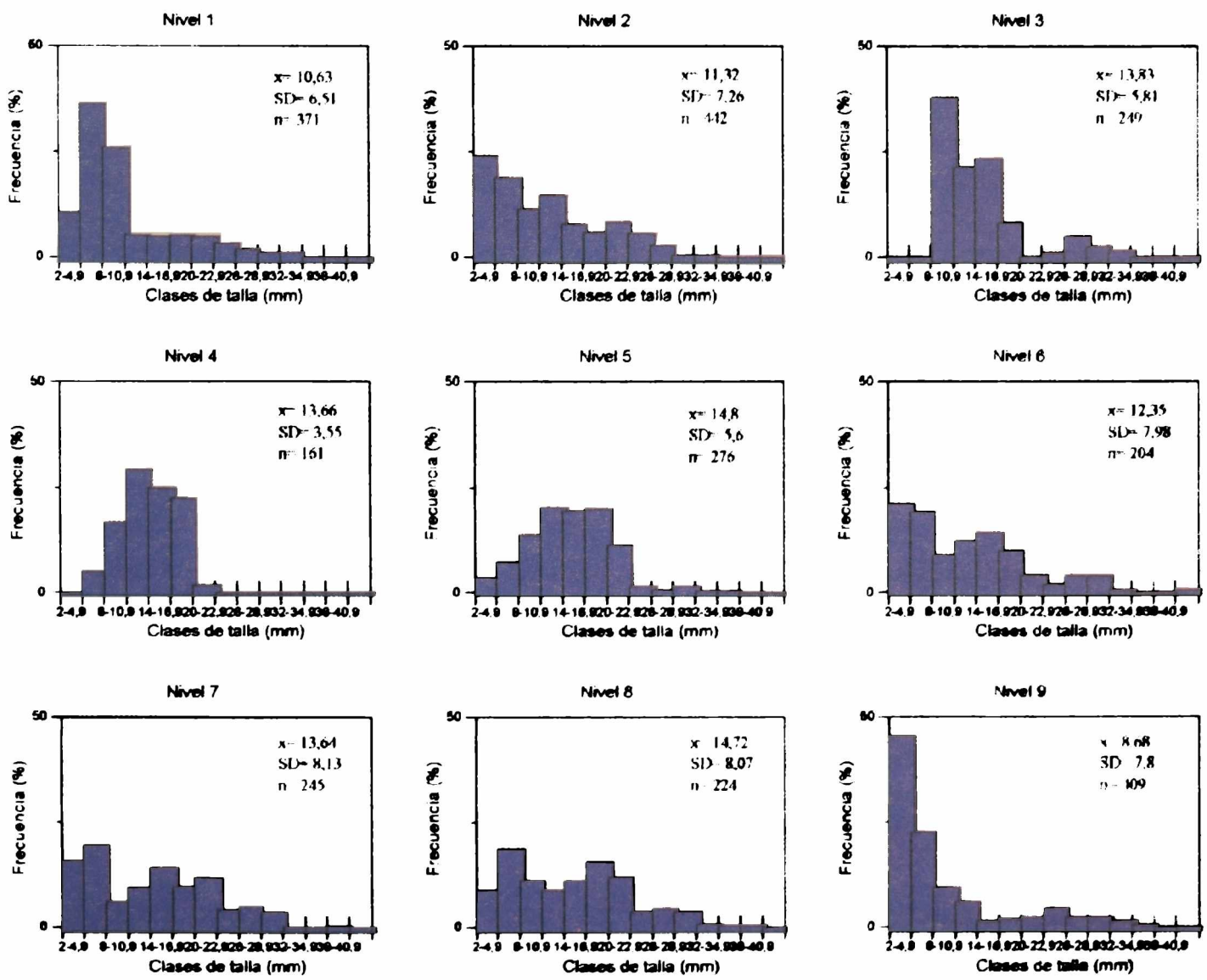

Fig. 14. Estructura poblacional *de Brachidontes rodriguezi* en los diferentes niveles. Monte Hermoso.

CONCLUSIONES

Las **comunidades asentadas sobre los sustratos artificiales** estudiados, muestran una clara dominancia del mitílido *Brachidontes rodriguezi*. Las especies acompañantes son diferentes de un sitio a otro y variables con la profundidad del nivel muestreado.

En la localidad de **Reta** la comunidad incrustante presenta una densidad de *Brachidontes rodriguezi* de entre 9,35 y 3,08 ind./cm^2, la misma desciende al aumentar la profundidad. La diversidad específica de las muestras es en general baja, debido a la amplia dominancia de *B. rodriguezi* y al reducido número de especies acompañantes. Entre la fauna acompañante más importante en los dos primeros niveles muestreados, se destacan pequeños ejemplares de *Mytilus edulis platensis*, nemertinos y platelmintos policládidos. En los niveles subsiguientes, estos organismos son superados en número por el poliqueto *Syllis* sp., el cual va ganando importancia al aumentar la profundidad. Entre los organismos coloniales, el más abundante es el hidrozoo *Bougainvillia ramosa*.

En la localidad de **Monte Hermoso** *Brachidontes rodriguezi* se encuentra en densidades que varían entre 9,02 y 3,28 ind./ cm^2. También aquí la densidad del mitílido tiende a disminuir con el aumento de la profundidad. La riqueza específica de las muestras es superior a la hallada en la localidad de Reta. La fauna acompañante más importante en los niveles superiores del muestreo son las larvas de insectos Chironomidae y los nemertinos. Ambos organismos son reemplazados por el poliqueto *Syllis* sp. en los niveles subsiguientes del mediolitoral, en tanto que en los niveles del infralitoral los organismos acompañantes más importantes son el decápodo *Pachycheles haigae*, los ofiuros Amphiuridae y el anfípodo *Caprella* sp.. En los niveles más profundos también es importante la presencia del isópodo *Jaeropsis dubia*.

Los **diagramas de afinidad** evidencian claros agrupamientos de los distintos niveles de muestreo, en función de sus componentes específicos y de los diversos gradientes asociados con los niveles de marea. En **Reta** se puede distinguir el nivel superior perteneciente al piso supralitoral, con la presencia de *Siphonaria lessoni*; los niveles 2, 3 y 4, pertenecientes al mediolitoral superior, con la presencia de nemertinos, *Anoplodactylus petiolatus*, *Ulothrix* sp. y una mayor abundancia de *Mytilus edulis platensis* y los niveles 5, 6 y 7 correspondientes al mediolitoral inferior caracterizados por la presencia de *Sabellaria wilsoni*, *Clytia gracilis*, *Membranipora puelcha*, *Pachycheles haigae*, *Caprella* sp. y el alga *Ceramium* sp. En **Monte Hermoso** se distingue el nivel 1, perteneciente al supralitoral, con una alta abundancia de larvas de insectos *Chironomidae*, la presencia exclusiva de *Balanus glandula* y *Ulva lactuca*; los niveles 2, 3 y 4, pertenecientes al piso mediolitoral y caracterizadas por la presencia de *Mytilus edulis platensis*, Nemertinos, *Sabellaria wilsoni*, *Cyrtograpsus altimanus y Anoplodactylus petiolatus* y los niveles 5, 6, 7, 8 y 9, caracterizados por una mayor riqueza específica y la presencia de Amphiuridae, *Caprella* sp., *Tanystylum orbiculare*, *Jaeropsis dubia*, *Pachycheles haigae*, *Plumularia setacea*, *Obelia* sp. y *Clytia gracilis*,

La **composición del microfouling** es muy similar en ambas localidades, constituyendo una característica común la ausencia de algas cianoficeas y la escasez de protozoos. En los niveles superiores se destaca la presencia de la diatomea *Achnantes longipes*, en tanto que en los niveles más profundos predomina *Navicula* spp., junto a *Grammatophora* spp. y *Synedra* spp.

Los **procesos de epibiosis** se encuentran poco diversificados en ambas localidades, siendo *Brachidontes rodriguezi* el principal organismo sustrato. Entre los principales organismos epibiontes del mitílido se encuentran *B. rodriguezi*, *Tricnidactis errans*, *Membranipora puelcha*, *Pododesmus rudis*, *Bougainvillia ramosa* y *Clytia gacilis*.

La **población** de *Brachidontes rodriguezi* en ambas comunidades estudiadas se encuentra integrada principalmente por las clases de talla entre los 2 y 20 mm de largo, siendo alta la frecuencia de individuos reclutas.

Si bien la **composición específica** de las comunidades estudiadas presentan una mayor afinidad con la del fouling de Puerto Belgrano, se observan claras diferencias con las comunidades incrustantes de los ambientes portuarios bonaerenses. Ello se debe fundamentalmente a las acciones antrópicas que tienen lugar en estos últimos, como ser contaminación por diversas sustancias y el transporte pasivo de especies exóticas a través del "fouling" de cascos de buques y agua de sentinas.

BIBLIOGRAFIA

Bastida, R.. 1968. Preliminary notes on the marine fouling at the port of Mar del Plata (Argentina). **Compte Rendu 2 nd. Int. Congr. Mar. Fouling Corrosion**, Atenas, Grecia: 557-562.

Bastida, R. O.. 1971a. Las incrustaciones biológicas en el puerto de Mar del Plata, período 1966/67. **Rev. Mus. Arg. Cs. Nat. B. Rivadavia, Hidrobiol.**, 3 (2):203-285.

Bastida, R. y G. Brankevich. 1980. Estudios ecológicos preliminares sobre las comunidades incrustantes de Puerto Quequén (Argentina). **V Congreso Internacional de Corrosión Marina e Incrustaciones**, Barcelona, España, Biología Marina:113-138.

Bastida, R. y G. Brankevich. 1981. Estudios ecológicos preliminares sobre las comunidades incrustantes de Puerto Quequén (Argentina). I Características del microfouling. **CIDEPINT, Anales, 1981**: 199-232.

Bastida, R. y G. Brankevich. 1982. Estudios ecológicos preliminares sobre las comunidades incrustantes de Puerto Quequén (Argentina). II Características del macrofouling. **CIDEPINT, Anales 1982**: 155-153.

Bastida, R. y V. Lichtschein de Bastida. 1978. Las incrustaciones biológicas de Puerto Belgrano.III. Estudio de los procesos de epibiosis registrados sobre paneles acumulativos. **CIDEPINT, Anales 1978**:55-97.

Bastida, R. y M. R. Torti. 1973. Estudio preliminar de las incrustaciones biológicas de Puerto Belgrano (Argentina). **LEMIT, Anales, 3-1971**:45-75.

Bastida, R., H. Adabbo y V. Rascio. 1976. Toxic action of antifouling paints with different toxicant concentrations. **Corrosion Marine Fouling**, 1/76: 5-17.

Bastida, R., J. Caprari y V. Rascio. 1970. Las incrustaciones biológicas (fouling) y su control por medio de pinturas. **Actas IV Congreso Latinoamericano de Zoología** (Caracas, Venezuela), II: 427-456.

Bastida, R., M. Trivi de Mandri y E. Ieno. 1995. Los organismos incrustantes del puerto de Mar del Plata (Argentina). *Polydora ligni*; aspectos biológicos y ecológicos. **CIDEPINT Anales 1995**:253-266.

Bastida, R., A. Roux y C. Bremec. 1989. Investigaciones sobre las comunidades bentónicas en la zona común de pesca argentino-uruguaya. **Frente Marítimo**, 5:115-129.

Bastida, R., M. E. T. De Mandri, V. L. De Bastida y M. Stupak. 1980. Ecological aspects of marine fouling at the port of Mar del Plata (Argentina). **Comunicaciones del V Congreso Internacional de Corrosión Marina e Incrustaciones**: 299-320.

Bastida, R., E. Spivak, S. L'Hoste y H. Adabbo. 1974a. Las incrustaciones biológicas de Puerto Belgrano. I. Estudio de la fijación sobre paneles mensuales 1971-1972. **Corrosión y Protección**, 8, (8): 11-31.

Bastida, R., E. Spivak, S. L'Hoste y H. Adabbo. 1974b. Las incrustaciones biológicas de Puerto Belgrano. II. Estudio de los procesos de epibiosis registrados sobre paneles mensuales. **LEMIT, Anales, 3, 1974**, Ser. II, (274): 167-195.

Benítez, J.C., C.A. Giúdice y V. Rascio. 1990. Binders for self polishing antifouling paints. **European Coat. J.**, 11: 618.631.

Brankevich, G., R. Bastida y D. Martinez. 1984. Ecological aspects on the marine fouling at the Necochea power station (Puerto Quequén, Argentina). **VI International Congress on Marine Corrosion and fouling**, Atenas, Grecia, Marine Biology: 567-583.

Bremec, C.. 1986. Asociaciones del macrobentos infralitoral de Monte Hermoso (39 00' S- 61 17'W, República Argentina). **Spheniscus**, 2: 1-18.

del Amo, B., C.A. Giúdice, V. Rascio y O. Sindoni. 1986. Antifouling paints based on WW rosin and chlorinated rubber. Influence of binder composition and content. **J. Oil Col. Chem. Ass.**, 69 (7): 178-185.

Excoffon, A. C. y M. Zamponi. 1993. Anémonas de Mar del Plata y localidades vecinas. IV. *Tricnidactis errans* Pires ,1988 (Actiniaria, Haliplanellidae). **Hieringia, Ser. Zool.** (75):47-53.

Giúdice, C.A., J.C. Benítez, V. Rascio y M. Presta. 1980. Study of variables which affect dispersion of antifouling paints in ball mills. **J. Oil. Col. Chem. Ass.**, 63: 153-162.

Giúdice, C.A., B. del Amo, V. Rascio y R. Sanchez,. 1983. Reactivity of calcium carbonate and cuprous oxide with binder acid components in antifouling paints. **J. Coat. Technol.**, 55 (697): 23-28.

Giúdice, C.A., J.C. Benítez y V. Rascio. 1984. Influence of cuprous oxide particle size distribution on toxic efficiency of antifouling paints. **J. Oil Col. Chem. Ass.**, 67 (11): 283-288.

Giúdice, C.A., B. del Amo, V. Rascio y O. Sindoni,. 1986. Composition and dissolution rate of antifouling paint binders (soluble type) during their immersion in artificial seawater. **J. Coat. Technol.**, 58 (733): 45-50.

Giúdice, C.A., J.C. Benítez, B. del Amo y V. Rascio. 1987. High build antifouling paints based on rosin and chlorinated rubber. **J. of Chemical Technology and Biotechnology**, 38 (4): 265-276.

Giúdice, C.A., B. del Amo y V. Rascio. 1988. Influence of composition and film thickness on the bioactivity of antifouling paints containing castor oil as thixotropic agent. Adhesive, sealants and coatings for space and hard environments, ed. by Lieng-Huang Lee, Webster Research Center, Xerox Corporation, New York: 371-380.

Giúdice, C.A., B. del Amo y V. Rascio. 1988. The use of calcium resinate in the formulation of soluble matrix antifouling paints based on cuprous oxide. **Progress in Organic Coatings**, 16 (2), 165-176.

Hodge, G.. 1862. Observations on a especies of pycnogon (*Phoxochilidium coccineum* Johnston), with an attempt to explain the order of its development. **Ann. Mag. Nat. Hist.** 3 (9): 33-43.

Lichtschein de Bastida, V. y R. Bastida. 1980. Los briozoos de las comunidades incrustantes de puertos argentinos. **V Congreso Int. de Corrosión Marina e Incrustaciones**, Barcelona , España, Biología Marina: 371-390.

Martinez, D., R. Bastida y G. Brankevich. 1984. Ecological aspects of marine fouling at the port of Ingeniero White (Argentina).**VI International Congress Marine Corrosion and Fouling**, Atenas, Grecia, Marine Biology: 521-537.

Mouzo, F. H. y M. L. Garza. 1974. Contribución al conocimiento del substrato en un sector de la pltaforma continental argentina entre Mar del Palta y Bahía Blanca. **Contrib. Cient. IADO** 12: 19 pp.

Rascio, V. y J.J. Caprari. 1969. Contribution à l'étude du comportement des peintures antisalissures. I. Influence du type de toxique et de la solubilité du liant. **Peintures, Pigments, Vernis**, 45 (2): 102.

Rascio, V., J.J. Caprari y R. O. Bastida. 1969. Contribution à l'étude du comportement des peintures antisalissures. II. Influence de la concentration de toxique. **Peintures, Pigments, Vernis**, 45 (11): 724-735.

Rascio, V. y J.J. Caprari. 1970. Contribución al estudio del comportamiento de las pinturas antiincrustantes. III. Nuevas experiencias realizadas en el Puerto de Mar del Plata (Argentina), Período 1968-70. **Corrosión y Protección**, 1 (4): 19-33.

Rascio, V. y J.J. Caprari. 1972. Study of some variables affecting antifouling paints performance. **Latin Am. J. of Chem. Eng. and Applied Chem.**, 2 (2): 117-150.

Rascio, V. y J.J. Caprari. 1973. Contribución al estudio del comportamiento de las pinturas antiincrustantes. IV. Influencia del tipo de inerte. **Corrosión y Protección**, Número extraordinario dedicado al 1er Congreso Nacional de Corrosión y Protección, Madrid, España: 415-441.

Rascio, V. y R. Bastida. 1973. Contribución al estudio del comportamiento de las pinturas antiincrustantes. V. Acción de los tóxicos sobre algas a nivel de línea de flotación. **Corrosión y Protección**, 4 (3): 19-27.

Rascio, V., R. Bastida y W. Bruzzoni. 1973. Protección anticorrosiva y antiincrustante por medio de pinturas. **Corrosión metálica, SENID**: 229-319.

Rascio, V. y J.J. Caprari. 1974. The influence of whiting as extender in soluble antifouling paints based on cuprous oxide. **J. Oil Col. Chem. Ass.**, 57 (12): 407-414.

Rascio, V., J.J. Caprari, B. del Amo y R.D. Ingeniero. 1976. Peintures antisalissures a base de composés organiques d'étain et de plomb. **Corrosion Marine-Fouling,** 1 (2): 21-27.

Rascio, V., J.J. Caprari, M.J. Chiesa y R.D. Ingeniero. 1976. Peintures antisalissures au caoutchouc chloré pour systèmes type "high build". **Corrosion Marine-Fouling,** 1 (1): 15-20.

Rascio, V., J.J. Caprari, M.J. Chiesa y R.D. Ingeniero. 1977. The use of arsenates as reinforcing toxicants in soluble antifouling paints based on cuprous oxide. **J. Oil Col. Chem. Ass.**, 60 (5), 161-168.

Rascio, V. y J.J. Caprari. 1978. A new approach to the use of extenders in toxin leachable antifouling paints. **J. Coat. Technol.**, 50 (637): 65.

Rascio, V., C.A. Giúdice, J.C. Benítez y M. Presta. 1978. Ships' trials of oleoresinous antifouling paints. I. Formulations with high and medium toxicant content. **J. Oil Col. Chem. Ass.**, 61 (10): 383-389.

Rascio, V., C.A. Giúdice, J.C. Benítez y M. Presta. 1979. Ships' trials of oleoresinous antifouling paints. II. Formulations with medium and low toxicant content. **J. Oil Col. Chem. Ass.**, 62 (8): 282-292.

Rascio, V., C.A. Giúdice y B. del Amo. 1990. High-build antifouling paints tested on raft and ship bottom. **Progress in Organic Coatings**, 18 (4), 389-398.

Spivak, E., R. Bastida, S. L'Hoste y H. Adabbo. 1975. Los organismos incrustantes del puerto de Mar del Plata. II. Biología y ecología de *Balanus amphitrite* y *B. trigonus* (Crustacea-Cirripedia). **LEMIT Anales 3-1975**, ser.II, (294):41-123.

Stirn, J..1981. Manual of methods in aquatic environment research. **FAO Fisheries Technical Paper**, 209:1-70.

Trivi de Mandri, M., V. Lichtschein de Bastida y R. Bastida. 1978. Estudio sobre los procesos de epibiosis de las comunidades incrustantes del puerto de Mar del Plata. **CIDEPINT Anales 1984**: 209-232.

STUDIES ON BIOFOULING AT MAR DEL PLATA HARBOR. MONTHLY SETTLEMENT OF CALCAREOUS SPECIES ALONG A YEAR

"BIOFOULING" DEL PUERTO DE MAR DEL PLATA:ASENTAMIENTO MENSUAL DE ORGANISMOS CALCÁREOS

M.C. Pérez, M.T. García, M.E. Stupak[1]

SUMMARY

Monthly settlement of calcareous species was followed in Mar del Plata harbor (Argentina) along a year. Large number of calcareous organisms recruited onto ceramic panels. ***Balanus amphitrite*** *and* ***Hydroides elegans*** *were the most representative species settled on the primary space. Other barnacles,* ***B. glandula*** *+* ***B. improvisus*** *followed in importance, but the number of recruits per panel was always low. All of them were measured and total occupied areas estimated. The species showed different settlement cycles, different preferences by both depth levels and surface texture.*

The maximum peak of density for ***B. glandula*** *+* ***B. improvisus*** *was in December, for* ***B. amphitrite*** *in February and for* ***Hydroides elegans*** *in March. Virtually no settlement took place during colder months (June-September). Barnacles preferred to settle on the back side of the panels, with grooves and pits, while serpulids showed no texture preferences. In relation with depth all species preferred to colonize the three deepest levels. Data corresponding to growth rates indicated a rapid development during warmer months.*

Keywords: *macrofouling, calcareous species, test panels, barnacles, serpulids.*

INTRODUCTION

The settlement of macrofouling calcareous species on artificial submerged structures should be taken into account because of their rapid colonization and growth. The attachment of these organisms generate serious problems not only from the point of view of fouling, e.g. increase in frictional resistance and loss of hydrodynamics but also due to corrosion phenomena, bacteria living under calcareous coating consume the oxygen due to its respiratory activity and promote localized corrosion processes **[1]**.

The planktonic larval stages of many sessile marine invertebrates are recruited to surfaces in response to surface associated stimuli. Gregarious settling behavior are generally

[1] Jefe del Area Incrustaciones Biológicas y Biodeterioro en Medio Marino

mediated by chemical signals **[2,3]** and are responsible for aggregation of barnacles, serpulids, hydroids, and a host of other sessile invertebrates. Physical and chemical stimuli are important in determining a substratum for barnacle settlement and metamorphosis **[3,4]**. In addition, one source of cues for settlement is some component of the attached microflora **[5-7]**.

The local current adjacent to the substratum, the conditions in water column and the physical characteristics of the substratum either prevent the attachment of the planktonic propagules or make it more attractive **[8-14]**. Furthermore, earlier successional species may enhance or inhibit the arrival of later species by providing suitable or unsuitable environmental conditions.

The calcareous species alter the topography of hard substratum, increasing its heterogeneity and trapping sediment particles in the interstices among them.

Barnacles are among the commonest fouling organisms and are nearly world-wide in distribution. Their larvae settle in great numbers on newly exposed surfaces and grow so rapidly that the surfaces are covered completely in a short time. On ships, barnacles are usually the first forms to appear in numbers if the protective paints are inadequate or become so. The firm attachment of barnacles to the surface also favors their persistence on ships in active use **[15]**. The barnacle larval stage known as the cyprid is non-feeding and specialized for dispersal, settlement, and metamorphosis to the adult **[16]**. Barnacle cyprids use their antennules for settlement on a substratum and for subsequent permanent attachment to it **[17]**. These antennules secrete a proteinaceous adhesive **[18]**.

Due to their frequency and to their covering rate, tube-worms (serpulids) are considered as an important group in fouling communities all over the world. *Hydroides elegans* (often as *H. norvegica*), a cosmopolitan species, occurs throughout tropical and temperate seas and was probably widely distributed on the bottom of ships. Rapid and dense colonization of submerged surfaces, natural and experimental, by this species has been recorded in Australia **[19]**, India **[20,21]**, Egypt **[22,23]**, South Atlantic and elsewhere. In Pearl Harbor, Hawaii, it is probably the major problem fouler of Navy ships, being able to colonize submerged surfaces and build up layers several centimeters thick in one to two months **[24]**.

The tubiculous worms have a larval swimming stage known as trocophore that settles on a hard substratum in large number; under favorable conditions, the growth rate may be 10 times quicker in summer than in winter **[25]** and the tubes reach 2 to 3 cm in length **[26]**. Dean **[27]** suggested that both barnacle and serpulid tube-worm settlements are inhibited by the presence of other species, and they settled only in abundance on bare surfaces. Some serpulids proved to be an indicator for the oil polluted water **[22,23]**.

In a previous paper **[28]** recruitment patterns of dominant macrosessile foulers and the seasonal developmental sequence of the community at Mar del Plata harbor were studied. Multivariate cluster analysis revealed two trends, one from late autumn to spring and the other from summer to early autumn. During winter months *Ciona intestinalis* had an important functional role in the community, as an adult might enhance the arrivals of some species as secondary space recruiters; however, in summer, its larvae were poor competitors for seasonal

space occupiers and this situation favored the invasion of calcareous exoskeleton organisms, such as *Balanus* and *Hydroides*.

The aim of the present research is to study the recruitment trends of calcareous macrosessile foulers on the primary space all the year round, and their preferences for different textures and depth at the time of settlement.

MATERIALS AND METHODS

Mar del Plata harbor is situated in the Buenos Aires province (38° 02'S-57° 32'W). It is an important harbor which is affected by a naval complex, fishery industries and nautical recreation. The study site was located within the harbor at the Club de Motonáutica (Fig. 1).

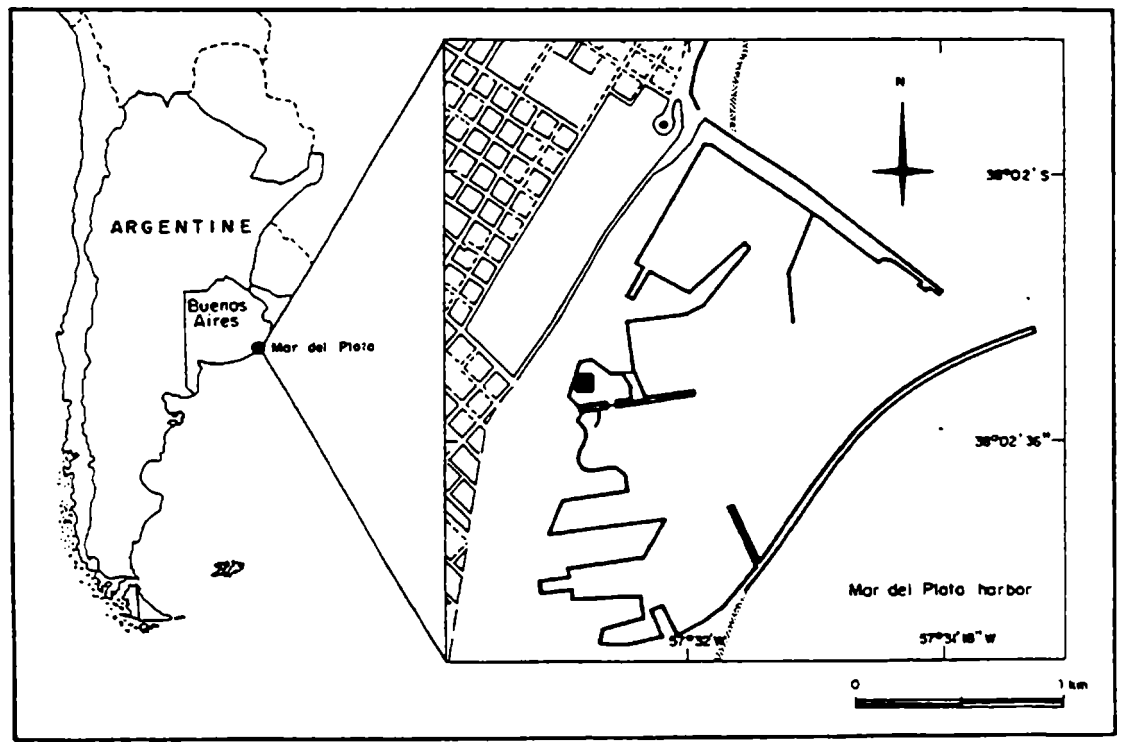

Fig. 1. -Site of study and location of test panels series (■).

The study was carried out since May 1991 up to April 1992. Fouling organisms were collected by submerging 128 cm^2 unglazed ceramic tiles (panels). A sample series included three ropes with four panels separated 20 cm one from each other. The series were vertically hung from a floating dock, about 0.3 m to 1.5 m below the water surface to provide the record of macrofouling organisms for four different depths (Fig. 2). Each series of panels was immersed for one month, then removed and transported in plastic cages in 4% neutral solution of formalin in sea water. A new series of clean panels was immersed at the same time. In order to check the density of barnacles and serpulids larvae, monthly plankton samples were taken with a 50 μm zooplankton net.

The front and the back surface of the panels have different rugosity. The front is smooth (total rugosity: 49.84 μm) and the back is with a design of 7 mm side-squares of 0.83 mm depth (with four edges each). The front and the back surface of the panels, from the top to the bottom were labeled as: **A**,**a**; **B**,**b**; **C**,**c** and **D**,**d**, respectively.

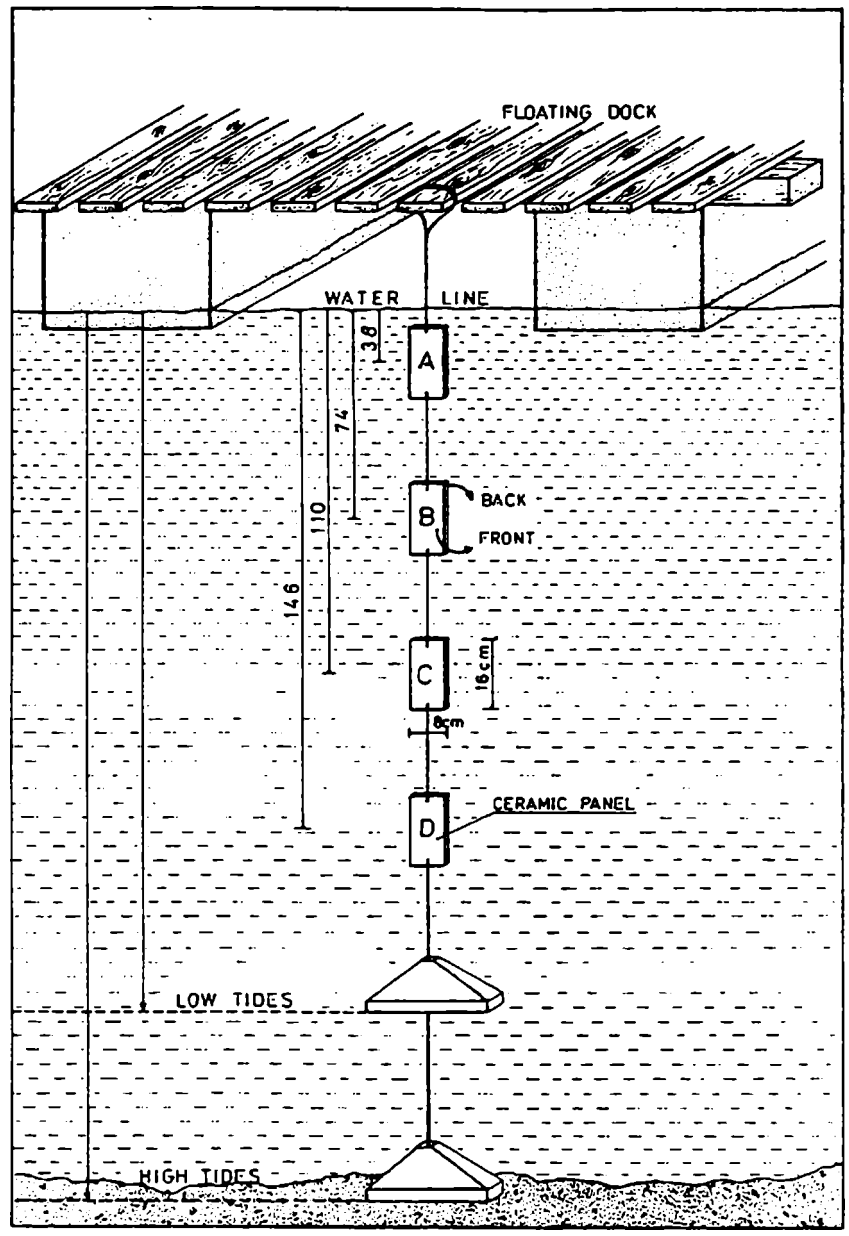

Fig. 2. -Ceramic panels series design.

After removing soft macrofouling organisms the panels were dried at room temperature. All sessile calcareous species growing on the primary space were counted and measured by a stereomicroscope with a 10x ocular micrometer. The outer 1 cm margin of the plates was excluded from examination to avoid an "edge effect" **[10]**. The rostral-carinal length and the lateral-lateral width of each barnacle were registered and then basal area was estimated. In the case of serpulids length and width of the calcareous tube for each serpulid were measured.

Because of it could not be determined exactly the age of each individual settled on panels, it was assumed that largest size specimens were 30 days old. In order to standardize the choice of those largest individuals a size frequency distribution of basal area was done. After considering the mean area occupied by larger size group by panel by month, it could be calculated the daily mean increase in basal area.

Temperature, pH and salinity were measured at sample time with a Luftman P300 Digital Meter, and a HI 8733 Portable Conductivity Meter. Mean water and air temperature

were also supplied by Centro Argentino de Datos Ocenográficos (Servicio de Hidrografia Naval).

Statistical analysis of the results was done with ANOVA and contrast LSD test (Fisher test) using SYSTAT program. In ANOVAs, the effect of temporal variation of recruitment, substratum texture and preference for depth were examined.

RESULTS

Large number of calcareous organisms recruited onto the tiles in Mar del Plata harbor. They showed different settlement cycles and different preferences by levels and surface texture. *Balanus amphitrite* (Cirripedia, Balanidae) and *Hydroides elegans* (Polychaeta, Serpulidae) were the most representative species settled on the primary space. Other barnacles, *B. glandula* and *B. improvisus*, were the third most abundant colonizers and they were considered together because of their settlement cycles were similar and the number of recruits per panel was always low. Some species like *B. trigonus* and *Conopeum* sp. (Bryozoa, Membraniporidae) were rare, only settled at low densities, and will not be considered in any detail.

Mean sea water temperature varied between 9.1 °C in July and 20.7 °C in January and mean air temperature ranged between 6.9 °C in July and 22.2 °C in March. The pH values maintained fairly constant between 7.9-8.2 and salinity ranged between 35.1-36.7 $^{0}/_{00}$.

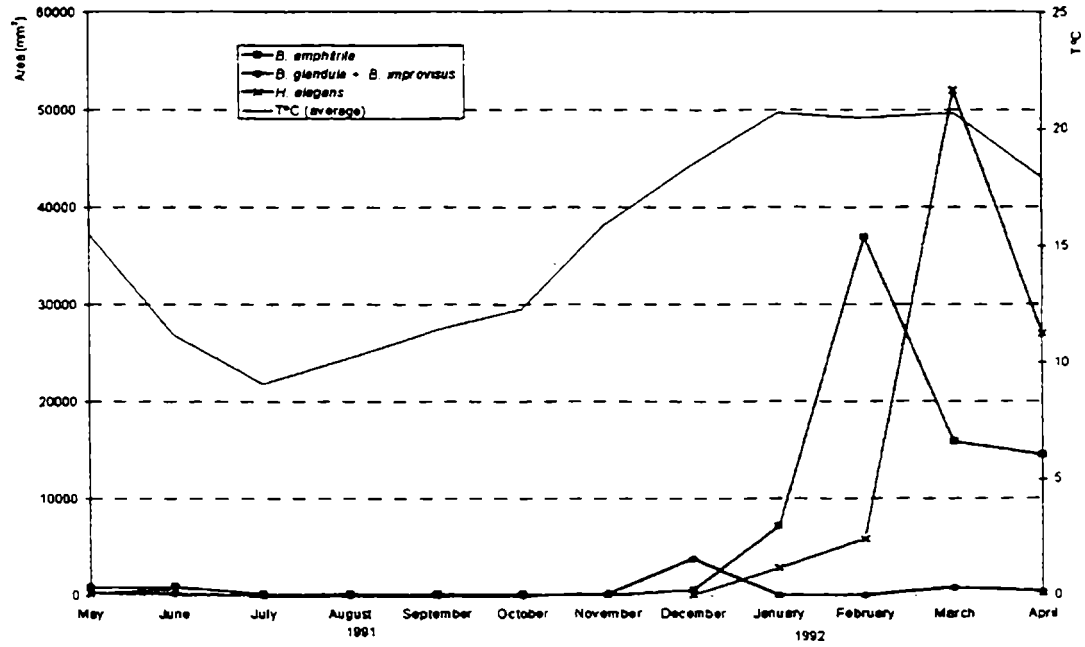

Fig. 3. -Mean water temperature from May 1991 to April 1992 and monthly total occupied area (A+B+C+D, levels) for each calcareous species.

Figure 3 shows a graphic with the recruitment of *B. amphitrite*, *B. glandula* + *B. improvisus* and *H. elegans* along a year. The total curves were very similar from May to October, in November they increased slowly with some oscillation in the first period and then *B. amphitrite* and *H. elegans* rapidly grew reaching the maximum in summer. Settlement cycles of these species were seasonal, and the peaks of recruitment were in accordance with the highest records of mean water temperature. The total cover area by calcareous species in Mar

del Plata harbor was characterized by three successive peaks every time higher, the first one corresponded to *Balanus glandula* + *B. improvisus*, the second to *B. amphitrite*, and the third to *Hydroids elegans*.

Barnacles

In May-June (Autumn) less than one third of the panels was colonized by *B. amphitrite*, reaching values about zero during colder months. From December to April maximum values of occupied area were observed. This species had its peak of attachment during January-February ($P<0.001$) and March-April ($P<0.05$) (Fig. 4).

In relation to substratum texture, larvae showed a strongly preference to adhere on the back side of the panels, with grooves and pits; thus, back sides had a heavier settlement than the front sides ($P<0.001$). However, a heavy colonization on the front side of February panels was registered ($P<0.05$). In plankton samples taken at the study area could be observed a great concentration of cyprids. When they explore the substratum, the more favorable sites are occupied during settlement before the less favorable ones; then, this behavior could explain the heavy colonization in plane surfaces.

On front side of the panels the adults were present at maximum densities of about 1.6 individuals per cm^2 in February, 1.7 individuals per cm^2 in March and 2.1 individuals per cm^2 in April, in all cases at **C** level. On the other hand, on the back side of the panels maximum density values were 2.6 individuals per cm^2 in February, 3.0 individuals per cm^2 in March and 2.3 individuals per cm^2 in April, these values were registered at **d** level.

The maximum occupied area was obtained during February when 306 barnacles covered about 70% of the **c** panel. Settlement data for *B. amphitrite* by levels on front and back sides of the panels are presented in Table I.

Table I

Total area occupied (mm^2) by *Balanus amphitrite*, total number of individuals in brackets

	Front side								Back Side							
Date	A		B		C		D		a		b		C		d	
May 91	2.6	(4)	2.0	(4)	11.3	(6)	17.6	(6)	29.8	(26)	168.9	(87)	137.0	(50)	234.0	(70)
Jun 91	2.9	(5)	2.7	(6)	14.7	(7)	23.5	(8)	41.8	(33)	200.6	(106)	148.2	(55)	262.5	(82)
Jul 91	0.0	(0)	0.0	(0)	0.0	(0)	0.0	(0)	0.7	(2)	4.1	(8)	0.0	(0)	0.0	(0)
Aug 91	0.6	(1)	0.0	(0)	0.0	(0)	0.0	(0)	9.5	(23)	2.5	(6)	0.0	(0)	0.0	(0)
Sep 91	0.0	(0)	0.0	(0)	0.0	(0)	0.0	(0)	0.0	(0)	0.0	(0)	15.8	(9)	0.0	(0)
Oct 91	0.0	(0)	0.0	(0)	0.0	(0)	1.6	(3)	0.0	(0)	0.0	(0)	11.9	(3)	3.9	(2)
Nov 91	0.0	(0)	0.0	(0)	0.0	(0)	4.8	(5)	0.8	(1)	0.0	(0)	0.4	(1)	20.4	20)
Dec 91	0.0	(0)	0.0	(0)	14.0	(2)	134.8	(14)	9.0	(1)	78.8	(6)	130.3	(13)	214.7	(19)
Jan 92	lost		2.5	(1)	32.7	4)	4.7	(6)	lost		2060.7	(48)	1089.6	(44)	3990.7	(105)
Feb 92	1595.5	(39)	2627.6	(129)	3424.0	(201)	2654.4	(152)	5405.6	(123)	4992.4	(189)	9053.8	(306)	7184.8	(333)
Mar 92	69.0	(12)	1635.9	(82)	878.0	(212)	257.8	(157)	1156.2	(131)	659.0	(134)	3944.6	(253)	7265.6	(386)
Apr 92	606.1	(64)	2742.5	(163)	2355.8	(271)	2079.1	(167)	1233.4	(109)	558.8	(101)	1093.5	(125)	3827.3	(294)

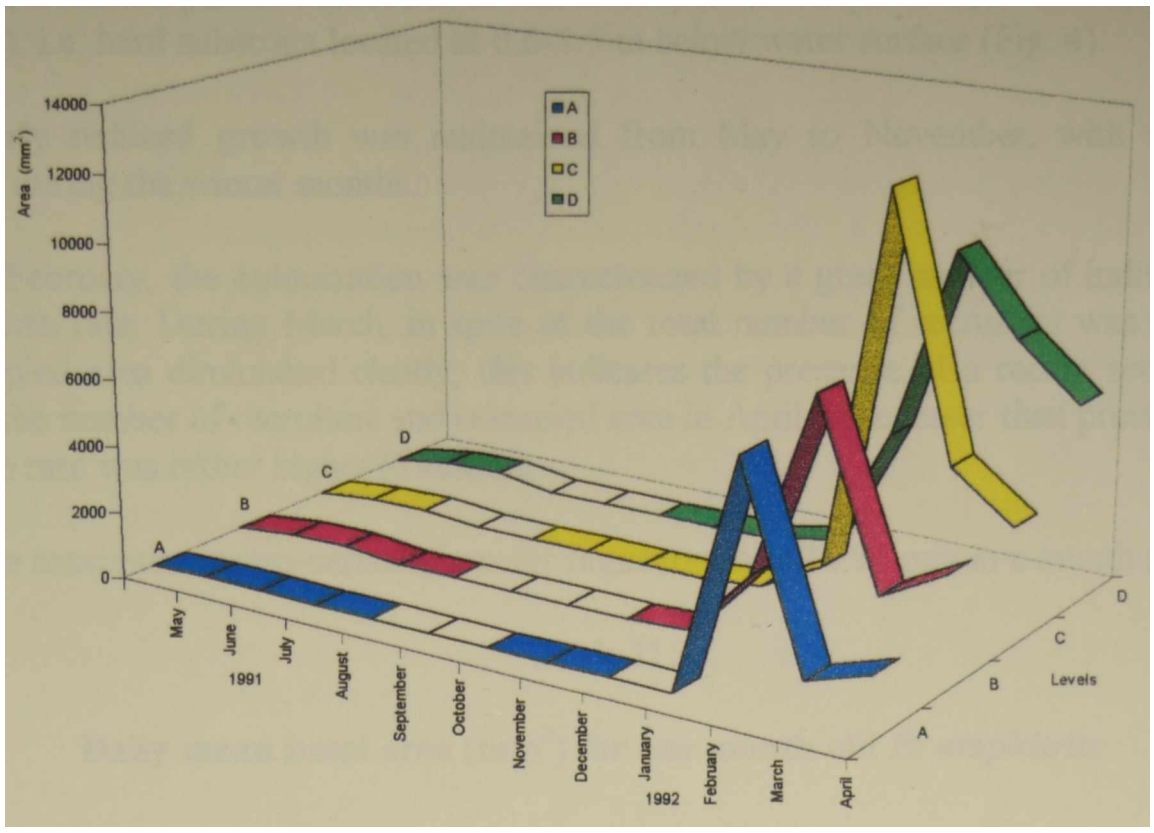

Fig. 4. -*Balanus amphitrite*, monthly total occupied area for level A (0.30-0.46 m), level B (0.66-0.82 m), level C (1.02-1.18 m) and level D (1.38-1.54 m).

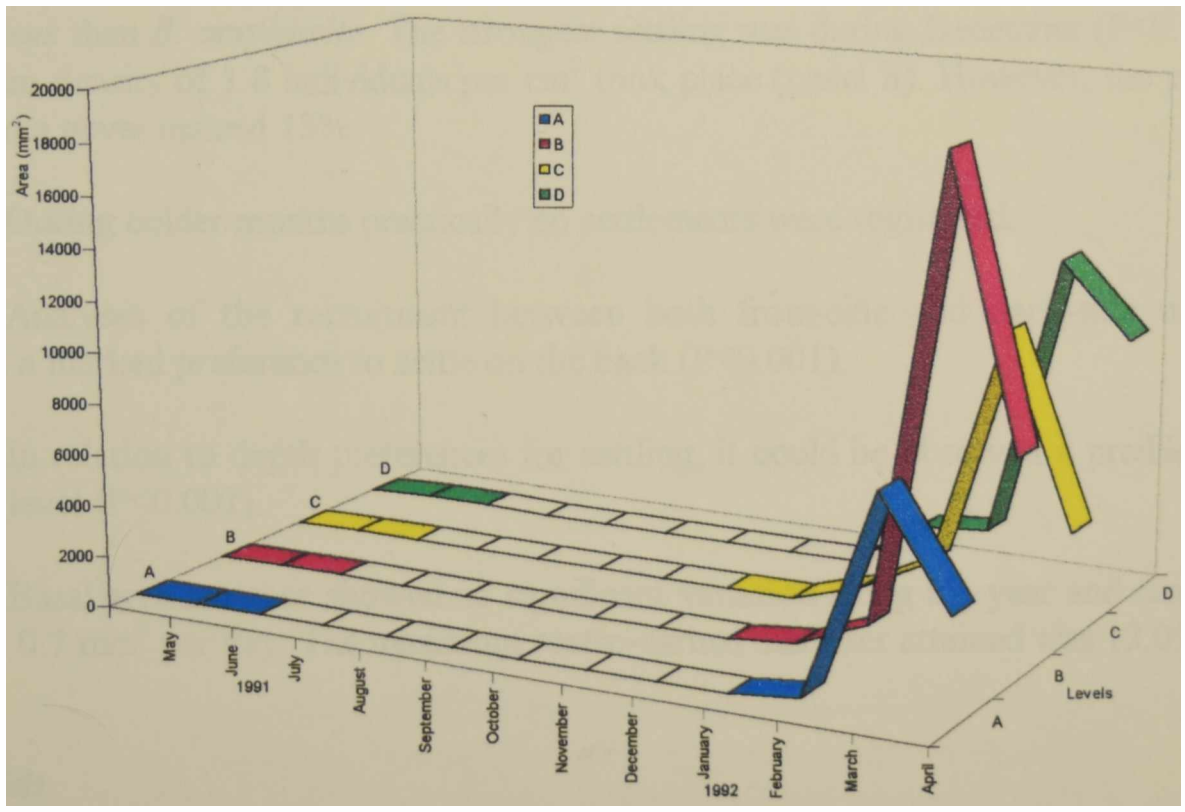

Fig. 5. -*Hydroides elegans*, monthly total occupied area for level A (0.30-0.46 m), level B (0.66-0.82 m), level C (1.02-1.18 m) and level D (1.38-1.54 m).

During the course of twelve months observations, *Balanus amphitrite* has mainly been observed to settle on panels exposed at the three deepest levels (level C, $P<0.001$; levels B and D, $P<0.05$), i.e. hard substrata located at 0.6-1.5 m below water surface (Fig. 4).

Fairly reduced growth was maintained from May to November, with virtually no settlement during the winter months.

In February, the colonization was characterized by a great number of individuals with faster growth rate. During March, in spite of the total number of recruiters was rather high, total occupied area diminished clearly, this indicates the presence of a recent settled cohort. Although the number of recruiters and occupied area in April were lesser than previous months the growth rate was rather higher (Table II).

The maximum rostro-carinal diameter registered was 14.95 mm in a month (February).

Table II

Daily mean basal area (mm^2) for one month old *B. amphitrite*

	Panels				Panels			
Date	**A**	**B**	**C**	**D**	**a**	**b**	**c**	**d**
Dec	0.0	0.0	0.2	0.7	0.0	0.7	0.6	1.0
Jan	lost	0.1	0.3	2.5	Lost	2.3	1.9	3.1
Feb	2.6	2.4	3.3	2.7	5.1	3.3	2.9	3.1
Mar	0.6	2.7	0.6	0.3	1.2	0.8	2.8	2.8
Apr	2.7	2.7	3.0	3.0	2.2	1.1	1.2	1.6

The number of individuals and occupied area were much lesser for *B. glandula* + *B. improvisus* than *B. amphitrite*. The strongest settling was during December ($P<0.001$) when a maximum density of 1.8 individuals per cm^2 took place (panel **b**). However, the percentage of cover area never exceed 13%.

During colder months practically no settlements were registered.

Analyses of the recruitment between both front-side and back-side of the panels showed a marked preference to settle on the back ($P<0.001$).

In relation to depth preferences for settling, it could be observed a predilection by the second level ($P<0.001$).

Basal area increase showed no significant variation along the year and ranged between 0.1 and 0.7 mm^2 per day. The maximum rostro-carinal diameter attained was 12.09 mm.

Serpulids

The temporal trend of serpulids showed a sudden increase at the beginning of summer, reaching a maximum in March when *Hydroides elegans* was the dominant species on panels. In this month maximum density ranged between 1.4- 4.3 individuals per cm^2. A period of stability

followed during May-June, then no individual was registered during winter and spring months (Table III).

Table III

Total area occupied (mm^2) by *Hydroides elegans*, total number of individuals in brackets

	Front side								Back Side							
Date	A		B		C		D		a		b		C		d	
May 91	3.2	(2)	10.0	(7)	13.4	(8)	35.4	(20)	11.0	(6)	22.0	(18)	19.6	(9)	55.8	(30)
Jun 91	3.7	(2)	21.8	(11)	16.2	(9)	35.4	(20)	14.2	(8)	22.0	(18)	19.6	(9)	50.0	(26)
Jul 91	0.0	(0)	0.0	(0)	0.0	(0)	0.0	(0)	0.0	(0)	0.0	(0)	0.0	(0)	0.0	(0)
Aug 91	0.0	(0)	0.0	(0)	0.0	(0)	0.0	(0)	0.0	(0)	0.0	(0)	0.0	(0)	0.0	(0)
Sep 91	0.0	(0)	0.0	(0)	0.0	(0)	0.0	(0)	0.0	(0)	0.0	(0)	0.0	(0)	0.0	(0)
Oct 91	0.0	(0)	0.0	(0)	0.0	(0)	0.0	(0)	0.0	(0)	0.0	(0)	0.0	(0)	0.0	(0)
Nov 91	0.0	(0)	0.0	(0)	0.0	(0)	0.0	(0)	0.0	(0)	0.0	(0)	0.0	(0)	0.0	(0)
Dec 91	0.0	(0)	0.0	(0)	12.1	(3)	0.0	0)	0.0	(0)	0.0	(0)	8.1	(3)	0.0	(0)
Jan 92	lost		129.8	(12)	523.5	(45)	923.8	(55)	lost		89.6	(15)	312.5	(39)	894.1	(75)
Feb 92	178.2	(33)	764.5	(76)	1314.6	(105)	1212.9	(97)	107.9	(20)	593.7	(45)	911.8	(78)	777.4	(79)
Mar 92	4469.5	(223)	7460.5	(376)	6607.9	(370)	8305.1	(370)	3794.6	(174)	11720.8	(555)	4866.5	(276)	4847.6	(235)
Apr 92	241.6	(36)	5534.5	(256)	501.7	(54)	4847.7	(237)	3917.6	(168)	2842.3	(128)	3678.0	(171)	5453.5	(256)

In relation with the depth, it could be observed that this species preferred the three deepest levels ($P<0.001$) (Fig. 5).

Settlement cycle was similar in smooth and rough side of the panels ($P>0.05$). Tubes are sinuous, often coiling in one or two regular turns at the beginning and then running fairly straight either along the panel or standing erect from it. Moreover, this disposition favored the increase of calcareous deposit and thicknesses about 1.5 cm for only one month were detected.

In spite of *Hydroides elegans* are single individuals which build white, contorted, calcareous tubes they are frequently found growing up straight the substratum in large masses. As a consequence it was difficult to measure exactly the length of the tubes. However, it could be estimated the daily mean increase in basal area (Table IV). On the back side of March and April panels the highest values happened.

The maximum length and width registered in a month were 48.6 mm and 1.5 mm, respectively.

Table IV

Daily mean increase in basal area (mm^2) for *Hydroides elegans*

	Panels				Panels			
Date	**A**	**B**	**C**	**D**	**a**	**b**	**c**	**d**
Dec	0.0	0.0	0.2	0.0	0.0	0.0	0.0	0.0
Jan	lost	0.7	1.0	1.1	lost	0.4	0.6	1.1
Feb	0.5	0.9	0.9	0.8	0.5	0.8	0.7	0.6
Mar	1.5	1.5	1.7	1.7	1.8	1.7	1.6	1.6
Apr	0.7	1.6	1.0	1.6	1.7	1.6	1.8	1.9

DISCUSSION

In this study the relationship between the seasonal increase in number of calcareous settlers and the temperature was evident.

A comparison carried out among settlement registered during summer months indicated that panels were alternately recruited by barnacles and tube-worm species. Calcareous organisms colonization began at the end of spring, when *Balanus glandula* + *B. improvisus* arrived to the tiles. In January both *B. amphitrite* and *Hydroides elegans* maintained in low abundances. In February *B. amphitrite* invaded the panels and during March, serpulids had a great peak and colonized rapidly the primary space. One possible source of this could be that high densities of both barnacles and serpulids larvae occurred in the plankton. Cyprids compete avidly for whatever space is free and spend their energy only in searching a place to settle, as a consequence result best competitors to colonize the panels. Then, when barnacle cyprids found an adequate hard substratum their density diminished in the plankton and serpulid larvae recruited and grew rapidly on all the panels. In April, serpulids diminished in abundance and showed, as barnacles, a fast growth rate.

The present results confirmed that the texture of the surface does indeed affect the amount of fouling which may attach under comparable conditions. Observations made along a year showed that barnacles were settled on the back of the panels with concavities and grooves, the choice of a rough substratum offer protection during the period immediately after metamorphosis. This is clearly demonstrated by maximum densities values obtained for back (2.3- 3.0 *B. amphitrite* per cm^2, 0.8- 1.8 *B. glandula* + *B. improvisus* per cm^2), and front sides (1.6- 2.1 *B. amphitrite* per cm^2, 0.1 *B. glandula* + *B. improvisus* per cm^2). Pomerat & Weiss **[29]** studied the attachment of barnacles and other fouling forms to various types of surfaces at Miami, Florida, found that smooth, non-porous, non-fibrous surfaces, especially if also hard, were relatively poor collectors of sedentary organisms. In addition, Crisp **[30]** and Crisp & Bourget **[31]** suggested that at the time of settlement, one of the last act of the still mobile cyprid is to orientate itself to the contour of the surface, they are capable of aligning to the long axis of a cylindrical cavity whose radius of curvature is many times the length of the cyprids itself, though narrow grooves into which it can fit snugly are preferred. Ardizzone & Chimenz **[32]** established that the substrates preferred by barnacles were those affected by water flow (cavities, angles) and only afterwards they did colonize the remaining surface. The present data support this conclusion because of in February panels not only the rough side of the panels were invaded by barnacles but also the plane side. It is noticeable that in the front sides of April tiles the total occupied area by *B. amphitrite* was higher than the back sides, this situation could be explained due to a great abundance of others non-calcareous species like the polychaete *Polydora ligni* **[28]**. In contrast with barnacles, *H. elegans* appeared to settle equally readily on rough and smooth surfaces, this observation is in accordance with those carried out by Pyefinch **[33]**.

Data corresponding to growth rates presented in this paper indicated a rapid development during warmer months, when the best conditions are given. Continuous immersion (e.g. ships anchored at harbors, raft trials, test panels), food availability and the range of temperature over which processes such as feeding and respiration can be carried out are the chief factors which influence on growth rate. Bourget & Crisp **[34]** established that

growth rates in barnacles dropped sharply when they were placed in air and normal growth was resumed soon after immersion.

Particularly interesting is a comparison of the present study with others conducted in 1966-69, 1969-70, 1973-74, 1976-77 periods in the same study area **[35-38]**. Their observations differed in a few aspects from the present study. They used sandblasted acrylic panels (460 cm^2 for level A, and 360 cm^2 for levels B, C and D), suspended vertically in a raft. It has been found **[39,40]** that ceramic and acrylic have about the same suitability for attachment and growth of organisms. In those experiences, *Balanus amphitrite* clearly preferred the upper levels A and B and only a few specimens settled on panel D. In the present study it showed preference to settle at the three deepest levels (B, C and D). Another difference is related to the size reached by individuals after one month exposure: in the period 1991/92 the maximum rostro-carinal diameter was 14.95 mm in February, and in the period 1973/74 this diameter attained 12 mm in January. Settlement peak was coincident in February and mean density value (taken as an average of panels A, B, C and D) was rather similar: 1.33 *B. amphitrite* per cm^2 in this research and 1.22 individuals per cm^2 in previous studies **[37]**.

In earlier studies four tube-worm species were registered: *Ficopomatus enigmaticus, Hydroides elegans, H. plateni* and *Serpula vermicularis*. During 1973-74 and 1976-77 periods serpulids were virtually absent in Mar del Plata harbor and filter-feeding mollusks, like *Mytilus edulis* colonized monthly panels in February-March. After a gap of fourteen years without any research, only *H. elegans* was registered again with a heavy recruitment in March and none mollusk was found. *B. trigonus* was found in both studies but with much higher number in 1973/74.

As regards to the distribution of the calcareous species on panels, in both serpulids and barnacles survival is thus limited by crowding. As a consequence of crowding changes in shell shape were detected, in the case of barnacles, the shell became tubular and the base narrow. At low population densities, barnacles may have troubles finding mates, since they are internally fertilized and have limited penis length in this sense, crowding may enhance the probability of cross-fertilization. Formation of great deposits of calcareous tubes is due to the ability of serpulids to build layers without damaging those pioneers which settled first and formed the base of the crust. Virtually the first settlers of *Hydroides* form the most strongly attaching layer, the tubes developed straight the substratum in order to expose branchial crown to water column **[22]**. Their importance is probably less than that of barnacles in that a given mass of tube-worms offers less resistance, but they have a tendency to settle on propellers from which they are not easily dislodged by rotation when well-established. This is one of the main problems on ships at Club de Motonáutica.

It is important to make short-term studies and to follow researches in order to achieve a more accurate information on recruitment tendencies. It is clear that a thorough knowledge on the composition of the fouling community at a given locality, their seasonal intensity, vertical distribution, growth and preferences to settle is an essential prerequisite for developing effective control methods. A concerted effort in this direction with interdisciplinary collaboration on a long term basis may yield methods that could be employed against the deleterious effect of the marine foulers. Nowadays, all over the world the trend is to check the biofouling by means of alternative methods; the development of new antifouling outlines by using non-toxic natural or artificial substances. In this sense, we are studying the effect of new

substances at laboratory scale in order to control biofouling at Mar del Plata harbor. However, further experiments are neccesary to integrate lab results with field tests.

ACKNOWLEDGMENTS

The authors would like to thank the Comisión de Investigaciones Científicas de la Provincia de Buenos Aires (CIC), the Consejo Nacional de Investigaciones Científicas y Técnicas (CONICET) for their support. We would also wish to thank to Dr. V. Rascio who provided useful comments on the manuscript and the Club de Motonáutica of Mar del Plata for the permission to use their marine testing site.

REFERENCES

[1] Stupak, M. E., Pérez, M. C., Di Sarli, A.- Relación entre la fijación de micro y macro "fouling" y los procesos de corrosión de estructuras metálicas. **Rev. Iberoam. Corr. Prot.** XXI(6), 219-225 (1990).

[2] Crisp, D. J.- Dispersal and reaggregation in sessile marine invertebrates, particularly barnacles. In: Larwood G., Rosen B. R. (eds.). **Biology and Systematics of Colonial Organisms.** Academic Press, New York, 3-327 (1979).

[3] Crisp, D. J.- Overview of research on marine invertebrate larvae, 1940-1980. In: Costlow, J. D., Tipper, R. C. (eds.). **Marine Biodeterioration: an Interdisciplinary Study**. Naval Institute Press, Annapolis, 103-126 (1984).

[4] Lewis, C. A.- A review of substratum selection in free-living and symbiotic cirripeds. In: Chia, F. S., Rice, M. E. (eds.). **Settlement and Metamorphosis of Marine Invertebrate Larvae**. Elsevier, New York, 207-218 (1978).

[5] Strathman, R. R., Branscomb, E. S.- Adequacy of cues to favorable sites used by settling larvae of two intertidal barnacles. In: S. E. Stancyk (ed.). **Reproductive Ecology of Marine Invertebrates**. Univ. South Carolina Press, Columbia, South Carolina, 77-89 (1979).

[6] Strathman, R. R., Branscomb, E. S., Vedder, K.- Fatals errors in set as a cost of dispersal and the influence of intertidal flora on set of barnacles. **Oecologia**, 48, 13-18 (1981).

[7] Maki, J. S., Yule, A. B., Rittschof, D., Mitchell, R.- The effect of bacterial films on the temporary adhesion and permanent fixation of cypris larvae, *Balanus amphitrite* Darwin. **Biofouling**, 8, 121-131 (1994).

[8] Williams, G. B.- The effects of extracts of *Fucus serratus* in promoting the settlement of larvae of *Spirorbis borealis* Daudin (Polychaeta). **J. Mar. Biol. Ass. U.K.**, 44, 397-414 (1964).

[9] Dayton, P. K.- Competition, disturbance, and community organization: the provision and subsequent utilization of space in a rocky intertidal community. **Ecol. Monogr.**, 41, 351-389 (1971).

[10] Foster, M. S.- Regulation of algal community development in a *Macrocystis pyrifera* forest. **Mar. Biol.**, 32, 331-342 (1975).

[11] Russ, G. R.- Effects of predation by fishes, competition and structural complexity of the substratum on the establishment of a marine epifaunal community. **J. Exp. Mar. Biol. Ecol.**, 42, 55-69 (1980).

[12] Connell, J. H.- The consequences of variation in initial settlement vs. post-settlement mortality in rocky intertidal communities. **J. Exp. Mar. Biol. Ecol.**, 93, 11-45 (1985).

[13] Possingham, H. P., Roughgarden, J.- Spatial population dynamics of a marine organism with a complex life cycle. **Ecology**, 71 (3), 973-985 (1990).

[14] Marques, J. C., Rodrigues, L. B., Nogueira, A. J. A.- Intertidal macrobenthic communities, in the Mondego estuary (Western Portugal): reference situation. **Vie Milieu**, 43 (2-3), 177-187 (1993).

[15] **Woods Hole Oceanographic Institution.**- Marine fouling and its prevention. United States Naval Institute, Annapolis, Maryland, 368 pp. (1952).

[16] Maki, J. S., Rittschof, D., Costlow, J. D., Mitchell, R.- Inhibition of attachment barnacles, *Balanus amphitrite*, by bacterial surface films. **Mar. Biol.**, 97, 199-206 (1988).

[17] Nott, J. A., Foster, B. A.- On the structure of the antennular attachment organ of the cypris larva of *Balanus balanoides* (L.). **Philos. Trans. R. Soc. Lond.**, Ser. B 256, 115-134 (1969).

[18] Walker, G., Yule, A. B.- Temporary adhesion of the barnacle cyprid: the existence of an antennular adhesive secretion. **J. Mar. Biol. Assoc. U.K.**, 64, 679-686 (1984).

[19] Wisely, B.- The development and settling of a serpulid worm, *Hydroides norvegica* Gunnerus (Polychaeta). **Austr. J. Mar. Freshwr. Res.**, 9, 351-361 (1958).

[20] Paul, M. D.- Studies on the growth and breeding of certain sedentary organisms in the Madras harbour. **Proc. Indian Acad. Sci.**, 15B, 1-42 (1942).

[21] Sasikumar, N., Rajagopal, S., Nair, K.- Seasonal and vertical distribution of macrofoulants in Kalpakkam coastal waters. **Indian J. Mar. Sci.**, 18, 270-275 (1989).

[22] Ghobashy, A. F.- Polychaetous fouling in the Egyptyan marine waters. **6th International Congress on Marine Corrosion and Fouling, Marine Biology**, 39-51 (1984).

[23] Ghobashy, A. F., Shalaby, I., Shalla, S.- Lake Timsah as a barrier for the serpuloid (tube worms) migration along the Suez Canal. **7th International Congress on Marine Corrosion and Fouling, Marine Biology**, 1-12 (1988).

[24] Hadfield, M. G., Unabia, C. C., Smith, C. M., Michael, T. M.- Settlement preferences of the ubiquitous fouler *Hydroides elegans*. In: Thompson, M. F., Nagabhushanam, R., Sarojini, R., Fingerman, M. (eds.). **Recent Developments in Biofouling Control**, 65-74 (1996).

[25] Roscoe, D., Walker, G.- Observations on the adhesion of the calcareous tube of *Pomatoceros lamarckii* and the holdfast of *Laminaria digitata*. **Biofouling**, 9(1), 39-50 (1995).

[26] Chandra Mohan, P., Aruna, Ch.- The biology of serpulid worms in relation to biofouling. In: Thompson, M. F., Nagabhushanam, R., Sarojini, R., Fingerman, M. (eds.). **Recent Developments in Biofouling Control**, 59-64 (1996).

[27] Dean, T.- Structural aspects of sessile invertebrates as organizing forces in an estuarine fouling community. **J. Exp. Mar. Biol. Ecol.**, 53(2-3), 163-80 (1981).

[28] Pezzani, S., Pérez, M., Stupak, M.- Macrofouling community at Mar del Plata harbor during one-year period (1991-1992). **Corrosion Reviews**, Special issue on industrial paints for corrosion control, 14 (1-2), 73-86 (1996).

[29] Pomerat, C. M., Weiss, C. M.- The influence of texture and composition of surface on the attachment of sedentary marine organisms. **Biol. Bull. Mar. Biol. Lab.**, 91(1), 57-65 (1946).

[30] Crisp, D. J.- Settlement responses in marine organisms. In: R. C. Newell (ed.). **Adaptations to the Environment.**, Butterworths, London, 83-124 (1976).

[31] Crisp, D. J., Bourget, E.- Growth in barnacles. **Advances in Marine Biology**, 22, 199-244 (1985).

[32] Ardizzone, G. D., Chimenz, C.- Primi insediamenti bentonici della barriera artificial di Fregene. **Atti Conv. P.F. C.N.R. Oceanogr. Fondi Mar.**, Roma, November 1981,165-181 (1982).

[33] Pyefinch, K. A.- Studies on marine fouling organisms. **J. Iron Steel Inst.**, 165, 214-220 (1950).

[34] Bourget, E., Crisp, D. J.- Factors affecting deposition of the shell in *Balanus balanoides* (L.). **J. Mar. Biol. Assoc. U. K.**, 55(1), 231-249 (1975).

[35] Bastida, R.- Las incrustaciones biológicas de las costas argentinas. La fijación anual en el puerto de Mar del Plata durante tres años consecutivos. **Corrosión y Protección**, 2(1), 21-37 (1971).

[36] Bastida, R.; Adabbo, H.- Fijación de fouling en el puerto de Mar del Plata (Período 1969/70). **LEMIT-Anales** (3), 1-39 (1975).

[37] Bastida, R. O., Mandri, M. T. de, Bastida, V. L de, Stupak, M.- Ecological aspects of the marine fouling at the Port of Mar del Plata, during the period 1973/74. **5th International Congress on Marine Corrosion and Fouling, Marine Biology**, 299-320 (1980).

[38] Stupak, M., Bastida, R. O., Arias, P.-Las incrustaciones biológicas del Puerto de Mar del Plata (Argentina), período 1976/77. **CIDEPINT-Anales**, 173-231 (1980).

[39] Capitoli, R. R.- Sequència temporal de colonição e desenvolvimento da comunidade incrustante na região mixohalina da lagos dos Patos; RS, Brasil. Tesis, Universidade do Rio Grande, 99 pp. (1983).

[40] Pérez, M., Stupak, M.- Revisión sobre los aspectos biológicos del "fouling". **CIDEPINT-Anales**, 95-154 (1996).

HIGH PERFORMANCE ANTICORROSIVE EPOXY PAINTS PIGMENTED WITH ZINC MOLYBDENUM PHOSPHATE

PINTURAS EPOXIDICAS ANTICORROSIVAS DE ALTA EFICIENCIA PIGMENTADAS CON FOSFATO DE CINC MODIFICADO CON MOLIBDATO DE CINC

R. Romagnoli[1], B. del Amo[2] , V. F. Vetere[3], L. Vèleva[4]

SUMMARY

Zinc molybdenum phosphate belongs to the so called second generation phosphate pigments and is claimed to have equal or greater anticorrosive properties than chromates and better than zinc phosphate alone. Little information is available in the literature about its anticorrosive performance.

The aim of this research was to study the anticorrosive performance of zinc molybdenum phosphate in solvent borne epoxy paints employing two anticorrosive pigment loadings. The effect of incorporating zinc oxide as complemetary pigment was also studied.

SAE 1010 steel panels were primed and coated with three different paint systems containing the anticorrosive paint and this paint plus a sealer and/or a topcoat. The anticorrosive efficiency of the different paint systems was assessed by accelerated tests (salt spray, humidity and accelerated weathering). Electrochemical measurements were done employing the anticorrosive paints alone.

Results showed that the highest anticorrosive effect was obtained employing 30% of zinc molybdenum phosphate. Polarization measurements showed that the anodic film formed on steel blocked the active sites for oxygen reduction. The incorporation of zinc oxide to pigment formula was detrimental due to its high water absorption and to the fact that it reduced zinc molybdenum phosphate solubility by the common ion effect. Polarization curves of pigments mixtures could be used as a guideline to predict the anticorrosive coating performance in accelerated and electrochemical tests. However, the final decision on pigment selection must be taken on the basis of accelerated trials.

Keywords: *zinc molybdenum phosphate, epoxy anticorrosive paints, zinc oxide, accelerated tests, electrochemical tests.*

---

[1] Miembro de la Carrera del Investigador del CONICET; Profesor Adjunto, UNLP
[2] Miembro de la Carrera del Investigador del CONICET
[3] Profesor Titular, UNLP; Jefe Area Estudios Electroquímicos Aplicados a Problemas de Corrosión y Anticorrosión
[4] Investigador del Centro de Investigación y Estudios Avanzados (CINVESTAV), México

INTRODUCTION

Zinc molybdenum phosphate belongs to the so called second generation phosphate pigments. It is basically composed by zinc phosphate added with zinc molybdate up to 1% (expressed as MoO_3) and is claimed to have equal or greater anticorrosive behaviour than chromates and undoubtely better than zinc phosphate alone **[1-6]**. The active inhibitive species in this pigment is molybdate anion which is thought to repassivate corrosion pits in steel **[7]**.

Little information is available in the literature about zinc molybdenum phosphate anticorrosive performance. Adrian and Bittner **[3, 5, 6]** reported the behaviour of zinc molybdenum phosphate in alkyd paints in comparison with zinc phosphate and zinc chromate. The performance of zinc molybdenum phospahte and other pigments belonging to the second generation phosphate pigments series in compliant primers was also tested **[6]**.

The purpose of the present research was to study the anticorrosive properties of zinc molybdenum phosphate in solvent borne epoxy paints employing two anticorrosive pigment loadings. The effect of incorporating zinc oxide was also studied. Zinc oxide was selected because of its ability to polarize cathodic areas by precipitating sparingly soluble salts **[8]**. Painted panels with either the anticorrosive paint alone or with a complete paint system were subjected to the salt spray, humidity chamber and accelerated ageing tests. Electrochemical tests were also performed on steel panels coated only with the anticorrosive paint to avoid higher barrier effects due to the complete paint system.

EXPERIMENTAL

Binder. The film forming material was an epoxy bisphenol polyamide resin.

Pigment. Micronized zinc molybdenum phosphate (average particle diameter 1 μm) was employed as anticorrosive pigment with two different loadings, 10 and 30 % by volume with respect to the total pigment content. The complementary pigments were ferric oxide and barium sulfate and the mixture resulting on partially replacing these pigments (20% by volume) by zinc oxide. Ferric oxide was also introduced in the pigment formula because its colloidal particles are said to interact with metallic substrates increasing its coverage **[9-11]**. Solids contained in the tested anticorrosive paints is shown in Table I.

Table I

Solids in anticorrosive paints compositions (% by volume)

Paint	1	2	3	4
Zinc molybdenum phosphate	12.1	4.1	12.1	4.1
Ferric oxide	14.1	18.1	11.3	14.5
Barium sulfate	14.1	18.1	11.3	14.5
Zinc oxide	-----	----	5.6	7.2
Epoxy resin	59.7	59.7	59.7	59.7

Note: The solvent mixture employed for epoxy paints was toluene/ methyl isobutyl ketone/ butyl alcohol (36/52/12, by weight)

The inhibitive properties of pigments mixtures were evaluated by means of anodic and cathodic polarization curves. In each case the swept began in the vicinity of corrosion potential at a sweep rate of 3 $mV.s^{-1}$. The electrolytic cell was composed by an iron electrode (working electrode), a saturated calomel electrode (SCE) as reference and a platinum counterelectrode. The electrolyte was 0.5 M sodium perchlorate solution. Cathodic curves were obtained immediately after the anodic swept.

Paints manufacture and application. It was carried out employing a ball mill with a 3.3 liters jar. The resin solution was added firstly while the pigments were incorporated later; the system was dispersed for 24 hours to achieve an acceptable dispersion degree, grade 4 in Hegman's scale **[12]**.

A sealer and a topcoat, whose composition may be seen in Table II, were prepared with a similar method. In the case of the sealer, the non leafing aluminium was incorporated after pigment dispersion to avoid reaction with chlorinated rubber resin.

Table II

Sealer and topcoat compositions expressed as % by volume

Components	Percentage	
	Sealer	Topcoat
Ferric oxide	2.2	---
Barium sulfate	2.2	---
Non leafing aluminium	4.7	---
Zinc oxide	0.8	---
Titanium dioxide	---	7.3
Alkyd resin (solids)	5.6	20.8
Chlorinated rubber (R10)	16.8	4.8
Chlorinated paraffin (42%)	7.2	2.1
Pine oil	0.5	0.5
Xilene	40.0	43.0
Aromasol H	20	21.5

Test panels were previously sandblasted to Sa 2 1/2 (SIS 05 59 00-67) attaining 20 ± 4 μm maximum roughness, degreased with toluene and coated with a wash primer (SSPC-PT 3-64). Paints applied by means of a spray gun on SAE 1010 steel panels (15.0 x 7.5 x 0.2 cm) and three different paint systems were studied (Table III) to assess their anticorrosive performance.

Salt spray test (ASTM B 117). After 1500 hours exposure panels were evaluated to establish the oxidation degree according to ASTM D 610. In all cases experiences were carried out in triplicate, determining the mean value of the results obtained in the test. Accelerated test were done on panels coated with the anticorrosive paint alone and with different paint systems (Table III).

Table III

Tested paint systems

Identification	Paint systems (thickness, between brackets)
1	Anticorrosive paint alone (75 ± 5 μm)
2	Anticorrosive paint (40 ± 5 μm) + Sealer (30 ± 5 μm)
3	Anticorrosive paint (40 ± 5 μm) + Sealer (30 ± 5μm) + Topcoat (40 ± 5 μm)

Humidity cabinet test (ASTM D 2247). Panels were placed in the humidity chamber at 38 ± 1^0 C for 2650 hours. The blistering degree was established according to the ASTM D 714 standard specification.

Accelerated ageing test (ASTM G 26). The accelerated degradation of painted samples was carried out in a Atlas Weather Ometer (Xenon arc type). The test program consisted of a 102 minutes light cycle followed by 18 minutes light water spray cycle. The overall time of each cycle was 2 hours and that of the complete test 1100 hours. The degree of rusting was evaluated according to the above mentioned standard specification.

Corrosion potential measurements. The cells to perform these measurements were constructed by delimiting 3 cm^2 circular zones on the painted surface. A cylindrical open acrylic tube, with one flat end, 7 cm long, was then placed on the specimen and the electrolyte (0.5 M sodium perchlorate solution) placed in the tube. The measurements of the corrosion potential of the painted steel substrate with respect to the SCE, were made employing a high impedance voltmeter. Electrochemical tests were carried out on steel panels covered only with anticorrosive paints.

Ionic resistance measurements. The resistance between the steel substrate and a platinum electrode was also measured employing the cells described previously and an ATI Orion, model 170, conductivity meter which operates at a 1000 Hz frequency.

Polarization resistance measurements. The polarization resistance of painted specimens was determined as a function of immersion time employing an electrochemical cell with three electrodes. The reference electrode was the SCE and the counterelectrode a platinum grid. The voltage swept was ± 10 mV, starting from the corrosion potential. Measurements were carried out employing an EG&G PAR Potentiostat/Galvanostat, Model 273A and the software SOFTCORR 352. Polarization resistance of uncoated steel was also monitored as a function of the immersion time.

RESULTS AND DISCUSSION

Pigments mixtures. Anodic polarization curves (Fig. 1) reveal that pigments mixtures 1 and 3 (with the highest zinc molybdenum phosphate content) have the best inhibitive properties because they have the lowest passivation current for the second peak. In this sense, the presence of zinc oxide was detrimental because it made difficult to achieve an effective steel passivation (pigment mixture 2). However, zinc oxide restrained the effect of lowering the zinc molybdenum phosphate content (pigment mixture 4). It is thought that the passive film formed by corrosion is similar to that formed at potentials previous to the second peak (which corresponds to the oxidation of ferrous species to ferric ones); in the case of mixtures 1 and 3 a more protective film seemed to be formed because, as it was said before, the current corresponding to the second peak decreased notably.

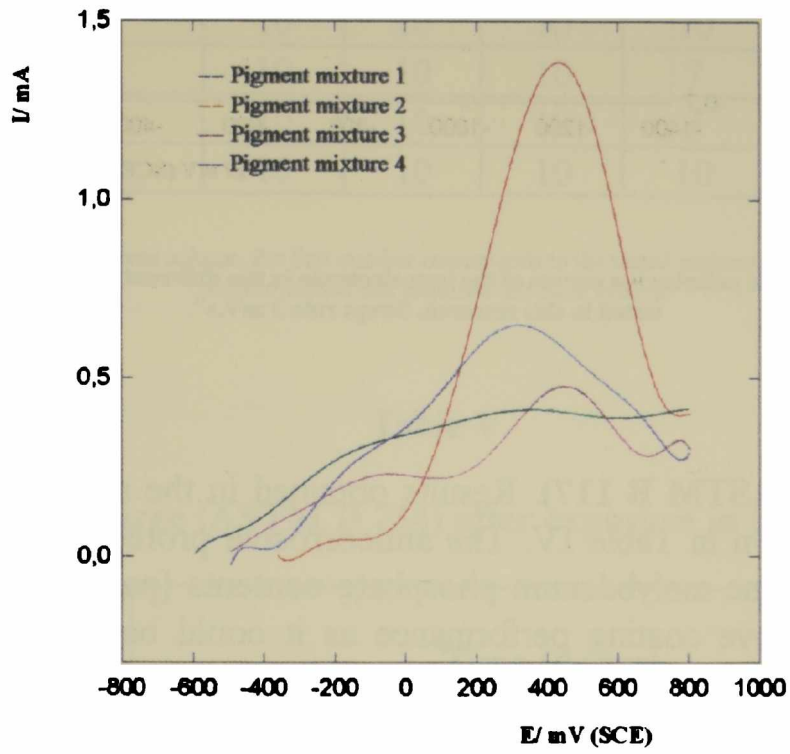

Fig.1.- Anodic polarization curves of the iron electrode in the different pigment mixtures tested. Swept rate 3 mV.s^{-1}.

From the cathodic polarization curves (Fig. 2), it may be seen that the higher the zinc molybdenum phosphate content in the pigment mixture the lower the oxygen diffusion current is. The presence of zinc oxide in mixture 3 resulted detrimental because it increased the oxygen diffusion current. It must be remembered that the highest the oxygen diffusion current the higher the corrosion rate would result.

As the cathodic curve was obtained after performing the anodic one, it was concluded that the film formed on the electrode during the anodic scan blocked the actives sites for oxygen reduction.

According to the foregoing discussion, it may be expected that paints formulated with the pigment mixture 1 must show the best anticorrosive performance and paints incorporating mixtures 2 and 4 the worst one.

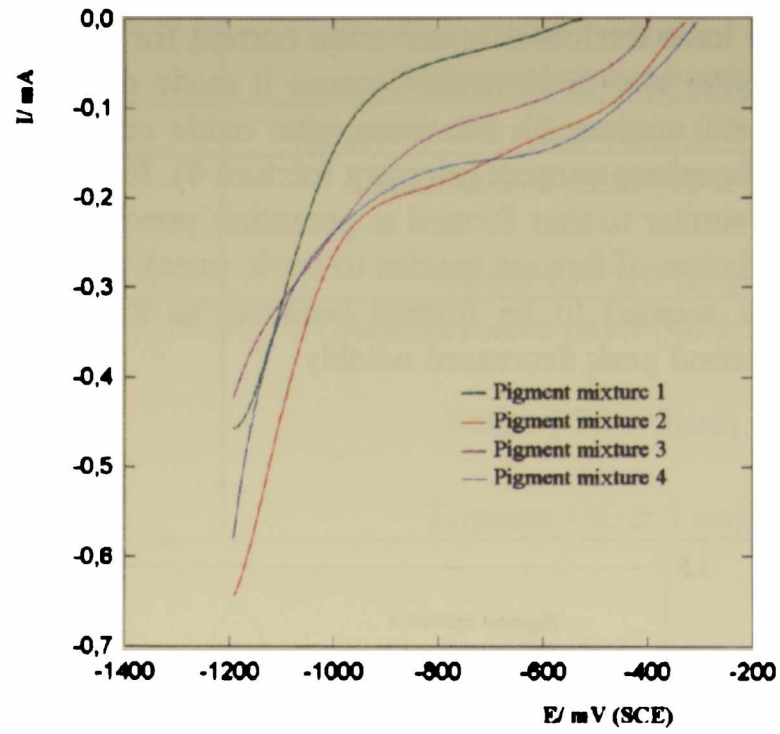

Fig.2.- Cathodic polarization curves of the iron electrode in the different pigment mixtures tested in this research. Swept rate 3 mV.s^{-1}.

Salt spray test (ASTM B 117). Results obtained in the salt spray cabinet after 1500 hours of testing are shown in Table IV. The anticorrosive protection was more efficient for paints with the highest zinc molybdenum phosphate contents (paint 1). The incorporation of zinc oxide did not improve coating performance as it could be expected from data in the literature [12] and previous results obtained with alkyd paints **[13]**. This is due to the fact that zinc oxide has a relatively high water absorption **[14]** and that it reduces zinc molybdenum phosphate solubility by the common ion effect. Evidently, these characteristics prevailed over the catodic protection provided by this pigment.

Paint system 2 (anticorrosive paint+sealer) proved to be as efficient as system 1 (two coats of the anticorrosive paint); this may be attributed to initial high barrier effect developed for anticorrosive paints as it will be said later. The presence of a topcoat (Paint system 3) enhanced the barrier effect and all systems showed high effciency including those containing zinc oxide. Results were confirmed after paint system removal.

Humidity cabinet test (ASTM D 2247). Paints blistering results are presented in Table V. Paint with the higher anticorrosive pigment content (paint 1, Table I) did not present blistering after 2640 hours exposition . Blistering increased as the zinc oxide content did. It was not observed signs of corrosion under the blisters except for paint 4.3 after 1500 hours (Table IV and V). In all cases the blistering was higher in system 3 but blisters originated between at the anticorrosive sealer paint interfase.

Table IV

Rusting degree (ASTM D 610) after exposure in the salt spray test

Paint systems	Time (hours)				
	360	720	960	1300	1500
1.1	10	10	10	9	8
1.2	10	10	10	10	9
1.3	10	10	10	10	10
2.1	10	10	10	8	7
2.2	10	10	9	8	6
2.3	10	10	10	10	10
3.1	10	10	10	8	6
3.2	10	10	10	9	7
3.3	10	10	10	10	10
4.1	10	10	10	7	6
4.2	10	10	10	7	6
4.3	10	10	10	10	8

Note. In the paint system column, the first number corresponds to the tested anticorrosive paint (Table 1) and the second one identifies the paint system.

Table V

Blistering degree (ASTM D 714) after exposure in humidity test

Paint Systems	Time (hours)					
	360	720	960	1500	1872	2640
1.1	10	10	10	10	10	10
1.2	10	10	10	8F	8F	8F
1.3	10F	8F	8F	8F	8F	8F
2.1	8F	8M	8M	8M	8M	8M
2.2	6F	6F	6M	6M	4MD	4MD
2.3	4F	4MD	4D	4D	4D	4D
3.1	8F	8F	8F	8F	8F	8F
3.2	8F	8MD	8MD	8D	6F	6F
3.3	6F	6F	6F	6F	6F	6F
4.1	8F	8MD	8MD	8MD	8MD	8MD
4.2	8F	8D	8D	6F	6F	6F
4.3	6F	6MD	6MD	6MD	6MD	6MD

Note: The numeral represents blister size: 10 no blistering, 8 the smallest size blister, etc. Letters indicate the frequency: D, dense; MD, medium dense; M, medium; F,few.

Accelerated ageing test (ASTM G 26). All paints exhibited a good behaviour after 1100 hours exposure. No signs of corrosion were observed neither on the painted surface nor

on the steel substrate. Blistering was, as a general rule, low and increased slightly for paints containing zinc oxide. It may be expected that these paint systems would perform acceptably in outdoor exposure for at least three years without showing signs of corrosion because, as it was stated in the literature, because 1100 hours of accelerated wheathering may be considered, as an average, equivalent to 3 years outdoor exposure [15].

Corrosion potential measurements.The best anticorrosive protection was afforded by paints 1 and 3 and the high barrier effect showed by these paints made it impossible to measure accurately the painted panel potential. As it was predicted by polarization curves obtained with the iron electrode dipped into the different pigment suspensions, the diminishing of zinc molybdenum phosphate content impaired the paint performance (paint 2) as well as the incorporation of zinc oxide. In both cases corrosion potential of painted panels derived towards negative values during the test period (Fig. 3).

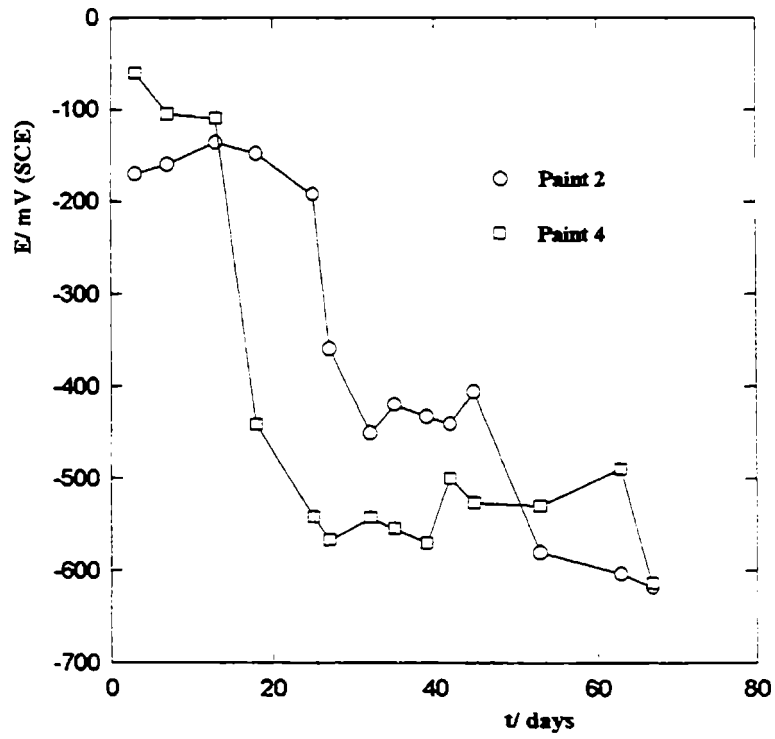

Fig. 3.- Corrosion potential of painted steel panels as a function of the exposure time, in 0.5 M sodium perchlorate solution.

Ionic resistance measurements. The measured resistance is composed by two contributions: the solution resistance and the paint film resistance. As the solution resistance is low (84 Ω) the paint film resistance is responsible of the measured values. Polarization effects may be neglected at the measuring frequency employed in this test.

The ionic resistance of paints 1 and 3 was higher than 10^8 and 10^7 $\Omega.cm^{-2}$ respectively, giving full protection to the steel substrate by barrier effect. Paints 2 and 4 showed high ionic resistance at the beginning of the test but this barrier effect was lost as time elapsed (Fig.4). The more impervious films corresponded to the highest anticorrosive pigment content; this led to think that pigment-binder interaction is responsible for higher barrier effect of paints 1 and 3. In the case of paint 3 this was slightly impaired by the presence of zinc oxide in the film, turning it more susceptible to electrolyte penetration.

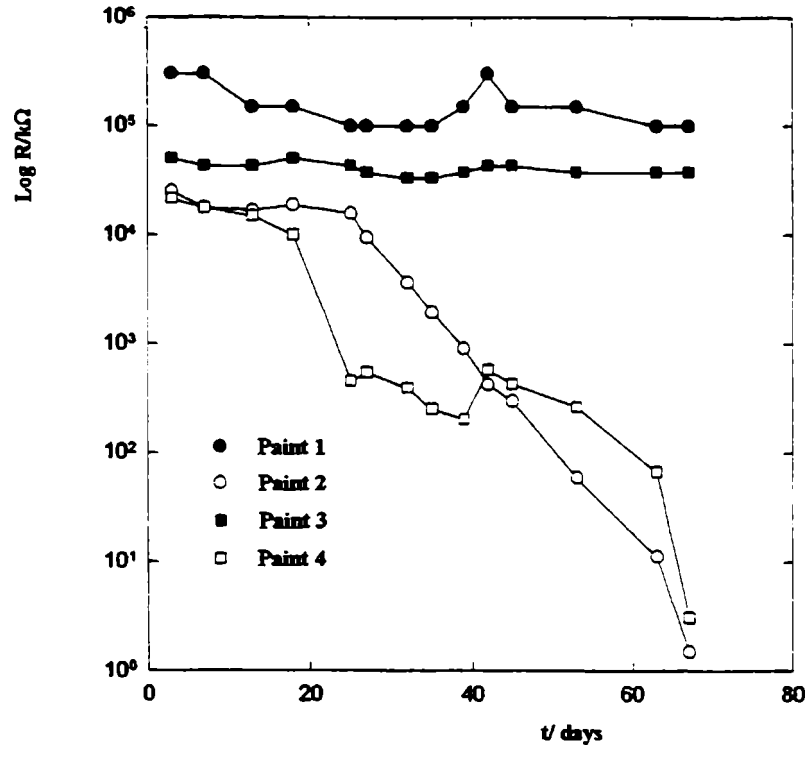

Fig. 4.- Resistance of painted steel as a function of the exposure time in 0.5 M sodium perclorate solution.

Polarization resistance measurements. The high barrier effect showed by paints 1 and 3 controlled paint behaviour. In these cases a linear response is to be obtained and it makes no sense to measure the variation of polarization resistance as a function of time. However, once paints 2 and 4 lost part of their barrier properties polarization resistance was measured and it was found that it exceeded the ionic resistance indicating that zinc molybdenum phosphate inhibited steel corrosion **[16]**.

CONCLUSIONS

1. The obtained results showed that the highest anticorrosive effect is obtained employing 30 % by volume of zinc molybdenum phosphate in the pigment composition. Polarization measurements show that the anodic film formed on steel blocked the active sites for oxygen reduction.

2. The ferric oxide and barium sulfate employed as extenders gave an additional barrier effect.

3. Zinc oxide is not recommended in epoxy paints pigmented with zinc molybdenum phosphate. This may be due to its high water absorption and to the fact that it reduces zinc molybdenum phosphate solubility by the common ion effect.

4. Polarization curves of pigments mixtures may be used as a guideline to predict the probable anticorrosive coating performance in accelerated and electrochemical tests. However, the final decision on pigment selection must be taken on the basis of accelerated trials.

AGKNOWLEDGEMENTS

The authors are grateful to CONICET (Consejo Nacional de Investigaciones Científicas y Técnicas), CIC (Comisión de Investigaciones Científicas de la Provincia de Buenos Aires) and UNLP (Universidad Nacional de La Plata) for their sponsorship to do this research. The authors also want to thank Colores Hispania for providing the anticorrosive pigment.

REFERENCES

[1] Meyer, G.- **Farbe+Lack, 69** (7), 528 (1963).
[2] Meyer, G.- **Farbe+Lack, 71** (2), 113 (1965).
[3] Adrian, G.; Gerhard, A.; Bittner, A.; Gawol, M.- **European Supplement to Polymer Paint Colour Journal**, 62 (1981).
[4] Leidheiser (Jr.), H.- **J. Coat. Tech., 53** (678), 29 (1981).
[5] Gerhard, A.; Bittner, A.- **J. Coat. Tech., 58** (740), 59 (1986).
[6] Bittner, A.- **J. Coat.Tech., 61** (777), 111 (1989).
[7] Ambrose, J.R.- **Corrosion (NACE), 34** (1), 27 (1978).
[8] Szklarska-Smialowska, Z.; Mankowsky, J.- **Br. Corros. J., 4** (9), 271 (1969).
[9] Andrade, E.M.; Molina, F.V.; Posadas, D.- **J. Colloid and Interface Science, 165,** 450 (1994)
[10] Andrade, E.M.; Gordillo, G.J.; Molina, F.V.; Posadas, D.- **J. Colloid and Interface Science, 173,** 231 (1995)
[11] Andrade, E.M.; Molina, F.V.; Gordillo, G.J.; Posadas, D.- **J. Colloid and Interface Science, 165,** 459 (1994)
[12] Giúdice, C.; Benítez, J.C.; Rascio, V.- **J.Oil Col. Chem Assoc., 62** (3), 151 (1980).
[13] del Amo, B.; Romagnoli, R.; Vetere, V.F.- **Corrosion Reviews, 14** (1-2), 121-133 (1996).
[14] Payne, H.F.- ***Organic Coatings Technology***, vol II: Pigments and Pigmented Coatings, p.1095, N.Y., Wiley, 1961.
[15] Rascio, V.; Caprari, J.J.; del Amo, B.; Ingeniero, R.- **JOCCA, 62** (12), 475(1979).
[16] Szauer, T.- **Prog. Org. Coatings, 10,** 157 (1982).

STEEL CORROSION PROTECTION BY MEANS OF ALKYD PAINTS PIGMENTED WITH CALCIUM ACID PHOSPHATE

PINTURAS ALQUIDICAS A BASE DE FOSFATO ACIDO DE CALCIO PARA LA PROTECCION ANTICORROSIVA DEL ACERO

B. del Amo[1], R. Romagnoli[2], V. F. Vetere[3]

SUMMARY

The use of classic anticorrosive pigments is being more and more restricted by increasing environmental concerns; they are gradually replaced by zinc phosphate and related compounds. Other anticorrosive pigments such as surface exchanged silicas were also proposed.

The object of this research is to study the anticorrosive properties of calcium acid phosphate as inhibitive pigment introducing a careful selection of complementary pigments in order to achieve an efficient anticorrosive protection. Several paints were prepared and tested through accelerated and electrochemical tests. The nature of the passive film was also studied.

Paints containing zinc oxide and calcium carbonate (50/50) showed the best performance and a higher resistance in the salt spray test. Zinc oxide and calcium carbonate decreased film permeability and improved steel passivation.

The passive film was composed by a ferric oxyhydroxide film whose pores became plugged by ferric phosphate.

Keywords: *calcium acid phosphate, alkyd anticorrosive paints, zinc oxide, calcium carbonate.*

INTRODUCTION

The use of classic anticorrosive pigments is being more and more restricted by increasing environmental awareness as well as stringent national and international regulations and directives. This situation takes into account that the use of chromate pigments implies cancerigenous risk.

---

[1] Miembro de la Carrera del Investigador del CONICET
[2] Miembro de la Carrera del Investigador del CONICET, Profesor Adjunto, UNLP
[3] Profesor Titular, UNLP; Jefe Area Estudios Electroquímicos Aplicados a Problemas de Corrosión y Anticorrosión

The long awaited reduction in usage of classical active pigments has induced considerable search for adequate alternative products for more than 15 years. Particular attention has been paid to zinc phosphate since it was found that its effectiveness could be improved by controlled chemical modification of its structure with suitable elements or by changing the anion orthophosphate by polyphosphate one **[1-8]**.

Comparative anticorrosive performance of calcium acid phosphate and zinc phosphate was established in a previous paper **[9, 10]**.

The aim of this paper is to study the anticorrosive properties of calcium acid phosphate as inhibitive pigment, introducing an important modification with respect to authors' previous studies **[9, 10]**. This modification is concerned with a careful selection of complementary pigments in order to achieve an efficient anticorrosive protection.

To test the performance of calcium acid phosphate two different studies were conducted. One series of studies involved the preparation of several paints employing an alkyd resin and different pigment compositions. Painted panels were subjected to accelerated and electrochemical tests. Another series was conducted in order to assess the inhibitive properties of aqueous pigment suspensions by different techniques, studying the properties of the passive layer.

EXPERIMENTAL

Paints composition and manufacture

Binder. The film forming material was an alkyd resin (50% solution in white spirit). The resin employed in this research had the infrared (IR) spectrum corresponding to a medium alkyd resin. It showed the characteristic peak of alkyds at 1275 cm^{-1} and other peaks assigned to the stretching of the C-H bond in oil (2870 and 2930 cm^{-1}), the stretching of the C=C bond (1490, 1580 and 1600 cm^{-1}) and to the bending of the benzene ring (705 and 745 cm^{-1}) **[11]**.

Pigment. Calcium acid phosphate was employed as anticorrosive pigment and its content was 30% by volume with respect to the total pigment formula. Other pigments such as titanium dioxide, magnesium silicate, calcium carbonate, zinc oxide and barium sulphate were used as complementary pigments. The PVC/CPVC relationship for all the paints was 0.8, resulting this value in a similar free binder content in all cases. Paints solids percentages, expressed as % by volume, are shown in Table I.

Paints preparation. It was carried out employing a ball mill with 3.3 liters jar. The resin solution was added firstly and pigments were incorporated later. The system was dispersed during 24 hours to achieve an acceptable dispersion degree **[12]**.

Paints application. They were applied by means of a spray gun on ASTM 1010 steel panels (15.0x7.5x0.2 cm) up to a thickness of 75 ± 5 μm. Tested panels were previously sandblasted to Sa 2 ½ (SIS 05 59 00) and degreased with toluene. The painted panels were kept in the laboratory for 7 days before testing. Two series of panels were tested; one with the

primer and the other with a complete system (a conventional alkyd enamel was used as a topcoat) up to a film thickness of 125 ±5 μm.

Table I

Solids in paint composition (% by volume)

Paint	1	2	3	4
Calcium acid phosphate	10.0	10.0	10.0	10.0
Talc	9.6	—	--	—
Calcium carbonate	---	9.6	--	4.8
Zinc oxide	---	---	9.6	4.8
Titanium dioxide	3.8	3.8	3.8	3.8
Barium sulphate	9.6	9.6	9.6	9.6
Alkyd resin	46.0	46.0	46.0	46.0

Laboratory tests

Standardized accelerated salt spray and humidity cabinet tests were performed using painted panels to assess paints anticorrosive properties. In addition, electrochemical measurements were done on similar panels to elucidate the anticorrosive performance of these paints.

Water vapour transmission was evaluated to determine coating permeability.

Finally, the nature of the passive layer was investigated by scanning electron microscopy (SEM) on both, bare steel submerged in a pigment suspension and at the metal/coating interface.

Accelerated tests

Salt spray test (ASTM B 117). A scratch line was made through the coating with a sharp instrument so as to expose the underlying metal to the aggressive environment. The panels were periodically observed, without removing the coating, to assess both the rusting degree (ASTM D 610) and the failure at the scribe (ASTM D 1654). In all cases experiences were carried out in triplicate, determining the mean value of the obtained results. Results after 720 hours exposure are displayed in Table II.

Humidity chamber test. Another series of panels coated with the anticorrosive paints alone, was placed in the humidity chamber at 38 ± 1°C for 1600 hours (ASTM D 2247). The blistering degree was established according to the ASTM D 714 standard specification.

Table II

Rusting degree (ASTM D 610), failure at the scribe (ASTM D 1654) and blistering (ASTM D 714) after 720 hours exposure in the salt fog chamber for steel panels covered with the selected painting systems

Painting system	Anticorrosive paint				Anticorrosive paint + topcoat	
Tests	Rusting degree			Blistering	Rusting degree	
Paint	Without removing the coat	After coat removal	Failure at the scribe	Without removing the coat	Without removing the coat	After coat removal
1	8	5	6	4D	10	10
2	9	6	5	6M	6	6
3	10	9	6	0	10	10
4	10	10	7	8F	10	10

Electrochemical measurements

Corrosion potential. The electrochemical cells to measure corrosion potential of painted steel as a function of time were constructed by delimiting 3 cm^2 circular zones on the painted surface. An acrylic tube, with one flat end and 7 cm high, was placed on the specimen and filled with the electrolyte (0.5 M sodium perchlorate solution). Corrosion potential of coated steel was measured against a saturated calomel electrode (SCE) with a high impedance voltmeter.

Ionic resistance. The resistance between the painted steel substrate and a platinum electrode was also measured employing the cells described previously and an ATI Orion, model 170, conductivity meter at a 1000 Hz frequency. Similar measurements were performed on uncoated steel.

Polarization resistance. The polarization resistance of painted panels was determined as a function of the immersion time for specimens whose ionic resistance was less than $10^5\ \Omega.cm^{-2}$. The electrochemical cell had three electrodes, a calomel one as reference and the counterelectrode was a platinum grid. The voltage swept was ± 10 mV, starting from the corrosion potential. Measurements were done employing an EG&G PAR Potentiostat/Galvanostat, Model 273A and the software SOFTCORR 352. Polarization resistance of uncoated steel was also monitored as a function of the immersion time.

Water vapour transmission

Water vapour transmission was evaluated according to ASTM D 1653, test method B, applying the paint films by means of a brush on a filter paper (dry film thickness 70 μm). Perm cups consisting of a container made of non-corroding, impervious to water and water vapour material, 25 cm^2 area, were employed (Fig. 1).

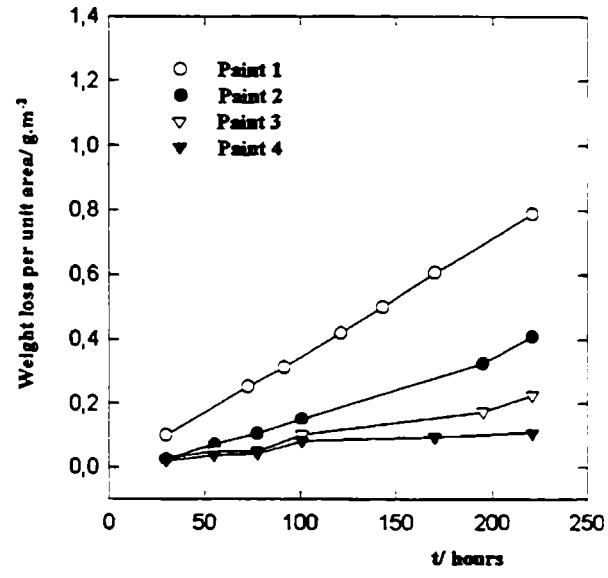

Fig. 1. Water vapour transmission as a function exposure of time (ASTM D 1653, test method B).

The nature of the passive film

The corrosion potential of an ASTM 1010 steel electrode was measured against a calomel electrode. The electrolyte was a pigment suspension in 0.1 M sodium perchlorate. The nature of the passive film formed on the steel surface was studied by scanning electron microscopy (SEM) and its composition determined by Mössbauer spectroscopy. The final product resulting from the reaction with calcium acid phosphate and iron powder was also identified by means of an IR spectrum.

The passive layer formed on painted specimens was examinated by SEM after removing the alkyd binder by means of a suitable solvent; then, the passive layer was scraped and its composition analysed by IR spectrometry.

RESULTS AND DISCUSSION

Accelerated tests

Salt spray test (ASTM B 117). The rusting and blistering degree after 720 hours are shown in Table II. The anticorrosive protection achieved with paint 1, without topcoating, was poor and closely related with the blistering observed in this case which was the greatest of the

series (4D grade). This behaviour drastically changed when a complete painting system was applied since after coat removal no signs of corrosion were found.

The results obtained show that replacing talc with calcium carbonate (paint 2) the corrosion degree diminished but failure at the scribe showed the greatest value of the series; blistering was also important. When the replacement was made with zinc oxide (paint 3) a full protection and no blistering were observed. Similar results were obtained when talc was completely replaced by zinc oxide and calcium carbonate (paint 4); but in this case the protection at the scribe was improved. The performance in the salt spray test was notably improved by the presence of zinc oxide and calcium carbonate in the pigment composition **[10]**.

Humidity chamber test. Results obtained after 1600 hours in the humidity cabinet test are presented in Table III. Paints 3 and 4, containing zinc oxide in the pigment composition, showed no blistering. On the other hand, paints 1 and 2, pigmented with talc and calcium carbonate, showed the worst behaviour. The anticorrosive performance was in accordance with the observed blistering.

Table III

Rusting degree (ASTM D 610) and blistering (ASTM D 714) after 1600 hours exposure in the humidity cabinet test for steel panels covered with the anticorrosive paint alone

Paint	Blistering	Rusting degree after coat removal
1	4D	4
2	6M	5
3	10	8
4	10	8

Electrochemical measurements

Corrosion potential. Corrosion potential was monitored for 51 days, being this period enough to detect the most important changes in paint film (Fig. 2). Paints 3 and 4 showed the best behaviour in this test while paints 1 and 2 the worst. Taking into account that all pigment compositions contained the same volume of calcium acid phosphate, the differences must be attributed to in the complementary pigments used in this research. The presence of calcium carbonate and zinc oxide in the pigment mixture improved steel passivation, which was closely related to the pH value of the pigments suspension. The presence of these complementary pigments changed the pH value from 6.4 in paint 1 to 6.6 in paint 2, 7 in paint 3 and 7,1 in paint 4. Passivation of iron in phosphate solution begins at pH values close to 7 because at this pH phosphate and oxides could precipitate together **[13]**. It is important to point out that paints 3 and 4, in which talc was not used, showed a noticeable ability to repassivate. It is

thought that this improved steel passivation is responsible for the better anticorrosive performance observed in the salt spray test.

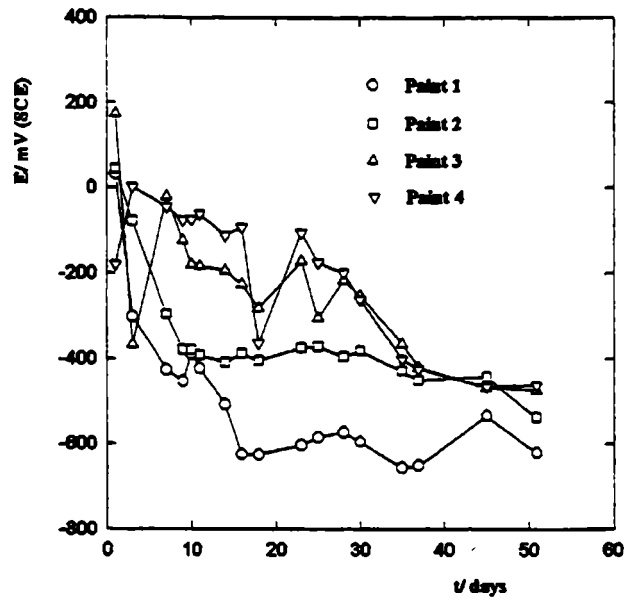

Fig. 2.- Corrosion potential of painted steel panels as a function of the exposure time, in 0.5 M sodium perchlorate solution.

Ionic resistance. Among all tested paints, paint 4 ($R>10^8$ $\Omega.cm^{-2}$) and paint 3 ($R>10^7$ $\Omega.cm^{-2}$) showed the highest barrier properties (Fig. 3) which was maintained greater than 10^6 $\Omega.cm^{-2}$ for 30 days. All the paints had the same PVC/CPVC value and the coat must have the same porosity [14]; however, paints containing calcium carbonate and zinc oxide showed the highest ionic resistance value. The most impervious film, at least during the initial phase of the immersion period, was that obtained replacing talc by calcium carbonate and zinc oxide (50/50).

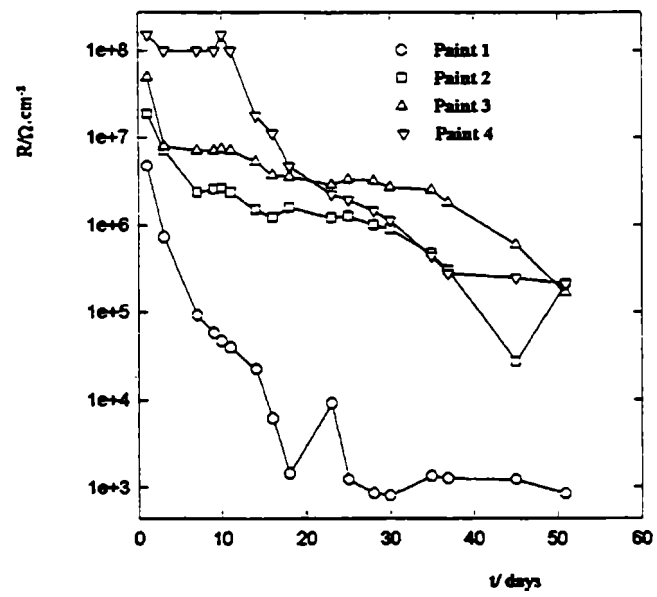

Fig. 3- Resistance of painted steel as a function of the exposure time in 0.5 M sodium perchlorate solution.

The reduced ionic permeability was due to the reaction between zinc pigments and the alkyd resin. This interaction was confirmed by determining the zinc content in extracts obtained by milling together either zinc phosphate and the alkyd resin or zinc oxide with the alkyd binder for 24 hours. The extracts were dried at 110 °C, calcined to eliminate organic matter and diluted with hydrochloric acid (1+1). The zinc content was determined by atomic absorption and was found to be equal to 113 and 165 mg of zinc cation per gram of resin, respectively.

Considering Funke´s oppinion about the fact that the future of corrosion control by organic coatings more likely lies in developing the barrier properties of the coat **[15]**, the findings of this research are relevant.

Polarization resistance. As a general rule, it must be said that polarization resistance was higher than the ionic one, indicating that the pigment inhibited steel corrosion. Polarization resistance for paints 3 and 4 showed that the corrosion process was controlled by the high barrier effect due to the presence of a very impervious film; it stood higher than 0,5 $M\Omega.cm^{-2}$ during the test period and it was impossible to measure it accurately because of instrumental limitations.

Water vapour transmission

To obtain efficient anticorrosive paints it is necessary not only the addition of active anticorrosive pigments but also the reduction of water and oxygen permeability as much as possible. The reduction of water uptake avoids adhesion loss at the metal-coating interface diminishing, at the same time, undercutting and underfilm rusting of injured coatings. As far as the PVC/CPVC ratio is concerned all tested paints must have similar permeabilities **[14]**; however, paint 4 showed the lowest permeability to water vapour and paint 1 the highest one (Table IV). At the same time, paint 4 exhibited a very good performance in accelerated and electrochemical tests and paint 1 the poorest. This behaviour may be partially related to the capacity of coatings to restrain the passage of water vapour as time elapsed (Fig. 1); paint 4 showed the lowest weight loss as a function of time and paint 1 the highest, as it could be deduced from the slopes of the both curves.

Table IV

Water vapour transmission after 24 hours ($g\ m^{-2}$)

Paints	1	2	3	4
Water vapor transmision	0.10830	0.02259	0.04090	0.01066

The nature of the passive film

The variation of steel corrosion potential, as a function of time, in the presence of a calcium acid phosphate suspension (Fig. 4), showed that it inhibited steel corrosion and that caused potential shiftings towards more positive values with respect to zinc phosphate.

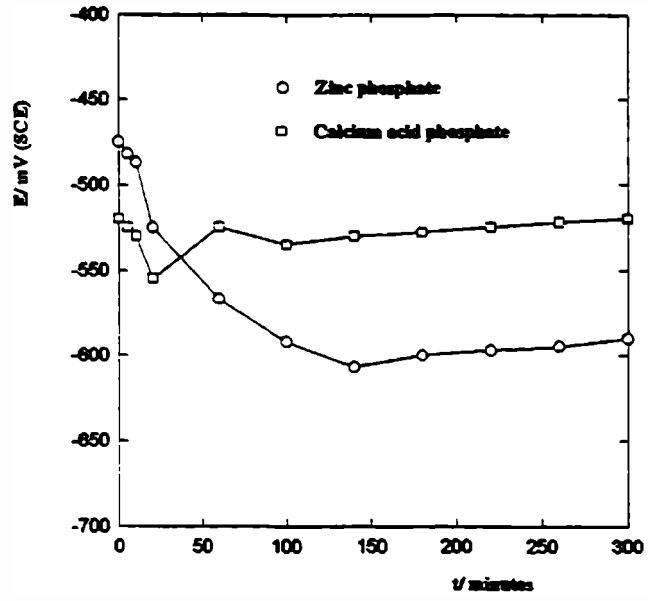

Fig. 4.- Corrosion potential of bare steel, as a function of the exposure time, in anticorrosive pigment suspensions in 0.5 M sodium perchlorate solution: a) zinc phosphate, b) calcium acid phosphate.

The steel plate kept in contact with the calcium acid phosphate suspension was examined by SEM and it was detected the formation of an ordered layer on the metallic surface (Fig.5). The EDAX analysis showed that the main component of the passive layer was Fe; Ca and P were encountered in very low proportions (less than 1%). This layer was identified by Mössbauer spectroscopy and the analysis of the spectrum revealed two types of interactions. One of them was a sextuple interaction corresponding to a magnetic material, in this case the base metal. The other was a doublet corresponding to a superparamagnetic phase with an isomer shift with respect to iron of 0.309 $\pm$ 0.2 mm/s (Fig.6). This phase was identified as an FeOOH **[16]** with a low crystallinity degree and a smaller particle size as it was deduced from the broad line observed in the spectrum.

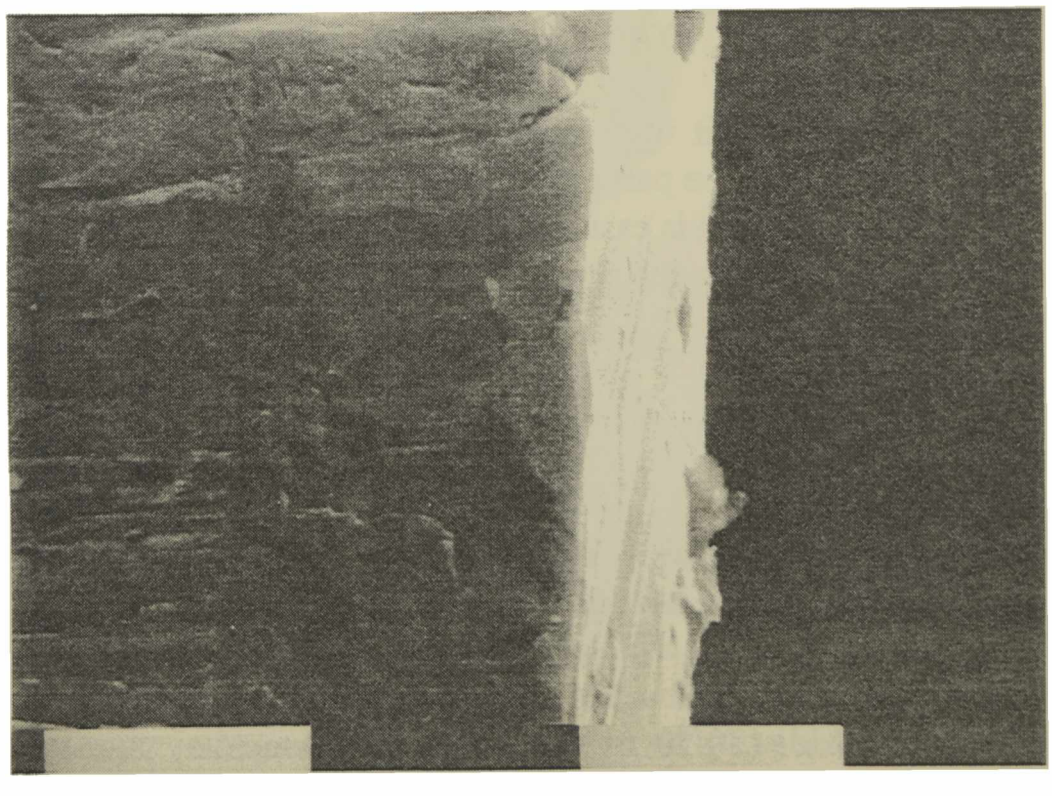

Fig. 5.- SEM photomicrograph of the passive layer formed on a steel substrate in a calcium acid phosphate suspension after 3 days exposure.

When the steel plate was put in contact with the calcium acid phosphate suspension, some loose products appeared at the bottom of the container. In order to know the nature of the whole set of products formed in the reaction between steel and calcium acid phosphate, a moistened mixture of iron powder and calcium acid phosphate was allowed to react during 2 weeks and the resulting products identified by IR spectrometry. The spectra revealed that ferric phosphate was formed (absorption bands at ~ 1050, 1100 and 1270 cm^{-1}).

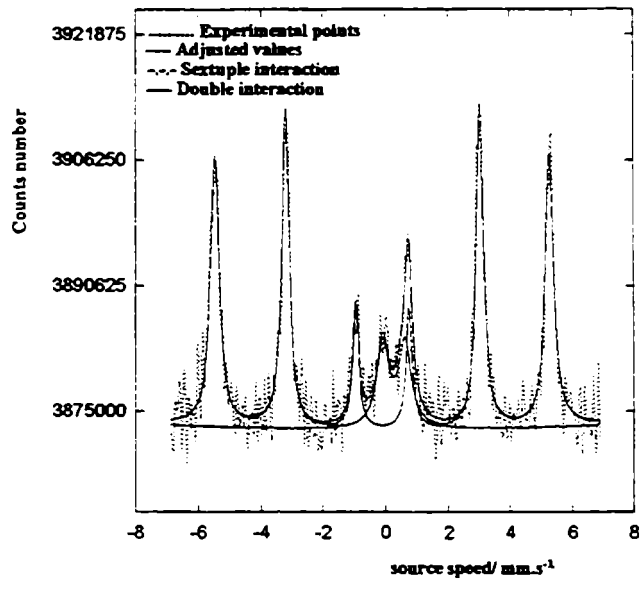

Fig. 6.- Mössbauer spectrum of the passive layer formed on a steel substrate in a calcium acid phosphate suspension after 3 days exposure.

The passive layer formed under the paint film was also examined by SEM (Figs 7a and 7b). Instead of the globular morphology of deletereous ferric oxide, a rather compact film was observed. It showed, at higher magnifications (5000X), the presence of crystals. The IR spectrum, obtained by scrapping corrosion products off the test panel, revealed the presence of ferric phosphate (absorption bands at ~ 1100 and 1270 cm^{-1}) and ferrous phosphate (absorption bands at ~ 743, 876, 1070 and 1270 cm^{-1}).

From these experiences it was concluded that the passive film is mainly composed of ferric oxyhydroxide which may be partially converted in ferric phosphate. Ferrous phosphate is an intermediate compound which is easily oxidized to ferric phosphate by atmospheric oxygen. Ferric phosphate was said to plug the pores of the ferric oxyhydroxide film **[6]**.

CONCLUSIONS

1) Calcium acid phosphate performance in anticorrosive paints was highly improved by incorporating suitable complementary pigments.

2) The best results were achieved when calcium acid phosphate was employed with calcium carbonate and zinc oxide (50/50, by volume) as complementary pigments.

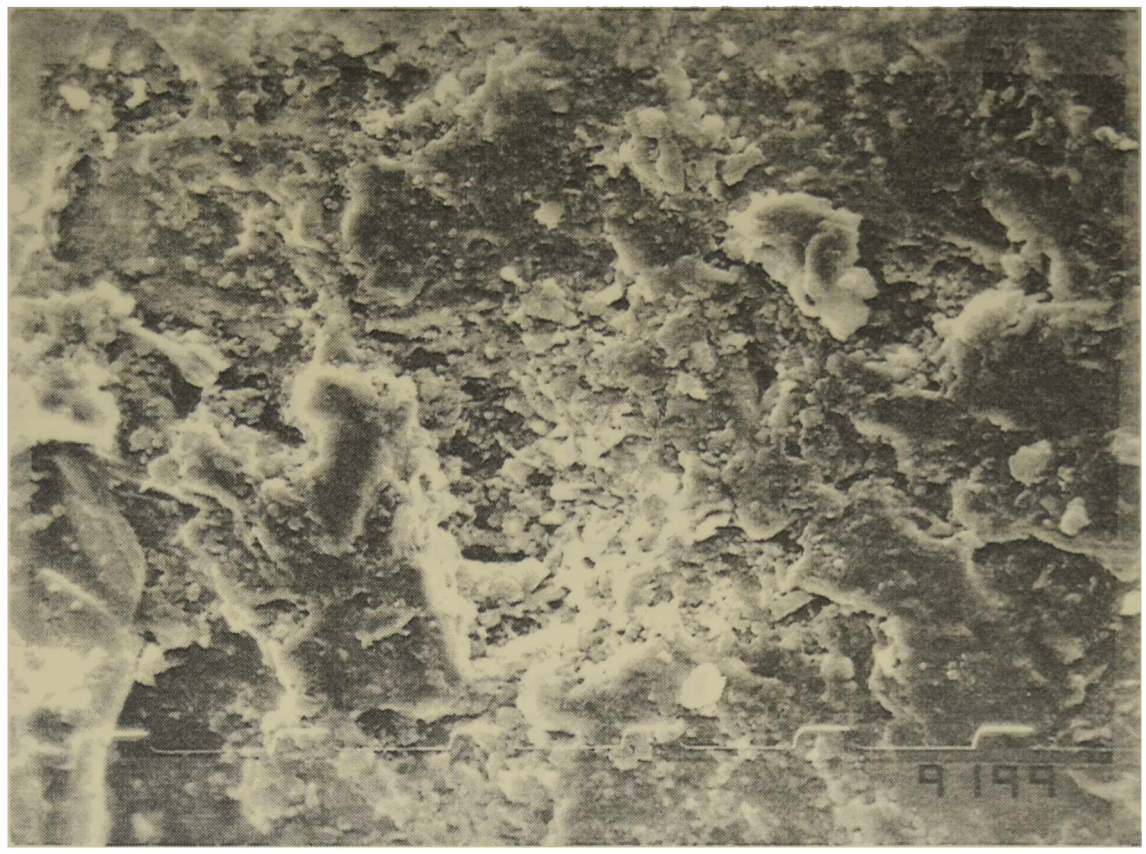

(a)

(b)

Fig. 7.- SEM photomicrograph of the passive layer formed on a steel substrate coated with an anticorrosive paint pigmented with calcium acid phosphate (Paint 4) after 720 exposure in the salt spray cabinet; a) 2000X, b) 5000X.

3) The improved anticorrosive performance was due to a combined effect: a higher barrier effect plus a more efficient passivation of steel substrate due to pH increase of the solution retained in the coating pores.

4) The passive film was to be composed of an ordered layer of ferric oxyhydroxide and small amounts of ferric phosphate.

ACKNOLEDGEMENTS

The authors are grateful to: CONICET (Consejo Nacional de Investigaciones Científicas y Técnicas) and CIC (Comisión de Investigaciones Científicas de la Provincia de Buenos Aires) for their sponsorship to do this research, Colores Hispania for providing the anticorrosive pigment and Polidur for suplying the alkyd resin. The authors also thanks to Professor Dr. Francisco Sánchez for his help in Mössbauer spectroscopy.

REFERENCES

[1] Bittner, A.- **J. Coat. Technol.**, **61** (777), 111 (1989).
[2] Cohen, M.- **Corrosion**, **32** (12), 461 (1976).
[3] Gerhard, A.; Bittner, A.- **J. Coat. Technol.**, **58** (740), 59 (1986).
[4] Meyer, G.- **Farbe+Lack**, **69** (7), 528 (1963).
[5] Meyer, G.- **Farbe+Lack**, **71** (2), 113 (1965).
[6] Pryor, M.J.; Cohen, M.- **J. Electrochem. Soc.**, **100,** 203 (1953).
[7] Romagnoli, R.; Vetere, V.F.- **Corrosion** (NACE), **51** (2), 116 (1995).
[8] Szklarska-Smialowska, Z.; Mankowsky, J.- **Br. Corrosion J., 4** (9), 271 (1969).
[9] Vetere, V.F.; Romagnoli, R.- **Br. Corros. J., 29** (2), 115 (1994).
[10] Romagnoli, R.; del Amo, B.; Vetere, V.F.- **Pitture e Vernici, 72** (10), 7 (1996).
[11] Sadtler Research Laboratories (Researchers, Editors an Publishers), Division of Bio-Rad Laboratories Inc. The Sadtler standard spectra. Inorganic and related compounds. USA 1976. vol.1 1K-300K; vol. 2 301K-600K; vol. 3 601K-900K, vol. 4 901K-1200K
[12] Giúdice, C.; Benítez, J.C.; Rascio, V.- **J. Oil Co. Chem. Assoc.**, **62** (3), 151 (1980).
[13] Szklarska-Smialowska, Z.; Staehle, R.W.- **J. Electrochem. Soc., 121** (11), 1393 (1974).
[14] Castells, R.C.; Meda, J.; Caprari, J.J.; Damia, M.- **J. Coat. Technol.**, **55** (707), 53 (1983).
[15] Funke, W.; Kendig, M,W.; Leidheiser, H. Jr. (Eds).- Proc. of the Symposium on Corrosion Protection by Coatings. vol.87-2. The Electrochemical Society, Pennington, NJ, 1987.
[16] Kundig, W.; Bommel, H.- **Phys. Rev., 142** (2), 327 (1966).

ANEXO

PUBLICACIONES CIENTIFICAS Y TECNICAS REALIZADAS POR EL CIDEPINT (Período 1993-1998)

SCIENTIFIC AND TECHNICAL PAPERS PUBLISHED BY CIDEPINT (Period 1993-1998)

PUBLICACIONES EN REVISTAS INTERNACIONALES DE LA ESPECIALIDAD

AÑO 1993

1. *Resistant lamellar micaceous iron oxides.*
   C.A. Giúdice.
   European Coatings Journal, (3), 134-144 (1993).

2. *Heavy duty offshore protection.*
   C.A. Giúdice.
   European Coatings Journal, (5), 344-354 (1993).

3. *Binders for marine paints.*
   A.R. Di Sarli.
   European Coatings Journal, (4), 252-258 (1993).

4. *Electrochemical testing of anticorrosion systems.*
   A.R. Di Sarli.
   European Coatings Journal, (10), 706-712 (1993).

5. *An electrochemical impedance spectroscopy study of zinc rich paints on steels in artificial sea water by a transmission line model.*
   S.G. Real, A.C. Elías, J.R. Vilche, C.A. Gervasi, A.R. Di Sarli.
   Electrochimica Acta, **38**, 2029-2035 (1993).

6. *The use of electrochemical impedance measurements to assess the performance of organic coating systems on naval steel.*
   E. Cavalcanti, O. Ferraz, A.R. Di Sarli.
   Progress in Organic Coatings, **23**, 183-198 (1993).

7. *Evaporation of the liquid phase during drying of oleoresinous emulsion binders.*
   J.J. Caprari, O. Slutzky, P. Pessi.
   Pitture e Vernici, **69** (9). 17-20 (1993).

8. *A phenomenological approach to ionic mass transfer at rotating disc electrodes with a hanging column of electrolyte solutions.*
   C.I. Elsner, P.P. Schilardi, S.L. Marchiano.
   Journal of Applied Electrochemistry, **23**, 1181-1186 (1993).

9. *Kinetics of the electroreduction of anodically formed cadmium oxide layers in alkaline solutions.*
   J.I. de Urraza, C.A. Gervasi, S.B. Saidman, J.R. Vilche.
   Journal of Applied Electrochemistry, **23**, 1207-1213 (1993).

10. *The mechanism of the anti-corrosive action of zinc ethyl silicate paints.*
    R. Romagnoli, V.F. Vetere.
    Journal of the Oil and Colour Chemists' Association, **76**, 208-213 (1993).

11. *Halomethanes in tri-n-octyllamine and squalane mixtures at infinite dilution.*
R.C. Castells, E.L. Arancibia, A.M. Nardillo.
Journal of Solution Chemistry, **22**, 85-94 (1993).

12. *Use of EIS to characterize the performance of naval steel/organic coating systems in NaCl solution.*
A.R. Di Sarli, E. Cavalcanti, O. Ferraz.
Corrosion Prevention and Control, **40** (3), 66-70 (1993).

13. *Development of a mathematical treatment for electrochemical impedance data obtained from coated metals: Part 2.*
V. Ambrosi, A. Di Sarli.
Anti-Corrosion, October, 9-13 (1993).

14. *Binder dissolution in antifoulings.*
C.A. Giúdice, D.B. del Amo.
European Coatings Journal, (1-2), 16-23 (1993).

AÑO 1994

15. *Zinc hydroxy phosphite for corrosion protection.*
C.A. Giúdice, D.B. del Amo.
European Coatings Journal, (7-8), 490-496 (1994).

16. *The role of calcium acid phosphate as a corrosion inhibitive pigment.*
V.F. Vetere, R. Romagnoli.
British Corrosion Journal, **29** (2), 115-119 (1994).

17. *Adhesion of lamelar iron oxide vinyl paints.*
C.A. Giúdice, B. del Amo.
European Coatings Journal, (5), 292-299 (1994).

18. *Pulsating diffusional boundary layers. III. A redox electrochemical reaction under intermediate kinetics control involving soluble species in solution. Theory and experimental test.*
C.I. Elsner, L. Rebollo Neira, W.A. Egli, S.L. Marchiano, A. Plastino, A.J. Arvía.
Acta Chimica Hungarica - Models in Chemistry, **131** (2), 121 (1994).

19. *The influence of cathodic currents on biofouling attachment to painted metals.*
M. Pérez, C.A. Gervasi, R. Armas, M.E. Stupak, A.R. Di Sarli.
Biofouling, **8**, 27-34 (1994).

20. *Evaluation of electrical and electrochemical parameters for painted steel/artificial sea water systems by using EIS.*
V. Ambrosi, A.R. Di Sarli.
Bulletin of Electrochemistry, **10** (2-3), 91-95 (1994).

21. *The excess enthalpies of (dinitrogen oxide + toluene) at the temperature 313.15 K and at pressures from 7.60 MPa to 15.00 MPa.*
R.C. Castells, C. Menduina, C. Pando, J.A.R. Renuncio.
Journal of Chemical Thermodynamics, **26**, 641 (1994).

22. *Fireproof pigments in flame retardant paints.*
B. del Amo, C.A. Giúdice.
European Coatings Journal, (11), 826-832 (1994).

23. *Influence of the composition of zinc-ethyl silicate paints.*
R. Romagnoli, V.F. Vetere, R.A. Armas.
Journal of Applied Electrochemistry, **24**, 1013-1018 (1994).

24. *Rheology of pigment dispersion during paint manufacture.*
C.A. Giúdice, J.C. Benítez.
Pitture e Vernici, **11**, 33-36 (1994).

25. *Comparison between electrochemical impedance and salt spray tests in evaluating the barrier effect of epoxy paints.*
C.I. Elsner, A.R. Di Sarli.
Journal of the Brazilian Chemical Society, **51**, 15-18 (1994).

26. *The corrosion protection of steel in sea water using zinc rich alkyd paints. An assessment of the pigment-content effect by EIS.*
C.A. Gervasi, A.R. Di Sarli, E. Cavalcanti, O. Ferraz, E.C. Bucharsky, S.G. Real, J.R.Vilche.
Corrosion Science, **36**, 1963-1972 (1994).

27. *Elektrochemische und in situ Rastertunnelmikroskopische Untersuchungen in den systemen HOPG(0001)/Ag^{+}.*
G.A. Gervasi, R.T. Põtzschke, G. Staikov, V.J. Lorenz.
Wiss. AbschluBber. Int. Sem. Univ. Karlsruhe, **29**, 34-46 (1994).

28. *Corrosión en la Industria Naval. Guía Práctica de la Corrosión.*
V. Rascio
CYTED - Programa Iberoamericano de Ciencia y Tecnología para el Desarrollo. 32 pp (1994).

29. *Excess molar enthalpies of nitrous oxide-toluene in the liquid and supercritical regions.*
R.C. Castells, C. Meduina, C. Pando, J.A.R. Renuncio.
J. Chem. Soc. Faraday Trans., **90**, 2677-2681 (1994).

30. *Pinturas antiincrustantes vinílicas tipo alto espesor basadas en resina colofonia desproporcionada.*
J.C. Benítez, C.A. Giúdice.
Rivista di Merceología, **33** (I), 1-15 (1994).

AÑO 1995

31. *Evaluation of zinc rich paint coatings performance by electrochemical impedance spectroscopy.*
E.C. Bucharsky, S.G. Real, J.R. Vilche, A.R. Di Sarli, C.A. Gervasi.
Journal of the Brazilian Chemical Society, **6** (1), 39-42 (1995).

32. *Heterogeneous reaction between steel and zinc phosphate.*
R. Romagnoli, V.F. Vetere.
Corrosion (NACE), **51**, 116-122 (1995).

33. *The characterization of protective properties for some naval steel/polymeric coatings/3% NaCl solution systems by EIS and visual assessment.*
O. Ferraz, E. Cavalcanti, A.R. Di Sarli.
Corrosion Science, **38** (8), 1267-1289 (1995).

34. *Electrochemical evaluation of the oxygen permeability for anticorrosive coating films.*
C.I. Elsner, R.A. Armas, A.R. Di Sarli.
Portugaliæ Electrochimica Acta, **13**, 5-18 (1995).

35. *Corrosion monitoring of ZRP on steel by EIS to evaluate the performance of different coating formulation.*
C.A. Gervasi, R. Armas, A.R. Di Sarli, E.C. Bucharsky, S.G. Real, J.R. Vilche.
Materials Science Forum, **192-194**, 357-362 (1995).

36. *Non-pollutant inhibitive pigments: Zinc phosphate and modified zinc phosphate. A review.*
R. Romagnoli, V.F. Vetere.
Corrosion Reviews, **13** (1), 45-64 (1995).

37. *Coatings for corrosion prevention of seawater structures.*
C.A. Giúdice, J.C. Benítez.
Corrosion Reviews, **13** (2-4), 81-190 (1995).

38. *Infinite dilution activity coefficients of hydrocarbons in tetra-n-alkyltin solvents between 313.15 K measured by gas-liquid chromatography.*
R.C. Castells, C.B. Castells.
Journal of Solution Chemistry, **24**, 285 (1995).

39. *Excess enthalpies of nitrous oxide+ pentane at 308.15 K from 6.64 to 12.27 MPa.*
J.A.R. Renuncio, C. Pando, C. Menduiña, R.C.Castells.
Journal of Chemical Engineering Data, **40**, 642 (1995).

40. *Thermodynamic consideration of the retention mechanism in a poly(perfluoroalkyl ether) gas chromatographic stationary phase used in packed columns.*
R.C. Castells, L.M.Romero, A.M. Nardillo.
Journal of Chromatography, **715**, 299 (1995).

41. *Separation of low-boiling pyridine bases by gas chromatography.*
M.C. Titón, A.M. Nardillo.
Journal of Chromatography, **699**, 403-407 (1995).

42. *Electrochemical characterization of anodic passive layers on cobalt.*
E.B. Castro,C.A. Gervasi, J.R. Vilche,C.P. Fonseca.
Journal of the Brazilian Chemical Society, **6** (1), 43-47 (1995).

AÑO 1996

43. *Semicontinuous emulsion polymerization of methyl methacrylate, ethyl acrylate, and methacrylic acid.*
J.I. Amalvy.
Journal of Applied Polymer Science, **59**, 339-344 (1996).

44. *High build antifouling paints based on disproportionated calcium resinate.*
C.A. Giúdice, J.C. Benítez.
Corrosion Reviews, "Special Issue on Industrial Paints for Corrosion Control", **14** (1-2), 1-14 (1996).

45. *Anticorrosive paints with flame retardant properties.*
C.A. Giúdice, B. del Amo.
Corrosion Reviews, "Special Issue on Industrial Paints for Corrosion Control", **14** (1-2), 35-46 (1996).

46. *Influence of the hydrolysis degree of the binder on the electrochemical properties of zinc-ethyl silicate paints.*
R. Romagnoli, C.A. Aznar, V.F. Vetere.
Corrosion Reviews, "Special Issue on Industrial Paints for Corrosion Control", **14** (1-2), 59-71 (1996).

47. *Macrofouling community at Mar del Plata harbor along a year (1991-1992).*
S. Pezzani, M. Pérez, M. Stupak.
Corrosion Reviews, "Special Issue on Industrial Paints for Corrosion Control", **14** (1-2), 73-86 (1996).

48. *Study of commercially available epoxy protective coatings by using non-destructive electrochemical techniques.*
P.R. Seré, D.M. Santágata, A.R. Di Sarli, C.I. Elsner.
Corrosion Reviews, "Special Issue on Industrial Paints for Corrosion Control", **14** (1-2), 87-97 (1996).

49. *Application of powder coatings. A bibliographic review to obtain a calculation system for the design of a conventional fluidized bed.*
J.J. Caprari, A.J. Damia, M.P. Damia, O. Slutzky.
Corrosion Reviews, "Special Issue on Industrial Paints for Corrosion Control", **14** (1-2), 99-120 (1996).

50. *Study of the anticorrosive properties of micronized zinc phosphate and zinc molybdophosphate in alkydic paints.*
D.B. del Amo, R. Romagnoli, V.F. Vetere.
Corrosion Reviews, "Special Issue on Industrial Paints for Corrosion Control", **14** (1-2), 121-133 (1996).

51. *Effect of the cathodic protection on coated steel/artificial sea water systems.*
D.M. Santágata, C. Morzilli, C.I. Elsner, A.R. Di Sarli.
Corrosion Reviews, "Special Issue on Industrial Paints for Corrosion Control", **14** (1-2), 135-144 (1996).

52. *Preliminary study of the biofouling of the Parana river (Argentina).*
M.E. Stupak, M.C. Pérez, M.T. García, E. García Solá, A. Leiva Azuaga, A. Mendivil, G. Niveyro.
Corrosion Reviews, "Special Issue on Industrial Paints for Corrosion Control", **14** (1-2), 145-155 (1996).

53. *The surface condition effect on adhesion and corrosion resistance of carbon steel/chlorinated rubber/artificial sea water systems.*
P.R. Seré, A.R. Armas, C.I. Elsner, A.R. Di Sarli.
Corrosion Science, **38** (6), 853-866 (1996).

54. *Influence of aluminium pretreatment on coating adhesion.*
C.A. Giúdice, B. del Amo, M. Morcillo Linares.
Corrosion Prevention and Control, **43** (1), 15-20 (1996).

55. *Coating systems for underwater protection.*
C.A. Giúdice, B. del Amo.
Corrosion Prevention and Control, **43** (2), 43-47 (1996).

56. *Activity coefficients of hydrocarbons at infinite dilution in di-n-octyltin dichloride. Comparison with results obtained in other alkyltin solvents.*
A.M. Nardillo, B.M. Soria, C.B. Castells, R.C. Castells.
Journal of Solution Chemistry, **25,** 369 (1996).

57. *Gas chromatographic separation of low-boiling pyridine bases.*
M.C. Titon, F.R. González, A.M. Nardillo.
Chromatographia, **42**, 465 (1996).

58. *Thermodynamics of solutions of hydrocarbons in low molecular weight poly(isobutylene): a gas chromatographic study.*
R.C. Castells, L.M. Romero, A.M. Nardillo.
Macromolecules, **29**, 4278 (1996).

59. *Vibrational spectroscopic study of distribution of sodium dodecyl sulfate in latex films.*
J.I. Amalvy, D.B. Soria.
Progress in Organic Coatings, **28**, 279-283 (1996).

60. *The influence of electrolyte composition on the diffusion process through chlorinated-rubber and vinyl films.*
C.I. Elsner, A.R. Di Sarli
Corrosion Prevention and Control, **43** (5), 124-130 (1996).

61. *Analisi comparativa dei pigmenti inorganici a base di fosfati nei p.v. anticorrosivi alchidici.*
R. Romagnoli, B. del Amo, V.F. Vetere
Pitture e Vernici, **72** (10), 7-11 (1996).

62. *Evaluation of theoretical models of non electrolyte solutions in the prediction of Kováts retention indices of branched alkanes in alkane stationary phases.*
C.B. Castells, R.C. Castells
Journal of Chromatography, **755**. 49-55 (1996).

AÑO 1997

63. *Flow properties of acrylic latices.*
J.I. Amalvy, B. del Amo.
Surface Coatings International (JOCCA), **80** (2), 78-82 (1997).

64. *Lamellar zinc-rich epoxy primers.*
C. Giúdice, J. Benítez, M.M. Linares
Surface Coatings International (JOCCA), **80** (6), 279-284 (1997).

65. *Solubility and toxic effect of the cuprous thiocyanate antifouling pigment on barnacle larvae.*
V.F. Vetere, M.C. Pérez, R. Romagnoli, M.E. Stupak, B. del Amo.
Journal of Coatings Technology, **69** (866), 39-45 (1997).

66. *Study of formulation variables of thermoplastic reflecting materials for traffic marking.*
A.C. Aznar, J.J. Caprari, J.F. Meda, O. Slutzky.
Journal of Coatings Technology, **69** (868), 33-38 (1997).

67. *Efecto del tipo y cantidad de plastificante sobre las propiedades de barrera de los film de barniz.*
C.I. Elsner, A.R. Di Sarli.
Pitture e Vernici, **73** (3), 11-17 (1997).

68. *High-build soluble matrix antifouling paints tested on raft and ship's bottom.*
V.J.D. Rascio, C.A. Giúdice, D.B. del Amo.
Pitture e Vernici, **73** (9), 27-38 (1997).

69. *Manufacture and testing of water-based tannic pretreatment.*
C.A. Giúdice, J.C. Benítez, M.L. Tonello.
Pitture e Vernici, **73** (11), 10-16 (1997).

70. *Extraction and characterisation of quebracho (Schinopsis sp.) tannins.*
M.L. Tonello, C.A. Giúdice, J.C. Benítez.
Pitture e Vernici, **73** (14), 9-16 (1997).

71. *Study of intermetallic phases growth in a hot-dip galvanized process by SEM.*
P.R. Seré, D. Culcasi, C.I. Elsner, A.R. Di Sarli.
The Journal of Scanning Microscopies, **19** (3), 244-45 (1997).

72. *Barrier protection of steel surfaces by a varnish coat. An electrochemical monitoring.*
A.R. Di Sarli.
Bulletin of Electrochemistry, **13** (6), 253-256 (1997).

73. *Reactive surfactants in heterophase polymerization. VIII. Emulsion polymerization of alkyl sulfopropyl maleates with styrene.*
H.A.S. Schoonbrood, M.J. Unzué, J.I. Amalvy, J.M. Asua.
Journal of Polymer Science Part A. Polymer Chemistry, **35** (13), 2561-2568 (1997).

74. *Influence of differences between sample and mobile phase viscosities on the shape of chromatographic elution profiles.*
R.C. Castells, C.B. Castells, M.A. Castillo.
Journal of Chromatography A, **775**, 73 (1997).

75. *Theoretical and practical aspects in flow control in programmed-temperature gas chromatography.*
F.R. González, A.M. Nardillo.
Journal of Chromatography A, **757**, 97 (1997).

76. *Retention in multistep programmed-temperature gas chromatography and flow control. Linear head pressure programs.*
F.R. González, A.M. Nardillo.
Journal of Chromatography A, **757**, 109 (1997).

77. *Integration of the equation of peak motion in programmed-pressure and -temperature gas chromatography.*
F.R. González, A.M. Nardillo.
Journal of Chromatography A, **766**, 147 (1997).

78. *Concurrent solution and adsorption of hydrocarbons in gas chromatographic columns packed with different loadings of 3-methylsydnone on chromosorb P.*
R.C. Castells, L.M. Romero, A.M. Nardillo.
Journal of Colloid Interface Science, **192**, 142 (1997).

79. *Aspects of the elution order inversion by pressure changes in programmed-temperature gas chromatography*
F.R. González, A.M. Nardillo
Journal of Chromatography A, **779**, 263-274 (1997).

80. *Mass transport processes through chlorinated rubber films.*
C.I. Elsner, P.R. Seré, A.R. Di Sarli.
European Coatings Journal, **12**, 1136-1140 (1997).

81. *Dilute-solution viscosimetry of carboxylated acrylic latices.*
J.I. Amalvy
Pigment & Resin Technology, **26** (6), 363-369 (1997).

82. *Factores que afectan a la estructura de los recubrimientos de cinc obtenidos por inmersión*
P.R. Seré, J.D. Culcasi, C.I. Elsner y A.R. Di Sarli.
Revista de Metalurgia, **33** (6), 376-381 (1997).

AÑO 1998

83. *Phosphorous-based intumescent coatings*
J.C. Benítez, C.A. Giúdice
European Coatings Journal, **1-2**, 52-59 (1998).

84. *Evaluation, using EIS, of anticorrosive paints pigmented with zinc phosphate*
L.S. Hernández, G. García, C. López, B del Amo, R. Romagnoli
Surface Coatings International, **81** (1), 19-25 (1998).

85. *The influence of the method of application of the paint on the corrosion of the substrate as assessed by ASTM and electrochemical method*
P.R. Seré, D.M. Santágata, C.I. Elsner, A.R. Di Sarli
Surface Coatings International, **81** (3), 128-134 (1998).

86. *Study of the anticorrosive properties of zinc phosphate in vinyl paints*
B. Del Amo, R. Romagnoli, V.F. Vetere, L.S. Hernández.
Progress in Organic Coatings, **33** (1), 28-35 (1998).

87. *Evaluation of the surface treatment effect on the corrosion performance of paint coated carbon steel*
D.M. Santágata, P.R. Seré, C.I. Elsner, A.R. Di Sarli
Progress In Organic Coatings, **33**, 44-54 (1998).

88. *Colloidal and film properties of carboxylated acrylic latices-affect of surfactant concentration*
J.I. Amalvy
Pigment & Resin Technology, **27** (1), 20-27 (1998).

PUBLICACIONES EN PROCEEDINGS DE CONGRESOS Y REUNIONES CIENTIFICAS

AÑO 1993

1. *Algunas variables que influyen sobre la concentración crítica de pigmento en volumen (CPVC) de una pintura anticorrosiva.*
   J.C. Benítez, C.A. Giúdice.
   Anales de las II Jornadas Argentinas en Ciencia de los Materiales, I, 53-56 (1993).

2. *Reología en pinturas. Esfuerzo de corte involucrado en el fenómeno de escurrimiento.*
   B. del Amo, J.C. Benítez.
   Anales de las II Jornadas Argentinas en Ciencia de los Materiales, I, 57-60 (1993).

AÑO 1994

3. *Influencia del electrolito en los procesos difusionales a través de películas de pintura.*
   C.I. Elsner, R.A. Armas, A.R. Di Sarli.
   Anales de las Jornadas SAM'94, Bahía Blanca, Argentina, 7-10 de junio (1994).

4. *An EIS analysis of gradual deterioration of zinc rich paint coatings in sea water by a transmission line model.*
   S.G. Real, J.R. Vilche, C.A. Gervasi, A.R. Di Sarli.
   Symposium on Electrochemical Impedance Analysis of Geometrically Awkward and Mathematically Complex Structures, San Francisco, California, EE.UU., 22-27 de mayo (1994).

5. *Derniers developpements en peintures antisalissures autopolissantes en Argentine.*
   J.C. Benítez, C.A. Giúdice, V. Rascio.
   Proceedings 22nd FATIPEC Congress, Vol. III, 214-225 (1994).

6. *Propiedades físicas y mecánicas de productos para la impermeabilización de mampostería y mortero.*
   A.C. Aznar, J.J. Caprari, J.F. Meda.
   Anales 1° Simposio Argentino de Impermeabilización, Mar del Plata, 17-18 de noviembre, pp. 35-44 (1994).

AÑO 1995

7. *Correlación de parámetros magnéticos con la concentración de óxido ferroso en sedimentos cuaternarios de la localidad de Hernández, La Plata, Provincia de Buenos Aires.*
   J.C. Bidegain, R.R. Iasi, R.H. Pérez, R. Pavlicevic.
   Anales Cuartas Jornadas Geológicas y Geofísicas Boanerenses, Junín, 15-17 de noviembre (1995).

8. *Influence of binders used in the formulation of zinc rich paints (ZRP) on the performance of the final coatings on naval steel in sea water.*
   J.R. Vilche, E.C. Bucharsky, S.G. Real, A.R. Di Sarli.
   Proceedings Symposium on Marine Corrosion (T-7C), NACE, Orlando, Florida, EE.UU., 26-31 de marzo (1995).

9. *Electrochemical testing to assess some protective properties of vinyl coatings.*
   E. Cavalcanti, P. Seré, E.I. Elsner, A.R. Di Sarli.
   Proceedings 18° Congreso Brasilero de Corrosión, Río de Janeiro, Brasil, 20-24 de noviembre (1995).

10. *Electrochemical evaluation of steel/plasticized chlorinated rubber/sea water systems.*
    E. Cavalcanti, O. Ferraz, C.I. Elsner, A.R. Di Sarli.
    Proceedings 18° Congreso Brasilero de Corrosión, Río de Janeiro, Brasil, 20-24 de noviembre (1995).

AÑO 1996

11. *Evaluación electroquímica de los criterios de protección catódica del acero en el hormigón.*
    V.F. Vetere, R.O. Batic, R. Romagnoli, I.T. Lucchini, J.D. Sota, R.O. Carbonari
    Anales Jornadas SAM'96, San Salvador de Jujuy, Argentina, 11-14 de junio (1996)

12. *Evaluación química y electroquímica de taninos y de imprimaciones acuosas a base de taninos.*
    V.F. Vetere, R. Romagnoli
    Anales Jornadas SAM'96, San Salvador de Jujuy, Argentina, 11-14 de junio (1996)

13. *Protección anticorrosiva por medio de imprimaciones reactivas a base de taninos.*
    V.F. Vetere, R. Romagnoli, J.I. Amalvy, O.R. Pardini
    Anales VII Jornadas Argentinas de Corrosión y Protección, Mendoza, Argentina, 17-19 de setiembre (1996).

14. *Variación de la adherencia en la interfase acero-mortero de cemento portland en probetas protegidas catódicamente en función del sobre potencial aplicado.*
    R.O. Batic, V.F. Vetere, R. Romagnoli, J.D. Sota, R.O. Carbonari, I.T. Lucchini
    Anales VII Jornadas Argentinas de Corrosión y Protección, Mendoza, Argentina, 17-19 de setiembre (1996).

15. *Evaluación de modelos teóricos de soluciones de no-electrolitos en la predicción de índices de retención de Kováts de parafinas en escualano.*
R.C. Castells, C.B. Castells
Anales XXI Congreso Argentino de Química, Bahía Blanca, Argentina, 18-20 de setiembre (1996).

16. *Efecto de la diferencia de viscosidad entre la fase móvil y el pulso inyectado sobre el perfil de elución de un pico de cromatografía líquida.*
R.C. Castells, C.B. Castells
Anales XXI Congreso Argentino de Química, Bahía Blanca, Argentina, 18-20 de setiembre (1996).

17. *Cromatografía gaseosa con temperatura y presión programadas en etapas múltiples.*
F.R. González, A.M. Nardillo
Anales XXI Congreso Argentino de Química, Bahía Blanca, Argentina, 18-20 de setiembre (1996).

18. *Control de la corrosión de estructuras metálicas en ambientes agresivos por medio de sistemas de recubrimiento.*
V. Rascio
Anales Jornadas Especializadas sobre la Corrosión, Buenos Aires, Argentina, 5-6 de setiembre (1996).

19. *Susceptibilidad magnética y concentraciones de FeO en Loess y paleosuelos cuaternarios como indicadores de cambios paleoambientales y paleoclimáticos.*
J.C. Bidegain, R. Pavlicevic, R.R. Iasi, R.H. Pérez
Anales III Congreso de Exploración de Hidrocarburos, Buenos Aires, Argentina, 13-18 de octubre (1996).

20. *Comportamiento anticorrosivo de pinturas vinílicas pigmentadas con fosfato de cinc.*
B. del Amo, R. Romagnoli, V.F. Vetere, L.S. Hernández
Anales XII Congreso Iberoamericano de Electroquímica y IX Encuentro Venezolano de Electroquímica, Mérida, Venezuela, 24-29 de marzo (1996).

21. *Recent developments in miniemulsion polymerization.*
I. Aizpurua, J.I. Amalvy, M.J. Barandiaran, J.C. de la Cal, J.M. Asua
Proceedings IUPAC 2nd International Symposium on Free Radical Polymerization: Kinetics and Mechanisms, Santa Margherita Ligure, Génova, Italia, 26-31 de mayo (1996).

22. *Anticorrosive behavior of paints pigmented with zinc phosphate with EIS.*
B. del Amo, L.S. Hernández, C. López
Proceedings Simposio 13 del International Materials Research Congress, Cancún, México, 1-6 de setiembre (1996).

23. *New trends in industrial painting.*
V. Rascio
Proceedings 2nd NACE Latin American Region Corrosion Congress, Rio de Janeiro, Brasil, 9-13 de setiembre (1996).

24. *The use of polymerisable surfactants in emulsion copolymerisation for coatings application.*
J.I. Amalvy, M.J. Unzué, H.A.S. Schoonbrood, J.M. Asua
Proceedings 16th Conference on Waterborne, High Solids and Radcure Technologies, Frankfurt, Alemania, 11-13 de noviembre (1996).

AÑO 1997

25. *Influencia de los parámetros del proceso de galvanizado por inmersión sobre el crecimiento de cristales de cinc.*
J.D. Culcasi, P.R. Seré, C.I. Elsner, A.R. Di Sarli
Jornadas SAM'97 y 1° Taller Nacional sobre Materiales para la Construcción, Tandil, 14-16 de mayo de 1997.

26. *Influencia del electrolito sobre la protección catódica del acero por recubrimientos metálicos de base Zn.*
C.I. Elsner, P.R. Seré, J.D. Culcasi, A.R. Di Sarli
Jornadas SAM'97 y 1° Taller Nacional sobre Materiales para la Construcción, Tandil, 14-16 de mayo de 1997.

27. *Desarrollo de un simulador del proceso de galvanizado por inmersión.*
P.R. Seré, G.W. Mugica, J.D. Culcasi
Jornadas SAM'97 y 1° Taller Nacional sobre Materiales para la Construcción, Tandil, 14-16 de mayo de 1997.

28. *Efecto de los parámetros del proceso y de la rugosidad superficial del acero base sobre la microestructura del acero galvanizado por inmersión.*
P.R. Seré, J.D. Culcasi, C.I. Elsner, A.R. Di Sarli
Jornadas SAM'97 y 1° Taller Nacional sobre Materiales para la Construcción, Tandil, 14-16 de mayo de 1997.

29. *The performance of zinc molybdenum phosphate in anticorrosive paints measured by accelerated and electrochemical tests.*
D.B. del Amo, R. Romagnoli, V.F. Vetere
Proccedings 1997 Joint International Meeting de ISE y The Electrochemistry Society, Paris, Francia, 31 de agosto al 5 de setiembre de 1997.

AÑO 1998

30. *Evaluation of non toxic alkyd primers by electrochemical impedance spectroscopy*
L.S. Hernández, G. García, B. del Amo, R. Romagnoli, C. López
Corrosion 98 NACE, San Diego, del 23 al 27 de marzo de 1998.

31. Evaluación de la capacidad protectora del sistema dúplex (galvanizado pintado)
P.R. Seré, C.I. Elsner, A.R. Di Sarli
XIII Congreso de la Sociedad Iberoamericana de Electroquímica, Reñaca, Viña del Mar, Chile del 29 de marzo al 3 de abril de 1998.

32. *Estudio por EIS del comportamiento frente a la corrosión de recubrimientos de cinc*
P.R. Seré, J.D. Culcasi, C.I. Elsner, A.R. Di Sarli
XIII Congreso de la Sociedad Iberoamericana de Electroquímica, Reñaca, Viña del Mar, Chile del 29 de marzo al 3 de abril de 1998.

33. *Study of zinc crystals orientation effect on the corrosion behavior*
J.D. Culcasi, P.R. Seré, C.I. Elsner, A.R. Di Sarli
Scanning 98, Baltimore, Maryland, USA del 9 al 12 de mayo de 1998.

34. *Study of the corrosion process at the galvanized steel/organic coating interface*
P.R. Seré, J.D. Culcasi, C.I. Elsner, A.R. Di Sarli
Scanning 98, Baltimore, Maryland, USA del 9 al 12 de mayo de 1998.

35. *Análisis de la interfase acero-mortero en probetas polarizadas catódicamente*
R. Romagnoli, V.F. Vetere, J.D. Sota, P.J. Maiza, I.T. Lucchini, O.R. Batic.
1st International Congress of Concrete Technology, Bauen Hotel, Buenos Aires, Argentina, del 1 al 4 de junio de 1998.

36. *Modificación del circuito de corriente impresa para protección catódica para un mejor control del potencial en la interfase acero-mortero*
V.F. Vetere, R. Romagnoli, J.D. Sota, I.T. Lucchini, R.O. Carbonari, O.R. Batic.
1st International Congress of Concrete Technology, Bauen Hotel, Buenos Aires, Argentina, del 1 al 4 de junio de 1998.

37. *Variación de la adherencia en la interfase acero-mortero en probetas polarizadas catódicamente durante dos años*
O.R. Batic, R. Romagnoli, V.F. Vetere, J.D. Sota, I.T. Lucchini, R.O. Carbonari.
1st International Congress of Concrete Technology, Bauen Hotel, Buenos Aires, Argentina, del 1 al 4 de junio de 1998.

38. *Steel corrosion protection by means of alkyd paints pigmented with calcium acid phosphate*
B. del Amo, R. Romagnoli, V. Vetere.
3rd NACE Latin American Region Corrosion Congress, Cancún, del 30 de agosto al 4 de setiembre de 1998.

39. *High performance anticorrosive epoxy paints pigmented with zinc molybdenum steel corrosion protection by means of alkyd paints pigmented with calcium acid phosphate*
R. Romagnoli, B. del Amo, V.F. Vetere, L. Veleva.
3rd NACE Latin American Region Corrosion Congress, Cancún, del 30 de agosto al 4 de setiembre de 1998.

40. *Evaluation of the Corrosion behaviour of painted steel/Zn on 55 % Al-Zn systems in salt spray*
P. Seré, C. I. Elsner, A. R. Di Sarli
3rd NACE Latin American Region Corrosion Congress, Cancún, del 30 de agosto al 4 de setiembre de 1998.

PUBLICACIONES EN REVISTAS NACIONALES Y EN CIDEPINT-ANALES

AÑO 1993

1. *Pinturas antiincrustantes basadas en resinas colofonia y colofonia modificada, esterificadas con óxido de tributil estaño*
   J.J. Caprari, O. Slutzky
   CIDEPINT-Anales, 49-59 (1993).

2. *Chemical and biocidal properties of the cuprous thiocyanate antifouling pigment.*
   V.F. Vetere, M.C. Pérez, R. Romagnoli, M.E. Stupak
   CIDEPINT-Anales, 161-172 (1993).

3. *Los fondos dificiles... Pintado y protección del acero galvanizado*
   B. del Amo.
   Color y Textura, **31**, 8-10 (1993).

AÑO 1994

4. *Propuesta de un método para la determinación de tensión de adhesión y cohesión de materiales termoplásticos para la demarcación de pavimentos.*
   A.C. Aznar.
   CIDEPINT-Anales, 215-226 (1994).

5. *Pinturas. Aspectos ecológicos relacionados con su empleo. Impacto ambiental producido por los disolventes, componentes del ligante y aditivos.*
   J.J. Caprari.
   CIDEPINT-Anales, 227-248 (1994).

6. *Velocidad de evaporación de la fase líquida durante el proceso de secado de ligantes oleorresinosos emulsionados.*
   J.J. Caprari, O. Slutzky, P.L. Pessi.
   Color y Textura, **32**, 15-18 (1994).

7. *Gas chromatography of aliphatic amines on diatomaceous solid supports modified by adsorption and crosslinking of polyethyleneimines.*
   A.M. Nardillo, R.C. Castells.
   Anales de la Asociación Química Argentina, **82** (5), 337-345 (1994).

8. *Estudio de la fase líquida de morteros afectados por la reacción alcali agregado.*
   O.R. Batic, R. Iasi, R. Pérez, J.D. Sota
   Hormigón, **27**, 19-28 (1994).

AÑO 1995

9. *Análisis teórico del comportamiento y de métodos electroquímicos utilizados para caracterizar sistemas metal/recubrimiento orgánico/electrolito acuoso.*
   A.R. Di Sarli.
   CIDEPINT-Anales, 181-251 (1995).

10. *Pinturas retardantes del fuego. Ensayos y clasificación de materiales.*
    C.A. Giúdice.
    Casa Nueva, Edición Nº 84, 72-74, Julio (1995).

11. *Los fondos difíciles... Pintado y protección del acero galvanizado.*
    B. del Amo.
    Casa Nueva, Edición Nº 86, 68-70, Setiembre (1995).

12. *Procesos de corrosión y su relación con el proyecto y diseño de edificios e instalaciones.*
    V. Rascio.
    Casa Nueva, Edición Nº 88, 70-74, Noviembre (1995).

13. *Pinturas. Aspectos ecológicos relacionados con su empleo. Impacto ambiental producido por los disolventes, componentes del ligante y aditivos.*
    J. J. Caprari.
    Industria y Química, **319**, 31-33 (1995).

14. *Parámetros de utilidad para la medición del comportamiento de pinturas.*
    V. Rascio.
    Industria y Química, **320**, 46-49 (1995).

15. *Toxicidad en relación con la elaboración y empleo de pinturas. 1ª parte.*
    C.A. Giúdice, D.B. del Amo.
    Industria y Química, **321**, 38-41 (1995).

16. *Toxicidad en relación con la elaboración y empleo de pinturas. 2ª parte.*
    C.A. Giúdice, D.B. del Amo.
    Industria y Química, **322**, 22-24 (1995).

AÑO 1996

17. *Chemical and electrochemical assessment of tannins.*
    V.F. Vetere, R. Romagnoli
    CIDEPINT-Anales 1996, 27-40.

18. *Revisión sobre los aspectos biológicos del "fouling".*
    M.C. Pérez, M.E. Stupak
    CIDEPINT-Anales 1996, 95-154

19. *Comparative corrosion behaviour of 55aluminium-zinc alloy and zinc hot-dip coatings deposited on low carbon steel substrates.*
P.R. Seré, M. Zapponi, C.I. Elsner, A.R. Di Sarli
CIDEPINT-Anales 1996, 175-195.

20. *Pinturas. Riesgos involucrados en la elaboración y empleo.*
C.A. Giúdice, B. del Amo
Casa Nueva, Edición N° 90, 70-74, Enero (1996).

21. *Pigmentos inhibidores de la corrosión de bajo impacto ambiental: fosfato de cinc y fosfatos de cinc modificados.*
R. Romagnoli, V.F. Vetere
Industria y Química, **323**, 22-30 (1996).

22. *Métodos para estudiar la corrosión de metales recubiertos con materiales poliméricos.*
A.R. Di Sarli
Industria y Química, **324**, 36-41 (1996).

23. *Demarcación para seguridad del tránsito en rutas y ciudades.*
A.C. Aznar
Revista de Ingeniería, Centro de Ingenieros de la Provincia de Buenos Aires, **136**, 25-29 (1996).

AÑO 1997

24. *De pinturas, tecnologías e instituciones.*
V.J.D. Rascio
Formas y Color, pags. 24-28 (1997).

25. *Reparación de esculturas y monumentos.*
C. Giúdice y J. Benítez.
Ingeniería y Ciencia Tecnológica, **1** (1), 24-28 (1997).

26. *El control de la corrosión de estructuras metálicas y su protección por medio de sistemas de pinturas.*
V. Rascio.
Materias Primas & Tecnología, **1** (2), 7-10 (1997).

27. *Pigmentos anticorrosivos: la importancia ecológica de su selección.*
V. Rascio.
Materias Primas & Tecnología, **1** (3), 25-27 (1997).

AÑO 1998

28. *Pinturas: Productos de última generación.*
V. Rascio.
Materias Primas & Tecnología, **1** (5), 10-14 (1998).

Teniendo en cuenta que algunos trabajos han sido publicados en Anales y en Revistas Internacionales o en Anales y Proceedings de Congresos, se deja constancia que en cada caso se lo menciona sólo una vez, considerando la cita de mayor relevancia.

Se incluyen trabajos realizados en colaboración con investigadores de otros organismos de ciencia y técnica.

ESTE EJEMPLAR SE TERMINO

DE IMPRIMIR EL DIA 15 DE

MAYO DE 1998

SERVICIOS CALIFICADOS QUE PRESTA EL CENTRO

Estudios y asesoramiento sobre problemas de corrosión de materiales en contacto con medios agresivos.
Estudios y asesoramiento sobre protección de los mencionados materiales por medio de cubiertas orgánicas (pinturas), inorgánicas (silicatos) o metálicas (galvanizado, cromado, niquelado).
Estudios sobre protección de metales, maderas, hormigones, plásticos, etc., empleados en estructuras de edificios, puentes, diques, instalaciones industriales, instalaciones navales, etc.
Estudio de medios agresivos.
Asesoramiento sobre diseño de estructuras y selección de los materiales a utilizar.
Diseño de esquemas de protección de acuerdo a las diferentes condiciones de servicio.
Formulación de recubrimientos para protección de superficies y estructuras.
Suministro de información sobre tecnología de preparación de superficies metálicas y no metálicas.
Estudio de operaciones y procesos involucrados en la preparación de pinturas y revestimientos protectores.
Preparación, a requerimiento de usuarios, de pinturas en escala de laboratorio o de planta piloto.
Normalización, en casos especiales no cubiertos por IRAM.
Formación y perfeccionamiento de personal científico calificado.
Transferencia de conocimientos a la industria, organismos estatales, universidades, etc., a través del dictado de conferencias, cursos, etc.

SERVICIOS NO CALIFICADOS

Control de calidad para la industria de pinturas (pigmentos, aceites, resinas, aditivos, etc.).
Control de calidad de pinturas, barnices y materiales para revestimiento, a requerimiento de fabricantes o usuarios.
Ensayos de resistencia a agentes corrosivos o de envejecimiento acelerado.
Control de calidad de materiales para señalización vial.
Suministro de documentación a través del servicio de repropgrafía del Centro.
Análisis de metales, cementos, cales y materiales para edificios, materiales refractarios y arcillas, minerales, etc.

ci
de
pint

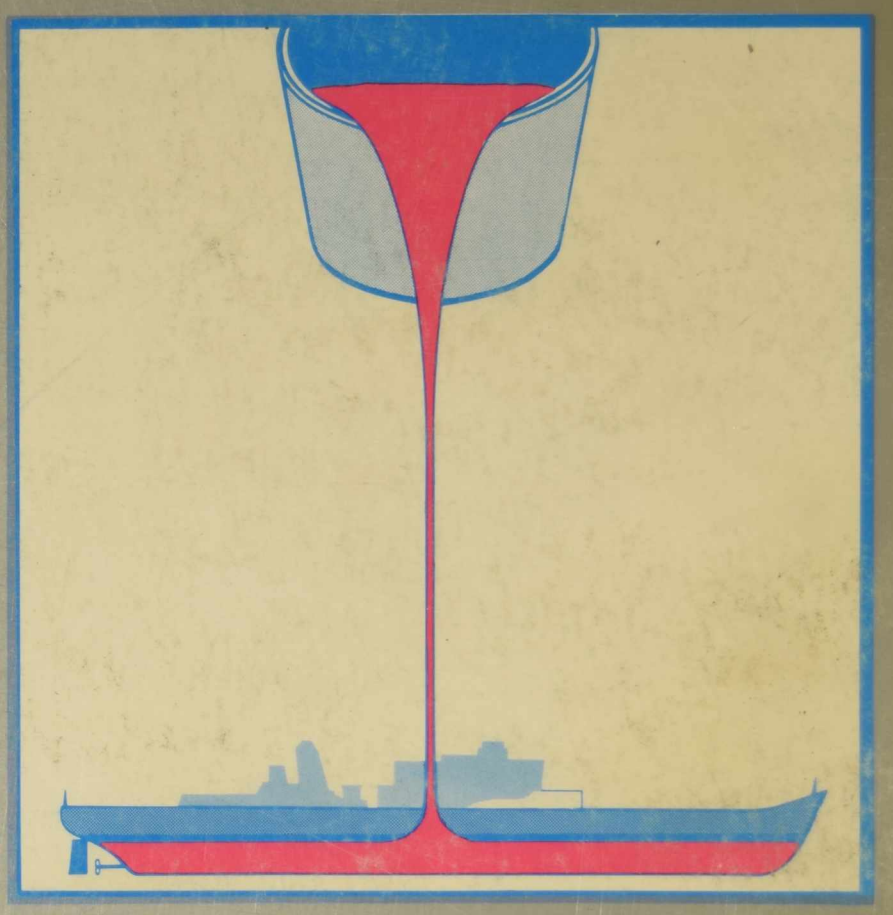

Centro de Investigación y Desarrollo en Tecnología de Pinturas (CIC-CONICET)

52 entre 121 y 122
1900 La Plata (Argentina)
Teléfonos (021) 831141-44/216214
Fax: 54-21-271587

Investigación y Desarrollo de pinturas anticorrosivas, antiincrustantes y productos especiales para protección industrial ecológicamente aceptables, en escala de laboratorio y planta piloto. Estudios electroquímicos aplicados a problemas de corrosión de materiales y estructuras.

Control de calidad para la industria de pinturas y materiales afines, asesoramientos, peritajes, etc.